

Department of Anatomy II:
Experimental Morphology
Centre for Experimental Medicine
University Medical Centre Hamburg-Eppendorf
Prof. Dr. Udo Schumacher

**Changes in Neurons, Glia and Extracellular Matrix
Molecules after Spinal Cord Hemisection
in Tenascin-C deficient Mice**

Dissertation

Thesis to earn a Doctoral Degree of Medicine
at the Faculty of Medicine of the University of Hamburg

presented by

Jenny Schreiber
Hamburg

Hamburg 2008

Accepted by the Faculty of Medicine
of the University of Hamburg at: 01.04.2009

Published with the authority of
the Faculty of Medicine of the University of Hamburg

Examination board, Chairman: Prof Dr. U. Schumacher

Examination board: 2. Consultant: Prof Dr. D. Lorke

Examination board: 3. Consultant: Prof Dr. M. Schachner

Lars, Emma and the Baby Boy

Table of content

1. Objectives	8
2. Introduction	9
3. Material and method.....	15
3.1. Animals	15
3.2. Surgery	15
3.3. Histology	17
3.4. Routine staining.....	18
3.5. Immunohistochemistry	18
3.6. Morphological analysis.....	22
3.7. Quantitative densitometry.....	26
3.8. Data analysis.....	31
3.9. Frequently used solutions.....	32
4. Results	34
4.1. TNC+/+ wild type mice	34
4.1.1. Routine histology.....	34
4.1.2. Collagen type IV	47
4.1.2.1. Morphology	47
4.1.2.2. Quantitative densitometry	53
4.1.3. Laminin.....	54
4.1.3.1. Morphology	54
4.1.3.2. Quantitative densitometry	60
4.1.4. Fibronectin.....	61

4.1.4.1. Morphology	61
4.1.4.2. Quantitative densitometry	66
4.1.5. F4/80.....	67
4.1.5.1. Morphology	67
4.1.5.2. Quantitative densitometry	77
4.1.6. GFAP.....	79
4.1.6.1. Morphology	79
4.1.6.2. Quantitative densitometry	89
4.1.7. Neurofilament.....	91
4.1.7.1. Morphology	91
4.1.7.2. Quantitative densitometry	99
4.2. TNC-/- knock out mice.....	103
4.2.1. Routine histology.....	103
4.2.2. Collagen type IV	112
4.2.2.1. Morphology	112
4.2.2.2. Quantitative densitometry	116
4.2.3. Laminin.....	118
4.2.3.1. Morphology	118
4.2.3.2. Quantitative densitometry	122
4.2.4. Fibronectin.....	124
4.2.4.1. Morphology	124
4.2.4.2. Quantitative densitometry	128
4.2.5. F4/80.....	130
4.2.5.1. Morphology	130
4.2.5.2. Quantitative densitometry	138
4.2.6. GFAP.....	140

4.2.6.1. Morphology	140
4.2.6.2. Quantitative densitometry	148
4.2.7. Neurofilament.....	150
4.2.7.1. Morphology	150
4.2.7.2. Quantitative densitometry	157
5. Discussion	161
5.1. TNC+/+ wild type mice	161
5.2. TNC-/- knock out mice.....	185
6. Summary.....	197
7. References	198
8. Appendix	212
8.1. Acknowledgement	212
8.2. Curriculum Vitae.....	214
8.3. Statistical tables.....	215
9. Statement of Originality.....	227

Abbreviation

CNS	central nervous system
CS-PG	chondroitin sulphate proteoglycan
CST	corticospinal tract
DAB	3,3'diaminobenzidine
ECM	extracellular matrix
FNIII	fibronectin-type III domain
H&E	haematoxylin and eosin stain
IFN- γ	interferon- γ
NF	neurofilament
PAP	peroxidase-antiperoxidase
PB	phosphate buffer
PBS	phosphate buffer, saline
PFA	paraformaldehyde
RST	rubrospinal tract
TGF- α	transforming growth factor- α
TGF- β	transforming growth factor- β
TGF- β 1	transforming growth factor- β 1
TNC	tenascin C
TNC-/-	tenascin C knock out
TNC+/-	tenascin C wild type
TNF- α	tumour necrosis factor- α
UKE	University Medical Centre Hamburg-Eppendorf
ZMNH	Centre of Molecular Neurobiology Hamburg

1. Objectives

Patients suffering from spinal cord injury can anticipate a near-normal life expectancy. However, these predominantly young, male patients are challenged to maintain an acceptable quality of life. Until today, complete functional recovery after spinal cord injury has not been described. Therefore it is important to continue basic research on wound healing after spinal cord injury, in order to understand the basic mechanisms involved in spinal cord regeneration.

This is the first study to characterize axonal growth, glial response, extracellular matrix formation and inflammatory response following spinal cord hemisection in tenascin C (TNC)^{-/-} knock out and TNC^{+/+} wild type control mice over a time period of fourteen days. TNC is a physiologically important component of the central nervous system (CNS) extracellular matrix and is involved in wound healing after brain injury.

Objectives of the present study:

- 1.) Is TNC involved in wound repair mechanisms after spinal cord injury?
- 2.) How does wound healing after spinal cord injury in TNC^{-/-} knock out mice differ from wound healing in TNC^{+/+} wild type mice?
- 3.) What are the characteristics of axonal growth after spinal cord hemisection in TNC^{-/-} knock out mice?
- 4.) What is the spatiotemporal course of the glial response (microglia and astrocytes) after spinal cord hemisection in TNC^{-/-} knock out mice?
- 5.) What is the spatiotemporal course of extracellular matrix proteins (collagen type IV, laminin and fibronectin) after spinal cord hemisection in TNC^{-/-} knock out mice?
- 6.) What is the spatiotemporal course of the inflammatory response after spinal cord hemisection in TNC^{-/-} knock out mice?

2. Introduction

In Germany the incidence of traumatic paraplegia is 1,800 cases annually (Schwab et al. 2004). Approximately 55,000 patients suffering from spinal trauma, including paraplegia as one of its severest forms, require hospital care in Germany every year (Schwerdtfeger et al. 2004). The most common causes for traumatic spinal cord injury are road traffic accidents involving motorcycles, sport injuries, fall-related and assault-related trauma. Due to a progress in rehabilitation and acute care, life expectancy of these predominantly young male patients has improved considerably (Nacimientto 1999). However, spinal cord injury devastates the lives of those affected and a complete functional recovery of injured axons in the adult mammalian spinal cord has not been described to date (Rossignol et al. 2007).

Cellular and molecular sequences of wound healing and the functionally inadequate neurite outgrowth after spinal cord injury are only poorly understood in humans and inadequately explored in animals (Ramon y Cajal 1928; Bähr and Bonhoeffer 1994; Schwab and Bartholdi 1996; Fawcett and Geller 1998; Nacimientto et al. 1999). The complex interactions of cells, extracellular matrix (ECM) proteins and soluble mediators greatly contribute to the success of axonal growth and potential functional regeneration after spinal cord injury.

Out of several ECM molecules, tenascin C (TNC) plays an important role in axonal growth. TNC is a member of a family of at least five large ECM glycoproteins, i. e. TNC, tenascin R, tenascin W, tenascin X and tenascin Y (Erickson and Bourdon 1989; Erickson 1993; Chiquet-Ehrismann 1995; Hagios et al. 1996). Out of all tenascins, only TNC and TNR have been reported to occur in central nervous system (CNS) tissues (Faissner 1997).

All tenascin molecules share a common structure with a serial arrangement of a cysteine-rich N-terminal region followed by epidermal growth factor-like repeats, varying numbers of fibronectin-type III (FNIII) domains, and a C-terminal fibrinogen-like globular domain (Bartsch 1996). The basic structure of TNC

contains eight constitutively expressed FNIII repeats (Bartsch 1996). Different TNC forms are generated by alternative splicing of various FNIII domains (Bartsch 1996; Forsberg et al. 1996). The monomer molecule is linked to multimers by sulphide bridges at the N-terminal end and appears as a hexabrachion, which is the prevalent form of native TNC (Erickson and Bourdon 1989; Bartsch 1996).

TNC is highly expressed in embryonic tissues where it regulates cell migration during organogenesis, and plays an important functional role during development (Mackie 1997; Webb et al. 1997). TNC is found in muscle, tendon, bone, cartilage, hair follicle, teeth, mammary gland, bone marrow, haemopoietic cells, kidney, spleen and lung tissue (Mackie et al. 1987; Thesleff et al. 1987; Mackie et al. 1988; Rüegg et al. 1989; Bartsch 1996; Mackie 1997; Webb et al. 1997; Roth-Kleiner et al. 2004).

In normal adult tissue, TNC is only found in the CNS, bone marrow (Mackie et al. 1988) and in T cell-dependent areas of lymphoid organs (Chilosi et al. 1993). However, during tissue repair and remodelling TNC becomes re-expressed in adults. For example it is expressed at sites of endothelial cell damage (Aziz et al. 1997), proliferating and migrating endothelial cells (Schenk et al. 1999), in granulation tissue (Rüegg et al. 1989), during wound healing (Mackie et al. 1988), in lungs undergoing fibrosis (Zhao et al. 1998), in inflamed and scarred human corneas (Maseruka et al. 1997), in macrophage-rich atherosclerotic plaques (Wallner et al. 1999), during neovascularization and vascular disease (Jones and Jones 2000), during tumorigenesis (Talts et al. 1999, Mackie et al. 1988) and during nerve regeneration (Jones and Jones 2000).

The complex pattern of TNC deposition and the characterization of TNC as a multifunctional ECM molecule *in vitro*, suggest a critical role for several steps during wound repair *in vivo*. Wound healing after spinal cord injury is, unlike in other tissues, not a typical regenerative process, but a fibro-proliferative event that results in a fibrotic scar (Clark 1996). After spinal cord injury, primary and secondary damage occurs and several endogenous processes are triggered that foster or hinder axonal reconnection (Rossignol et al. 2007). Due to complex

interactions between numerous specific responses that occur after spinal cord injury, it is difficult to study a certain sub-issue of wound healing. However, with the advent of recombinant DNA technology and availability of embryonic stem cells, it has been feasible to create certain knock out mice (Schachner 1994). Using knock out mice, it is possible to thoroughly study the role of a particular gene product that is involved in post injury processes of the CNS.

This study uses TNC^{-/-} knock out mice created by Evers et al. (2002). These TNC^{-/-} knock out mice show morphological alterations in the cerebral cortex (Irintchev et al. 2005) and an impaired memory in the step down passive avoidance task (Strekalova et al. 2002). In addition, TNC^{-/-} knock out mice display enhanced novelty-induced exploration, reduced anxiety, delayed resynchronisation of circadian activity and reduced muscle strength (Morellini and Schachner 2006).

The above-mentioned results indicate that TNC is a physiologically important component of the CNS and regulates multiple functions during wound healing in diverse tissues. This strongly suggests that TNC is involved in the process of wound healing after spinal cord injury.

In this study a spinal cord hemisection in TNC^{-/-} knock out mice is performed. Traumatic spinal cord injury in humans varies from complete transection to mild contusion (Joosten 1997). Due to the wide range of spinal cord injuries in humans it is difficult to experimentally establish a definitive animal model for spinal cord injuries. Contusion models in animals are often not reproducible and a complete transection does not reflect human pathology. Because of its reproducibility a hemisection model is preferred in this investigation over the contusion model. The contralateral intact site of the spinal cord can serve as an intra-individual control. The level of incision is defined at L₁/L₂, in particular because of animal welfare reasons. A higher level of hemisection results in a more devastating motor impediment. In addition, high

spinal cord transections are described to result in notable impairment of wound healing (Kliesch et al. 1996).

The present study is performed to elucidate the role of TNC in wound repair after spinal cord injury. Therefore both TNC^{-/-} knock out and TNC^{+/+} wild type mice undergo spinal cord hemisection. Axonal growth, the glial response, ECM formation and the inflammatory response following spinal cord hemisection are characterized over a time period of fourteen days.

To evaluate the influence of TNC protein on axonal growth, neurofilament (NF) immunoreactivity is used as a marker for axons. Axonal sprouting is thought to be the initial step of regeneration and is the prerequisite of functional recovery after spinal cord injury.

Astrocytes contribute to the formation of the glial scar, which is thought to act as a barrier to growing neurites (Qiu et al. 2000). Following cortical stab injury in TNC deficient mice created by Saga et al. (1992), abnormally high numbers of astrocytes were morphologically described, but have not been quantitatively evaluated (Steindler et al. 1995). Therefore morphological evaluation and quantitative densitometry of GFAP immunoreactivity, demonstrating astrocytes and astroglial scarring will be performed in TNC^{-/-} knock out mice after spinal cord hemisection.

The activation of microglia is a feature of several CNS pathologies and an early response to CNS injury. Microglia may contribute to the resulting neuropathology and secondary necrosis that occurs after spinal cord injury (Bethea 2000). A recent study revealed no significant alteration in the density of microglial cells in the somatosensory or motor cortex of TNC deficient mice (Irintchev et al. 2005) and until today the role of TNC with regard to microglial activation and maintenance after injury is unknown. Therefore this study presents morphological and quantitative evaluation of microglia specific F4/80 antibody following spinal cord hemisection in TNC^{-/-} knock out mice.

Since the glycoprotein TNC is involved in the formation of ECM, three ECM molecules, which interact with TNC protein and which are additionally involved

in axonal growth will be studied as well. The first one is fibronectin, which is expressed during development and has an analogous expression in response to injury, suggesting a role in CNS repair processes (Tate et al. 2002). Particularly interesting is a quantitative evaluation of fibronectin immunoreactivity after spinal cord hemisection, since a reduction in fibronectin has been only morphologically described in skin and cornea wounds of TNC deficient mice (Forsberg et al. 1996; Matsuda et al. 1999).

The second and third ECM molecules investigated are collagen type IV and laminin. After injury collagen type IV and laminin are the major components of ECM formation (Hermanns et al. 2001) and are associated with the success or failure of neurite outgrowth (Sosale et al. 1988; Grimpe and Silver 2002; Liesi and Kauppila 2002). Degradation of ECM molecules in CNS lesions is known to promote fibre growth across the incision site (Stichel et al. 1999a; Stichel et al. 1999c), implying a mechanical or biochemical barrier to axonal growth. Absent TNC protein may pave the way to an altered ECM composition, which may be beneficial to axonal growth. To elucidate the interaction between TNC and collagen type IV and laminin, and to understand the influence of TNC upon ECM formation with regard to axonal growth, morphological and quantitative evaluation is performed for collagen type IV and laminin immunoreactivity. In addition, collagen type I is semi-quantitatively evaluated by combined Masson trichrome and Verhoeff stain.

Recruitment and survival of polymorphonuclear cells in chemically induced dermatitis of TNC deficient mice is enhanced compared to wild type mice (Mackie and Tucker 1999). Furthermore, increased numbers of monocytes in the stroma of spontaneously arising mammary tumours in TNC deficient mice was observed (Talts et al. 1999). Because of a potential role of TNC in the inflammatory process, the general inflammatory response following spinal cord hemisection in TNC-/- knock out mice is evaluated in haematoxylin and eosin stain (H&E) by semi-quantitative cell counting of leucocytes and monocytes.

Besides the TNC^{-/-} knock out mouse used in this study, two other independently generated TNC deficient mice exist (Saga et al. 1992; Forsberg et al. 1996). At first sight both mice seemed to develop normally and revealed no detectable morphological defects (Saga et al. 1992; Forsberg et al. 1996). However, subsequent studies have uncovered subtle biochemical and behavioural abnormalities in both strains, hence comparisons between TNC deficient mice with a different genetic background seem feasible (Cifuentes-Diez et al. 1998; Nakao et al. 1998; Kiernan et al. 1999; Cifuentes-Diez et al. 2002). This study uses TNC^{-/-} knock out mice created by Evers et al. (2002), because they have been reported to lack detectable levels of TNC protein.

3. Material and method

3.1. Animals

TNC^{-/-} knock out and TNC^{+/+} wild type mice with a mixed C57BL/6J-129SvJ genetic background were obtained from Prof. Dr. M. Schachner, Head of Centre of Molecular Neurobiology Hamburg (ZMNH).

Animals were bred and kept at the breeding facilities of the ZMNH under norm conditions ($22 \pm 1^\circ \text{C}$, 55 % humidity, 12 h day-night-rhythm). Animals had free access to water and rodent chow (ssniff® M-Z Alleindiät extrudiert, ssniff Spezialdiäten GmbH, Soest, Germany). 24 TNC^{-/-} knock out mice and 26 TNC^{+/+} wild type littermates of both sexes, aged 3 month \pm 2 weeks were experimental subjects. In addition 10 TNC^{-/-} knock out and 7 TNC^{+/+} wild type mice were used for establishing the operation technique and immunohistochemistry.

All procedures involving experimental animals were performed in accordance to local governmental body of animal care and welfare of the Freie und Hansestadt Hamburg (Tierversuchsnummer 62/00).

3.2. Surgery

The average body weight of TNC^{-/-} knock out and TNC^{+/+} wild type littermates did not differ significantly. Before surgery the mean body weight of TNC^{-/-} knock out mice was 27.46 g (\pm SD 3.50 g) and the mean body weight for TNC^{+/+} wild type animals was 27.51 g (\pm SD 3.74 g). Post surgery the mean body weight was slightly reduced in both genotypes. The mean body weight for TNC^{-/-} knock out mice was then 26.05 g (\pm SD 2.69 g) and for TNC^{+/+} wild type animals 25.96 g (\pm SD 3.29 g).

Animals were anesthetized with ketamine/xylazine, ((Ketamin 10, Atarost GmbH & Co., Twistingen, Germany; Rompun 2 %, Bayer Vital GmbH, Leverkusen, Germany) 0.1 ml/10 g body weight) intraperitoneal (i. p.) and skin was surgically scrubbed with Cutasept® F (Bode Chemie, Hamburg, Germany). The hair at the surgical field was removed and the eyes were covered with ointment (Vidisic®, Dr. Mann chemisch-pharmazeutische Fabrik GmbH, Berlin, Germany) to prevent them from drying.

In prone position animals were attached with tape to the dissecting table. Under aseptic conditions skin and thoracolumbar fascia were dissected 12 mm from the lumbar segment L₃/L₄ from caudal to cranial. The medial part of the back muscles was retracted to the side over two segments from the spinal processes, while producing as little tissue trauma and bleeding as possible. Searching the intervertebral foramina and cutting the lamina of one vertebral arch of each side resulted in a laminectomy. Using a blade (#11 blade, Bruno Bayha GmbH, Tuttlingen, Germany) at the level L₁/L₂ the spinal cord was gently hemitransected free at the right side in one movement from the medial dorsal septum to the lateral edge. Care was taken not to harm the anterior spinal artery. The superficial back muscles of both sides were repositioned and carefully sutured with absorbable Vicryl® (Ethicon GmbH, Norderstedt, Germany). Skin was closed with the same suture. The duration of the surgery without suturing ranged between 8 and 16 min.

Intraoperative animals received 0.02 ml Metamizol-WDT (WDT, Garbsen, Germany) subcutaneously. Mice were kept in cages individually and placed on soft bedding on a warming blanket held at 37° C for 24 h after surgery to prevent hypothermia. Then mice were kept in a temperature controlled (22° C) room with softened rodent chow ad libitum. Animals received 0.2 ml Novalgine® (Ratiopharm GmbH, Ulm, Germany) in 75 ml drinking water until they were sacrificed.

Six TNC^{+/+} wild type mice and four TNC^{-/-} knock out animals died post surgery. Therefore 20 TNC^{+/+} wild type and 20 TNC^{-/-} knock out spinal cord samples underwent immunohistochemistry.

3.3. Histology

Animals were sacrificed at day 1, 3, 7 and 14-post surgery. Mice were deeply anesthetized with ketamine/xylazine (0.15 ml/10 g body weight i. p.). Animals were fixed in supine position and the skin of the abdomen was cut median up to the throat. A thoracotomy was performed to gain access to the heart and the left jugular veins were laid open. After the left jugular veins were cut the right atrium was opened immediately. Using a Luer Lock cannula (G18, B. Braun Melsungen AG, Germany) mice were transcordially perfused through the left ventricle (pressure 90 mm Hg) with Ringer solution (Apotheke, University Medical Centre Hamburg-Eppendorf (UKE), Germany) for 30 sec, or until the liver appeared to be bloodless. This was followed by a transcordial perfusion with 4 % buffered paraformaldehyde (PFA; for details see chapter 3.9.) for 10 min.

The spinal cord was laid open through bilateral laminectomy and transected at the medulla oblongata and cauda equina. Spinal nerves were cut and the spinal cord was removed and placed in PFA for another 2 h. Thereafter tissue was left overnight at room temperature in 30 % sucrose.

The following day spinal cords were placed into small plastic forms surrounded by Tissue-Tek® O. C. T. Compound (Sakura Finetek Europe B.V., Zoeterwoude, Netherlands). Isopentane (Merck, Darmstadt, Germany) was frozen down to -80° C in nitrogen and plastic forms were situated in isopentane until tissue froze solid, i. e. Tissue Tek® turned from transparent into white. Frozen tissue was stored at -84° C in 1 ml Cryo-tubes (Nunc, Wiesbaden, Germany). Cryo-tubes were preserved in Falcon tubes (Greiner, Frickenhausen, Germany) surrounded by frozen distilled water, to prevent tissue from drying.

16 μm -longitudinal serial sections in the frontal plate from the dorsal pial surface to the ventral pial surface were cut using a Leica CM 3050 cryostat (Leica Instruments GmbH, Nussloch, Germany). Sections were collected on SuperFrost®Plus slides (Menzel-Gläser, Germany) through saline phosphate buffer (PBS; for details see chapter 3.9.) and air-dried for at least 20 min at room temperature. Sections were then fixed with acetone (Merck, Darmstadt, Germany) for 3 min and again air-dried for at least 20 min. Sections were stored in boxes at -84°C until staining was performed.

3.4. Routine staining

Two routine stainings, i. e. H&E and combined Masson trichrome and Verhoeff stain were performed on longitudinal cryostate sections of two TNC-/- knock out and two TNC+/+ wild type animals on each day post injury.

For both staining protocols, sections were air-dried for at least 40 min and then fixed with PFA for another 10 min. Routine staining was performed and sections were dehydrated through a series of increasing ethanol before sections were mounted with Eukitt® (O. Kindler GmbH & Co., Freiburg, Germany).

3.5. Immunohistochemistry

Immunohistochemical staining was performed on longitudinal sections of the spinal cord. Sections were differentiated according to location, i. e. dorsal tier, central tier and ventral tier, each of them showing a symmetrical distribution of grey and white matter.

The dorsal tier of the spinal cord displayed white matter tracts adjacent to the meninges. Medially to the tracts grey matter was displayed. These first few sections were discarded. The following four to six sections showed white matter

tracts medially and laterally and grey matter in between. Unlike in humans, in mice the dorsomedial tract was identified as the corticospinal tract (CST) (Uematsu et al. 1996; Bregman et al. 2002; Inman and Steward 2003), while the dorsolateral tract represented the rubrospinal tract (RST) (Bregman et al. 2002). To these sections NF antibody was applied (Fig. 1). In the central tier, sections displayed grey matter medially and white matter tracts laterally. Some sections revealed the central canal in the midline. These sections were labelled with antibodies detecting glial cells, i. e. F4/80 and GFAP (Fig. 1). Sections of the ventral tier presented white matter tracts medially and laterally, while grey matter was located in between. These sections were incubated with antibodies against ECM components, i. e. collagen type IV, laminin and fibronectin (Fig. 1).

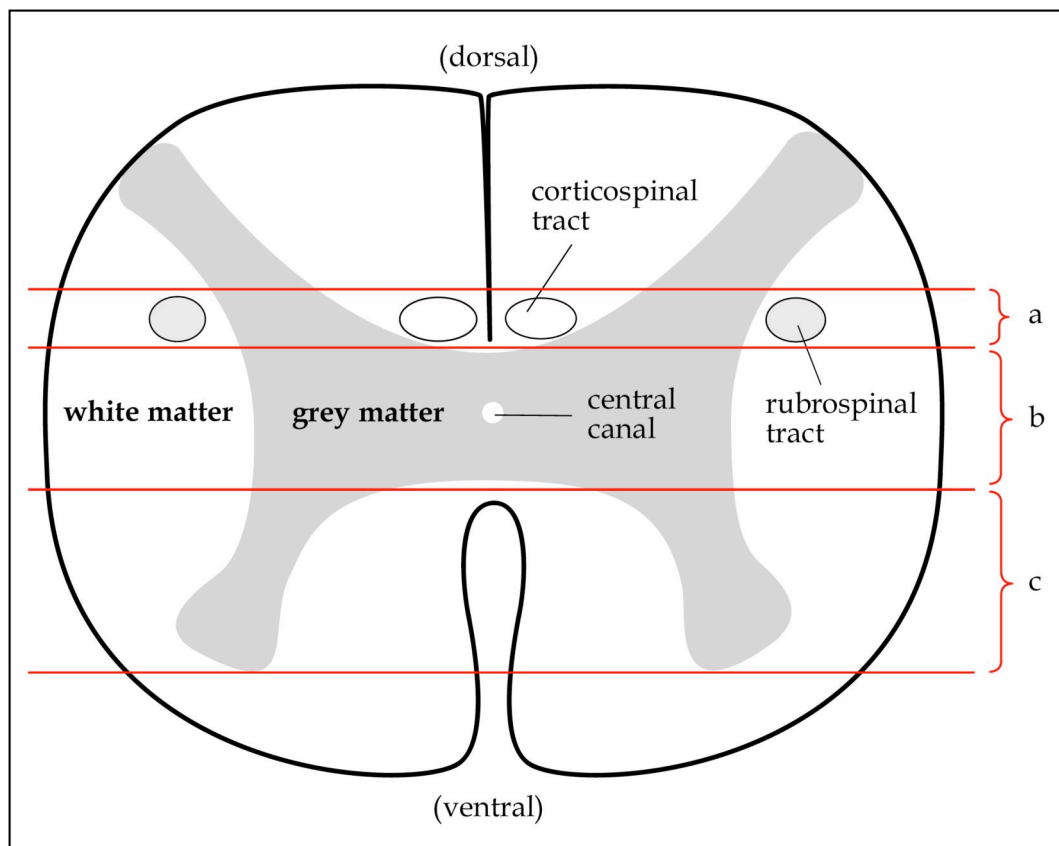


Fig. 1: Schematic drawing of a transverse section of the mouse spinal cord. Sections for immunohistochemistry were obtained from part (a) for neuronal marker (neurofilament), from part (b) for glial marker (F4/80 and GFAP) and from part (c) for extracellular matrix marker (collagen type IV, laminin and fibronectin). Tracts have been located according to Bregman et al. (2002).

For immunohistochemistry the following antibodies were used (Fig. 2, 3, 4):

Primary Antibody	Source	Final dilution	Secondary Antibody	Source	Final dilution
goat-anti-collagen type IV	Cat no. AB769 Chemicon Int., Hofheim, Germany	1:100	biotinylated rabbit- anti-goat immunoglobulin	DakoCytomation Glostrup, Denmark	1:250
anti-fibronectin	Product Nr. F3648 Sigma, München, Germany	1:500	biotinylated swine- anti-rabbit immunoglobulin	DakoCytomation Glostrup, Denmark	1:250
rabbit-anti-laminin	Product Nr. L9393 Sigma, München, Germany	1:200	biotinylated swine- anti-rabbit immunoglobulin	DakoCytomation Glostrup, Denmark	1:250

Fig. 2: Table of antibodies detecting extracellular matrix proteins (collagen type IV, laminin, fibronectin)

Primary Antibody	Source	Final dilution	Secondary Antibody	Source	Final dilution
rat-anti-mouse-F4/80	Product Nr. MCAP497 Serotec, Düsseldorf, Germany	1:200	biotinylated rabbit- anti-rat immunoglobulin	DAKO, Denmark	1:250
rabbit-anti-cow-GFAP	Code No. Z0334 DAKO, Hamburg, Germany	1:800	biotinylated swine- anti-rabbit immunoglobulin	DakoCytomation Glostrup, Denmark	1:250

Fig. 3: Table of antibodies detecting microglial cells (F4/80) and astrocytes (GFAP)

Primary Antibody	Source	Final dilution	Secondary Antibody	Source	Final dilution
rabbit-anti-neurofilament 200kD	No. N 4142 Sigma, München, Germany	1: 400	biotinylated swine- anti-rabbit immunoglobulin	DakoCytomation Glostrup, Denmark	1:250

Fig. 4: Table of antibodies detecting axonal structures (neurofilament)

When comparing knock out with wild type control animals, care was taken to use the same batch of diluted antibody and to stain the sections at the same time.

Sections who had been stored at -84° C had to air-dry at least 40 min before they were fixed with PFA for 10 min. All sections were washed in PBS (3 x 5 min),

only sections for F4/80 immunohistochemistry were continuously washed with 0.1 % Triton® X-100 (Serva Feinbiochemica GmbH & Co., Heidelberg, Germany) diluted in PBS to reduce background staining.

Predigestion with 0.1 % trypsin (1:250, Biochrom AG, Berlin, Germany) diluted in PBS for 2 min at 37° C was only performed for F4/80 immunohistochemistry. After washing sections with Triton® X-100 or PBS (3 x 5 min), endogenous peroxidase was blocked with 0.1 % H₂O₂ (Merck, Darmstadt, Germany) diluted in methanol (Merck, Darmstadt, Germany) for 30 min. Subsequently rinsing sections in PBS (3 x 5 min), sections stained for laminin, fibronectin, GFAP and NF were covered with 2 % normal swine serum (DakoCytomation, Glostrup, Denmark) diluted in PBS for 30 min at room temperature. Sections, which underwent labelling for collagen type IV and F4/80 were overlaid with 2 % normal rabbit serum (DakoCytomation, Glostrup, Denmark) for 30 min at room temperature. Sections were then incubated with the primary antibody overnight at 4° C in a humid chamber (for details see Fig. 2, 3, 4).

On the second day, sections were washed in PBS (3 x 10 min) and incubated with secondary antibody for 1 h (for details see Fig. 2, 3, 4). After rinsing with PBS (2 x 10 min) all sections, except sections for collagen type IV were treated with peroxidase-anti-peroxidase (PAP) complex. PAP complex was applied at a dilution of 1:200 in PBS for 30 min at room temperature. Sections for laminin, fibronectin, GFAP and NF received PAP rabbit serum (DAKO, Denmark), while sections for F4/80 were treated with PAP mouse serum (DAKO, Denmark). Subsequently all sections were washed in PBS (2 x 10 min) and covered with Elite PK-6100 Standard Vectastain® ABC Kit (Linaris Biologische Produkte GmbH, Wertheim, Germany) for 30 min at room temperature, followed by 10 min rinsing in PBS and 10 min washing in 0.1 M phosphate buffer, ph 7.4 (0.1 M PB; for details see chapter 3.9).

To visualize antibody-enzyme complexes, glucose-oxidase-treatment (for details see chapter 3.9.) was performed. Freshly prepared glucose-oxidase was used and solution was prepared rapidly as the reaction starts when glucose-oxidase is added. For glucose-oxidase-treatment each antibody had its own incubation period (8 to 17 min). The individual incubation period was strictly maintained with every staining procedure. Each incubation period of glucose-oxidase-treatment was previously tested and the time duration for each antibody with the best result (i. e. intense signal of immunoreactivity and minimal unspecific staining) was chosen. Glucose-oxidase-treatment showed a strong black reaction product, while background staining was weak. Sections were rinsed in distilled water (2 x 5 min) and finally mounted with Crystal/Mount® (Biomedica Corp. Foster City, California) and ClariØn® (Biomedica Corp. Foster City, California).

Control sections that had received PBS instead of primary antibody, but otherwise underwent the same staining procedure, were used to distinguish specific staining from non-specific antibody binding components of the lesion area. The control sections did not show any 3,3'-diaminobenzidine (DAB) reaction product and therefore yielded negative results.

3.6. Morphological analysis

Sections were analyzed using an Axiophot 2 microscope (Carl Zeiss, Göttingen, Germany) for general morphology. The extension of the lesion, the inflammatory reaction and the morphology of the spinal cord in general were described in H&E and combined Masson trichrome and Verhoeff stain sections. Immunohistochemical sections were analyzed to identify defined changes after spinal cord lesion. For routine staining and for each antibody different regions were defined for morphological analysis.

Routine staining

Morphological changes were observed in different areas in the lesioned spinal cord. The contralateral spinal cord of the incision site showed no morphological changes throughout the time course and was therefore defined as the normal control of the spinal cord. For routine staining and immunohistochemical staining the normal control was described and served as an intra-individual control. In addition three other regions were described in detail for routine staining; i. e. incision site, surrounding area and the ipsilateral distant white matter, cranial to the incision site (Fig. 5). The incision site was defined as the area between the wound edges. The surrounding area was defined as the ipsilateral area approximately 0.05 mm above and 0.05 mm beneath the incision site. The ipsilateral distant white matter cranial to the incision site was defined as the cranial white matter from the border of the surrounding area to the edge of the section (approximately 0.7-1.5 mm from the incision site).

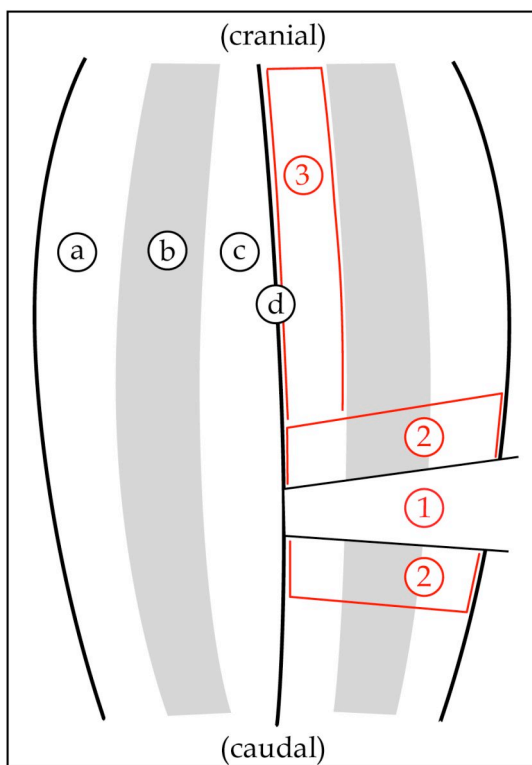


Fig. 5: Schematic drawing of a longitudinal section of the mouse spinal cord. (a) White matter; (b) Grey matter; (c) White matter, corticospinal tract; (d) Posterior median sulcus. The following regions were defined for morphological description (H&E and combined Masson trichrome and Verhoeff stain): (1) Incision site; (2) Surrounding area; (3) Distant white matter (corticospinal tract).

ECM marker

Morphological changes for ECM markers, i. e. collagen type IV, laminin and fibronectin were only seen at the incision site and in the surrounding area, therefore description was confined to these two regions (Fig. 6).

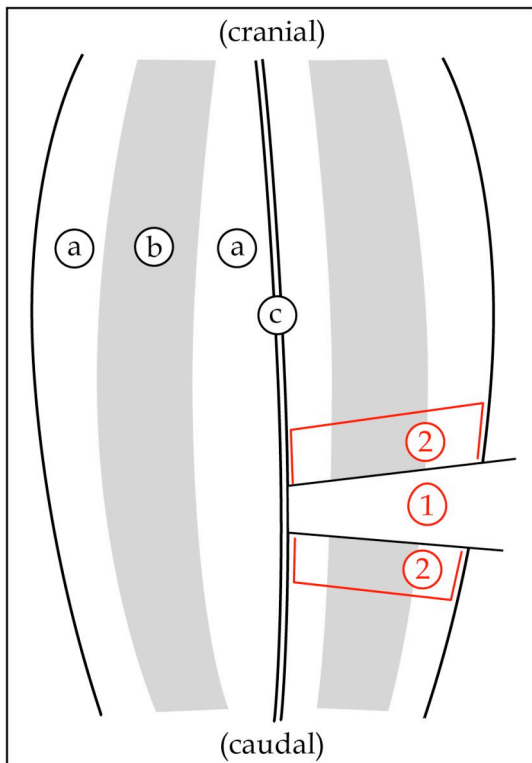


Fig. 6: Schematic drawing of a longitudinal section of the mouse spinal cord. (a) White matter; (b) Grey matter; (c) Anterior median fissure. The following regions were defined for extracellular matrix morphology (collagen type IV, laminin, and fibronectin): (1) Incision site and (2) Surrounding area.

Glial marker

For glial cell markers, i. e. microglia and astrocytes four regions, i. e. incision site, surrounding area, ipsilateral grey matter distant from the incision site and the ipsilateral white matter distant from the incision site were described (Fig. 7).

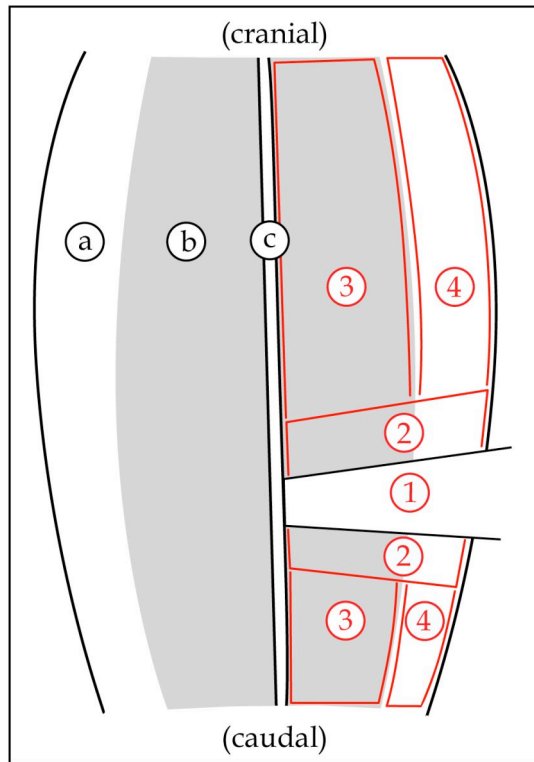


Fig. 7: Schematic drawing of a longitudinal section of the mouse spinal cord. (a) White matter; (b) Grey matter; (c) Central canal. The following regions were defined for glial morphology (F4/80, GFAP): (1) Incision site; (2) Surrounding area; (3) Distant grey matter; (4) Distant white matter.

Axonal marker

For NF immunoreactivity four regions of morphological changes were observed, therefore description was confined to the incision site, the surrounding grey matter, the surrounding white matter and the distant white matter (corticospinal tract) cranial to the incision site (Fig. 8).

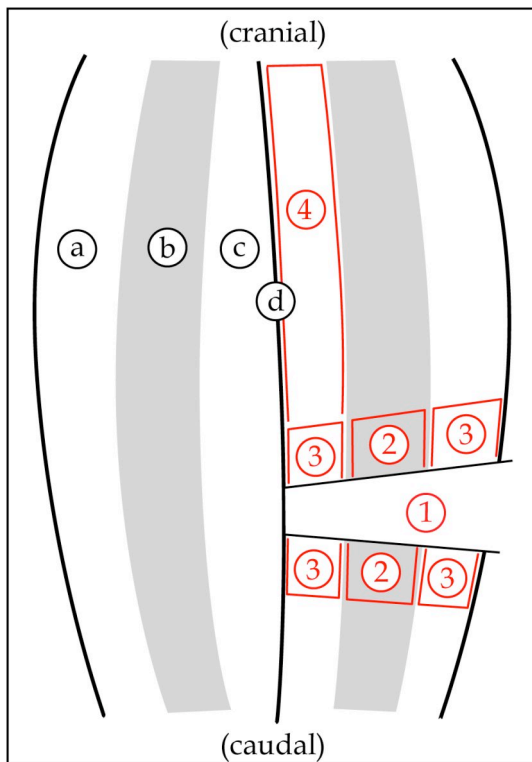


Fig. 8: Schematic drawing of a longitudinal section of the mouse spinal cord. (a) White matter, rubrospinal tract; (b) Grey matter; (c) White matter, corticospinal tract; (d) Posterior median sulcus. The following regions were defined for neuronal morphology (neurofilament): (1) Incision site; (2) Surrounding grey matter; (3) Surrounding white matter; (4) Distant white matter, corticospinal tract.

3.7. Quantitative densitometry

Sections were analyzed with the Axiophot 2 microscope to develop a system on how to perform a quantitative analysis. The examiner was blinded to the genotype of the animals.

For quantitative analysis, images were taken using an Axiophot 2 microscope and the Spot/AP software version 2.1. (Diagnostic Instruments Inc., Michigan). Images for collagen type IV, laminin, fibronectin, F4/80 and GFAP were digitised at a magnification of 10 x and images for NF were digitised at a magnification of 40 x. Images were captured at 1315 x 1035 pixels in RGB colours and saved as a

TIFF files. The setting for each antibody was kept constant throughout the image capturing. The captured images presented in this study were resized and labelled using Adobe Photoshop software (Version 5.5) and Adobe Illustrator (Version 8.01) for Macintosh. The contrast and brightness were adjusted to provide optimal clarity.

Densitometry to quantify the signal of the antibodies was performed by measuring Integrated Optical Density (IOD) using the Metamorph 4.0 software (Universal Imaging Corporation, Pennsylvania). The Optical Density (OD) is the inverse logarithm of the greyscale transmittance, where the transmittance at a given pixel is considered to be its greyscale value divided by the maximal possible number of greyscale levels (e. g. 256 for an 8 bit image). The transmittance stands for transmitted light divided by incident light.

$$OD = \text{Log}_0 (1/\text{transmittance})$$

The IOD is the sum of the optical densities of all pixels that make up the object (e. g. astrocytes above threshold). The unit of the IOD measurement is defined as IOD. GV stands for the greyscale value.

$$IOD = \sum (GV \log \text{MaxGV}/GV)$$

Densitometry was performed for all immunolabelled sections (i. e. collagen type IV, fibronectin, laminin, F4/80, GFAP and NF). IOD measurements were carried out on up to six different sections per animal and antibody, avoiding dark stained meninges, any folds, dirt, large vessels, cavities, or areas in which there were tightly packed clusters of erythrocytes or any technical artefacts. All measurements, except for NF, were restricted to the grey matter.

The IOD was determined within an analysis window of rectangular shape (89640 μm^2). Measurements for NF antibody were performed in a smaller rectangular shaped box (up to 43794.9 μm^2). The measured IOD value was divided by the area of the sampled region. Subsequently the median of the up to six IOD measurements was taken to perform statistical analysis.

ECM marker

For ECM proteins (collagen type IV, laminin and fibronectin) two measurements were carried out (Fig. 9). The first measurement was performed in the epicentre of the lesion, the second measurement was carried out in the surrounding area (approximately 0.05 mm away from the epicentre). At first, one measurement was carried out in the surrounding area cranially the incision site and one was carried out in the surrounding area caudally the incision site. Both regions presented comparable measurements, hence the cranial and caudal region of the surrounding area were combined into one region, which is referred to as the surrounding area. To provide intrasection control for differences in section thickness or overall level of immunoreactivity, the threshold was set manually 1.9 mm distant from the incision site on the contralateral side, where only background reaction was seen. This gauge threshold was then automatically used for the entire section, so that both measurements were taken under identical conditions.

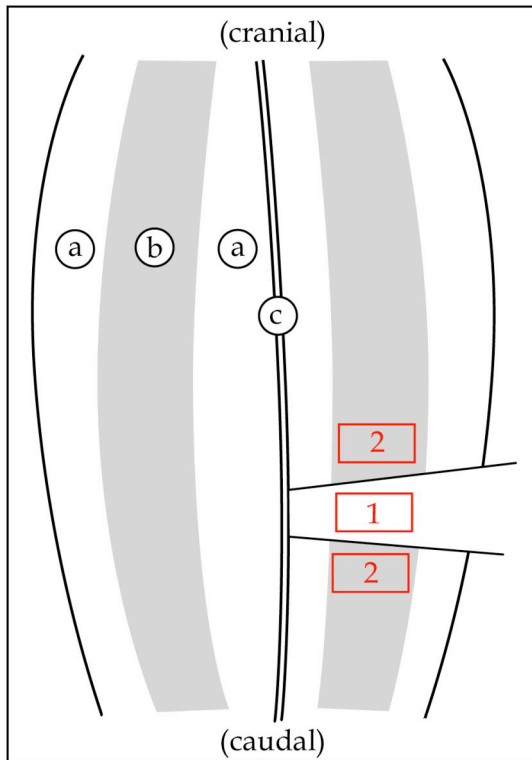


Fig. 9: Schematic drawing of a longitudinal section of the mouse spinal cord. (a) White matter; (b) Grey matter; (c) Anterior median fissure. Measurements of the density of immunoreactivity for extracellular matrix components (collagen type IV, laminin, and fibronectin) were performed in the following areas: (1) Incision site; (2) Surrounding area.

Glial marker

Measurements for glial cells (F4/80 and GFAP) were carried out in the same way as for ECM proteins (incision site and surrounding area). In addition two measurements were taken distant from the incision site (0.7-1.5 mm cranially and caudally to the epicentre of the incision site) to measure the long distance effect of glial cells, which was demonstrated in the morphological examination (Fig. 10). The threshold was set manually 1.9 mm distant from the incision site on the contralateral side, so that immunolabelled cells were above threshold and unlabelled areas were below threshold. This gauge threshold was then automatically used for all four measurements.

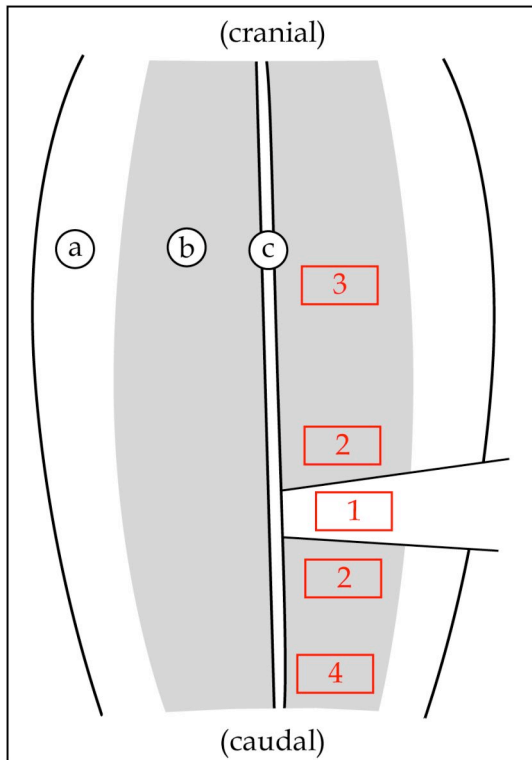


Fig. 10: Schematic drawing of a longitudinal section of the mouse spinal cord. (a) White matter; (b) Grey matter; (c) Central canal. Measurements of the density of immunoreactivity for glial cells (F4/80, GFAP) were performed in the following areas: (1) Incision site; (2) Surrounding area; (3) Distant grey matter, cranial to the incision site; (4) Distant grey matter, caudal to the incision site.

Axonal marker

For NF immunoreactivity, six measurements were performed, three in the grey and three in the white matter (Fig. 11). The first measurement in the grey matter was carried out directly at the incision site. The second and third measurements were performed in the immediate surrounding above and below, approximately 0.025 mm away from the epicentre of the incision site.

At first one measurement was carried out at the incision site adjacent to the CST white matter and one was carried out adjacent to the RST white matter. Measurements showed comparable findings, therefore both regions were combined and referred to as white matter incision site.

The second and third measurements in the white matter were performed in the immediate surrounding (CST and RST) above and below (approximately 0.025 mm) the incision site. At first, measurements in the white matter were carried out in the CST cranially and caudally to the incision site and in the RST cranially and caudally to the incision site. Both measurements taken in the white matter cranially the incision site (CST and RST) presented comparable findings, hence both regions were combined and referred to as surrounding white matter cranial.

In accordance with that, both measurements taken in the white matter caudally the incision site (CST and RST) presented similar findings, therefore these regions were combined and referred to as surrounding white matter caudal.

In order to measure very thin fibres, the threshold was set not within the tracts, but manually in the grey matter immediately above the epicentre of the lesion for each section. This gauge threshold was then automatically used for all measurements.

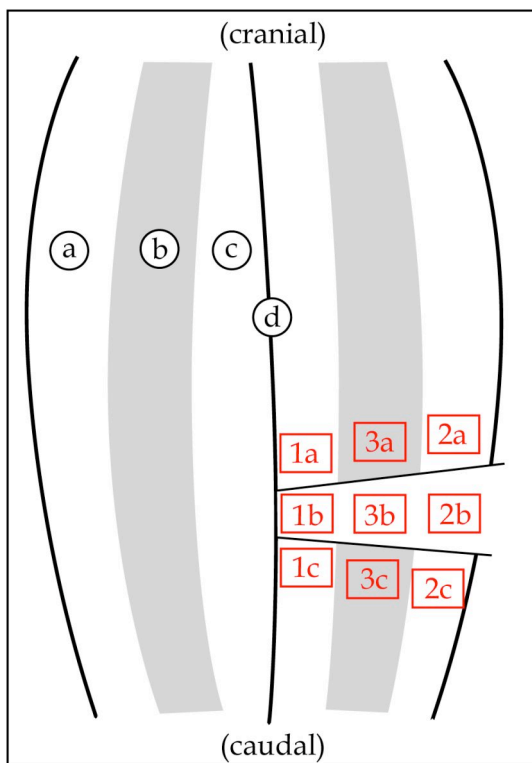


Fig. 11: Schematic drawing of a longitudinal section of the mouse spinal cord. (a) White matter, rubrospinal tract (RST); (b) Grey matter; (c) White matter, corticospinal tract (CST); (d) Posterior median sulcus. Measurements of the density of immunoreactivity for axons (neurofilament) were performed in the following areas: (1) White matter, CST, (a) surrounding cranial, (b) incision site, (c) surrounding caudal; (2) White matter, RST, (a) surrounding cranial, (b) incision site, (c) surrounding caudal; (3) Grey matter (a) surrounding cranial, (b) incision site, (c) surrounding caudal. Regions 1a and 2a are combined and referred to as surrounding white matter cranial. Region 1b and 2b are combined and referred to as white matter incision site. Region 1c and 2c are combined and referred to as surrounding white matter caudal.

3.8. Data analysis

Statistical analysis was performed using the statistical software program SPSS for Windows (Version 11). ANOVA was applied for repeated measurements by the method of General Linear Model (GLM) to detect differences in the IOD between regions, between time points and between genotypes for each antibody. If necessary, post-hoc comparisons of differences in IOD between regions and between post injury survival days were examined with the Games-Howell method. For differences between regions contrast was calculated with regard to the *incision* region. Differences were considered significant at $p \leq 0.05$.

3.9. Frequently used solutions

Frequently used solutions are listed in their order of appearance.

1. PFA (4 % paraformaldehyde, buffered in 0.2 M phosphate buffer)
40 g para formaldehyde (Merck, Darmstadt, Germany)
ad 400 ml distilled water, solution was heated up to 80° C
ad 1 N NaOH (Merck, Darmstadt, Germany) until solution turned from milky
into transparent
after solution cooled down, 500 ml 0.2 M phosphate buffer was added
2. PBS (0.1 M saline phosphate buffer, pH 7.4)
17.8 g Na₂HPO₄ × 2H₂O (Merck, Darmstadt, Germany)
16.0 g NaCl (J.T. Baker, Deventer, Netherlands)
ad 2000 ml distilled water
pH was adjusted with 1 N HCl (Merk, Darmstadt, Germany)
3. 0.2 M PB (0.2 M phosphate buffer, pH 7.2-7.4)
65.84 g Na₂HPO₄ × 2H₂O (Merck, Darmstadt, Germany)
5.52 g NaH₂PO₄ × H₂O (Merck, Darmstadt, Germany)
ad 2000 ml distilled water
4. glucose-oxidase-enhancement solution (stocks are described below)
 - a. 45 ml 0.1 M PB
 - b. 1 ml DAB
 - c. 100 µl ammonium chloride
 - d. 900 µl nickel sulphate
 - e. 900 µl glucose
 - f. 150 µl glucose oxidase
- 4a. 0.1 M PB (0.1 M phosphate buffer, pH 7.4)
4.03 g KH₂PO₄ (Merck, Darmstadt, Germany)

17.8 g $\text{Na}_2\text{HPO}_4 \times 2\text{H}_2\text{O}$ (Merck, Darmstadt, Germany)
ad 1000 ml distilled water, pH was adjusted with $\text{Na}_2\text{HPO}_4 \times 2\text{H}_2\text{O}$

4b. DAB (3,3'-diaminobenzidine)

2.25 g DAB (Sigma Aldrich Chemie GmbH, Steinheim, Germany)
ad 100 ml tris buffer (TB, see below)
solution was filtrated and stored at a dark place at -20°C

TB (0.05 M tris buffer, pH 7.6)

3.02 g trizma base (Sigma T-1503; Sigma Aldrich Chemie GmbH, Steinheim, Germany)
4.5 g NaCl (J.T. Baker, Deventer, Netherlands)
ad 500 ml distilled water; pH was adjusted with NaCl or HCl

4c. ammonium chloride

18 mg ammonium chloride (Sigma Aldrich Chemie GmbH, Steinheim, Germany)
ad 100 μl distilled water

4d. nickel sulphate

130 mg nickel sulphate (Sigma Aldrich Chemie GmbH, Steinheim, Germany)
ad 10 ml distilled water

4e. glucose

10 mg glucose (Merck, Darmstadt, Germany)
ad 100 ml distilled water

4f. glucose-oxidase

1.2 mg glucose-oxidase, stored at -20°C (G-2133; Sigma Aldrich Chemie GmbH, Steinheim, Germany),
ad 1 ml distilled water

4. Results

One TNC^{+/+} wild type animal and one TNC^{-/-} knock out animal only showed a moderate hemisection and therefore were not included in the analysis. Morphological description was done on 19 (5, 5, 5, 4 days post surgery) TNC^{+/+} wild type animals and on 19 (4, 5, 4, 6 days post surgery) TNC^{-/-}-knock out mice.

Out of these animals, one TNC^{+/+} wild type animal and one TNC^{-/-} knock out animal revealed a histology of severe necrosis of the spinal cord, presumably because the anterior spinal artery was harmed through the surgical procedure. Therefore these two animals were not taken into quantitative analysis. Quantitative densitometry was performed on 18 (5, 5, 4, 4 days post surgery) TNC^{+/+} wild type mice and 18 (3, 5, 4, 6 days post surgery) TNC^{-/-} knock out animals.

4.1. TNC^{+/+} wild type mice

4.1.1. Routine histology

The contralateral spinal cord distant from the incision site showed no pathological changes throughout the time course and was therefore considered as the normal control.

Underneath the most superficial layer, i. e. the meninges with spindle-shaped leptomeningeal cells, the lateral white matter tracts showed brightly stained fibre bundles usually seen parallel to the meninges. Occasionally small fibre bundles or single fibres were oriented perpendicularly to the meninges. Oval shaped nuclei, representing oligodendroglial cells, were frequently seen throughout the white matter, while astrocytes were only rarely seen. The next layer consisted of grey matter and showed a different picture in the ventral and dorsal part of the spinal cord. Dorsally located sections showed small neurons with oval nuclei. These neurons contained relatively few Nissl bodies. In contrast, the majority of neurons in the ventral tier presented with significantly larger cell bodies and nuclei. In

addition, plenty of Nissl substance was found in their cytoplasm, characterized by blue staining in H&E. These cells were therefore classified as large motor neurons. Occasionally, one or two satellite cells surrounding these neurons were detected. Only few oligodendrocytes with a round-shaped nuclei and relatively dense chromatin were seen in the grey matter. Astrocytes characterized by less compact round nuclei, were frequently found in the white matter. Microglial cells were predominantly seen in the grey matter and showed considerably smaller cell bodies compared to astrocytes. Both astrocytes and microglial cells were also identified by immunohistochemistry. Most medially, the central canal was composed of square-shaped cells with dark nucleole. Blood vessels devoid of erythrocytes were seen throughout the entire cord in a regular distribution, indicating adequate perfusion with the fixative.

Combined Masson trichrome and Verhoeff stain revealed moderate collagen deposits in the meninges and discrete collagen fibres surrounding large vessels, which were mainly seen near the meninges and close to the midline.

In routine staining histological changes in the lesioned spinal cord were observed in three regions. Therefore, description was confined to the incision site, the surrounding area and the ipsilateral distant white matter, containing the CST.

On the first day post injury, the incision site was devoid of neural tissue (Fig. 12A₁, 13A). This tissue-free gap was up to 0.025 mm wide and showed a clear separation of tissue on each side of the unilateral incision. The gap was filled with a moderate amount of erythrocytes, indicating haemorrhage. In one animal wound edges were adjacent to each other.

In the surrounding area numerous swollen neurons with brighter, enlarged karyoplasms and a light halo, indicated cell necrosis. The less intensely stained neuropil, indicating oedema and the necrotic tissue with cell debris was typical of this site. Infiltrating granulocytes, mainly neutrophils dominated the picture (Fig. 12A₂). They were found in great density adjacent to the incision, but extended throughout the surrounding area. Lymphocytes, monocytes or fibroblasts were

not detected yet. As a prominent feature, all sections showed ruptured blood vessels in the surrounding area, resulting in minor haemorrhages close to the incision site (Fig. 12A₂). Sometimes, eosinophilic accumulations, representing fibrin deposits, were detected. Extensive haemorrhage in the surrounding area only occurred in one animal. Vessels in the central part of the surrounding area showed a wider lumen than the ones seen in the normal control, indicating slight vasodilation.

1.5 mm away of the incision site, the morphological appearance of the CST resembled the picture seen in the normal control (Fig. 14A). Neither the contralateral spinal cord on the level of incision nor the ipsilateral distant grey matter distant from the incision site showed morphological changes throughout the time course.

On the third day post surgery, the wound edges of the incision were adjacent to each other (Fig. 12B₁). A gap was no longer visible and haemorrhage, when present, was less severe than on day one. Along the incision edges, combined Masson trichrome and Verhoeff stain showed bright green collagen fibres (Fig. 13B). These fibres were situated parallel and perpendicular to the incision site and did not extend the neighbouring tissue yet.

In the surrounding area, the most obvious change was the large amount of newly invading fibroblasts and a moderate penetration of monocytes and lymphocytes compared to day one. These fibroblasts with a relatively large nucleus and a visible ovoid cytoplasm were categorized as *active* fibroblasts (Bannister 1995). Active fibroblasts were preferentially located near the meninges and orientated perpendicular to the wound edges. Monocytes showed a large cell body and prominent nucleoli, while lymphocytes appeared as smaller cells with a narrow edge of cytoplasm. Lymphocytes and monocytes were scattered throughout the surrounding area. The amount of neutrophils remained similar to day one. Neurons still presented blurred cell borders and enlarged karyoplasms (Fig. 12B₂). Some of the neurons formed spike-like cytoplasmic ramifications, indicating a disintegration of Nissl bodies. In addition, two to four satellite cells

surrounding these neurons were detected. Destruction of blood vessels especially near the incision site was still obvious. Blood vessels in the central part of the surrounding area showed a larger diameter in lumen than seen on day one, now indicating marked vasodilation. Pseudocysts, devoid of endothelial lining were frequently seen in the surrounding white and grey matter (Fig. 12B₁). Pseudocysts occurring after spinal cord injury were categorized as cavitations (Zhang et al. 1996). In general, cavitations were small, except for one animal, which showed one large cavitation.

The distant CST was pale in staining, showing oedematous axons and scattered small cavitations (Fig. 14B₁, B₂).

On the seventh day, the margins of the incision site were joined together and lined with active fibroblasts (Fig. 12C₁, C₂). Combined Masson trichrome and Verhoeff stain still showed bright green collagen fibres along the incision site (Fig. 13C).

In addition, collagen fibres were now also found in the surrounding area, especially near the meninges (Fig. 13C). This collagen network indicated the beginning of a scar formation, which included fibroblasts, vessels and small cavitations. The predominant cell type was the activated fibroblast (Fig. 12C₂), seen in even higher density than on day three. Fibroblasts were again detected preferentially near the meninges and the incision site. Distribution and morphological pattern of neutrophils and lymphocytes remained comparable to day three, although the number of neutrophils slightly decreased compared to day three. The number of monocytes in the surrounding area remained stable, but cells presented different morphological characteristics and an altered distribution. Monocytes adjacent to fibre tracts generally presented as large round cells with vacuolated, bright cytoplasm (Fig. 12C₂), while monocytes in the grey matter frequently displayed smaller cell bodies with dark cytoplasm. Neurons displayed similar morphological features seen on day three, i. e. bright, huge karyoplasm, a light halo and surrounding satellite cells. Vessels, still displaying a dilated lumen in the surrounding area, now also appeared to be more numerous than on day

three. Multiple cavitations, which had slightly enlarged in size, were seen in all animals (Fig. 13C). Only one animal demonstrated a vast cavity in the centre of the lesion. Another animal presented a stronger inflammatory response i. e. stronger infiltration of neutrophils, lymphocytes and monocytes and a slightly higher number of fibroblasts in the surrounding area than seen in other animals. Furthermore, combined Masson trichrome and Verhoeff stain in this sample revealed a massive increase in collagen fibres. In this particular animal, a spinal root was adherent to the cord on the level of the incision.

The distant CST showed changes similar to those observed on day three, i. e. oedematous tissue with swollen axons (Fig. 14C₁). In addition, a mononuclear infiltration had become obvious (Fig. 14C₂).

Fourteen days post surgery, the incision site and the surrounding area were entangled and interwoven with each other. Therefore, they were described together. Compared to day seven, a much larger area was occupied by collagen, generating a fibre-net throughout the incision site and adjacent surrounding area (Fig. 13D₁, D₂). In places, where a light collagen network had been seen on day seven, a massive increase in newly formed collagen deposits was seen. In general, the incision site and the surrounding area had become increasingly dense, as the scar contracted and diminished in size (Fig. 12D). In addition, fibroblast infiltration remained massive throughout the surrounding area (Fig. 12D), and accumulated near the meninges. Furthermore fibroblasts now showed a shape morphologically distinct from the ones seen on day seven. Fibroblasts displayed longer and thinner cell bodies with less cytoplasm. The cytoplasm and nucleolus was hardly seen and the nucleus was smaller, spindle-shaped and more compact. Therefore, these cells were categorized as *inactive* fibroblasts (Bannister 1995). The density of monocytes remained the same, lymphocytes had slightly decreased in number and neutrophils had almost disappeared. Intact neurons were barely visible any longer.

As seen on day seven, the number of capillaries remained elevated. However, the previously dilated vessels had returned to a size comparable to those seen in

the normal control. In the surrounding area, all animals showed cavitations, with a size similar to those seen on day seven. One animal displayed a stronger inflammatory response, as well as a higher number of inactive fibroblasts and collagen fibres in the surrounding area. In this animal, an adhesion between the spinal root and the cord was detected on the level of incision.

In all mice, the distant CST still displayed a strong mononuclear infiltration next to damaged axons (Fig. 14D₁, D₂).

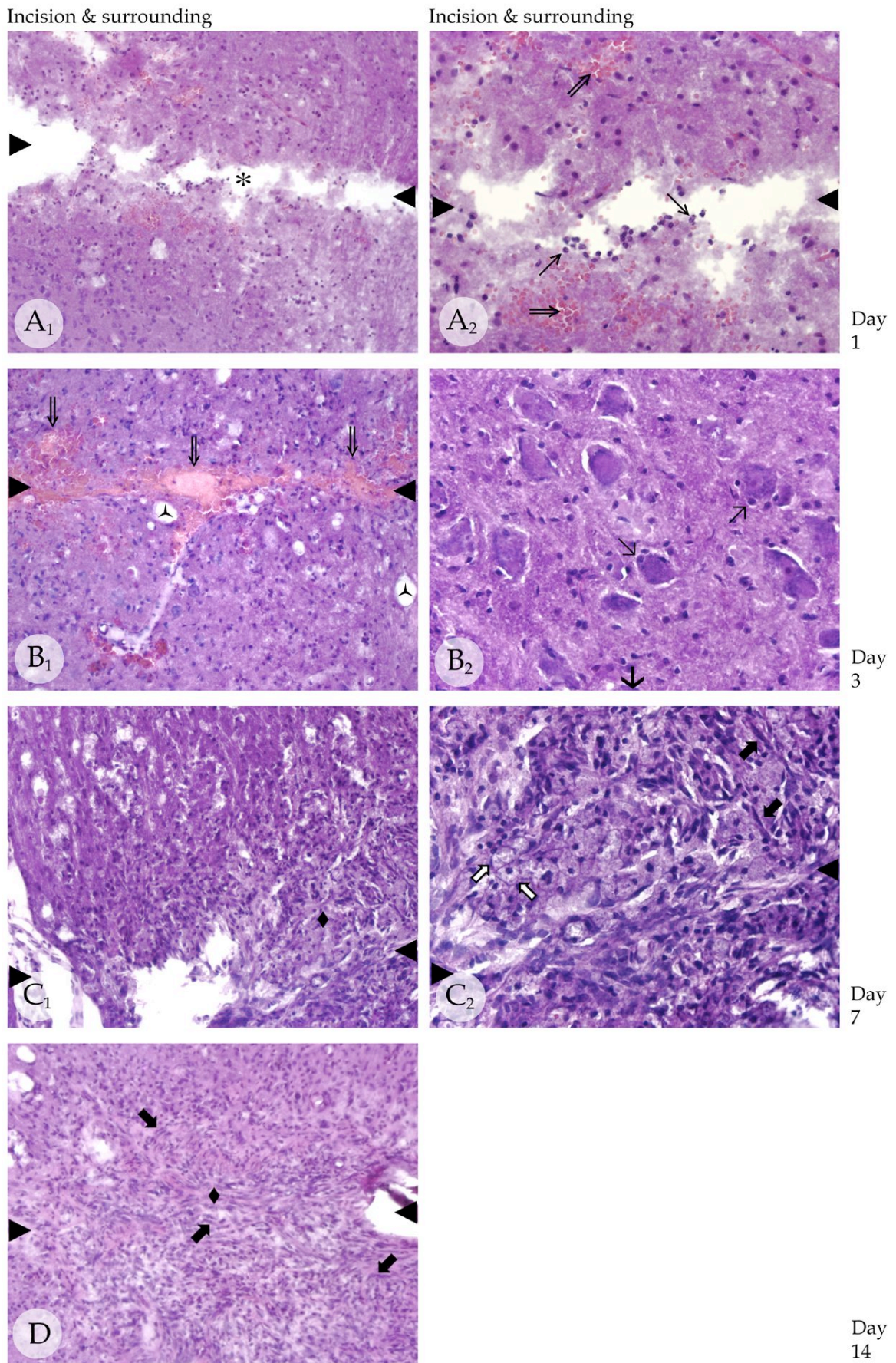


Fig. 12: Summary of morphological changes at the incision site in H&E staining for TNC+/+ wild type mice (for legend see next page).

Fig. 12: Summary of morphological changes at the incision site in H&E staining for TNC+/+ wild type mice after one (A₁, A₂), three (B₁, B₂), seven (C₁, C₂) and fourteen (D) days following spinal cord hemisection. Arrowheads (▶) indicate the location of incision. Arrows (→) indicate the direction of the incision. (A₁) One day post injury the incision site is devoid of neural tissue (*), with (A₂) minor haemorrhages (⇒) in the surrounding and neutrophils (→) invading the incision site; (B₁) Three days post injury the incision site has narrowed and the former gap is filled with erythrocytes (⇒) and multiple small cavitations (∧) are seen in the surrounding area. (B₂) Swollen neurons (→) with blurred cell borders and satellite cells are seen in the surrounding area; (C₁) Seven days post injury formation of the fibrous scar (◆) with (C₂) dense lining of activated fibroblasts (◆) and occasional macrophages (⇒); (D) Fourteen days post injury the incision site shows a fully developed scar (◆) with the predominant cell type being inactivated fibroblasts (◆). A₁, B₁, C₁, D: 100x; A₂, B₂, C₂: 200x

Incision & surrounding

Incision & surrounding

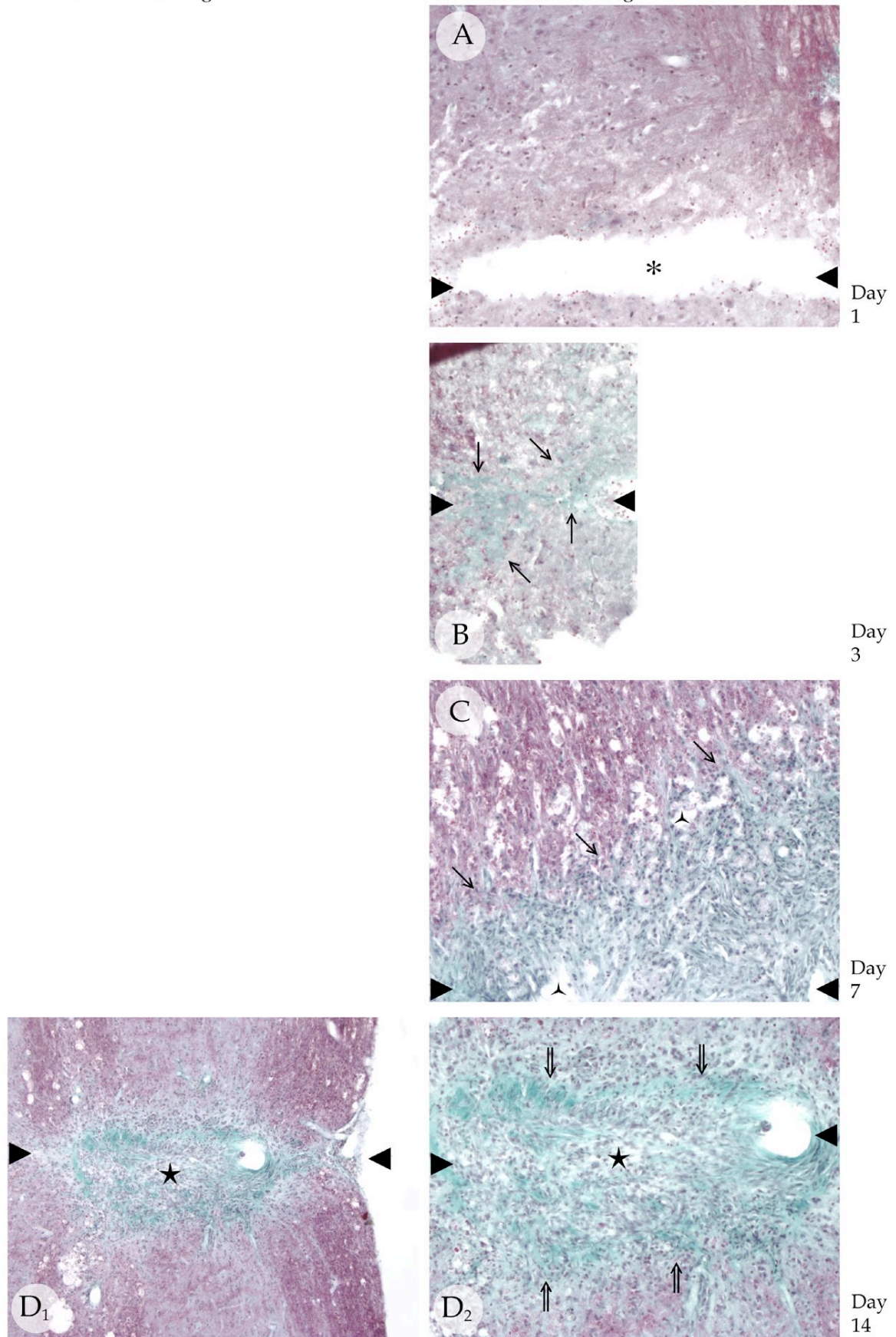


Fig. 13: Summary of morphological changes at the incision site in combined Masson trichrome and Verhoeff stain for TNC+/+ wild type mice (for legend see next page).

Fig. 13: Summary of morphological changes at the incision site in combined Masson trichrome and Verhoeff stain for TNC+/+ wild type mice after one (A), three (B), seven (C) and fourteen (D₁, D₂) days following spinal cord hemisection. Arrowheads (►) indicate the location of incision. (A) One day post injury the incision site is seen as a wide gap (*), devoid of connective tissue; (B) Three days post injury lightly stained collagenous tissue (→) is seen along the incision site, not extending into the surrounding area yet; (C) Seven days post injury the incision site shows an increase in collagenous fibres (→) compared to day three. Fibres are now clearly invading the surrounding area and multiple small cavitations (▲) are seen; (D₁, D₂) Fourteen days post injury an extensive collagenous scar (★) is seen, forming a dense rim (⇒) around the incision site, with radiating branches into the surrounding area as well as towards the incision centre. A, B, C, D₂: 100x; D₁: 50x

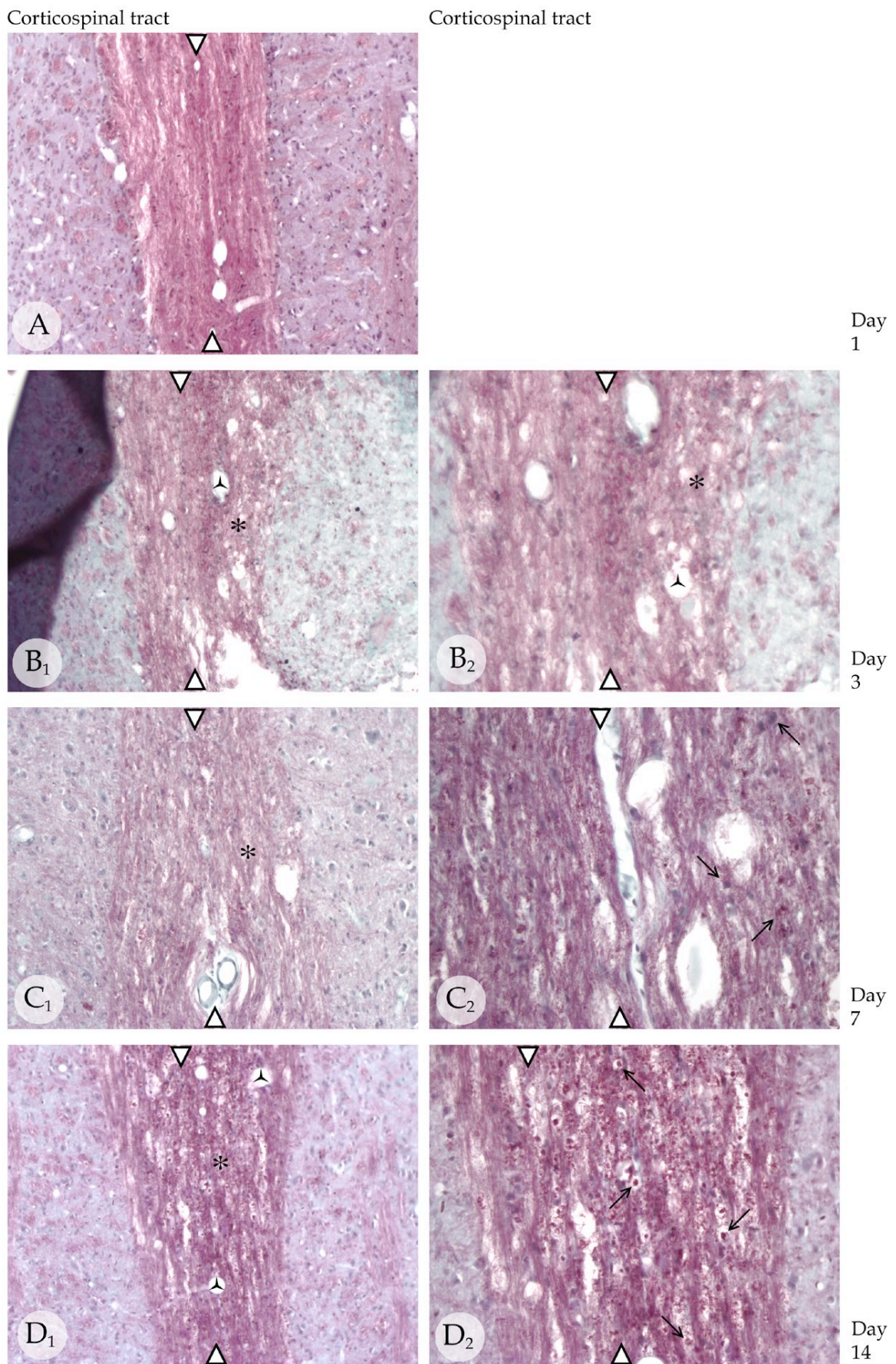


Fig. 14: Summary of morphological changes at the ipsilateral corticospinal tract in combined Masson trichrome and Verhoeff stain for TNC+/+ wild type mice (for legend see next page).

Fig. 14: Summary of morphological changes at the ipsilateral white matter distant from the incision site (distant white matter, corticospinal tract (CST)) in combined Masson trichrome and Verhoeff stain for TNC+/+ wild type mice after one (A), three (B₁, B₂), seven (C₁, C₂) and fourteen (D₁, D₂) days following spinal cord hemisection. Arrowheads (▷) indicate the border between ipsilateral (right hand side, incision) and contralateral (left hand side) of the spinal cord. (A) One day post injury the distant white matter shows its regular well-defined pattern; (B₁, B₂) Three days post injury oedematous tissue (*) with multiple small cavitations (∧) is seen within the CST; (C₁) Seven days post injury an oedematous CST (*) with (C₂) a mononuclear infiltration (→) is seen; (D₁) Fourteen days post injury destructed white matter (*) with multiple cavitations (∧) and (D₂) a strong mononuclear infiltration (→) is obvious. A, B₁, C₁, D₁: 100x; B₂, C₂, D₂: 200x

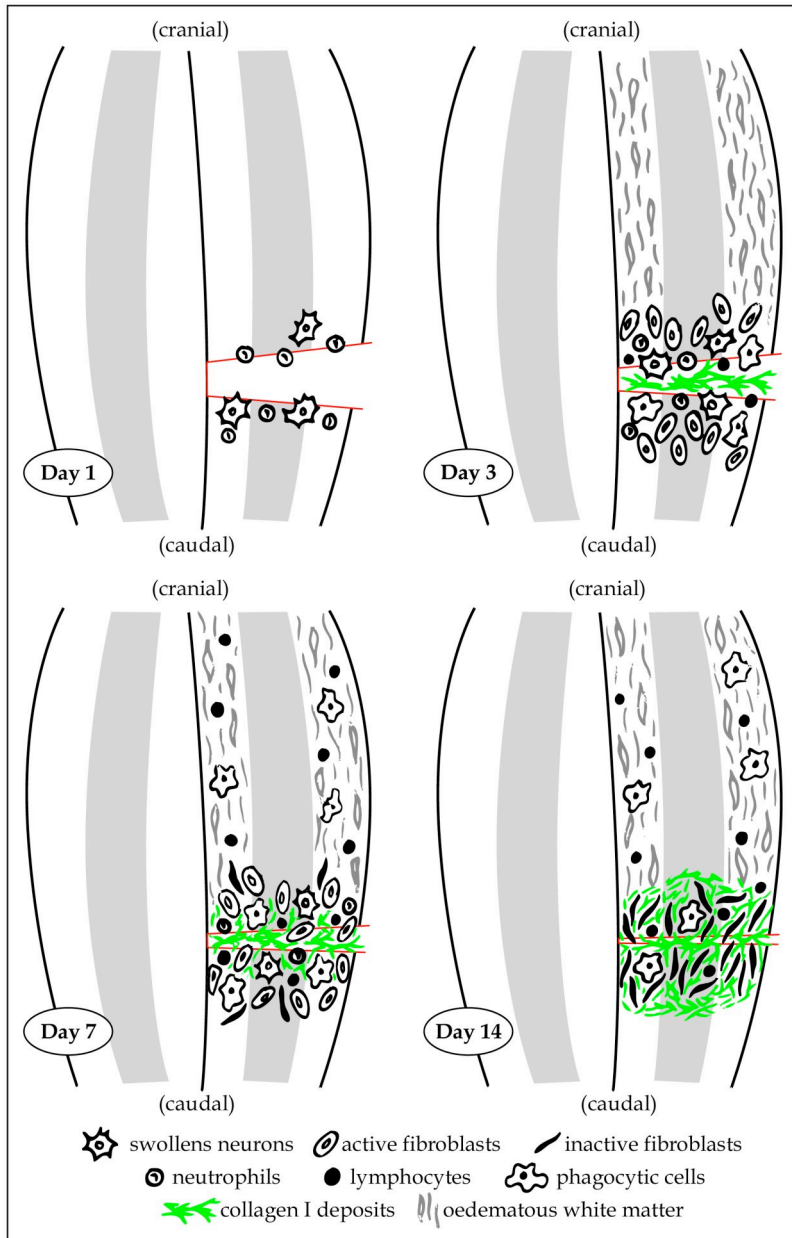


Fig. 15: Summary of morphological changes for TNC+/+ wild type mice after one, three, seven and fourteen days following spinal cord hemisection. On the first day the surrounding area shows swollen neurons and an infiltration of neutrophils. On the third day, first collagen type I fibres appear along the incision site. The surrounding area shows a large amount of activated fibroblasts, as well as a moderate infiltration of lymphocytes and phagocytes. Neutrophils are still seen. The corticospinal tract (CST) and the rubrospinal tract (RST) cranial to the incision site display oedema with swollen axons and scattered small holes. On day seven, the previously discrete collagen type I deposit extends into the surrounding area, while the density of activated fibroblasts, lymphocytes and monocytes remained similar compared to day three. Neutrophils slightly decrease in number compared to day three. The distant CST and RST are infiltrated by mononuclear cells. On day fourteen an extensive collagenous scar has formed. Inactive fibroblasts are dominating, while leucocytic infiltration has decreased. Some phagocytes are still present. The distant CST and RST remain oedematous and a strong mononuclear infiltration is still obvious.

4.1.2. Collagen type IV

4.1.2.1. Morphology

The normal control showed a strong collagen type IV immunoreactivity in the ECM meninges. Tender vessels throughout the cord were weakly labelled, while intermediate vessels, especially near the meninges were moderately labelled. Larger arteries, like the anterior spinal artery, presented with a strong staining intensity. In contrast, the cytoplasm of neurons or glial cells was collagen type IV-negative. The roots of the spinal nerves showed a strong collagen type IV immunoreactivity.

Changes in immunoreactivity for collagen type IV, as for all other connective tissue markers, i. e. laminin and fibronectin were only observed at the incision site and in the surrounding area. Therefore, description was confined to these two regions.

On the first day, the incision site was devoid of collagen type IV immunoreactivity (Fig. 16A₂).

In the surrounding area, collagen type IV was confined to blood vessels (Fig 16A₂). However, staining intensity slightly varied within the surrounding area. Vessels in the central part of the surrounding area demonstrated the most intense labelling. Distally to the lesion, the intensity gradually decreased to a level seen in the normal control (Fig. 16A₁). Collagen type IV-positive vessels near the incision site showed a wider lumen, indicating slight vasodilation. The cytoplasm of neurons and glial cells remained collagen type IV-negative, as on all other days post surgery. On the level of the incision, the meninges showed a stronger staining intensity than meninges seen in the normal control. This was also present on all other days post surgery.

On the third day, collagen type IV immunoreactivity was not only found around vessels, but also as ECM sheets along the narrow incision site (Fig. 16B).

The newly formed collagen type IV deposits were aligned parallel and perpendicular to the incision site, radiating into the white and the grey matter of the neighbouring tissue.

In the surrounding area, staining intensity of vessels and their density was comparable to day one. However, immunoreactive vessels, especially near the incision site displayed an even larger lumen than seen on day one, indicating marked vasodilation. Small cavitations were not associated with collagen type IV and remained collagen type IV-negative throughout the time course.

On day seven the incision site was filled with collagen type IV deposits, with an even higher their staining intensity compared to day three (Fig. 16C₁). In most animals, these deposits were now confined to the incision site and no longer spread into the neighbouring tissue. Only one animal still showed a fine collagen type IV network, radiating from the incision edges to thin vessels in the neighbouring tissue. However, that animal presented an adhesion between a spinal root and the cord, hence displayed greater density of collagen type IV immunoreactivity than seen in other animals.

The surrounding area was characterized by collagen type IV-positive blood vessels with a staining intensity similar to day three (Fig. 16C₂). While vessels in the central part of the surrounding area still demonstrated a discrete staining, vessels in the outer surrounding already displayed a staining intensity comparable to the normal control (Fig. 16C₁). However, all vessels in the central surrounding area still showed a dilated lumen. In addition, capillaries appeared to be more numerous in the lesioned area than on day three, indicating the formation of new blood vessels.

Fourteen days post injury, the incision site revealed collagen type IV deposits along the edges (Fig. 16D), which showed a higher staining intensity than seen on day seven. The majority of animals displayed the strongest collagen type IV immunoreactive deposits along the incision site throughout the time course (Fig. 16D). One animal, with an adhesion between a nerve root and the cord, showed

even more densely arranged collagen type IV deposits at the incision site and in the surrounding area.

The surrounding area was characterized by collagen type IV-positive vessels as seen on day seven. Rarely larger vessels with a strong staining intensity were detected in the central part of the surrounding area. A general vasodilation was no longer apparent, but the density of vessels in the central surrounding area remained elevated.

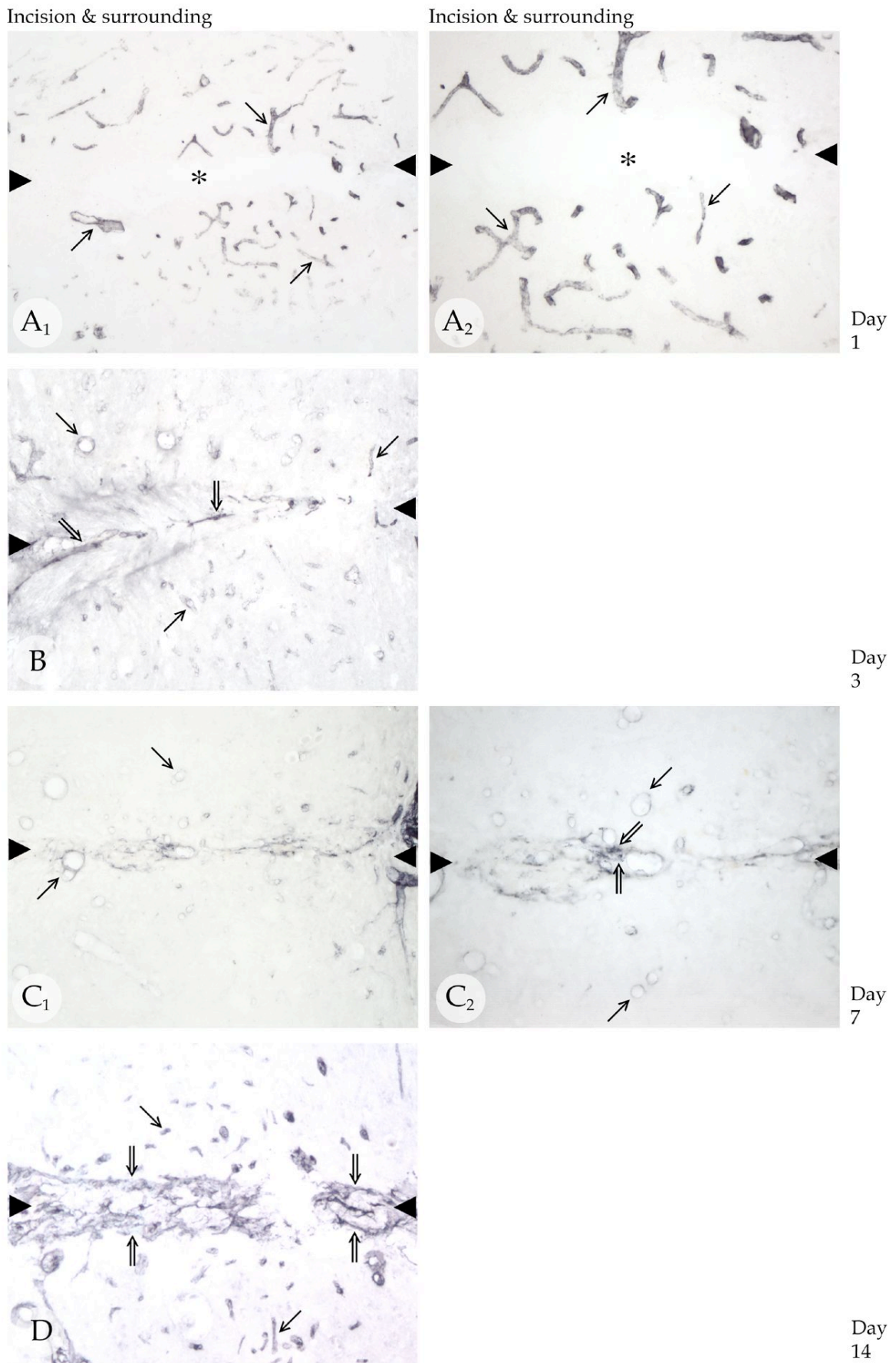


Fig. 16: Summary of collagen type IV immunoreactivity at the incision site for TNC^{+/+} wild type mice (for legend see next page).

Fig. 16: Summary of collagen type IV immunoreactivity at the incision site for TNC+/+ wild type mice after one (A₁, A₂), three (B), seven (C₁, C₂) and fourteen (D) days following spinal cord hemisection. Arrowheads (▶) indicate the location of incision. (A₁, A₂) One day post injury the incision site is devoid of collagen type IV immunoreactivity (*). Collagen type IV is confined to immunoreactive vessels (→) in the surrounding area, with gradually decreased staining intensity from the incision site towards the outer surrounding area; (B) Three days post injury, collagen type IV immunoreactivity is now also seen as extracellular matrix sheets along the incision site (⇒), spreading into the surrounding tissue. Staining intensity of collagen type IV-positive vessels (→) slightly decreased in the surrounding area; (C₁) On day seven, collagen type IV-positive vessels (→) are seen in the surrounding area. (C₂) Extracellular collagen type IV deposits (⇒) are now confined to the incision site; (D) Fourteen days post injury, the highest density of collagen type IV deposits (⇒) is seen along the incision site. Vasodilation of immunoreactive vessels (→) in the surrounding area is not evident anymore, though the density of vessels appears higher compared to the normal control, indicating neovascularization. A₁, B, C₁, D: 100x; A₂, C₂: 200x

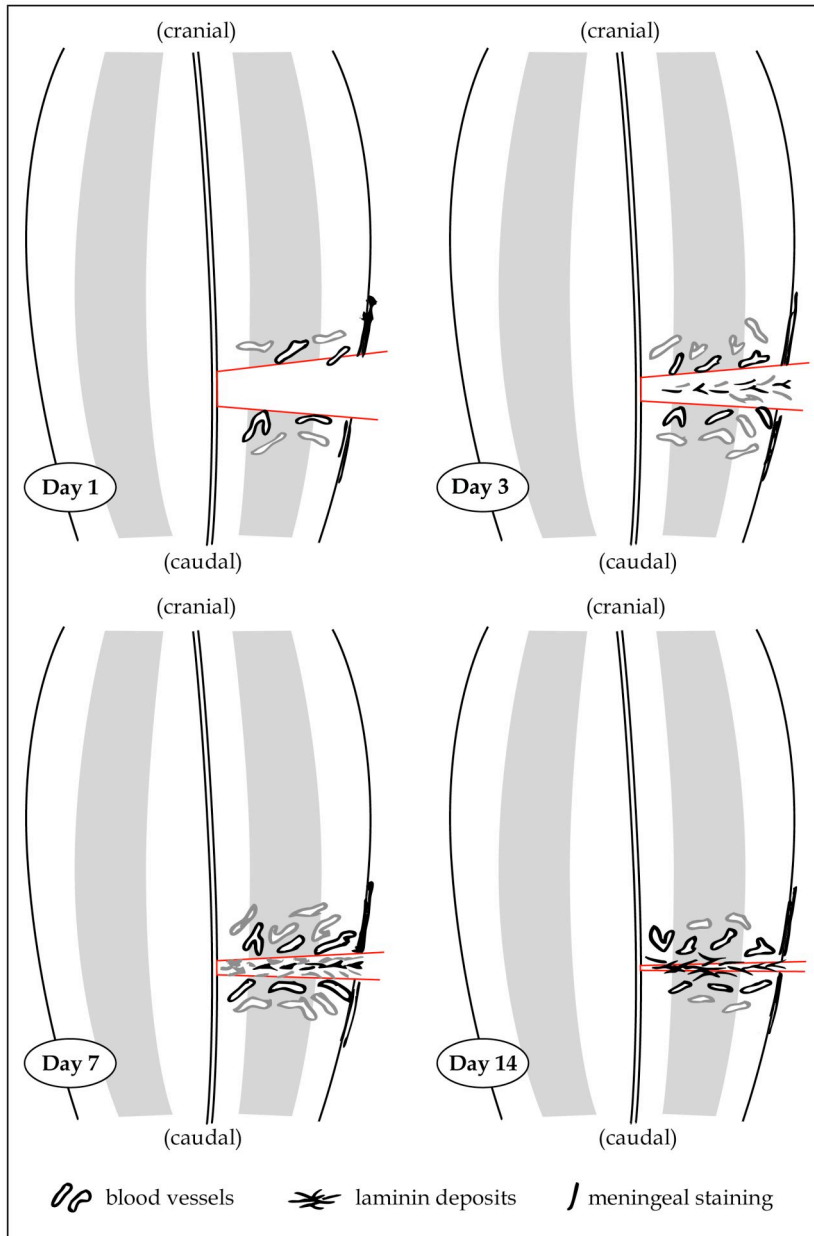


Fig. 17: Summary of changes for collagen type IV for TNC+/+ wild type mice after one, three, seven and fourteen days following spinal cord hemisection. The intensity of the immunoreactivity is coded: black - strong; grey - weak. On day one, collagen type IV is confined to vessels in the immediate vicinity of the incision site. Collagen type IV immunoreactive vessels show a wider lumen, compared to the normal control, indicating slight vasodilation. On the level of the incision, the meninges display a higher staining intensity compared to the normal control, which is evident throughout the time course. On day three, first collagen type IV extracellular deposits, unrelated to blood vessels, line the incision site and extend into the surrounding area. In the surrounding area collagen type IV-positive vessels display a marked vasodilation. On day seven, collagen type IV deposits are confined to the incision site and no longer extend into the surrounding area. Vasodilation and neovascularization is seen in the surrounding area. On day fourteen, the incision site shows extensive collagen type IV extracellular deposits, while in the surrounding area neovascularization is evident, but vasodilation no longer seen.

4.1.2.2. Quantitative densitometry

For collagen type IV, as for all other ECM markers, i. e. laminin and fibronectin, the immunoreactivity was quantified in two regions (incision site and surrounding area).

On the first day the incision site showed very low IOD levels for collagen type IV immunoreactivity, the median IOD being under 3.0. On day three, the IOD doubled and a gradual increase was seen throughout the time course. On day seven the median IOD reached 24.7 and subsequently scaled up to the highest peak on day fourteen with a median IOD of 34.7.

The surrounding area showed lower levels throughout the time course compared to the incision site. On day one, the median was on its maximum with an IOD of 2.0. Similar low median IOD levels were seen on day three (0.9), on day seven (1.6) and on day fourteen (1.4).

The difference between the incision site and the surrounding area was significant ($p < 0.0001$) over the time period tested. For neither of the regions a significant influence of the day ($p = 0.059$) was detected.

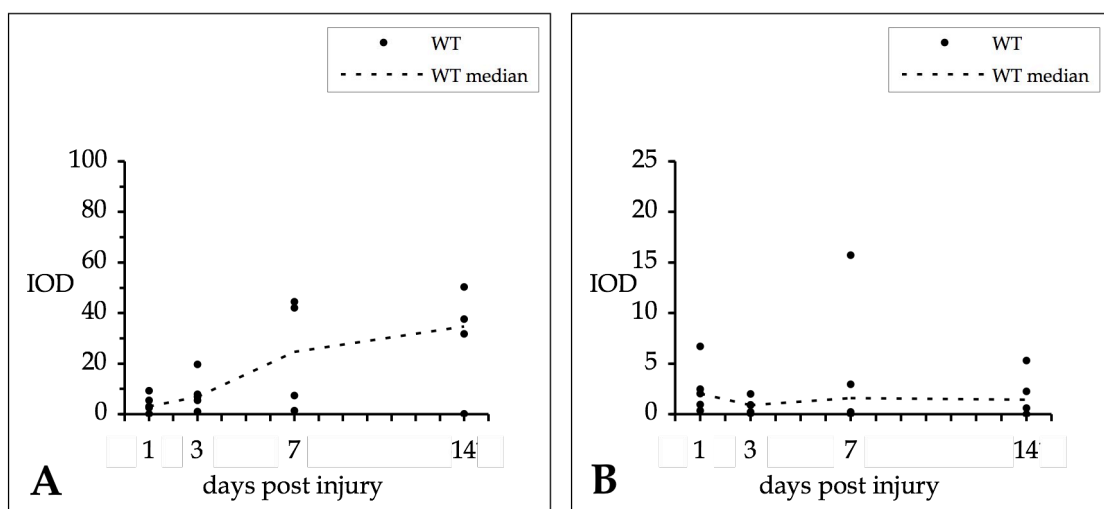


Fig. 18: Integrated optical density (IOD) for collagen type IV immunoreactivity at the incision site (A) and in the surrounding area (B) for TNC+/+ wild type mice (WT) from one to fourteen days after spinal cord hemisection. Measurements (●) are shown for three to five animals per day. The difference between the incision site and the surrounding area is significant ($p < 0.0001$) over the time period tested.

4.1.3. Laminin

4.1.3.1. Morphology

In the normal control, laminin demonstrated the strongest immunostaining in the meninges and around large vessels, especially close to the midline. Intermediate vessels were labelled moderately throughout the cord, while tender vessels were only weakly labelled. Spinal nerve roots presented strong laminin immunoreactivity.

On the first day, the incision site was devoid of laminin immunoreactivity.

The surrounding area displayed laminin-positive vessels (Fig. 19A₁, A₂). The staining intensity varied in the surrounding area, in that the staining was very strong adjacent to the incision site and became weaker further away. Hence, vessels in the outer surrounding area displayed a staining intensity comparable to the normal control. Labelled vessels showed a slightly wider diameter than in the normal control, indicating vasodilation. Extracellular laminin deposits were not observed yet. However, one animal revealed a subtle labelling of laminin-positive fibre-like deposits in the grey matter adjacent to the incision site. On the level of incision, the meninges showed a heavier staining intensity compared to the normal control, which was seen on all days post surgery.

On the third day, the incision edges appeared weakly labelled for laminin. This staining was unrelated to blood vessels. Short laminin fibre-like deposits were located perpendicular to the incision site, mainly orientated towards the adjacent grey matter. One animal showed larger and more intensely labelled laminin deposits along the incision site.

In the surrounding area, a higher density of vessels was found to be laminin-positive, though their staining intensity decreased from day one to day three. Vessels along the incision edges still showed the strongest immunoreactivity and in contrast to day one, now vessels in the outer part of the surrounding area were also moderately labelled laminin-positive (Fig. 19B₁, B₂). Vessels in the central part

of the surrounding area showed a larger lumen, compared to the normal control. One animal revealed laminin-positive fibre-like deposits, unrelated to laminin immunoreactivity of blood vessels. These fibre-like deposits came from white matter tracts, heading towards the incision site, presumably wrapping along axons. Cavitations were never associated with laminin.

Seven days after injury, the overall level of immunoreactivity at the incision site increased, while in the surrounding area staining intensity was comparable to day three. Three different morphologies between animals were observed for the incision site. Two animals revealed moderately labelled laminin deposits along the incision site and smaller deposits were scattered in the adjacent surrounding area. However, one of these animals showed an adhesion between a nerve root and the cord, hence displayed a stronger overall immunoreactivity of laminin. Two animals displayed only faintly labelled laminin deposits at the incision site and no laminin deposits in the surrounding area. In the remaining animal no extracellular laminin deposit at the incision site or in the surrounding area was present (Fig. 19C₁, C₂).

In all animals, laminin-positive capillaries, still showing vasodilation were found in the surrounding area (Fig. 19C₁, C₂). In addition, the density of vessels in the central part of the surrounding area appeared much higher than in the normal control, indicating newly formed vessels.

On day fourteen, again two different morphological groups between the animals could be distinguished for the incision site. Three animals, one being the one with an adhesion between a root and the cord, presented extensive laminin deposits along the incision edges. These sheet-like structures formed layers parallel to the incision site with fine extensions to perivascular deposits in the surrounding area (Fig. 19D). In one animal, only few laminin deposits were found as a narrow line along the incision site. In addition, laminin-positive fibre-like deposits, mainly longitudinally orientated to the white matter tracts were detected near the incision site. Occasionally laminin-positive small horseshoe-shape

deposits with a bright core, representing a transverse cut of the fibre-like deposits were observed predominantly in the grey matter adjacent to the incision site.

All animals presented laminin-positive vessels in the surrounding area, which had returned to a normal size, though their density remained higher compared to the normal control (Fig. 19D).

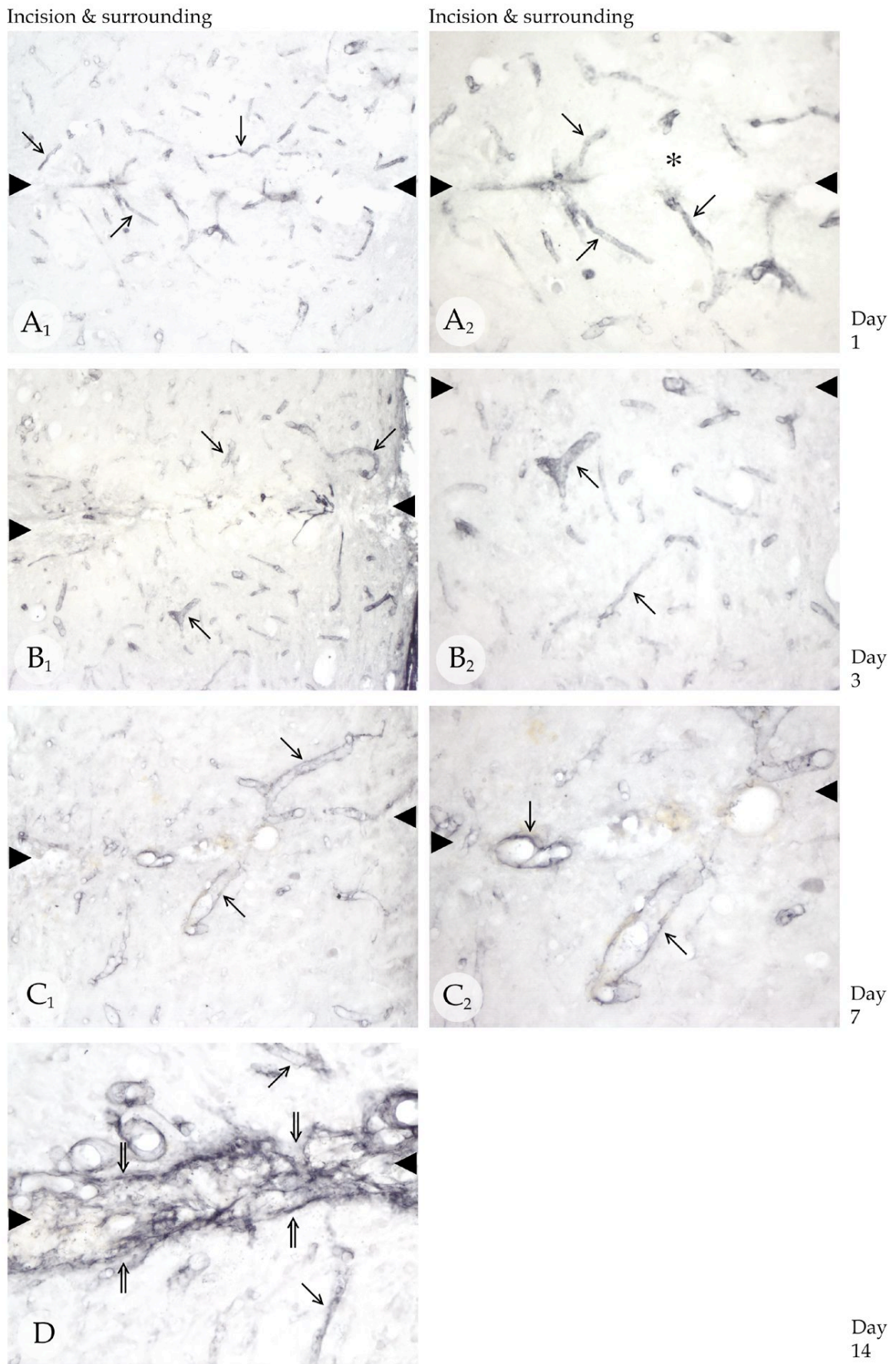


Fig. 19: Summary of laminin immunoreactivity at the incision site for TNC^{+/+} wild type mice (for legend see next page).

Fig. 19: Summary of laminin immunoreactivity at the incision site for TNC+/+ wild type mice after one (A₁, A₂), three (B₁, B₂), seven (C₁, C₂) and fourteen (D) days following spinal cord hemisection. Arrowheads (►) indicate the location of incision. (A₁, A₂) One day post injury the incision site is devoid of laminin immunoreactivity (*). Laminin labelled vessels (→) are seen near the incision edges, with a decreased staining intensity towards the outer surrounding area; (B₁, B₂) Three days post injury laminin-positive vessels (→) are seen in the surrounding area; (C₁, C₂) Seven days post injury, the density of laminin-positive vessels (→) near the incision site appears to be higher than in the normal control; (D) Fourteen days post injury, heavily labelled laminin extracellular deposits (⇒) and laminin immunoreactive vessels (→) are seen at the incision site. A₁, B₁, C₁: 100x; A₂, B₂, C₂, D: 200x

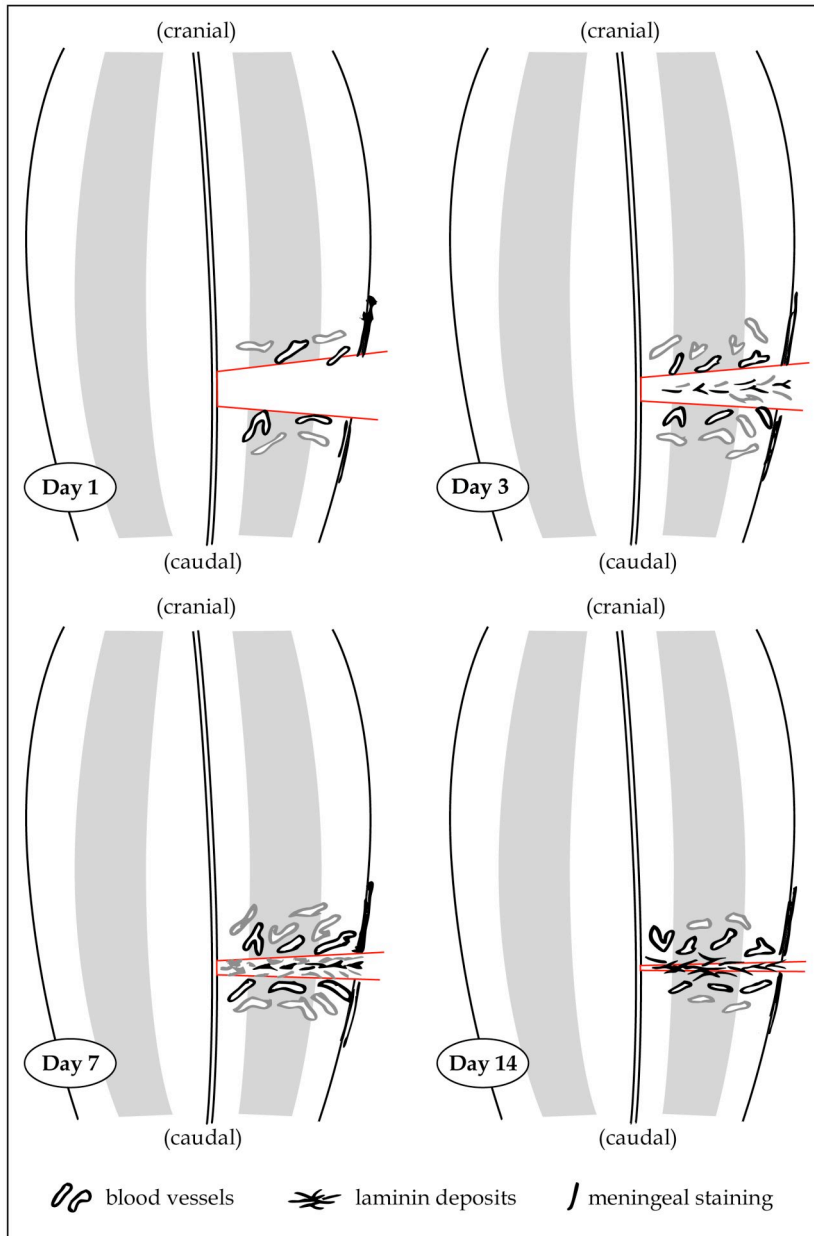


Fig. 20: Summary of changes for laminin for TNC+/+ wild type mice after one, three, seven and fourteen days following spinal cord hemisection. The intensity of the immunoreactivity is coded: black - strong; grey - weak. Immunoreactivity of laminin and collagen type IV is very similar. On day one, laminin is confined to vessels in the immediate vicinity of the incision site. The central surrounding area displays laminin-positive vessels, which are slightly dilated. On the level of the incision, the meninges display a higher staining intensity compared to the normal control, which is evident throughout the time course. On the third day post injury, the incision site first shows few, weakly labelled extracellular laminin deposits. Laminin labelled vessels and vasodilation in the surrounding area are still evident. On day seven, the incision site shows moderately labelled laminin deposits, while more numerous vasodilated vessels are seen in the surrounding area. On day fourteen the incision site shows extensive, strongly labelled laminin deposits, while the surrounding area displays neovascularization, but vasodilation is no longer evident.

4.1.3.2. Quantitative densitometry

On the first and third day, laminin immunoreactivity at the incision site showed a low median IOD of 11.4 and 5.2, respectively. From then on, a steep rise was observed with the median IOD being 40.0 on day seven and doubling on day fourteen to 85.0.

Throughout the time course, the surrounding area showed much lower IOD levels than the incision site. IOD levels presented as a straight line with a minimal rise over the time period. The lowest median IOD was seen on day one with 1.3. Similarly low median IOD values were seen on day three (1.7) and seven (2.7). This steady but low rise resulted in a maximum on day fourteen with a median IOD of 3.9.

The difference between the incision site and the surrounding area was significant ($p=0.001$) throughout the time course. Post injury days did not differ significantly ($p=0.213$) from each other in both regions investigated.

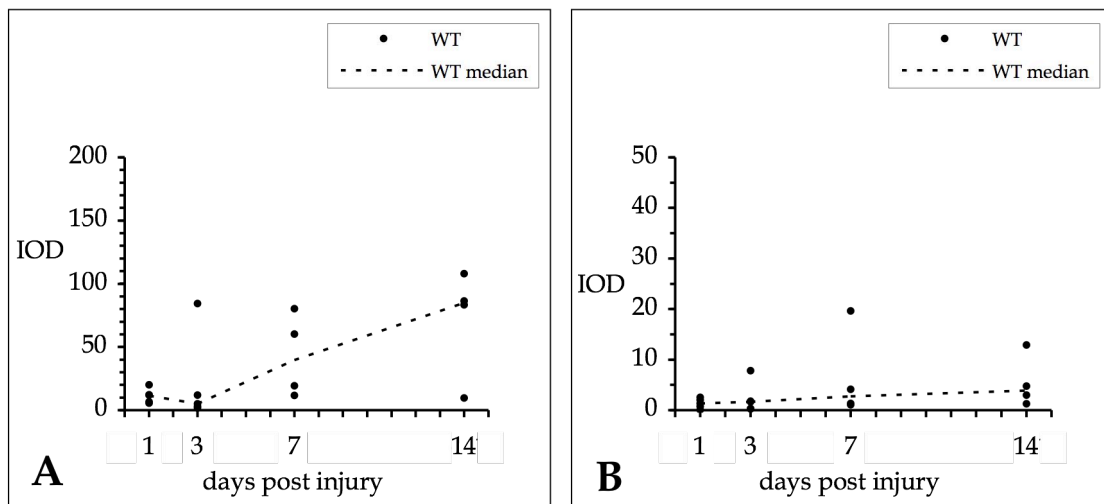


Fig. 21: Integrated optical density (IOD) for laminin immunoreactivity at the incision site (A) and in the surrounding area (B) for TNC^{+/+} wild type mice (WT) from one to fourteen days after spinal cord hemisection. Measurements (●) are shown for three to five animals per day. The difference between the incision site and the surrounding area is significant ($p \leq 0.001$) over the time period tested.

4.1.4. Fibronectin

4.1.4.1. Morphology

In the normal control, an intensive immunolabelling of fibronectin was detected in the meninges and around large vessels. In the white matter tracts, moderately labelled fibronectin-positive strands were located parallel to the meninges. In contrast, the grey matter only occasionally displayed fibronectin-positive strands, mostly orientated perpendicular to the meninges. Intermediate-size blood vessels showed a moderate staining intensity, while the root of the spinal nerve was weakly fibronectin positive.

On the first day after injury, the ECM of the incision site was heavily labelled with fibronectin (Fig. 22A₂). Along the wound edges and in the central part of the surrounding area, moderately labelled fibronectin-positive strands and smaller spherical structures, presumably strands in a transverse cut, were seen (Fig. 22A₁). The staining intensity was particularly strong at the wound edges.

In the surrounding area, fibronectin-positive strands were seen in both, the white and the grey matter (Fig. 22A₁). Strands near the incision site were heavier labelled in the white matter than in the grey matter. They expanded into the wound edges and were often orientated perpendicular to the incision site. However, none of these strands seemed to cross the incision site. On the level of incision, the meninges showed a heavier staining intensity compared to the normal control, which was seen on all days post surgery.

On the third day post surgery, fibronectin-positive strands along the incision site diminished compared to day one. Instead intensely labelled extracellular fibronectin deposits were seen at the incision site (Fig. 22B).

In the surrounding area, staining intensity of fibronectin-positive strands had also decreased compared to day one. Fibronectin extracellular deposits were not seen and cavitations were not associated with fibronectin.

Seven days post injury, fibronectin deposits at the incision site were seldom detected. The incision site was pale and displayed an extremely low level of fibronectin immunoreactivity (Fig. 22C₁, C₂).

The surrounding area occasionally presented thin fibronectin-positive strands and diffuse, vaguely labelled small spherical fibronectin deposits with a bright core, presumably strands in a transverse cut (Fig. 22C₂). These deposits were sometimes associated with capillaries. In contrast to day three, a minority of the multiple cavitations were now associated with fibronectin. The animal demonstrating an adhesion between a nerve root and the cord showed essentially the same pattern of fibronectin deposition as seen in all other animals.

Fourteen days after surgery, the overall level of immunoreactivity was slightly higher compared to day seven (Fig. 22D₁, D₂). Fibronectin deposits dominated the incision site and the central part of the surrounding area.

Fibronectin positive strands, mainly situated in the adjacent white matter, were diffusely distributed without traversing the incision site. The surrounding grey matter predominantly presented fibronectin-positive strands in a transverse cut (Fig. 22D₁, D₂). Again, these deposits were sometimes associated with capillaries. Like on day seven, only very few cavitations were surrounded by fibronectin. The animal with the adhesion showed a stronger labelling intensity, but an identical fibronectin arrangement compared to the other animals.

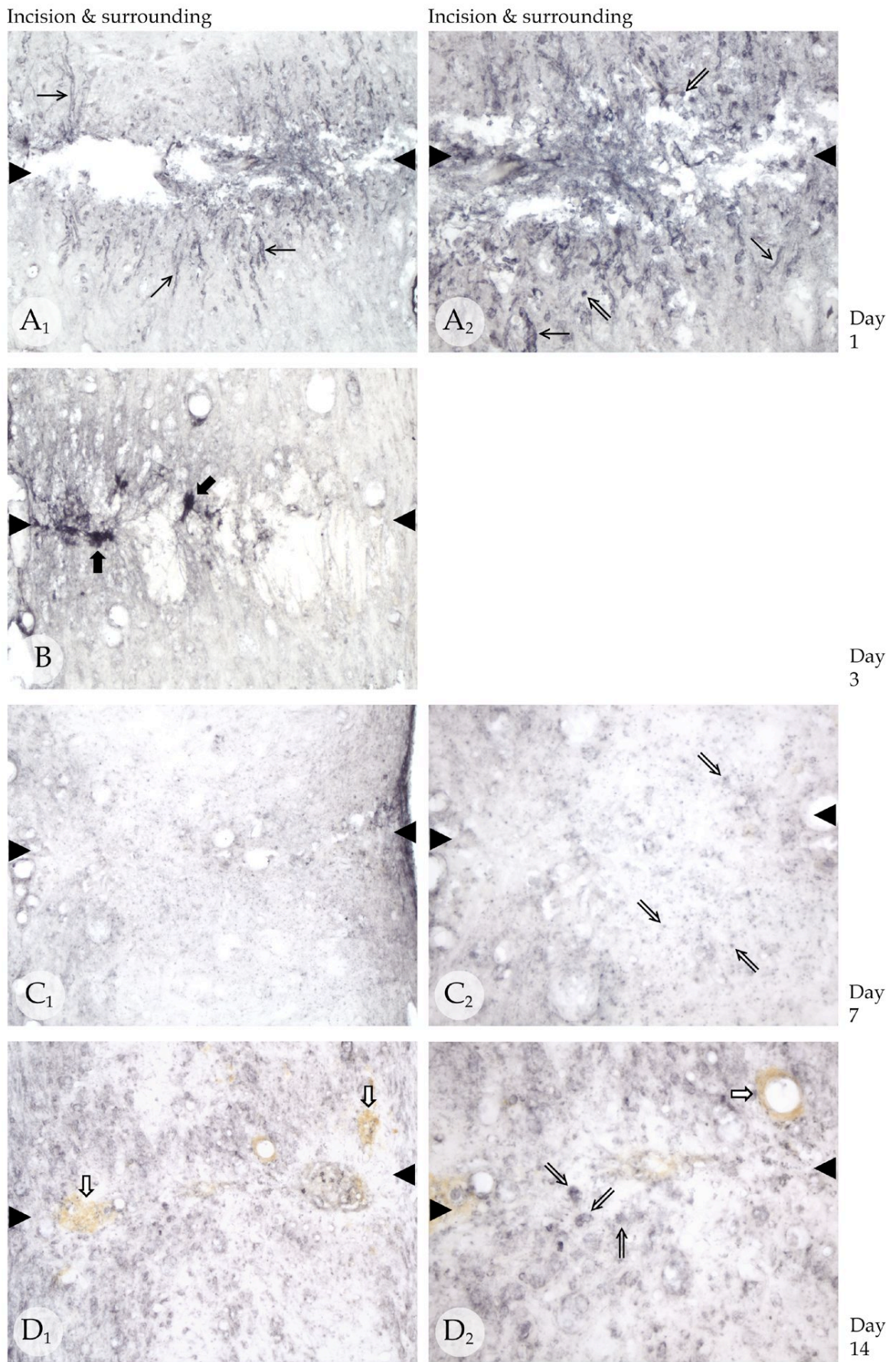


Fig. 22: Summary of fibronectin immunoreactivity at the incision site for TNC^{+/+} wild type mice (for legend see next page).

Fig. 22: Summary of fibronectin immunoreactivity at the incision site for TNC+/+ wild type mice after one (A₁, A₂), three (B), seven (C₁, C₂) and fourteen (D₁, D₂) days following spinal cord hemisection. Arrowheads (▶) indicate the location of incision. (A₁, A₂) One day post injury, many heavily labelled fibronectin-positive strands (→) and fibronectin spherical deposits (⇒), presumably strands in a transverse cut, are seen at the incision site and in the surrounding area; (B) Three days post injury, fibronectin-positive strands diminish, instead heavily labelled extracellular fibronectin deposits (➡) are obvious along the incision site; (C₁) Seven days post injury the incision site and the surrounding area are pale in labelling. (C₂) The surrounding area shows diffuse, vaguely labelled fibronectin-positive strands in a transverse cut (⇒); (D₁, D₂) Fourteen days post injury, a slight increase in immunoreactivity compared to day seven is seen, with round fibronectin deposits (⇒) and haemosiderin accumulations (⇒). A₁, B, C₁, D₁: 100x; A₂, C₂, D₂: 200x

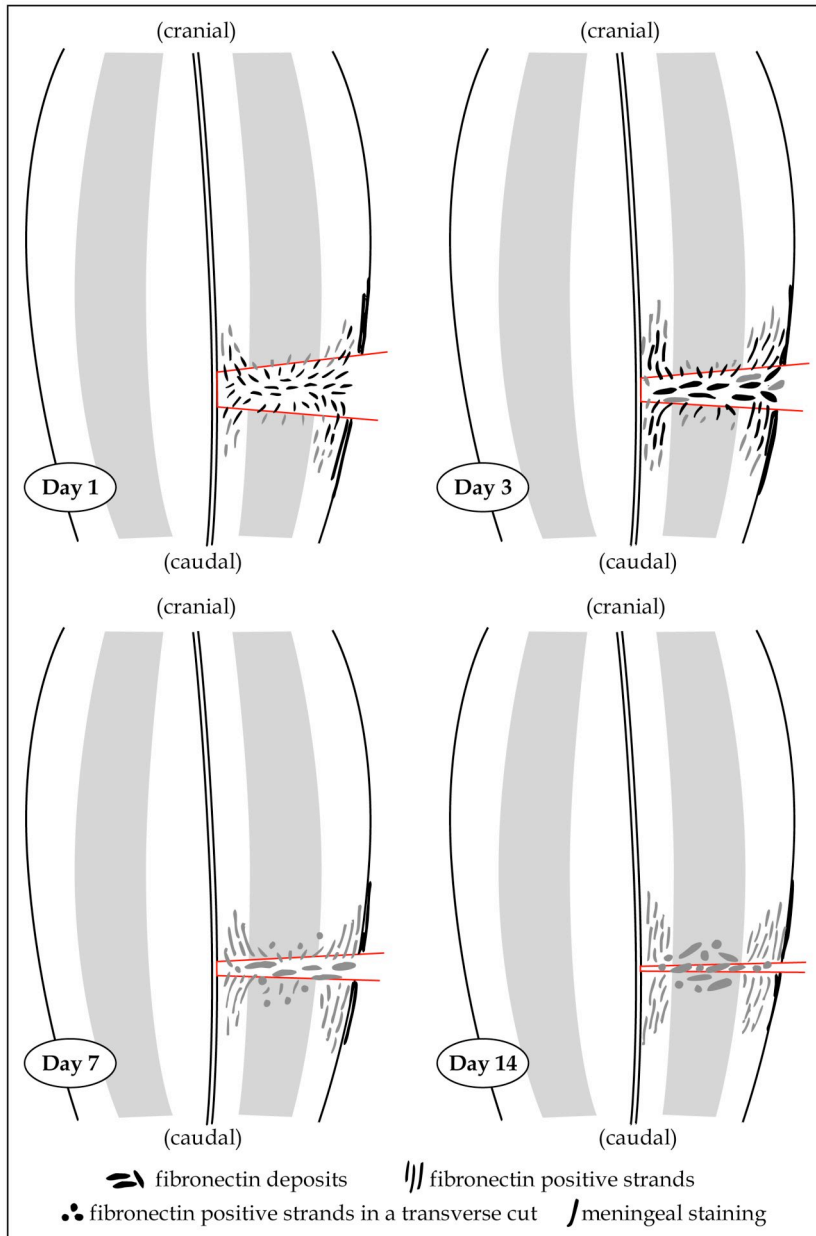


Fig. 23: Summary of changes for fibronectin for TNC+/+ wild type mice after one, three, seven and fourteen days following spinal cord hemisection. The intensity of the immunoreactivity is coded: black - strong; grey - weak. On the first day, the incision site and the surrounding area display fibronectin-positive strands. On the level of the incision, the meninges show a higher staining intensity compared to the normal control, which is evident throughout the time course. On day three the density of fibronectin-positive strands at the incision site diminishes. Instead fibronectin extracellular deposits are seen. Seven days post injury the incision site shows lightly labelled fibronectin deposits, while the surrounding area predominantly displays lightly labelled fibronectin-positive strands. On day fourteen fibronectin deposits dominate the incision site and the central surrounding area. The surrounding white matter predominantly shows fibronectin-positive strands, while the surrounding grey matter mainly displays spherical deposits.

4.1.4.2. Quantitative densitometry

Fibronectin immunoreactivity showed a maximum median IOD of 92.3 on day one at the incision site. Fibronectin immunoreactivity decreased to a median IOD of 45.5 on day three and reached the lowest median IOD level (4.3) on day seven. Subsequently a slight rise of the median IOD to 25.4 was seen on day fourteen.

The surrounding area showed lower levels of fibronectin immunoreactivity throughout the time course compared to the incision site. The highest level of fibronectin immunoreactivity was seen on day one with the median IOD being 18.8. A steep fall from day one to day three (3.2) on was observed. Median IOD levels of fibronectin immunoreactivity on day seven and fourteen remained low with 1.1 and 2.0, respectively.

The difference between the incision site and the surrounding area was significant ($p < 0.0001$) over the time period investigated. A significant influence of the day ($p = 0.038$) was detected with ANOVA for repeated measurements, though post-hoc comparisons by the method of Games-Howell did not confirm any significant differences between post injury days.

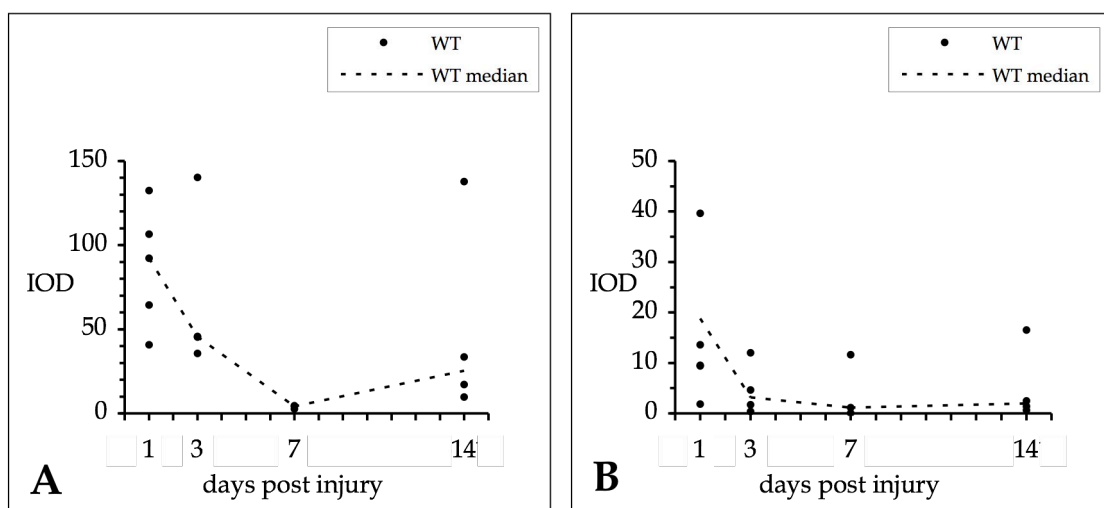


Fig. 24: Integrated optical density (IOD) for fibronectin immunoreactivity at the incision site (A) and in the surrounding area (B) for TNC+/+ wild type mice (WT) from one to fourteen days after spinal cord hemisection. Measurements (●) are shown for three to five animals per day. The difference between the incision site and the surrounding area is significant ($p \leq 0.0001$) over the time period tested.

4.1.5. F4/80

4.1.5.1. Morphology

In the normal control, F4/80-positive cells displayed a regular distribution in both, white and grey matter. In the grey matter, F4/80-positive cells presented with small cell bodies and frequently ramified branches. F4/80-positive cells situated in the white matter displayed a more oval shaped cell body and longer occasionally branching processes, orientated longitudinally to the cord. Both cell types presented morphological characteristics of resting microglia (Streit et al. 1999). F4/80-positive cells, associated with capillaries displayed small, oval shaped cell bodies with several primary processes, situated parallel to the vessels' axis. These cells were categorized as pericytes (Thomas 1999). No F4/80 immunoreactivity was seen in the spinal root or nerve.

Changes in immunoreactivity for glial markers, i. e. F4/80 and GFAP were observed in four regions. The description was therefore confined to the incision site, the surrounding area, the ipsilateral distant grey matter and the ipsilateral distant white matter far away from the incision site.

On the first day post surgery, the incision site was devoid of F4/80 immunoreactivity (Fig. 25A). Two samples revealed non-specific labelling of cell debris and necrotic material at the incision site and in the surrounding area. Resting microglia, as seen in the normal control was rarely seen in the surrounding area.

Further away, in the ipsilateral distant grey and white matter, resting microglia appeared as seen in the normal control (Fig. 26A, 27A). The contralateral side showed resting microglia throughout the entire time course investigated.

On the third day after injury, the overall level of immunoreactivity had increased immensely. The incision site was filled with tightly packed F4/80-positive cells (Fig. 25B₁). These cells showed large, round and pale cytoplasm and

were categorized as phagocytes (Streit et al. 1999) (Fig. 25B₂). These vacuolated cells were found in great density along the wound edges.

F4/80-positive cells in the surrounding area revealed different morphology in the grey and white matter. Cells in the grey matter revealed darkly labelled cytoplasm with hardly any processes, representing phagocytes. Cells in the surrounding white matter showed more lightly labelled cytoplasm, also representing phagocytes. F4/80-positive cells in the outer surrounding area displayed frequently branching ramifications, which were much shorter and thicker than seen in resting microglia, hence these cells were classified as activated microglia (Streit et al. 1999) (Fig. 25B₃). Occasionally F4/80-positive cells with increased ramifications, but slender processes were seen in the transitional zone between the surrounding area and the ipsilateral distant cord. These cells were characterized as hyper-ramified microglia (Streit et al. 1999) (Fig. 25B₃).

F4/80-positive cells in the ipsilateral distant grey matter displayed activated microglia (Fig. 26B₁, B₂). Occasionally hyper-ramified cells were detected.

In contrast, the ipsilateral distant white matter was packed with F4/80-positive cells (Fig. 27B₁). These cells displayed large round cell bodies with either darkly labelled cytoplasm or bright cytoplasm, both representing phagocytes (Fig. 27B₁, B₂). Rarely cells showed thick processes, which were then orientated parallel to the tracts, representing activated microglia.

Seven days after injury, the overall level of immunoreactivity had increased at the incision. The incision site displayed F4/80-positive cells in high density, mainly phagocytes, activated microglia and some pericytes (Fig. 25C₁, C₂).

At day seven, the surrounding area predominantly showed activated microglia and fewer phagocytes compared to day three. Phagocytes showed a brightly labelled cytoplasm near the white matter and darkly labelled cytoplasm close to the grey matter. Hyper-ramified microglial cells were predominantly seen in the outer surrounding area (Fig. 25C₃).

As seen on day three, the ipsilateral distant grey matter showed mainly hyper-ramified microglia, occasionally activated microglia was observed (Fig. 26C₁, C₂).

In the distant white matter phagocytes had diminished compared to day three. Instead activated microglia was now the predominant cell type (Fig. 26C₁, C₂). The animal presenting an adhesion between a spinal nerve root and the cord displayed similar features in the spinal cord compared to other animals. However, this animal demonstrated an invasion of strongly labelled F4/80-positive phagocytes in the spinal nerve root.

Fourteen days after surgery, the incision site showed activated microglia, while the amount of phagocytes had ceased (Fig. 25D₁, D₂).

F4/80 immunoreactivity had decreased in the surrounding area. Hyper-ramified cells dominated the surrounding area, while resting microglia was seen in the outer surrounding area (Fig. 25D₃). Many of the hyper-ramified cells were associated with newly formed capillaries and the density of pericytes was much higher compared to the normal control, most likely related to an increase in capillaries. Furthermore, F4/80-positive cells outlined small cavitations.

Microglial cells in the ipsilateral distant grey matter had completely returned to the state of resting microglia (Fig. 26D).

Parallel to this finding, the ipsilateral distant white matter predominantly displayed resting microglia. Sporadically hyper-ramified microglia, with processes orientated parallel to the tracts were detected (Fig. 27D₁, D₂). The cord of the animal demonstrating an adhesion resembled the histology seen in other mice, but in this sample F4/80-positive cells also appeared in the spinal root and nerve.

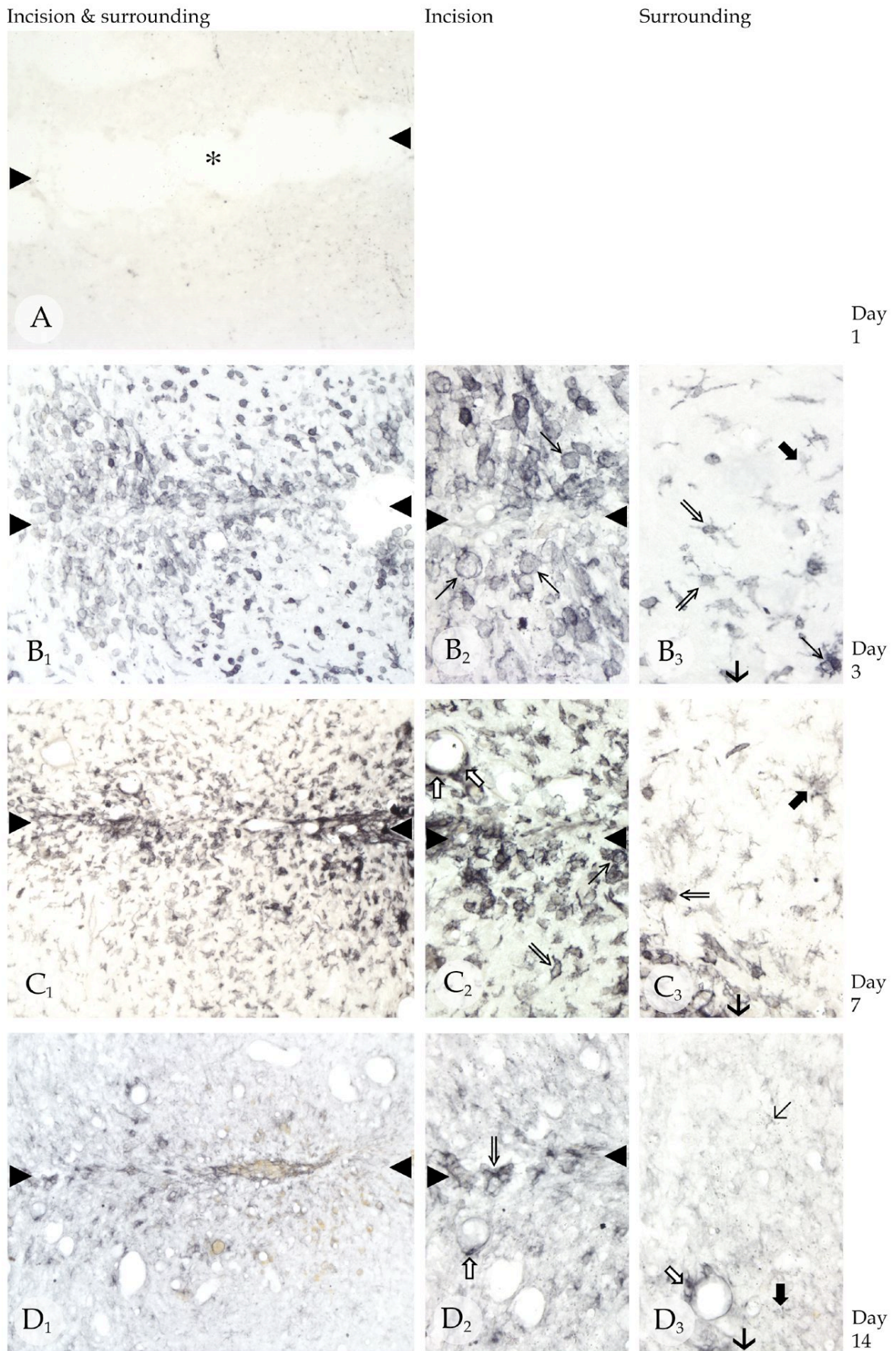


Fig. 25: Summary of F4/80 immunoreactivity at the incision site and the surrounding area for TNC^{+/+} wild type mice (for legend see next page).

Fig. 25: Summary of F4/80 immunoreactivity at the incision site for TNC+/+ wild type mice after one (A), three (B₁, B₂), seven (C₁, C₂) and fourteen (D₁, D₂) days and for the surrounding area after three (B₃), seven (C₃) and fourteen (D₃) days following spinal cord hemisection. Arrowheads (▶) indicate the location of incision. Arrows (→) indicate the direction of the incision. (A) One day post injury the incision site is devoid of F4/80 staining (*); (B₁) Three days post injury heavily labelled F4/80-positive cells, (B₂) mainly phagocytes (→) are seen at the incision site. (B₃) The surrounding area displays F4/80-positive phagocytes (→) close to the incision site, activated microglia (⇒) in the intermediate zone and hyper-ramified cells (➤) towards the distant spinal cord; (C₁) Seven days post injury, immunoreactivity for F4/80 increased at the incision site compared to day three, showing (C₂) phagocytes (→), activated microglial cells (⇒) and pericytes (⇨). (C₃) The surrounding area displays activated microglial cells (⇒) towards the incision site and hyper-ramified cells (➤) towards the distant spinal cord; (D₁) Fourteen days post injury, staining intensity at the incision site decreased compared to day seven. (D₂) The incision site shows activated microglial cells (⇒) and few pericytes (⇨). (D₃) The surrounding area displays hyper-ramified microglial cells (➤) and pericytes (⇨) near the incision site, and resting F4/80-positive microglia (→) towards the distant spinal cord. A, B₁, C₁, D₁: 100x; B₂, B₃, C₂, C₃, D₂, D₃: 200x

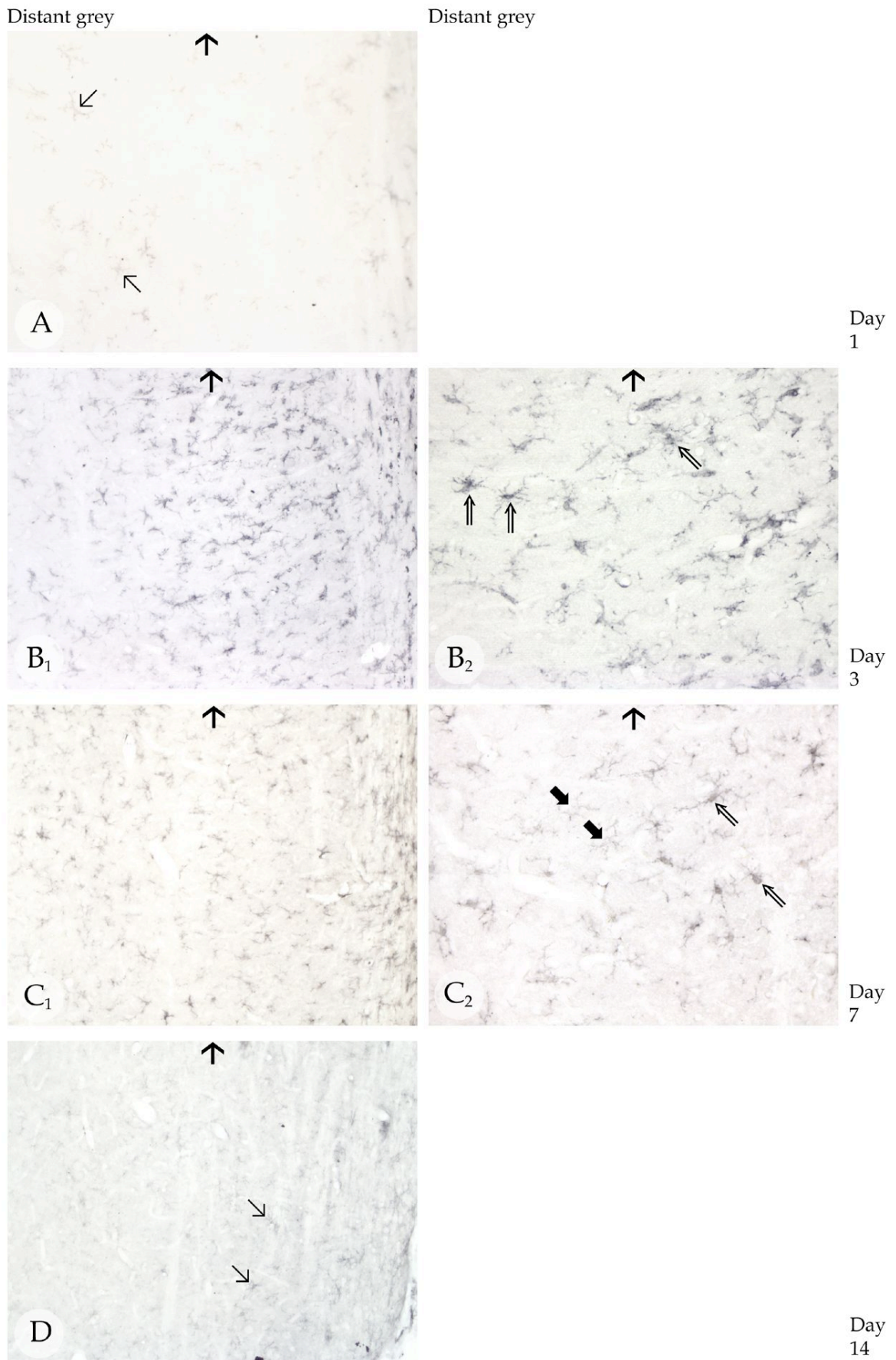


Fig. 26: Summary of F4/80 immunoreactivity at the ipsilateral grey matter distant from the incision site for TNC+/+ wild type mice (for legend see next page).

Fig 26: Summary of F4/80 immunoreactivity at the ipsilateral grey matter distant from the incision site (distant grey) for TNC+/+ wild type mice after one (A), three (B₁, B₂), seven (C₁, C₂) and fourteen (D) days following spinal cord hemisection. Arrows (→) indicate the direction of the incision. (A) One day post injury the distant grey shows lightly labelled F4/80-positive resting microglia (→); (B₁, B₂) Three days post injury heavily labelled F4/80-positive cells, mainly activated microglial cells (⇒) are seen; (C₁, C₂) Seven days post injury, F4/80 immunoreactivity in the distant grey decreased compared to day three, showing fewer activated microglial cells (⇒) with a reduced staining intensity. Instead, hyper-ramified microglial cells (➤) are seen more frequently; (D) Fourteen days post injury, F4/80 immunoreactivity has decreased compared to day seven, now mainly showing resting microglia (→). A, B₁, C₁, D: 100x; B₂, C₂: 200x

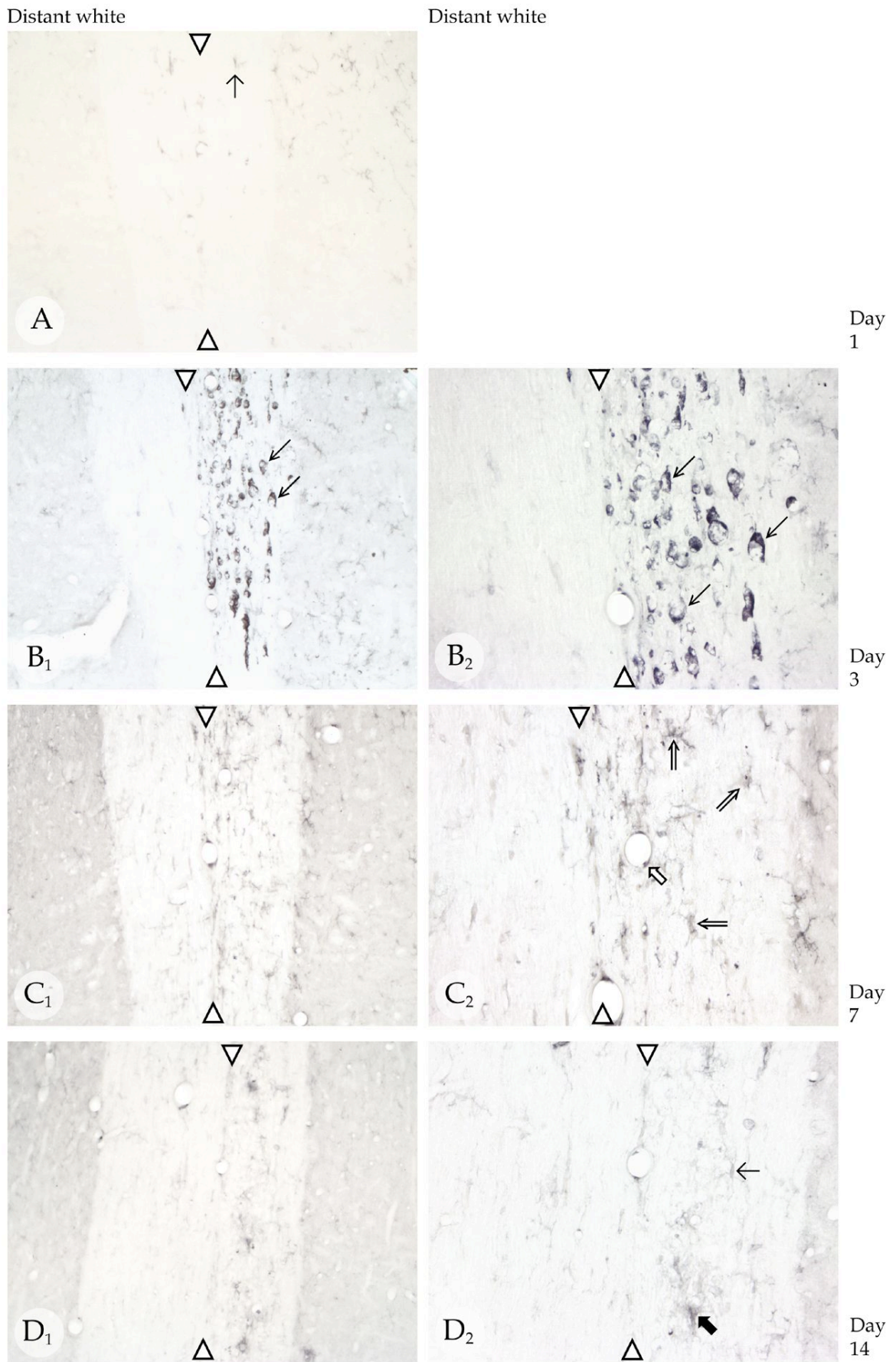


Fig. 27: Summary of F4/80 immunoreactivity at the ipsilateral white matter distant from the incision site for TNC+/+ wild type mice (for legend see next page).

Fig. 27: Summary of F4/80 immunoreactivity at the ipsilateral white matter distant from the incision site (distant white) for TNC+/+ wild type mice after one (A), three (B₁, B₂), seven (C₁, C₂) and fourteen (D₁, D₂) days following spinal cord hemisection. Arrowheads (▷) indicate the border between ipsilateral (right hand side, incision) and contralateral (left hand side) of the spinal cord. (A) One day post injury the distant white matter shows very few lightly labelled F4/80-positive resting microglia (→); (B₁, B₂) Three days post injury heavily labelled F4/80-positive cells, mainly phagocytes (→) are seen in the distant white matter; (C₁) Seven days post injury, F4/80-positive phagocytes have diminished compared to day three, now mainly showing (C₂) activated microglial cells (⇒) and some pericytes (⇔); (D₁) Fourteen days post injury F4/80 immunoreactivity has decreased compared to day seven, (D₁) now showing resting microglia (→) and few hyper-ramified microglial cells (➤). A, B₁, C₁, D₁: 100x; B₂, C₂, D₂: 200x

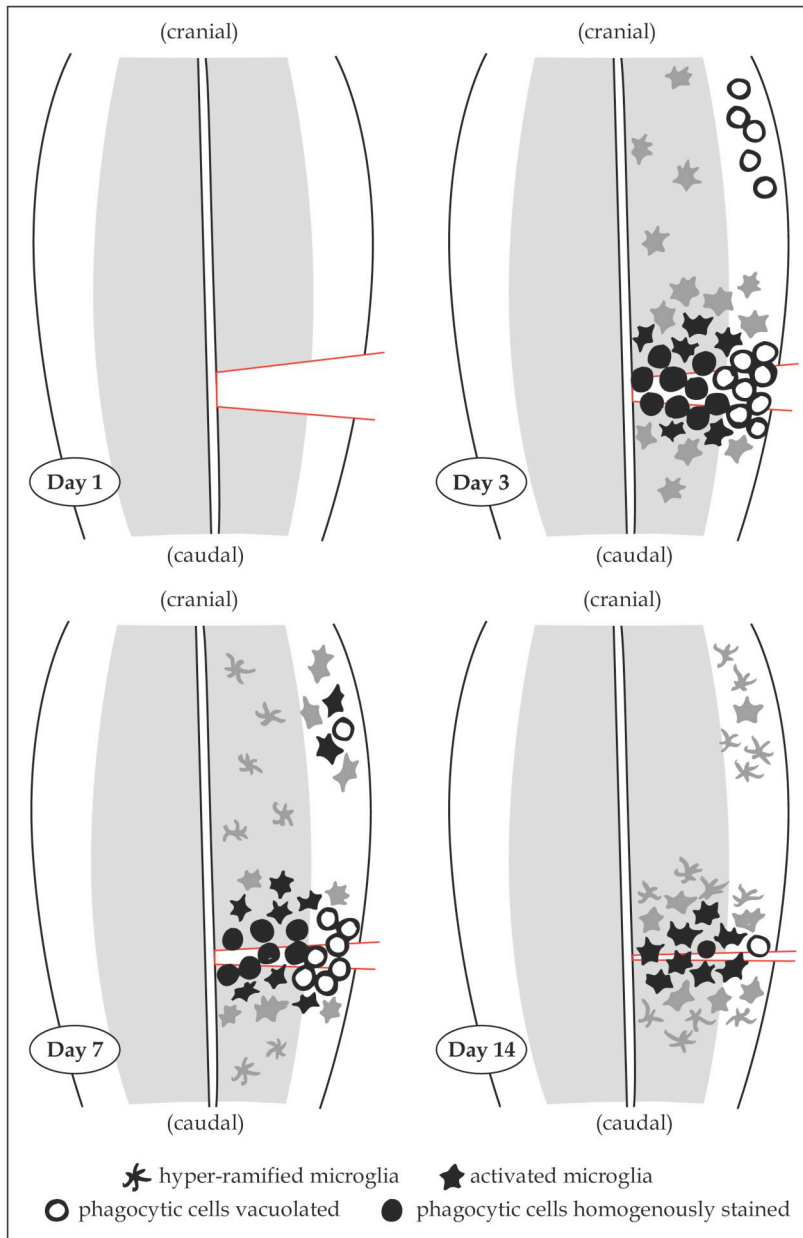


Fig. 28: Summary of changes for F4/80-positive microglia/macrophages for TNC+/+ wild type mice after one, three, seven and fourteen days following spinal cord hemisection. The intensity of the immunoreactivity is coded: black - strong; grey - weak. Resting microglia is not shown. On the first day, no F4/80 immunoreactivity is detected at the incision site. In the remaining spinal cord resting microglia is present. On the third day, phagocytes, vacuolated and homogeneously labelled first appear at the incision site. Activated microglia is seen in the surrounding area. The ipsilateral distant grey matter shows activated microglia as well, while the ipsilateral distant white matter predominantly displays vacuolated phagocytes. On the seventh day, phagocytes at the incision site and in the surrounding area have decreased compared to day three. Instead, the density of activated microglia has increased. The distant grey matter displays hyper-ramified microglia, while the distant white matter mainly presents activated microglia. On day fourteen, microglial activation has decreased. At the incision site, activated microglia is prominent, while the surrounding area shows hyper-ramified cells and resting microglia. In the distant grey matter cells return to the state of resting microglia, while in the distant white matter hyper-ramified and few activated microglial cells are still seen.

4.1.5.2. Quantitative densitometry

Quantitative densitometry for F4/80 as well as for GFAP was performed in four regions (incision site, surrounding area, distant grey matter cranial and distant grey matter caudal to the incision site).

On the first day, the incision site was negative for F4/80 immunoreactivity with a median IOD of 0.0. On day three, the median IOD at the incision site was 11.3, followed by an extremely steep increase to the maximum level of 88.8 IOD on day seven. Subsequently, a minor decrease of the median IOD to a level of 73.4 was observed on day fourteen.

The surrounding area showed lower IOD levels compared to the incision site throughout the time course. Again, on day one the median IOD was very low with 0.1. This was followed by a hundredfold increase on day three with a median IOD of 12.0. On day seven and fourteen a plateau was seen with a median IOD of 18.8 and 17.4, respectively.

The distant grey matter cranial to the incision site showed extremely low levels of F4/80 immunoreactivity throughout the time course. On day one (0.1) and three (0.5) the median IOD never exceeded levels above one. A maximum was seen on day seven with a median IOD of 4.2, while on day fourteen the median IOD level dropped to its starting point of 0.1.

Similar to that, the distant grey matter caudal to the incision site displayed low IOD levels for all post surgery days tested. On day one the median IOD was as low as 0.1. A slight rise was seen on day three with a median IOD of 2.5. On day seven and fourteen the median IOD stabilized with 1.7 and 1.4, respectively.

The difference between the incision site and the surrounding area ($p < 0.0001$), between the incision site and the distant grey matter, cranial to the incision ($p < 0.0001$) as well as between the incision site and the distant grey matter, caudal to the incision ($p < 0.0001$) was significant over the time course investigated. A

significant influence of the day ($p < 0.0001$) was detected for all regions and post-hoc comparisons with Games-Howell test revealed the following findings: The first day differed significantly from day seven ($p = 0.015$) and day fourteen ($p < 0.0001$). In addition, the third day differed significantly from day fourteen ($p = 0.033$).

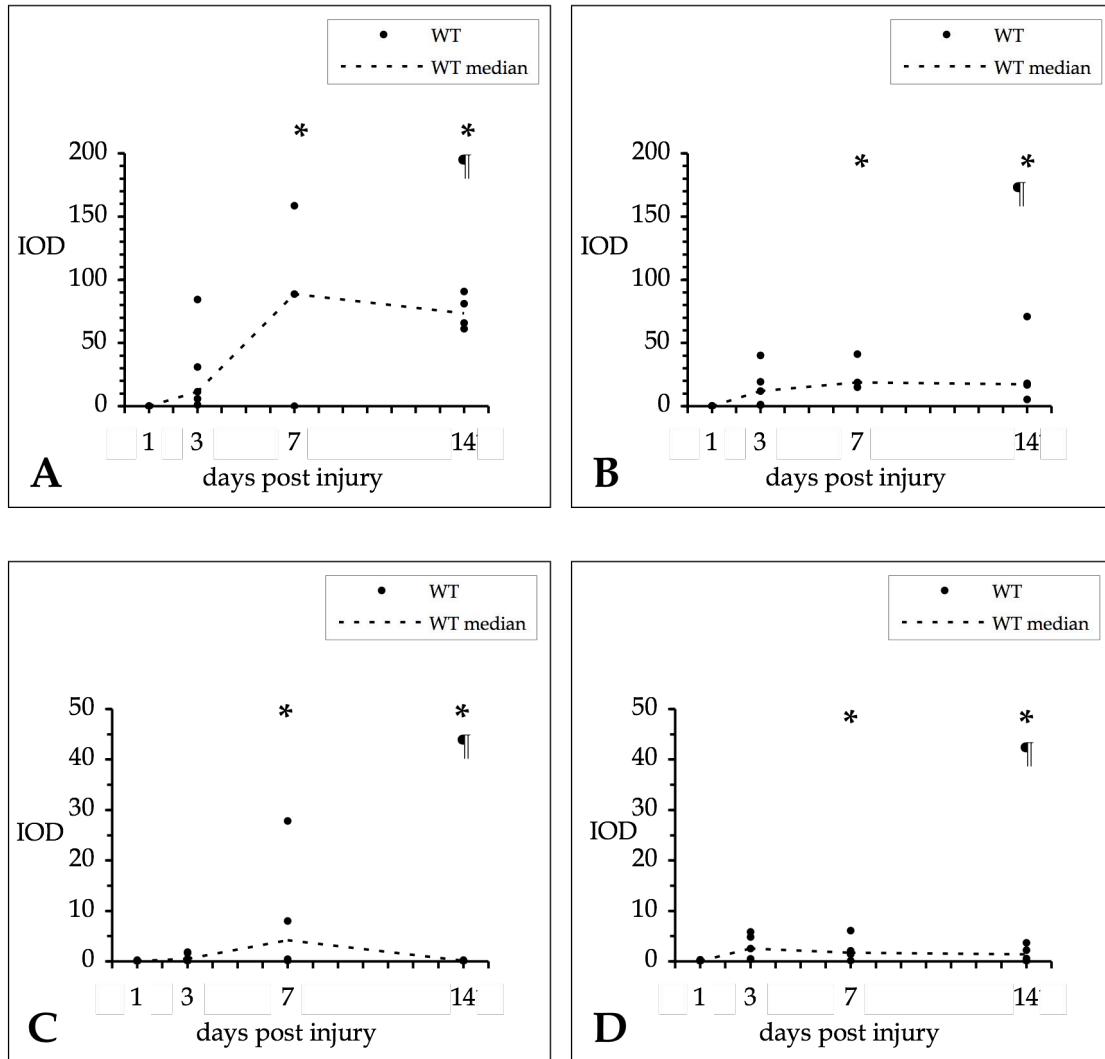


Fig. 29: Integrated optical density (IOD) for F4/80 immunoreactivity as a microglial marker is shown for TNC+/+ wild type (WT) mice from one to fourteen days after spinal cord hemisection at the incision site (A), the surrounding area (B), the distant grey matter approximately 1.5 mm cranial (C) and 1.5 mm caudal (D) to the incision site. Measurements (●) are shown for three to five animals per day. The surrounding area ($p \leq 0.0001$), the distant grey matter, cranial ($p \leq 0.0001$), and the distant grey matter, caudal ($p \leq 0.0001$) show a significant difference to the incision site over the time period investigated. In addition, the first day differs significantly from day seven ($p \leq 0.05$) (*) and day fourteen ($p \leq 0.0001$) (*); and the third day differs significantly from day fourteen ($p \leq 0.05$) (¶) for all regions investigated.

4.1.6. GFAP

4.1.6.1. Morphology

In the normal control, GFAP-positive cells were homogeneously distributed throughout the grey matter and sparsely, but in regular distribution, seen within the white matter. In the grey matter, GFAP-positive cells were weakly labelled and displayed an average size, round cell body. The cell body showed several tender branches, which ramified in the periphery. These star-shaped cells represented protoplasmic astrocytes. In the white matter, GFAP-positive cells displayed a smaller, oval-shaped cell body with few, but long processes orientated parallel to the meninges. These cells were identified as fibrous astrocytes. Protoplasmic astrocytes were often found near neurons, while GFAP-positive fibrous astrocytes in the white matter were often found adjacent to vessels. Their shorter and clumsier processes frequently reached the outer margins of capillaries. Some GFAP-positive cells, present near white matter tracts displayed short processes orientated towards the meningeal surface.

On the first day after surgery, the incision site was GFAP-negative.

The surrounding area was lightly labelled GFAP-positive. The morphology of astrocytes in the surrounding area was comparable to astrocytes seen in the normal control (Fig. 30A). Protoplasmic astrocytes, i. e. star-shaped cells with several tender ramifications were seen in the grey matter and fibrous astrocytes, i. e. oval-shaped cell bodies with few, long processes were found in the white matter.

As in the normal control, the ipsilateral distant grey matter presented protoplasmic astrocytes (Fig. 31A), while the distant white matter showed mainly fibrous astrocytes (Fig. 32A).

Three days after injury, the incision site is lightly labelled positive for GFAP immunoreactivity (Fig. 30B₁).

In the surrounding area, GFAP-positive cells had accumulated at day three. These cells were larger and had processes that were more complex compared to day one. In addition, GFAP-positive cells appeared to be more numerous. Therefore these cells were classified as reactive astrocytes (Eng et al. 2000, Sofroniew 2005). A boundary of reactive astrocytes had formed around the incision site with thick processes, preferentially pointing towards the incision site (Fig. 30B₂).

The ipsilateral distant spinal cord has shown an increase in GFAP immunoreactivity, compared to day one (Fig. 31B₁). Different morphological characteristics were found for GFAP-positive cells in the distant grey and white matter. In the grey matter reactive astrocytes, i. e. increase in size and complexity of their processes, dominated the picture (Fig. 32B₂).

The ipsilateral distant white matter showed GFAP-positive phagocytic-like cells. These large, round cells, lacking any processes, displayed a strong staining intensity (Fig. 32B₁, B₂). Their clearly visible, large cytoplasm was presumably filled with fatty debris. These cells showed a morphology reminiscent of gemistocytes (Kros et al. 2000).

Seven days following injury, the incision site was completely invaded by reactive astrocytes (Fig. 30C₁). These cells showed thick, heavily labelled and numerous processes, demonstrating nicely the process of astroglial scarring (Fig. 30B₂). The strongest intensity of immunoreactivity was found along the edges of the incision site.

Reactive astrocytes were frequently found in the surrounding area, often adjacent to cavitations.

The ipsilateral distant grey matter displayed a picture similar to day three, i. e. reactive astrocytes with large cytoplasm and thick processes (Fig. 31C₁, C₂).

The morphology of the distant white matter had changed from day three to day seven. Cells now presented a strong GFAP immunoreactivity with small cell bodies and multiple processes, typical of reactive astrocytes (Fig. 32C₁, C₂). GFAP-positive phagocytic-like cells were no longer detected. The animals with an

adhesion between the cord and the nerve root showed no difference in GFAP immunoreactivity, compared to the remaining animals.

Fourteen days after surgery, the incision site presented the highest density of accumulated GFAP-positive cells throughout the time course investigated (Fig. 30D₁, D₂). Reactive astrocytes at the incision site and in the surrounding area showed tightly interwoven processes attached to one another, representing the formation of astroglial scarring (Fig. 30D₁). In the outer surrounding area reactive astrocytes had returned to the morphology of protoplasmic astrocytes as seen in the normal control. As on day seven, multiple small cavitations were surrounded by astroglial processes.

Astrocytic cells in the ipsilateral distant grey matter showed a decreased immunoreactivity compared to day seven and a comparable morphology to protoplasmic astrocytes seen in the normal control (Fig. 31D).

The immunoreactivity in the distant white matter was reduced compared to day seven, although reactive astrocytes were still the predominant cell type (Fig. 32D). The animal with an adhesion between the spinal nerve root and the cord displayed a morphology similar to remaining samples.

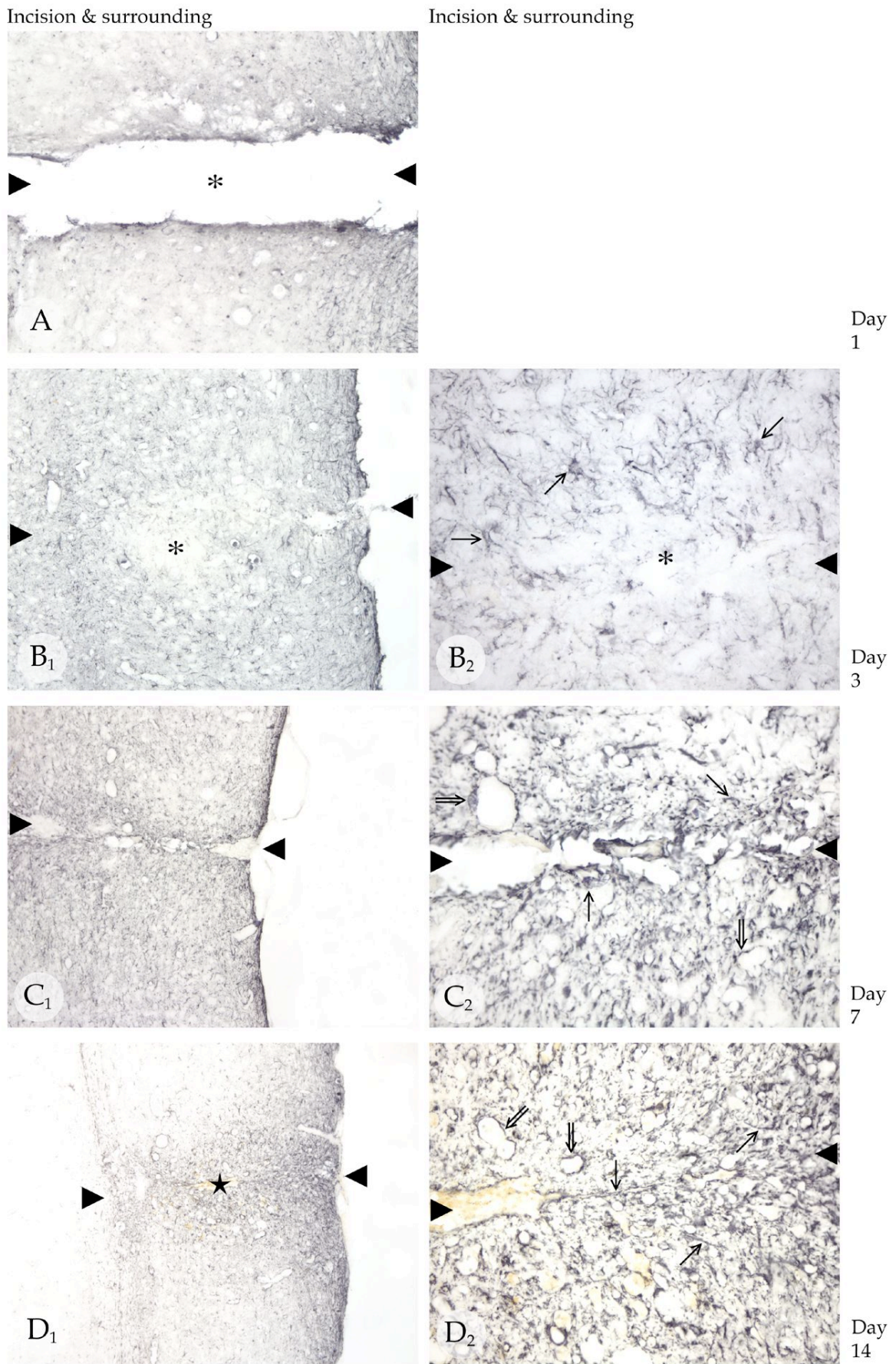


Fig. 30: Summary of GFAP immunoreactivity at the incision site for TNC^{+/+} wild type mice (for legend see next page).

Fig. 30: Summary of GFAP immunoreactivity at the incision site for TNC+/+ wild type mice after one (A), three (B₁, B₂), seven (C₁, C₂) and fourteen (D₁, D₂) days following spinal cord hemisection. Arrowheads (►) indicate the location of incision. (A) One day post injury the incision site is GFAP-negative (*); (B₁) Three days post injury GFAP staining spares the incision centre (*), (B₂) but shows reactive astrocytes (→) in the immediate surrounding area; (C₁) Seven days post injury GFAP immunoreactivity at the incision site has increased compared to day three, showing (C₂) reactive astrocytes (→) lining the incision site and GFAP-positive cells lining small cavitations (⇒); (D₁) Fourteen days post injury the incision site and the surrounding area show the strongest GFAP immunoreactivity throughout the time course tested. A fully developed astroglial scar (★), with (D₂) tightly interwoven processes of reactive astrocytes (→) and GFAP-positive cells surrounding small cavitations (⇒) is seen. A, B₁, C₁, D₁: 100x; B₂, C₂, D₂: 200x

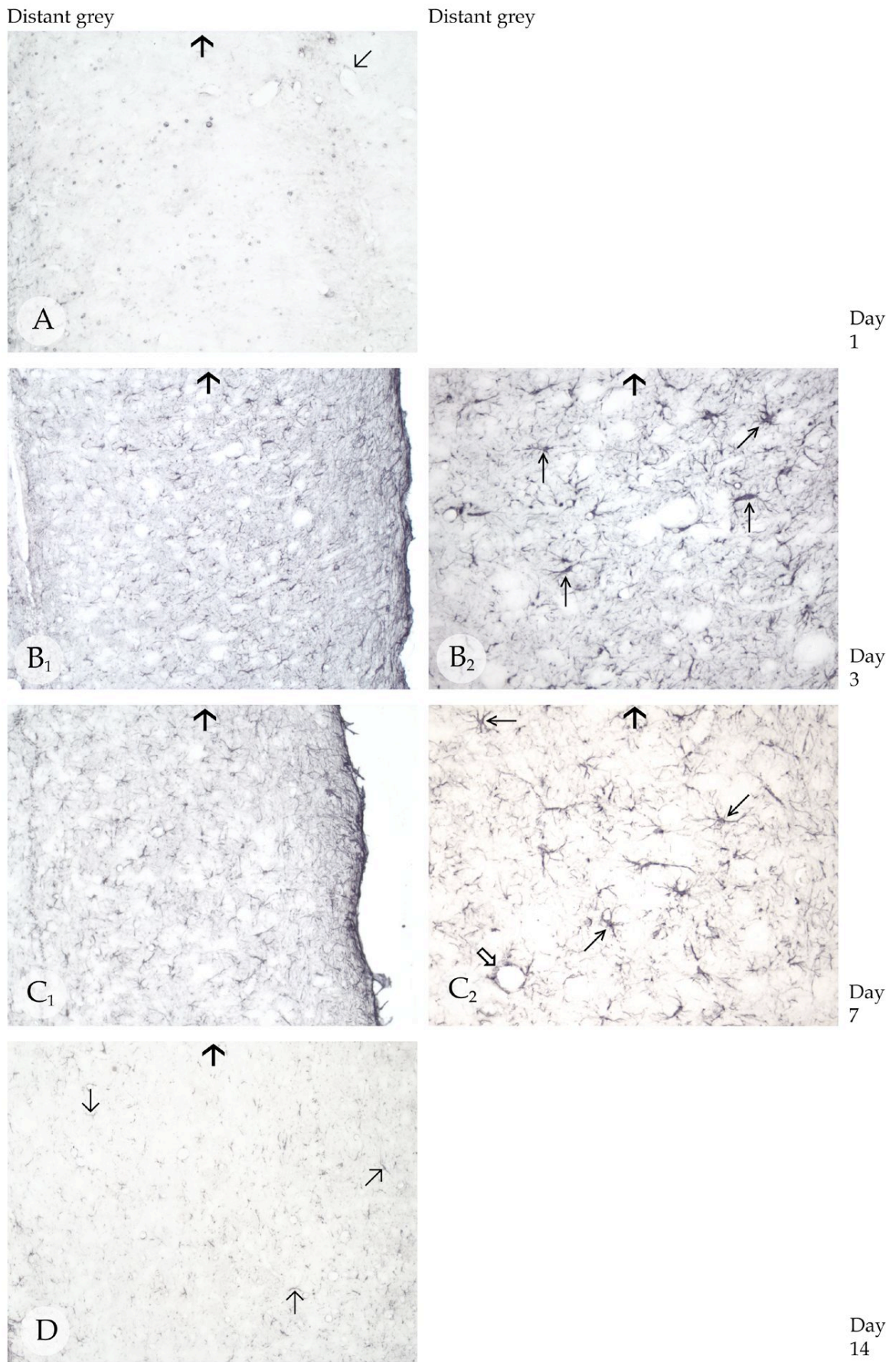


Fig. 31: Summary of GFAP immunoreactivity at the ipsilateral grey matter distant from the incision site for TNC+/+ wild type mice (for legend see next page).

Fig. 31: Summary of GFAP immunoreactivity at the ipsilateral grey matter distant from the incision site (distant grey) for TNC+/+ wild type mice after one (A), three (B₁, B₂), seven (C₁, C₂) and fourteen (D) days following spinal cord hemisection. Arrows (→) indicate the direction of the incision. (A) One day post injury the distant grey shows GFAP-positive protoplasmatic astrocytes (→); (B₁, B₂) Three days post injury heavily labelled GFAP-positive cells in the distant grey, mainly reactive astrocytes (→) are seen; (C₁, C₂) Seven days post injury GFAP immunoreactivity in the distant grey is similar to day three, still showing reactive astrocytes (→). In addition GFAP-positive cells around small vessels (⇨) are seen; (D) Fourteen days post injury GFAP immunoreactivity in the distant grey matter has decreased compared to day seven, mainly showing protoplasmatic astrocytes (→). A, B₁, C₁, D: 100x; B₂, C₂: 200x

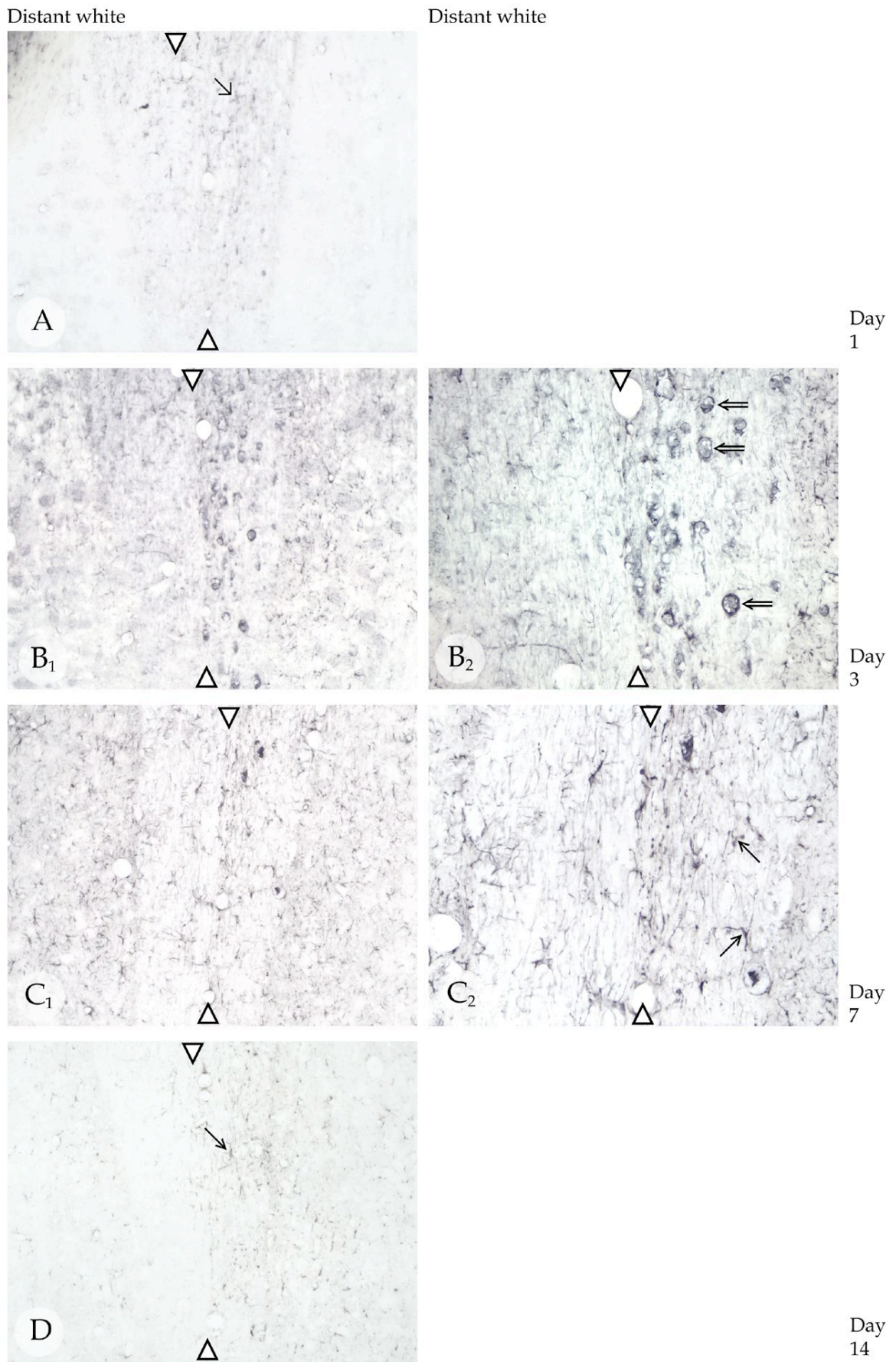


Fig. 32: Summary of GFAP immunoreactivity at the ipsilateral white matter distant from the incision site for TNC+/+ wild type mice (for legend see next page).

Fig. 32: Summary of GFAP immunoreactivity at the ipsilateral white matter distant from the incision site (distant white) for TNC+/+ wild type mice after one (A), three (B₁, B₂), seven (C₁, C₂) and fourteen (D) days following spinal cord hemisection. Arrowheads (▷) indicate the border between ipsilateral (right hand side, incision) and contralateral (left hand side) of the spinal cord. (A) One day post injury the distant white shows fibrous astrocytes (→); (B₁, B₂) Three days post injury heavily labelled GFAP-positive cells, predominantly vacuolated phagocytic-like astrocytes (⇒) are seen; (C₁, C₂) Seven days post injury, phagocytic-like astrocytes have diminished, instead GFAP-positive reactive astrocytes (→) with multiple processes are seen; (D) Fourteen days post injury, GFAP immunoreactivity has decreased and reactive astrocytes (→) are seen less frequently. A, B₁, C₁, D: 100x; B₂, C₂: 200x

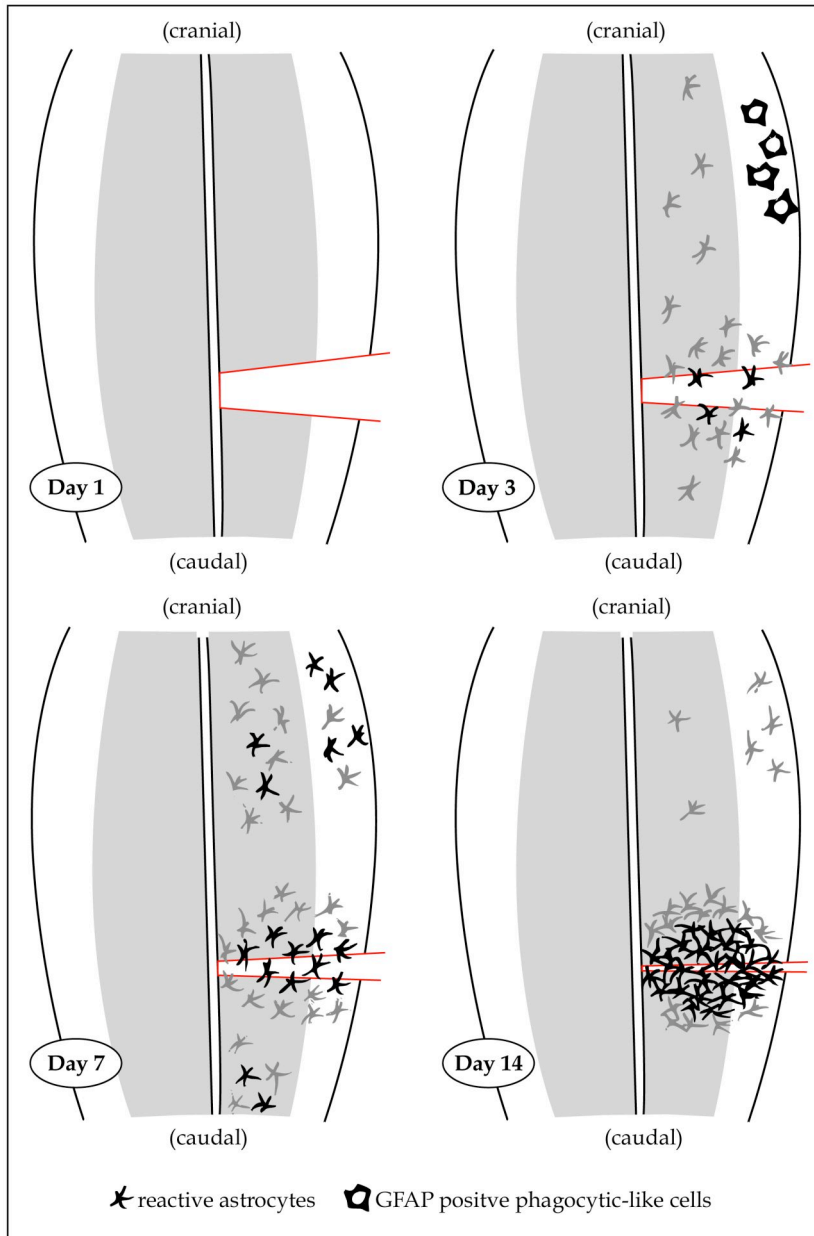


Fig. 33: Summary of changes for GFAP-positive astrocytes for TNC+/+ wild type mice after one, three, seven and fourteen days following spinal cord hemisection. The intensity of the immunoreactivity is coded: black - strong; grey - weak. Non-reactive protoplasmatic and fibrous astrocytes are not shown. On the first day, the incision site is devoid of GFAP immunoreactivity. In the remaining spinal cord protoplasmatic and fibrous astrocytes are found. On the third day, hardly any reactive astrocytes are seen at the incision site. A rim of reactive astrocytes is obvious in the surrounding area. The ipsilateral distant grey matter displays reactive astrocytes, while the ipsilateral distant white matter shows GFAP-positive phagocytic-like cells. On day seven, heavily labelled reactive astrocytes penetrate the incision site. In the surrounding area reactive astrocytes are seen in higher density compared to day three. The ipsilateral distant white and grey matter displays reactive astrocytes. On day fourteen, the incision site shows tightly interwoven GFAP-positive processes presenting the astroglial scar. In the distant grey and white matter reactive astrocytes have decreased, the prominent cell type now being protoplasmatic and fibrous astrocytes.

4.1.6.2. Quantitative densitometry

GFAP immunoreactivity (astrocytes) at the incision site showed a steady rise of IOD levels throughout the time course. Starting with a very low median IOD of 1.3 on day one and 1.7 on day three, the median IOD reached 7.7 on day seven and resulted in a maximum of 15.5 on day fourteen.

The surrounding area showed a curve, starting with a low median IOD of 0.3 on day one, followed by 6.6 on day three. The median IOD then nearly doubled to 10.4 on day seven and stabilized with a median IOD of 9.6 on day fourteen.

The distant grey matter cranial to the incision site showed extremely low levels of IOD throughout the time course, with all median IOD values being beneath two. Day one and three showed median IOD levels of 0.0 and 0.9, respectively. This was followed by a slight rise to a median IOD of 1.8 on day seven and declined to a level of 0.8 IOD on day fourteen.

The distant grey matter caudal to the incision site showed comparable low IOD values to the ones seen cranial to the incision site. On day one, the median IOD was as low as 0.1 and raised to a maximum of 2.4 on day three. A slight decline to a median IOD of 1.0 was observed on day seven, and the curve stabilized with a median IOD of 1.8 on day fourteen.

The difference between the incision site and the distant grey matter, cranial to the incision site ($p < 0.0001$) and the distant grey matter caudal to the incision site ($p = 0.001$) was significant over the time period investigated. No significant difference between the incision site and the surrounding area ($p = 0.391$) was detected throughout the time course investigated. A significant influence of the day ($p = 0.001$) was detected for all regions tested. Post-hoc comparisons with Games-Howell test revealed the following findings: The first day differed significantly from day seven ($p = 0.014$) and day fourteen ($p < 0.0001$).

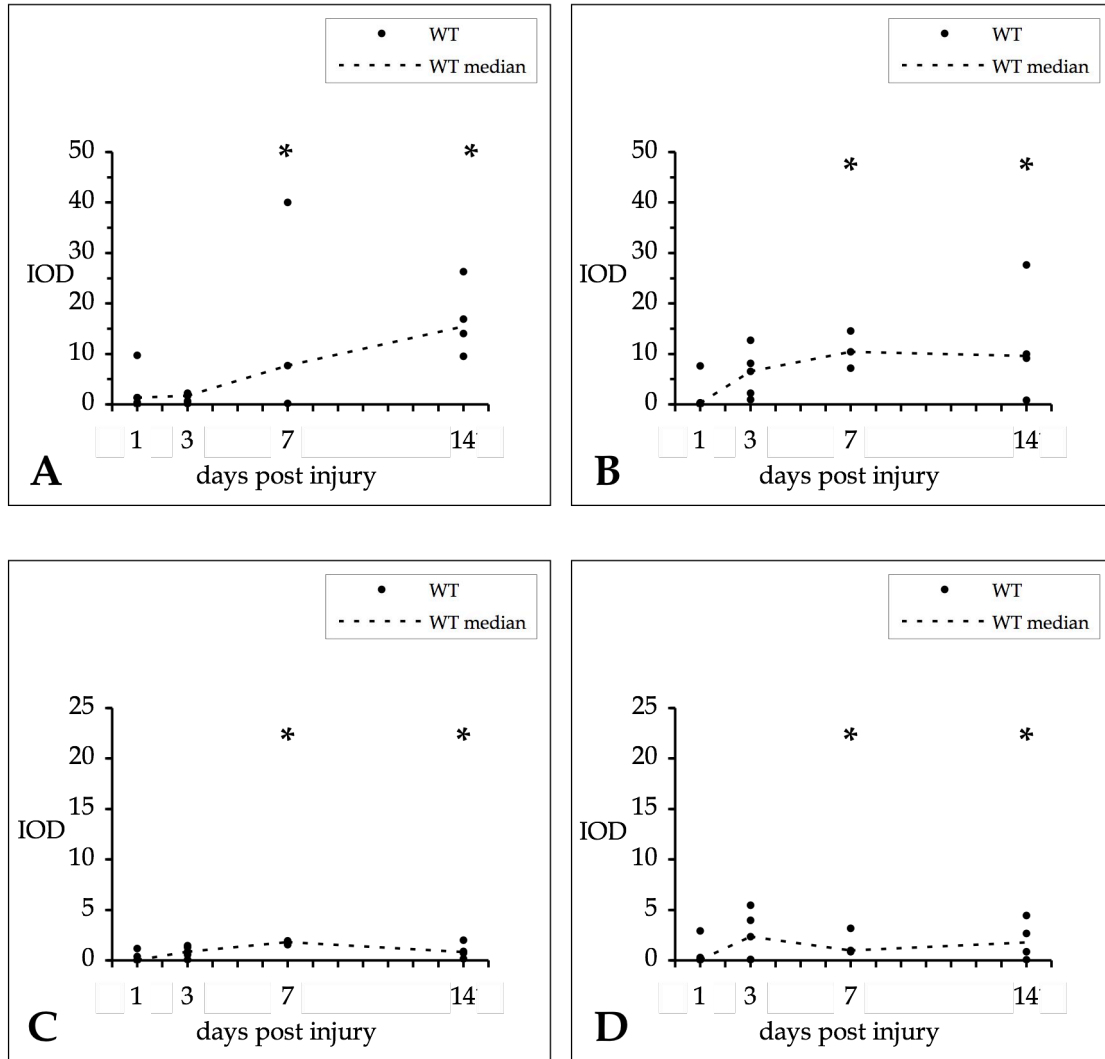


Fig. 34: Integrated optical density (IOD) for GFAP immunoreactivity as an astroglial marker is shown for TNC+/+ wild type (WT) mice from one to fourteen days after spinal cord hemisection for the incision site (A), the surrounding area (B), the distant grey matter approximately 1.5 mm cranial (C) and 1.5 mm caudal (D) to the incision site. Measurements (●) are shown for three to five animals per day. The distant grey matter, cranial ($p \leq 0.0001$) and the distant grey matter caudal ($p \leq 0.001$) show a significant difference to the incision site over the time period investigated. The difference between the incision site and the surrounding area is not significant. In addition, the first day differs significantly from day seven ($p \leq 0.05$) (*) and day fourteen ($p \leq 0.0001$) (*) for all regions investigated.

4.1.7. Neurofilament

4.1.7.1. Morphology

The normal control showed strongly labelled NF-positive, thick fibres in the entire white matter, orientated parallel to the meninges. The grey matter sporadically revealed fine NF-positive fibres, which were only weakly labelled. Most of these thin fibres were situated perpendicular to the meninges, occasionally longitudinal fine fibres were observed. Grey matter, adjacent to white matter tracts frequently displayed heavily labelled small, round spots, presumably NF-positive fibres in a transverse cut. Spinal nerves and roots showed strong NF immunoreactivity, displaying thick axons. Meninges appeared faintly labelled, but cells were NF-negative in the entire normal control.

Morphological changes for NF were observed in four regions: incision site, surrounding grey matter, surrounding white matter, containing the RST and CST, and the ipsilateral distant white matter cranial from the incision site, also containing the CST. No changes were observed in the contralateral spinal cord or the ipsilateral distant grey matter throughout the time course investigated.

On the first day after surgery, the incision site was NF-negative (Fig. 35A₁). Along the incision edges NF-positive fibres were situated, presumably fibres, which were shifted away during the procedure of spinal cord hemisection.

In the surrounding grey matter, fine NF-positive fibres were randomly orientated in all directions (Fig. 35A₂). These fine fibres were seen in greater density compared to the grey matter in the normal control.

In the surrounding white matter, strongly labelled NF-positive, thick fibres pointing towards the incision site, but never invading the incision site were seen (Fig. 35A₃). These fibres were swollen and deformed, growth cones were not detected yet.

The distant CST, cranial to the incision site displayed the same morphological features seen in the normal control (Fig. 36A), i. e. a well-defined tract with heavily labelled, thick NF-positive fibres, orientated parallel to the meninges.

On the third day post surgery, the incision edges were adjacent to each other and NF immunoreactivity at the incision site had increased compared to day one (Fig. 35B₁). Fine NF-positive fibres were frequently seen parallel to the incision edges, but never crossed the incision site.

NF immunoreactivity in the surrounding grey matter had decreased compared to day one. However, fine NF-positive fibres were still detected more frequently than in the normal control (Fig. 35B₂). These thin fibres presented a vermicular shape, often curled around their axis and appeared to meander through the tissue in a disorganized way. Some of these thin fibres pointed towards the incision site, but turned away once they had reached the edges of the incision site. Many of these thin fibres showed a club-shape structure at the end, a morphology reminiscent of growth cones (Fig. 35B₂). NF aggregates represented necrotic material.

In the surrounding white matter, NF immunoreactivity also decreased compared to day one, indicating an ongoing axonal damage (Fig. 35B₃). The regular pattern of the white matter was no longer detected, i. e. fewer thick NF-positive fibres were seen compared to day one. Dense aggregates of NF immunoreactivity were scattered in the surrounding white matter, representing necrotic material.

The regular pattern of the distant CST cranial to the incision site had disappeared and signs of axonal damage were obvious. Growth cones were not detected (Fig. 36B₁, B₂).

On day seven, the incision site was pale and little NF immunoreactivity was confined to very few thin NF-positive axons (Fig. 35C₁).

Immunoreactivity in the surrounding grey matter was comparable to day three. Again, thin NF-positive fibres, with club-shaped ends were randomly orientated in all directions (Fig. 35C₂). The density of these fibres was comparable to day three. In addition, the surrounding grey matter showed small round NF-positive deposits, most likely NF-positive fibres in a transverse cut. These round deposits appeared in a higher density compared to the normal control, indicating an overall increase of NF-positive fibres.

NF immunoreactivity in the surrounding white matter had further decreased and the formerly highly organized thick NF-positive axons had vanished (Fig. 35C₃). Necrotic material and some fine NF-positive fibres dominated the picture of the surrounding white matter (Fig. 35C₃).

The distant CST displayed a massive axonal damage (Fig. 36C₁, C₂). Thick NF-positive fibres were seldom detected, instead heavily labelled large NF deposits were frequently observed. These NF deposits, representing necrotic material, were situated along former axons as bead-like structures and accumulated at certain sites.

On the fourteenth day, the incision site was still pale and little NF immunostaining was confined to very few NF-positive thin fibres (Fig. 35D₁), a similar picture to that seen on day seven.

The surrounding grey matter also displayed a picture similar to that seen on day seven. Thin NF-positive fibres, with growth cones were observed (Fig. 35D₂).

The well-defined white matter tract in the surrounding area was completely destroyed and NF-positive necrotic material dominated the picture. Fine NF-positive fibres, pointing towards the incision site and small round NF-positive spots, representing fibres in a transverse cut were often observed (Fig. 35D₃).

The distant CST showed a decreased staining intensity, compared to day seven (Fig. 36D₁). Thick axons were no longer observed. Instead, fine NF-positive fibres were seen occasionally, situated mainly parallel or perpendicular to the meninges (Fig. 36D₂).

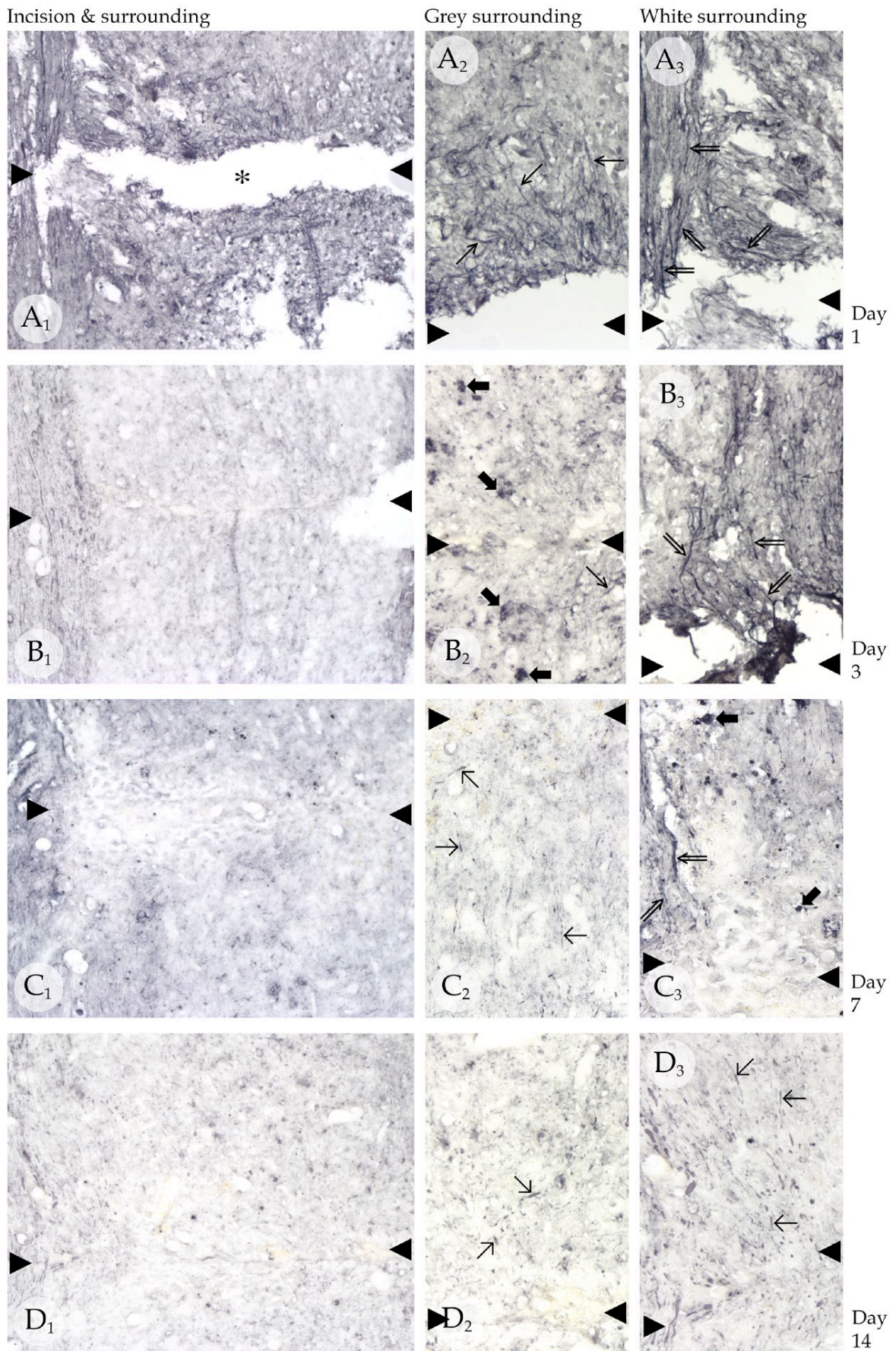


Fig. 35: Summary of neurofilament immunoreactivity at the incision site and in the immediate grey and white surrounding for TNC^{+/+} wild type mice (for legend see next page).

Fig. 35: Summary of neurofilament (NF) immunoreactivity at the incision site and in the immediate grey and white surrounding for TNC+/+ wild type mice after one (A₁, A₂, A₃), three (B₁, B₂, B₃), seven (C₁, C₂, C₃) and fourteen (D₁, D₂, D₃) days following spinal cord hemisection. Arrowheads (►) indicate the location of incision. (A₁) One day post injury the incision site is NF-negative (*). (A₂) The grey surrounding shows thin NF-positive fibres (→) randomly orientated in all directions, while (A₃) the surrounding white matter displays heavily labelled thick NF-positive fibres (⇒), mainly orientated towards the incision site; (B₁) Three days post injury the incision edges are adjacent to each other. (B₂) The grey surrounding shows thin NF-positive fibres (→) and necrotic material (►). (B₃) The surrounding white matter displays fewer thick NF-positive fibres (⇒) compared to day one; (C₁) Seven days post injury the incision site is pale and shows a decrease in NF immunoreactivity compared to day three. (C₂) Thin NF-positive fibres (→), which often show a club shaped end, representing growth cones are obvious in the surrounding grey matter. (C₃) Thick NF-positive fibres (⇒) in the surrounding white matter are seen less frequently compared to day three. Instead NF-positive necrotic material (►) is seen frequently; (D₁) Fourteen days post injury the incision site is still pale in NF immunoreactivity. (D₂) In the surrounding grey matter thin NF-positive fibres (→) are seen sporadically. (D₃) The usually well-defined thick NF-positive fibres of the surrounding white matter have disappeared, instead thin NF-positive fibres (→) are seen. A₁, B₁, C₁, D₁: 100x; A₂, A₃, B₂, B₃, C₂, C₃, D₂, D₃: 200x

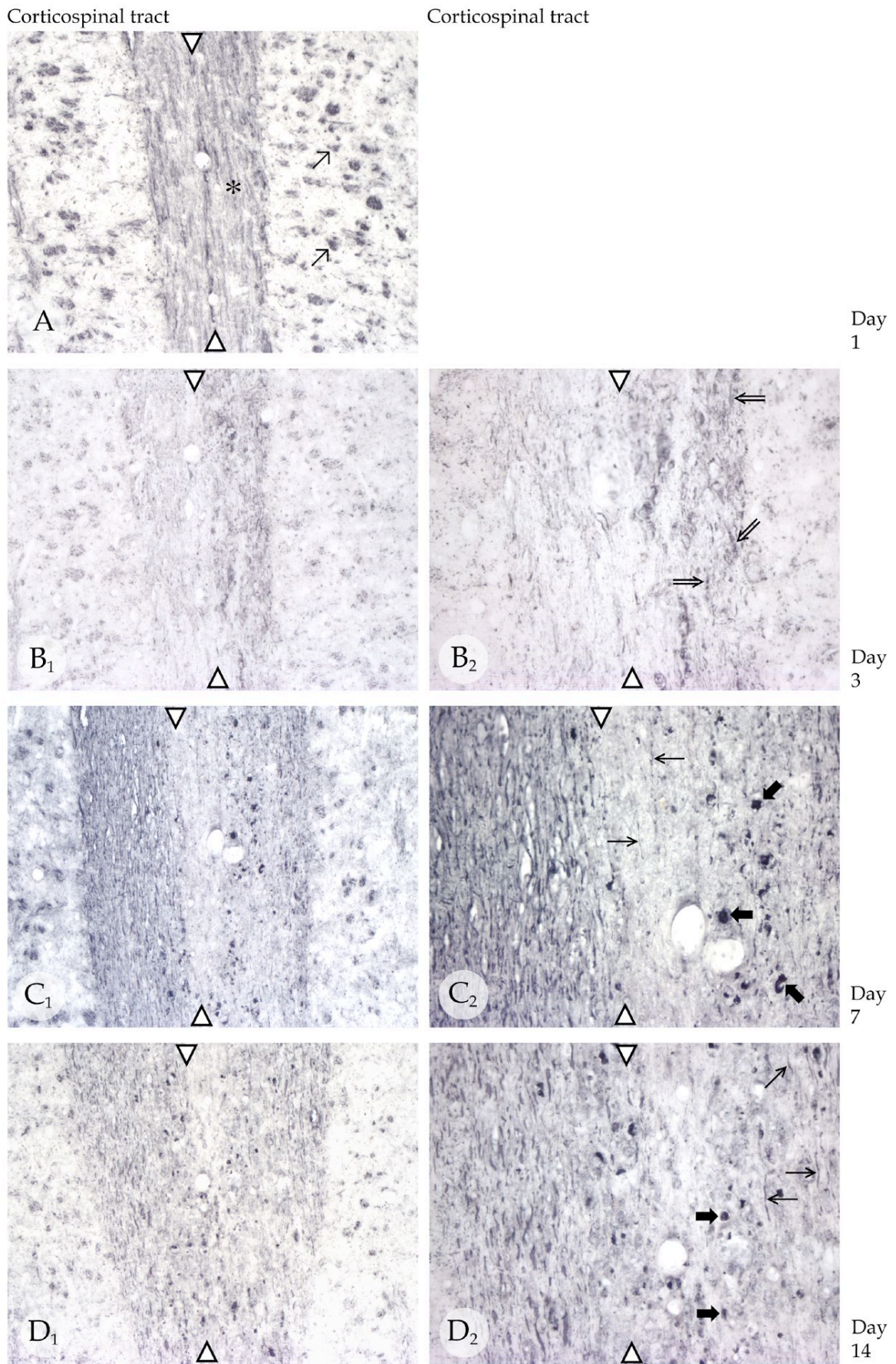


Fig. 36: Summary of neurofilament immunoreactivity at the ipsilateral corticospinal tract distant from the incision site for TNC^{+/+} wild type mice (for legend see next page).

Fig. 36: Summary of neurofilament (NF) immunoreactivity at the ipsilateral white matter distant from the incision site (distant corticospinal tract (CST)) for TNC+/+ wild type mice after one (A), three (B₁, B₂), seven (C₁, C₂) and fourteen (D₁, D₂) days following spinal cord hemisection. Arrowheads (▷) indicate the border between ipsilateral (right hand side, incision) and contralateral (left hand side) of the spinal cord. (A) One day post injury the distant CST shows thick NF-positive fibres in a well-organized and regular distribution (*). The ipsilateral grey matter distant from the incision site displays heavily labelled round spots, representing axons in a transverse cut (→); (B₁, B₂) Three days post injury the distant CST shows an irregular pattern of NF labelled oedematous fibres (⇒); (C₁, C₂) Seven days post injury the distant CST displays axonal damage. NF-positive necrotic material (➡) dominates the picture, while few thin NF-positive fibres (→) are seen in the ipsilateral CST; (D₁, D₂) Fourteen days post injury the ipsilateral CST displays signs of massive axonal damage, predominantly showing necrotic material (➡) with few thin NF-positive fibres (→). A, B₁, C₁, D₁: 100x; B₂, C₂, D₂: 200x

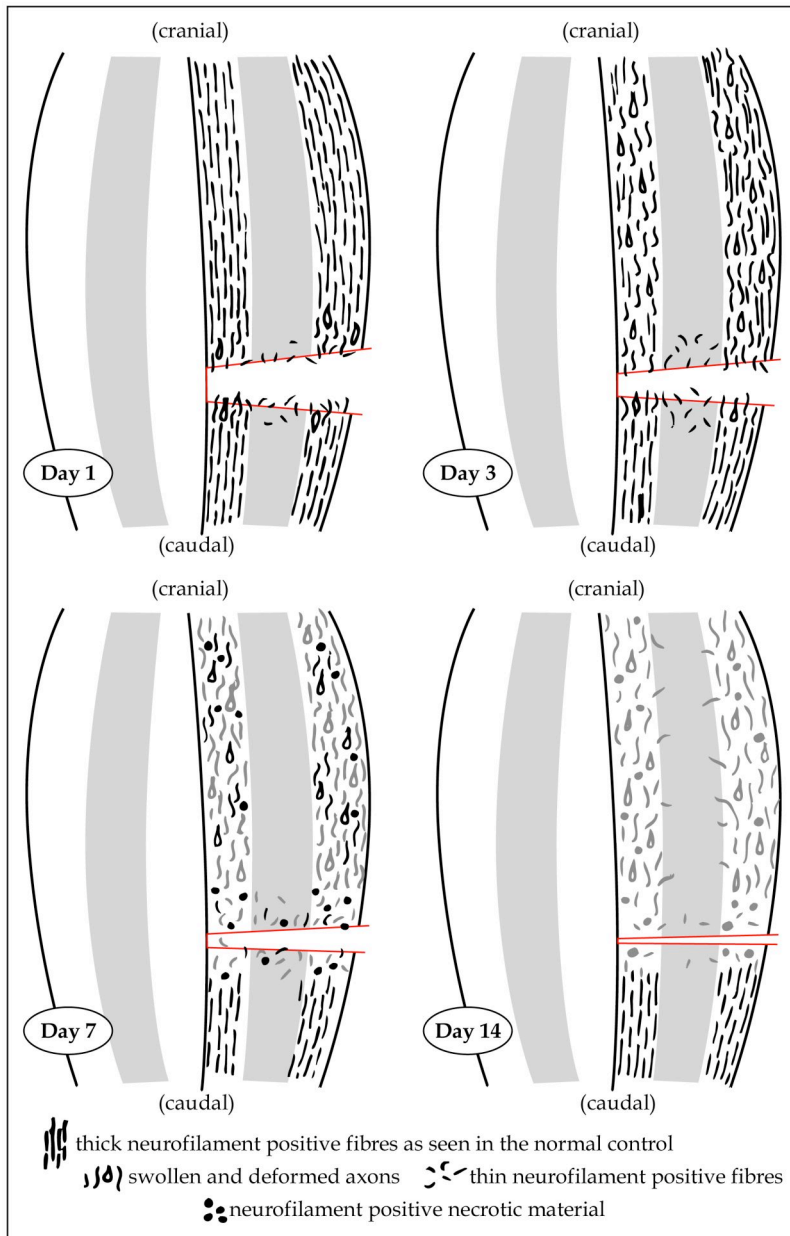


Fig. 37: Summary of changes for neurofilament (NF) for TNC+/+ wild type mice after one, three, seven and fourteen days following spinal cord hemisection. The intensity of the immunoreactivity is coded: black - strong; grey - weak. Normal NF staining pattern on the contralateral site of the incision is not shown. On the first day after surgery the incision site is NF-negative. The surrounding grey matter displays randomly orientated thin NF-positive fibres. The surrounding white matter shows oedematous thick NF-positive fibres. The corticospinal tract (CST) distant from the incision site shows a similar histology to the normal control. On the third day, thin NF-positive fibres enter, but never traverse the incision site. Thin NF-positive fibres meander through the surrounding grey matter. The surrounding white matter and the distant CST show oedematous and deformed axons. On the seventh day, the incision site is pale. The surrounding grey matter predominantly displays fine NF-positive fibres and necrotic material. In the surrounding white matter, thick NF-positive fibres diminish and necrotic material dominates. The distant CST displays massive axonal damage showing NF-positive necrotic material. On the fourteenth day, the incision site is devoid of NF-positive fibres. Thin NF-positive fibres in the surrounding grey matter are still seen. In the surrounding white matter thick NF-positive fibres are no longer detected. Instead necrotic material and some thin NF-positive fibres are seen. The distant CST still shows dense aggregates of NF-positive necrotic material and few NF-positive thin fibres.

4.1.7.2. Quantitative densitometry

For the analysis of NF immunoreactivity, measurements were taken in three regions of the grey (incision site, surrounding cranial, surrounding caudal) and in three regions of the white matter (incision site, surrounding cranial, surrounding caudal).

The incision site in the grey matter showed extremely low IOD values for NF immunoreactivity throughout the time course, with a median IOD maximum of 7.6 on day three. Extremely low median IOD values were observed on day one (1.0), day seven (0.6) and day fourteen (0.2).

The surrounding grey matter cranial and caudal to the incision site showed higher IOD levels than incision site adjacent to the grey matter. The surrounding grey matter cranial to the incision site showed a peak median IOD of 69.7 on day one and then declined to 21.1 on day three. This plateau was steady with a median IOD of 18.2 and 19.6 on day seven and fourteen, respectively.

The surrounding grey matter caudal to the incision site showed a similar curve to the surrounding grey matter cranial. On the first day a maximum median IOD of 48.3 was seen, followed by a steep decline to the lowest median IOD value of 18.7 on day three. The plateau stabilized with a median IOD level of 19.6 on day seven and 22.9 on day fourteen.

In general, the white matter revealed persistently higher IOD levels than the grey matter. The white matter incision site showed a median IOD of 2.6 on day one. A steep rise was seen to a maximum of 48.6 on day three, followed by a decline to a median IOD of 2.3 on day seven. Subsequently a slight increase to 5.5 IOD was seen on day fourteen.

The surrounding white matter cranial to the incision site showed much higher IOD values compared to the incision site adjacent to the white matter. Starting with the highest median IOD level of 196.9 the curve steadily declined to a median IOD of 127.9 on day three and subsequently reached the lowest point of 47.4 IOD

on day seven. Thereafter an increase of the median IOD was observed to 89.4 on day fourteen.

The white matter caudal to the incision site showed similarly high IOD values compared to the surrounding white matter caudal to the incision site. The highest median IOD was 146.0 on day one. A steady fall to a median IOD of 89.0 on day three and subsequently to the lowest value of 50.3 on day seven was observed. This was followed by a steady rise up to a median IOD value of 112.5 on day fourteen.

The difference between the incision site adjacent to the white matter and the white matter surrounding, cranial ($p=0.001$) and the white matter surrounding, caudal ($p<0.0001$) was significant for the time course investigated. In addition, the difference between the incision site adjacent to the grey matter and the grey matter surrounding, cranial ($p=0.034$) was significant for the time period tested. No significant difference between the incision site next to the grey matter and the surrounding grey matter caudal ($p=0.098$) was detected. In addition, post surgical days did barely not differ significantly from each other ($p=0.051$).

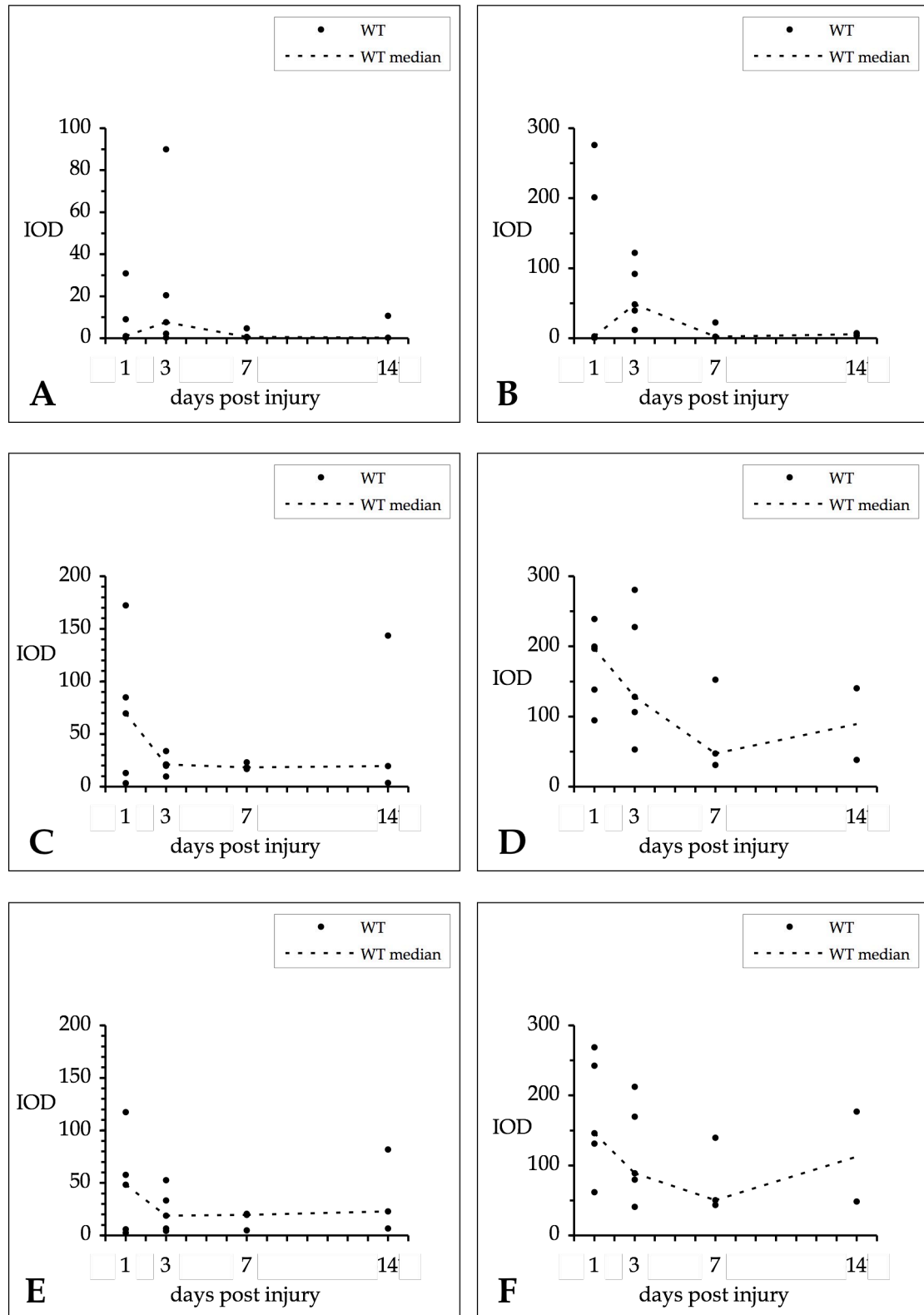


Fig. 38: Integrated optical density for neurofilament immunoreactivity as an axonal marker for TNC+/+ wild type mice (for legend see next page).

Fig. 38: Integrated optical density (IOD) for neurofilament (NF) immunoreactivity as an axonal marker is shown for TNC+/+ wild type (WT) mice from one to fourteen days after spinal cord hemisection at the incision site next to the grey matter (A), in the surrounding grey matter cranial (C) and caudal (E) to the incision site, at the incision site next to the white matter (B), and in the surrounding white matter cranial (D) and caudal (F) to the incision site. Measurements (●) are shown for three to five animals per day. The differences between the incision site next to the white matter and the surrounding white matter, cranial ($p \leq 0.001$), and the white matter surrounding, caudal ($p \leq 0.0001$) are significant for the time course investigated. In addition the difference between the incision site next to the grey matter and the surrounding grey matter, cranial to the incision site ($p \leq 0.05$) is significant for the time period tested.

4.2. TNC^{-/-} knock out mice

4.2.1. Routine histology

TNC^{-/-} knock out animals appeared phenotypically normal. They revealed a similar body size compared to their TNC^{+/+} wild type littermates and were fertile. On cursory histological examination no gross deficits of the CNS or other principal organ systems was detected.

In H&E stain, the normal control of TNC^{-/-} knock out mice showed a morphology similar to TNC^{+/+} wild type animals. No apparent malformation was observed. Neurons and glial cells were similar in density, size and distribution to TNC^{+/+} wild type findings. No signs of an astrogliosis, demyelination or ongoing inflammatory process were detected in the normal control of TNC^{-/-} knock out mice. Combined Masson trichrome and Verhoeff stain revealed the same distribution of collagen deposits in both strains.

On the first day post injury, one major difference between genotypes was observed. Lymphocytes, which were only seen on day three in TNC^{+/+} wild type animals, already invaded the surrounding area on day one in TNC^{-/-} knock out mice (Fig. 39A₂). The remaining morphological characteristics were identical to TNC^{+/+} wild type findings (Fig. 39A₁, 40A, 41A). For a detailed morphological description see chapter 4.1.1.

On the third day post injury, no morphological differences between TNC^{+/+} wild type and TNC^{-/-} knock out mice were observed (Fig. 39B₁, B₂, 40B, 41B₁, B₂). For a detailed morphological description see chapter 4.1.1.

On day seven, one major difference between genotypes was observed. TNC^{-/-} knock out animals showed a further increase in neutrophilic granulocytes, while in TNC^{+/+} wild type mice the number of neutrophils had already decreased,

compared to day three. However, the distribution of neutrophils in both genotypes was similar, they were mainly found in the central part of the surrounding area.

Other morphological characteristics, seven days after injury, were identical in both genotypes (Fig. 39C₁, C₂, 40C, 41C₁, C₂). For a detailed morphological description see chapter 4.1.1.

On the fourteenth day, no morphological difference between TNC^{+/+} wild type and TNC^{-/-} knock out mice was detected (Fig. 39D, 40D₁, D₂, 41D₁, D₂). For a detailed morphological description see chapter 4.1.1.

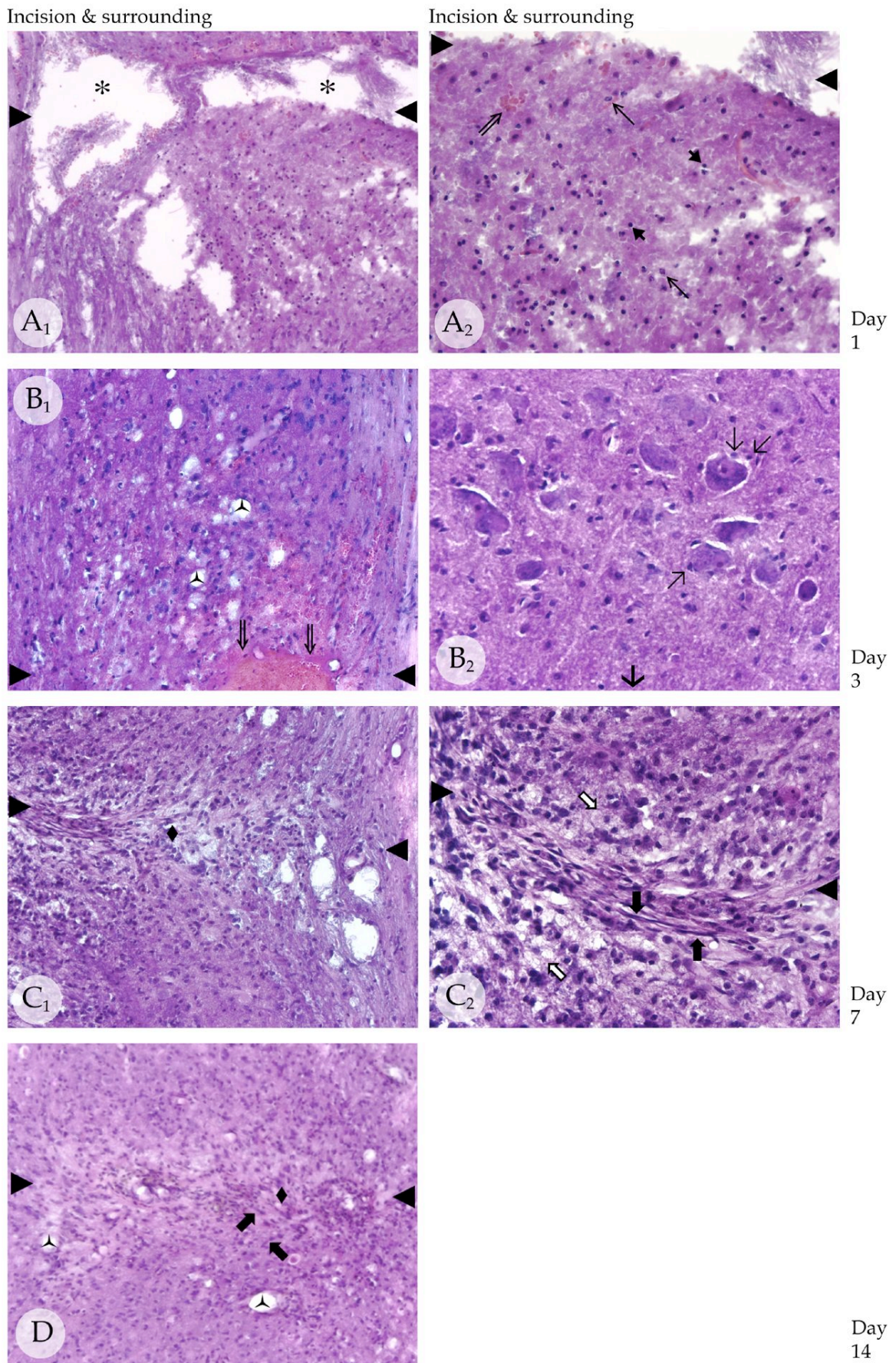


Fig. 39: Summary of morphological changes at the incision site in H&E staining for TNC-/- knock out mice (for legend see next page).

Fig. 39: Summary of morphological changes at the incision site in H&E staining for TNC^{-/-} knock out mice after one (A₁, A₂), three (B₁, B₂), seven (C₁, C₂) and fourteen (D) days following spinal cord hemisection. Arrowheads (▶) indicate the location of incision. Arrows (→) indicate the direction of the incision. (A₁) One day post injury the incision site is seen as a wide gap (*), with (A₂) granulocytes (→), mainly neutrophils and minor haemorrhages (⇒) in the surrounding. Lymphocytes (➔), which are only seen on day three in TNC^{+/+} wild type mice, are already invading the incision site in TNC^{-/-} knock out animals; (B₁) Three days post injury the incision site has narrowed, the former gap is filled with erythrocytes (⇒) and multiple small cavitations (⋈) are seen in the surrounding area. (B₂) Swollen neurons (→) with blurred cell borders and satellite cells in the surrounding area are seen; (C₁) Seven days post injury the formation of the fibrous scar (◆) with (C₂) a high density of activated fibroblasts (➔) along the incision site and some vacuolated macrophages (⇒) is evident; (D) Fourteen days post injury the incision site shows a fully developed scar (◆) with mainly inactivated fibroblasts (➔) and small cavitations (⋈).

In summary, the scar formation in H&E staining is very similar between TNC^{+/+} wild type and TNC^{-/-} knock out mice. However, two morphological differences are detected. On day one, TNC^{-/-} knock out mice already show a lymphocytic infiltration in the surrounding area, which is only seen on day three in TNC^{+/+} wild type animals. In addition, on day seven TNC^{-/-} knock out mice display a stronger neutrophilic infiltration, while in TNC^{+/+} wild type mice neutrophilic density has already diminished (not shown here). A₁, B₁, C₁, D: 100x; A₂, B₂, C₂: 200x

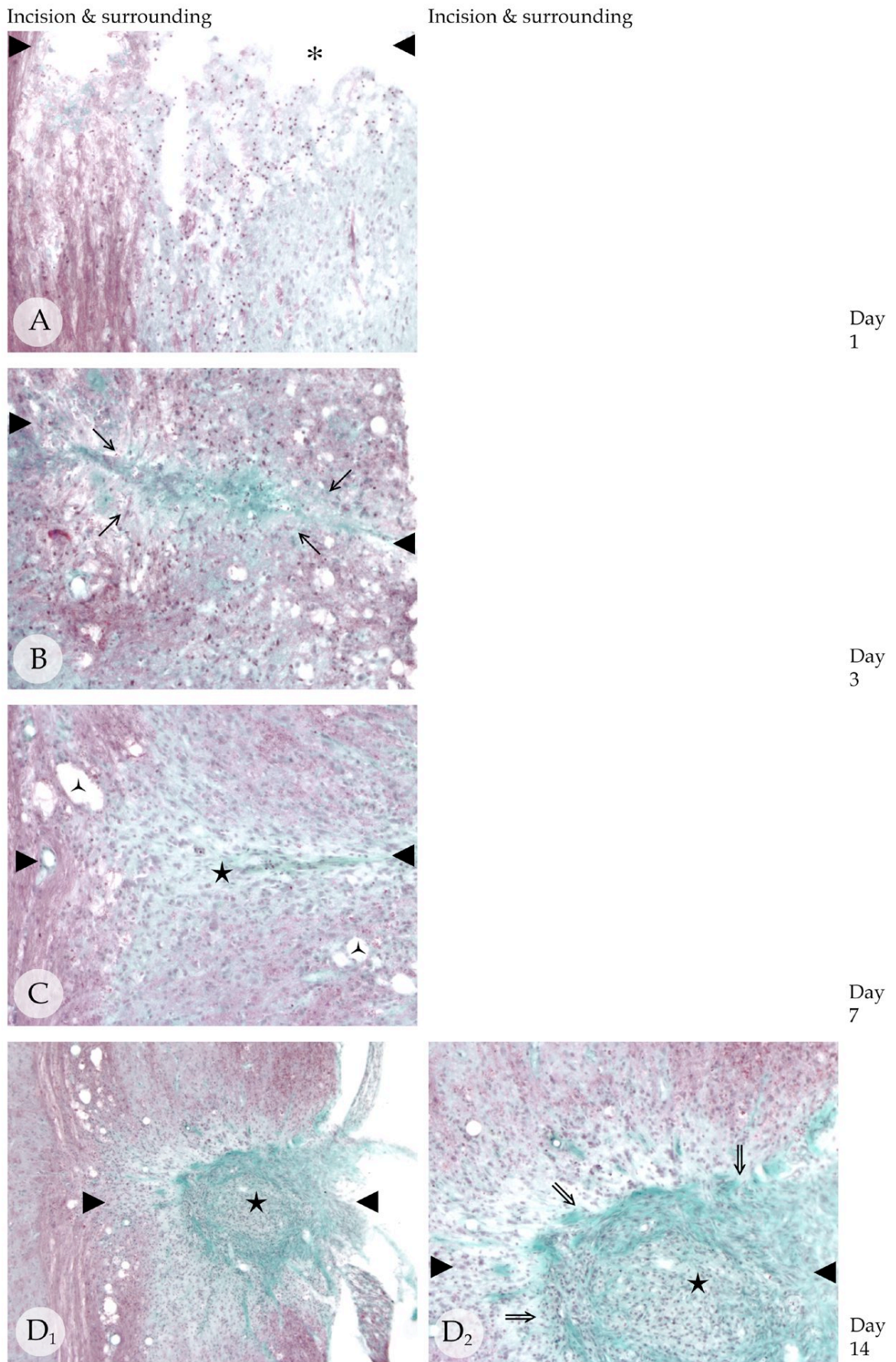


Fig. 40: Summary of morphological changes at the incision site in combined Masson trichrome and Verhoeff stain for TNC^{-/-} knock out mice (for legend see next page).

Fig. 40: Summary of morphological changes at the incision site in combined Masson trichrome and Verhoeff stain for TNC^{-/-} knock out mice after one (A), three (B), seven (C) and fourteen (D₁, D₂) days following spinal cord hemisection. Arrowheads (►) indicate the location of incision. (A) One day post injury the incision site is devoid of connective tissue (*); (B) Three days post injury collagenous tissue (→) is seen along the incision site, not extending into the surrounding area yet; (C) Seven days post injury collagen fibres (★) are more widespread, now also seen in the surrounding tissue. Multiple slightly larger cavitations (∧) are seen in the surrounding area compared to day three; (D₁) Fourteen days post injury an extensive collagenous scar (★) is seen, (D₂) forming a dense rim around the incision site, with radiating branches into the surrounding area as well as towards the incision centre.

In summary, the scar formation in combined Masson trichrome and Verhoeff stain is indistinguishable between TNC^{+/+} wild type and TNC^{-/-} knock out animals. A, B, C, D₂: 100x; D₁: 50x

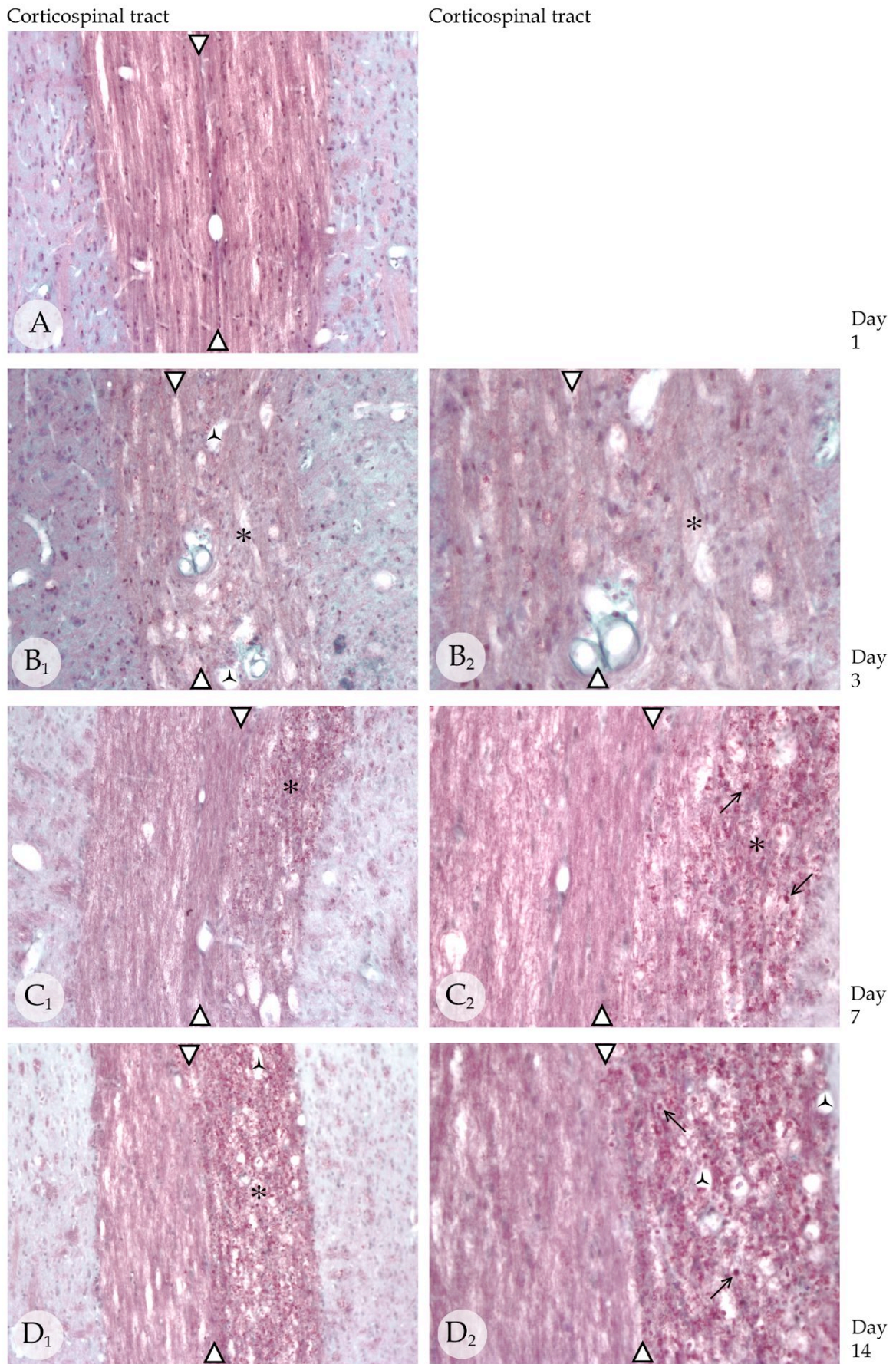


Fig. 41: Summary of morphological changes at the ipsilateral corticospinal tract in combined Masson trichrome and Verhoeff stain for TNC-/- knock out mice (for legend see next page).

Fig. 41: Summary of morphological changes at the ipsilateral white matter distant from the incision site (distant white matter, corticospinal tract (CST)) in combined Masson trichrome and Verhoeff stain for TNC^{-/-} knock out mice after one (A), three (B₁, B₂), seven (C₁, C₂) and fourteen (D₁, D₂) days following spinal cord hemisection. Arrowheads (▷) indicate the border between ipsilateral (right hand side, incision) and contralateral (left hand side) of the spinal cord. (A) One day post injury the CST shows its regular well-defined pattern; (B₁, B₂) Three days post injury oedematous tissue (*) and small cavitations (∧) are seen in the CST; (C₁) Seven days post injury an oedematous CST (*) with (C₂) a massive mononuclear infiltration (→) is seen; (D₁) Fourteen days post injury the destroyed CST displays small cavitations (∧) and (D₂) a strong mononuclear infiltration (→).

In summary, the morphology of the distant CST in combined Masson trichrome and Verhoeff stain is indistinguishable between TNC^{+/+} wild type and TNC^{-/-} knock out mice. A, B₁, C₁, D₁: 100x; B₂, C₂, D₂: 200x

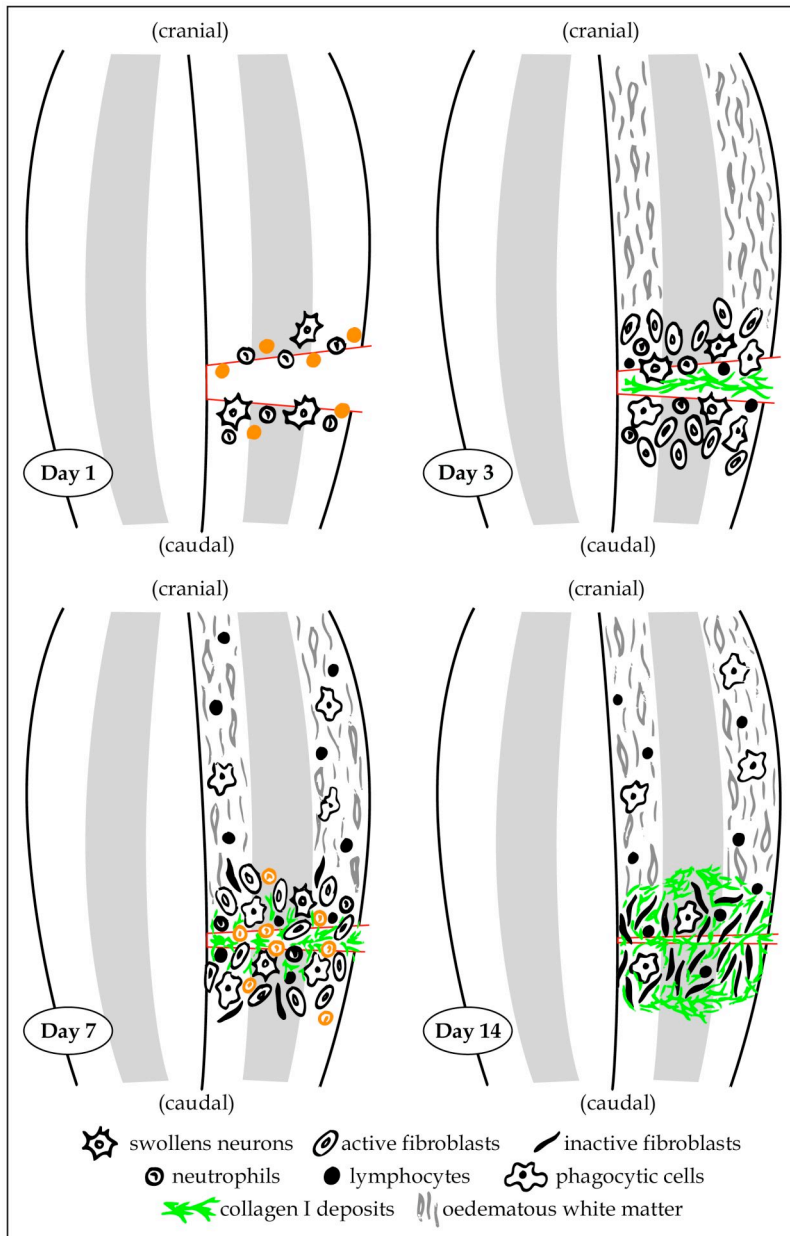


Fig. 42: Summary of morphological changes for TNC^{-/-} knock out mice after one, three, seven and fourteen days following spinal cord hemisection. Objects highlighted in orange demonstrate a higher density of cells compared to TNC^{+/+} wild type animals. The histology of the scar formation throughout the time course is very similar between TNC^{+/+} wild type and TNC^{-/-} knock out mice. However, two morphological differences are detected. On day one, in TNC^{-/-} knock out animals a lymphocytic infiltration into the surrounding area is already seen, while in TNC^{+/+} wild type mice lymphocytes are first seen on day three. However, the density of lymphocytes on day three is similar in both genotypes. On day seven TNC^{-/-} knock out animals display a much stronger neutrophil infiltration than seen in TNC^{+/+} wild type mice. On day fourteen, neutrophils in TNC^{-/-} knock out mice have decreased in numbers and have become comparable in both genotypes. On day three and fourteen no morphological alterations between TNC^{+/+} wild type and TNC^{-/-} knock out mice are observed.

4.2.2. Collagen type IV

4.2.2.1. Morphology

The normal control of TNC^{-/-} knock out mice showed an identical distribution and intensity of collagen type IV immunoreactivity, compared to TNC^{+/+} wild type animals.

On the first, third and seventh day post injury, the incision site and the surrounding area of TNC^{-/-} knock out mice revealed the same histology and staining intensity of collagen type IV immunoreactivity as observed in TNC^{+/+} wild type animals (Fig. 43A, 43B₁, B₂, 43C₁, C₂). For a detailed description of collagen type IV immunoreactivity see chapter 4.1.2.1.

On day fourteen, all TNC^{-/-} knock out animals displayed less intensely labelled collagen type IV deposits compared to TNC^{+/+} wild type mice. The incision site of TNC^{-/-} knock out mice revealed more weakly labelled and much fewer collagen type IV deposits compared to TNC^{+/+} wild type animals (Fig. 43D).

The surrounding area showed identical morphological features and an equal staining intensity between TNC^{-/-} knock out and TNC^{+/+} wild type mice. For a detailed description of collagen type IV immunoreactivity fourteen days after injury see chapter 4.1.2.1.

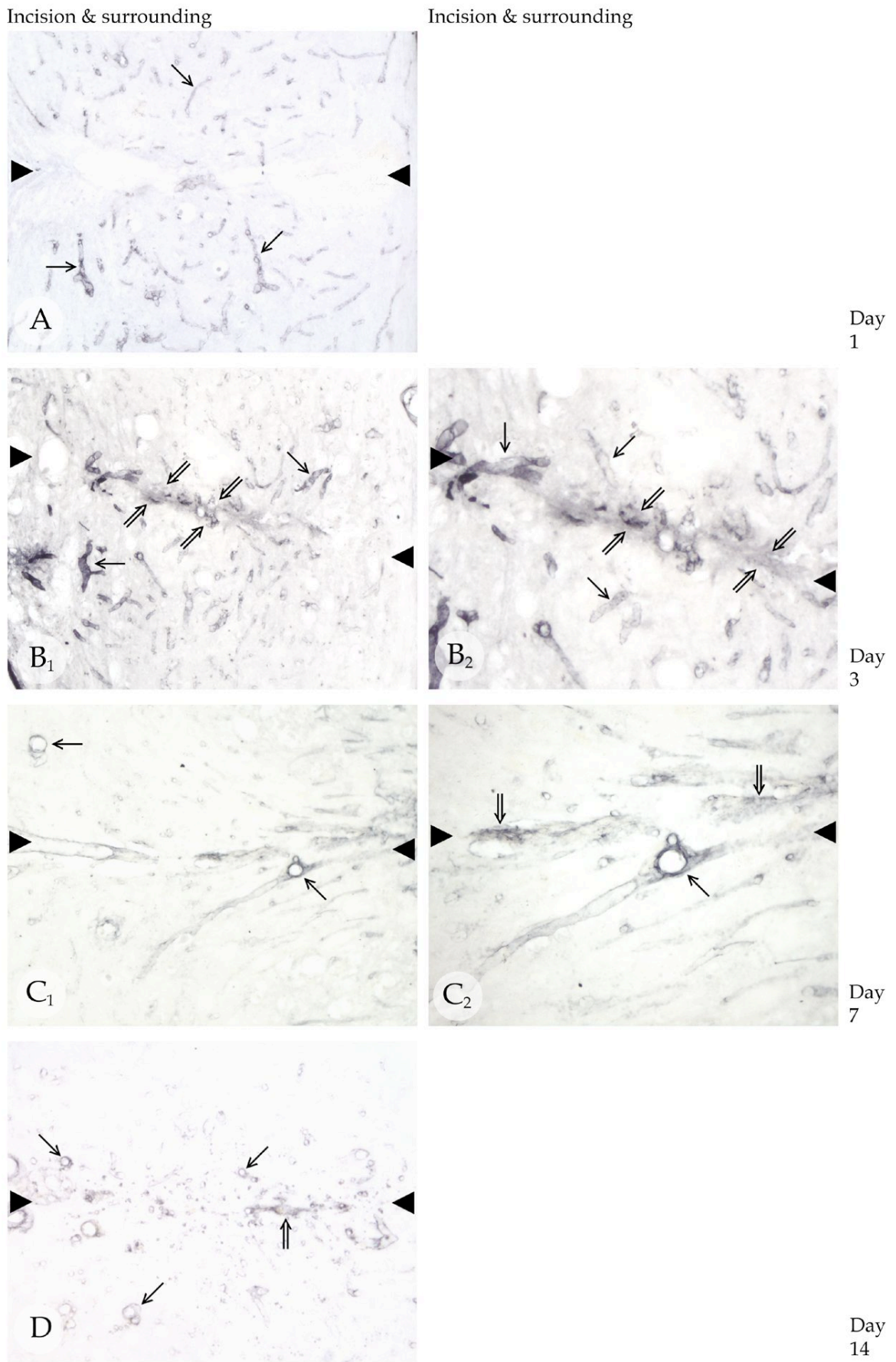


Fig. 43: Summary of collagen type IV immunoreactivity at the incision site for TNC^{-/-} knock out mice (for legend see next page).

Fig. 43: Summary of collagen type IV immunoreactivity at the incision site for TNC^{-/-} knock out mice after one (A), three (B₁, B₂), seven (C₁, C₂) and fourteen (D) days following spinal cord hemisection. Arrowheads (▶) indicate the location of incision. (A) One day post injury collagen type IV deposition is confined to dilated vessels (→) in the surrounding area; (B₁, B₂) Three days post injury collagen type IV immunoreactivity first appears as extracellular matrix deposits (⇒) along the incision site, radiating into the surrounding area. Collagen type IV-positive dilated vessels (→) are still obvious in the surrounding area; (C₁, C₂) Seven days post injury extracellular collagen type IV deposits are now confined to the incision site. Collagen type IV-positive vessels (→) appear to be more numerous compared to day three; (D) Fourteen days post injury collagen type IV deposits (⇒) along the incision site are seen less frequently, compared to TNC^{+/+} wild type mice. In the surrounding area collagen type IV immunoreactive vessels (→) are seen in a higher density compared to the normal control, indicating neovascularization.

In summary, collagen type IV immunoreactivity is very similar in both genotypes throughout the time course investigated. However, on day fourteen TNC^{-/-} knock out mice show markedly fewer collagen type IV deposits at the incision site compared to TNC^{+/+} wild type findings. The surrounding area is indistinguishable between strains over the time period tested. A, B₁, C₁, D: 100x; B₂, C₂: 200x

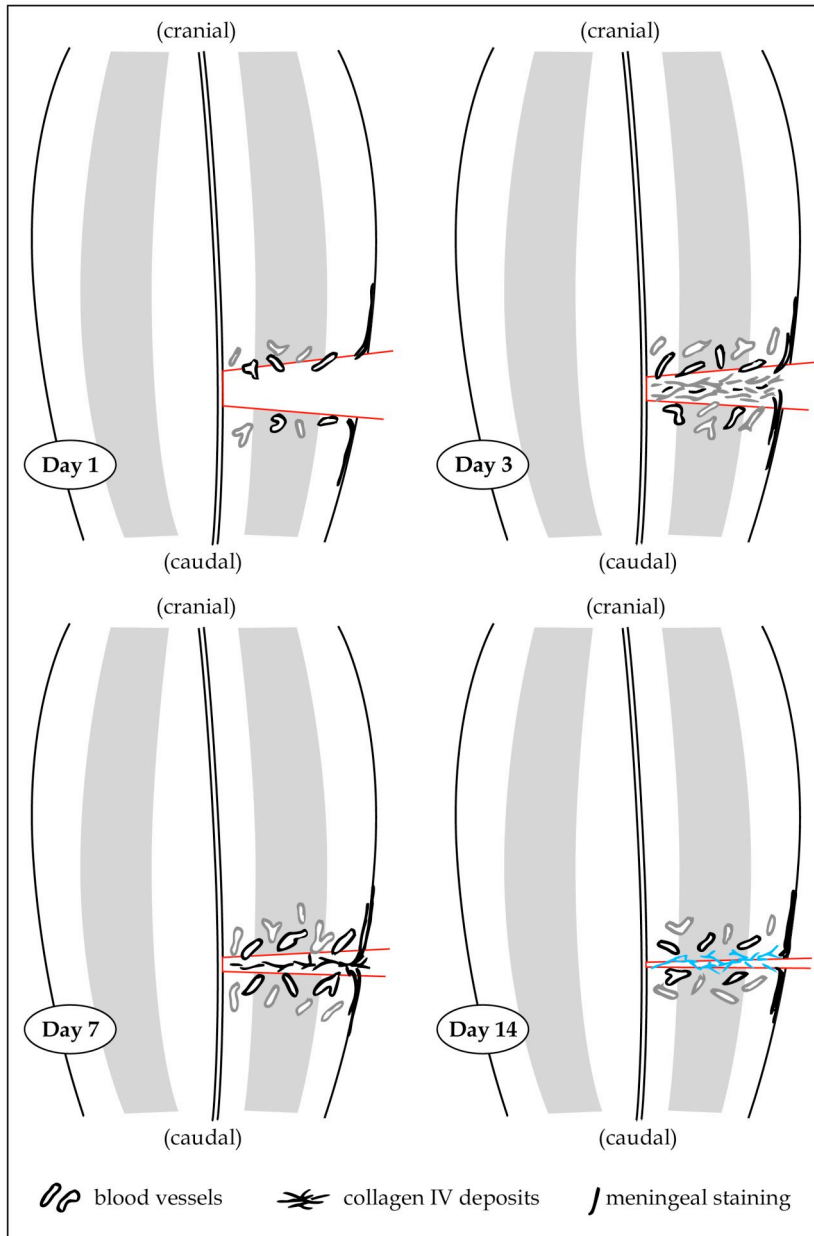


Fig. 44: Summary of changes for collagen type IV for TNC^{-/-} knock out mice after one, three, seven and fourteen days following spinal cord hemisection. The intensity of the immunoreactivity is coded: black - strong; grey - weak. Objects highlighted in blue demonstrate less collagen type IV immunoreactivity compared to TNC^{+/+} wild type animals. Immunoreactivity for collagen type IV is very similar between TNC^{-/-} knock out and TNC^{+/+} wild type mice throughout the time course investigated. However, on day fourteen a difference at the incision site is noted. TNC^{-/-} knock out mice show markedly fewer collagen type IV deposits at the incision site compared to TNC^{+/+} wild type animals. The surrounding area is indistinguishable between genotypes for the time period investigated.

4.2.2.2. Quantitative densitometry

On the first day, the incision site showed a median IOD as low as 1.3. Subsequently, on day three the median IOD had increased to 11.3, reaching a maximum of 29.2 IOD on day seven. On day fourteen, the median IOD decreased to an extremely low level of 2.7. Collagen type IV immunodensity at the incision site showed similar IOD values between genotypes on day one, three and seven. However, on day fourteen the median IOD of TNC^{-/-} knock out mice decreased to an extremely low level, with all IOD values being lower than TNC^{+/+} wild type IOD values.

The surrounding area on day one, showed a median IOD as low as 0.3, followed by a slight rise to 2.3 IOD on day three. Subsequently the median IOD dropped to 0.0 and 0.1 on day seven and fourteen, respectively. Collagen type IV immunodensity at the surrounding area showed IOD levels comparable to TNC^{+/+} wild type mice.

The difference between the incision site and the surrounding area was significant ($p < 0.0001$) over the time period tested. On day fourteen, an obvious difference of the median IOD at the incision site was observed between genotypes. Although all IOD values of TNC^{-/-} knock out mice were markedly lower than IOD values of TNC^{+/+} wild type animals, no significant difference between genotypes ($p = 0.651$) was detected throughout the time period tested. Furthermore, for both regions no significant difference between post injury days ($p = 0.059$) was detected.

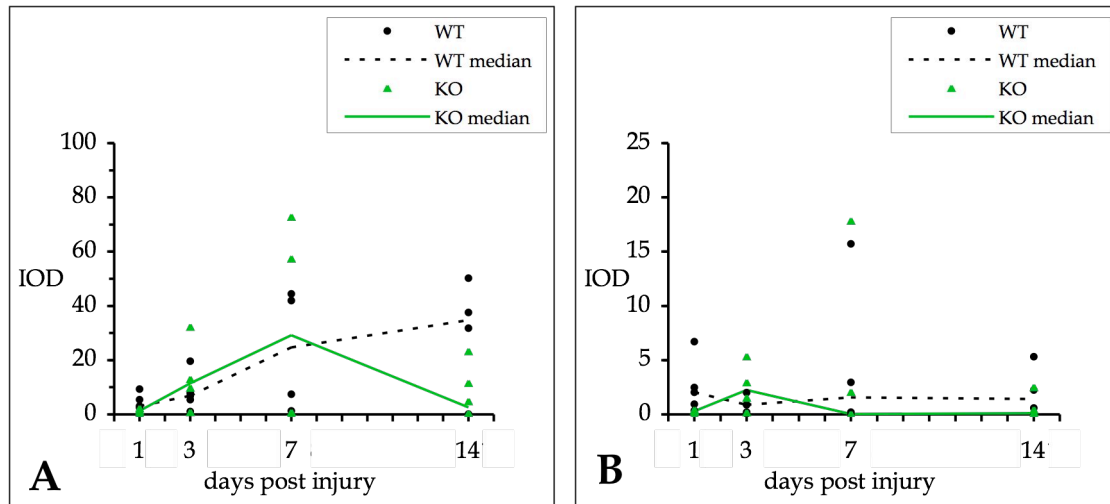


Fig. 45: Integrated optical density (IOD) for collagen type IV immunoreactivity at the incision site (A) and in the surrounding area (B) for TNC^{+/+} wild type (WT, ●) and TNC^{-/-} knock out (KO, ▲) mice from one to fourteen days after spinal cord hemisection. Measurements are shown for three to six animals per day. For both genotypes the difference between the incision site and the surrounding area is significant ($p \leq 0.0001$) over the time period tested. Although on day fourteen all IOD values of TNC^{-/-} knock out mice are markedly lower than IOD values of TNC^{+/+} wild type mice, a significant difference between genotypes is not detected for all post injury days tested.

4.2.3. Laminin

4.2.3.1. Morphology

The normal control of TNC^{-/-} knock out animals, showed a laminin immunoreactivity comparable to TNC^{+/+} wild type mice.

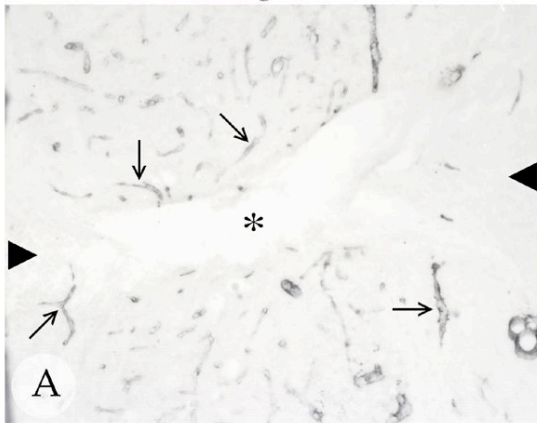
On the first, third and seventh day post surgery, the incision site and the surrounding area of TNC^{-/-} knock out mice showed a laminin immunoreactivity, which was indistinguishable from TNC^{+/+} wild type animals (Fig. 46A, 46B₁, B₂, 46C). For a detailed description of laminin immunoreactivity see chapter 4.1.3.1.

Fourteen days after surgery, the incision site of TNC^{-/-} knock out mice revealed a different histology compared to TNC^{+/+} wild type findings. The overall laminin immunoreactivity at the incision site was lower in all TNC^{-/-} knock out mice, showing fewer and weaker labelled laminin deposits compared to TNC^{+/+} wild type findings (Fig. 46D). Only one TNC^{-/-} knock out animal displayed extensive laminin deposits along the incision site, a feature which was frequently seen in TNC^{+/+} wild type mice.

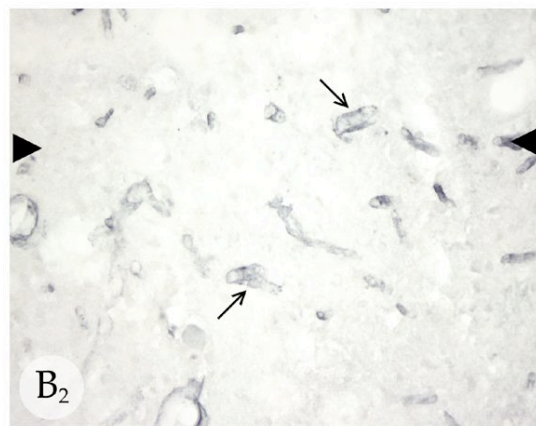
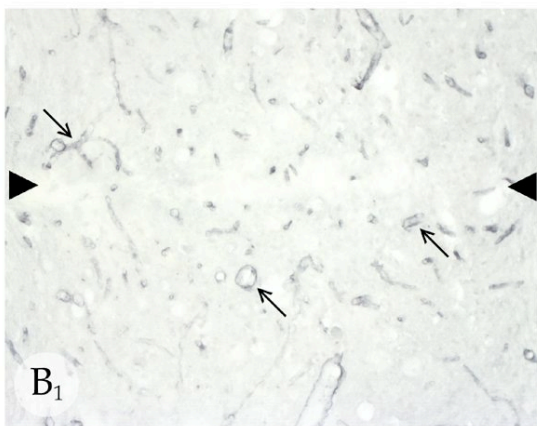
The surrounding area displayed a similar morphology and staining intensity of laminin in both genotypes. For a detailed description of laminin immunoreactivity fourteen days after injury see chapter 4.1.3.1.

Incision & surrounding

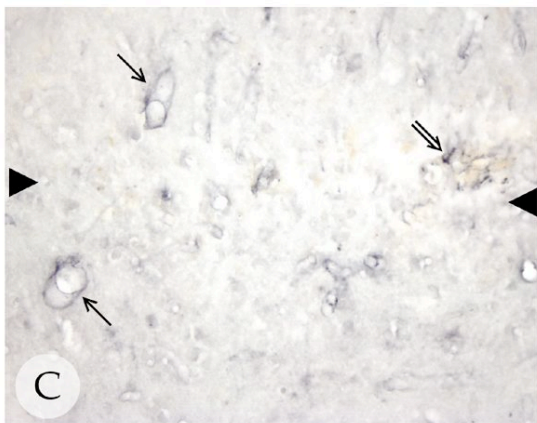
Incision & surrounding



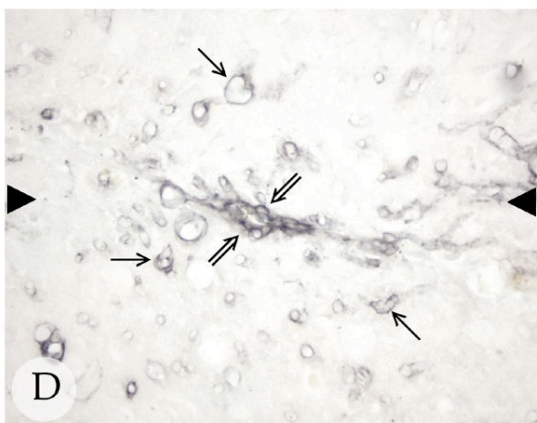
Day
1



Day
3



Day
7



Day
14

Fig. 46: Summary of laminin immunoreactivity at the incision site for TNC^{-/-} knock out mice (for legend see next page).

Fig. 46: Summary of laminin immunoreactivity at the incision site for TNC^{-/-} knock out mice after one (A), three (B₁, B₂), seven (C) and fourteen (D) days following spinal cord hemisection. Arrowheads (►) indicate the location of incision. (A) One day post injury the incision site is laminin-negative (*). Laminin labelled vessels (→) are seen near the incision edges, with a decreased staining intensity towards the outer surrounding area; (B₁, B₂) Three days post injury laminin-positive vessels (→) are seen in the surrounding area; (C) Seven days post injury laminin-positive vessels (→) along the incision site and occasionally laminin extracellular deposits (⇒) are seen; (D) Fourteen days post injury fewer and weaker labelled laminin extracellular deposits (⇒) are seen at the incision site compared to TNC^{+/+} wild type mice. Laminin-positive vessels (→) appear to be more numerous than in the normal control, indicating neovascularization.

In summary, laminin immunoreactivity is very similar in both genotypes over the time period studied. However, on day fourteen all TNC^{-/-} knock out mice show considerably fewer extracellular laminin deposits at the incision site, compared to TNC^{+/+} wild type mice. The surrounding area is indistinguishable between genotypes over the time period tested A, B₁: 100x; B₂, C, D: 200x

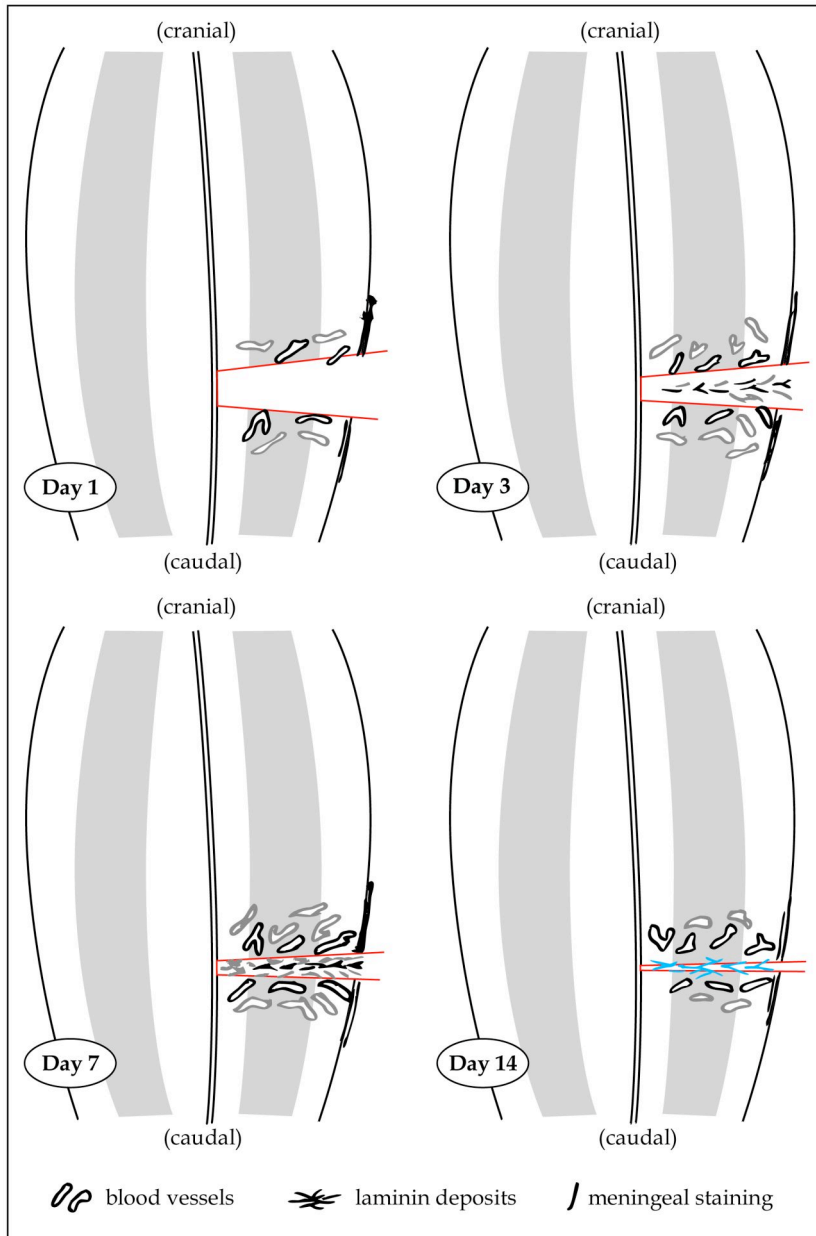


Fig. 47: Summary of changes for laminin for TNC^{-/-} knock out mice after one, three, seven and fourteen days following spinal cord hemisection. The intensity of the immunoreactivity is coded: black - strong; grey - weak. Objects highlighted in blue demonstrate less laminin immunoreactivity compared to TNC^{+/+} wild type animals. Immunoreactivity for laminin is very similar between TNC^{-/-} knock out and TNC^{+/+} wild type mice throughout the time course investigated. However, on day fourteen a difference at the incision site is noted. At the incision site TNC^{-/-} knock out mice show markedly fewer extracellular laminin deposits compared to TNC^{+/+} wild type animals. Laminin immunoreactivity in the surrounding area is indistinguishable between genotypes throughout the time course investigated.

4.2.3.2. Quantitative densitometry

At the incision site, laminin showed median IOD levels of 2.3 and 9.7 on day one and day three, respectively. On day seven, the median IOD doubled to 18.1 and stabilized at a similar level with a median IOD of 15.0 on day fourteen. At the incision site from day one to day seven, median IOD values for laminin immunoreactivity were similar between genotypes. However, a considerable difference was seen on day fourteen. Whereas in TNC^{+/+} wild type animals a steep increase in the median IOD was observed, the median IOD of TNC^{-/-} knock out mice remained low. The median IOD of TNC^{+/+} wild type mice on day fourteen was as high as 85.0, whereas the median IOD for TNC^{-/-} knock out animals was only as 15.0.

IOD levels at the surrounding area presented as a straight line over the time. On day one the median IOD was as low as 1.0. Similar low IOD values were seen on day three and seven with a median IOD of 1.5 and 2.1, respectively. The lowest point was reached on day fourteen with a median IOD of 0.9. The surrounding area of TNC^{-/-} knock out mice showed similar IOD levels compared to TNC^{+/+} wild type animals.

The difference between the incision site and the surrounding area was significant ($p=0.001$) throughout the time course. Despite a major difference of IOD values at the incision site on day fourteen between genotypes; i. e. all but one TNC^{-/-} knock out mice revealed considerably lower IOD values than TNC^{+/+} wild type animals, no significant difference between the genotype ($p=0.895$) was observed. In addition, no significant influence of the day ($p=0.213$) was detected.

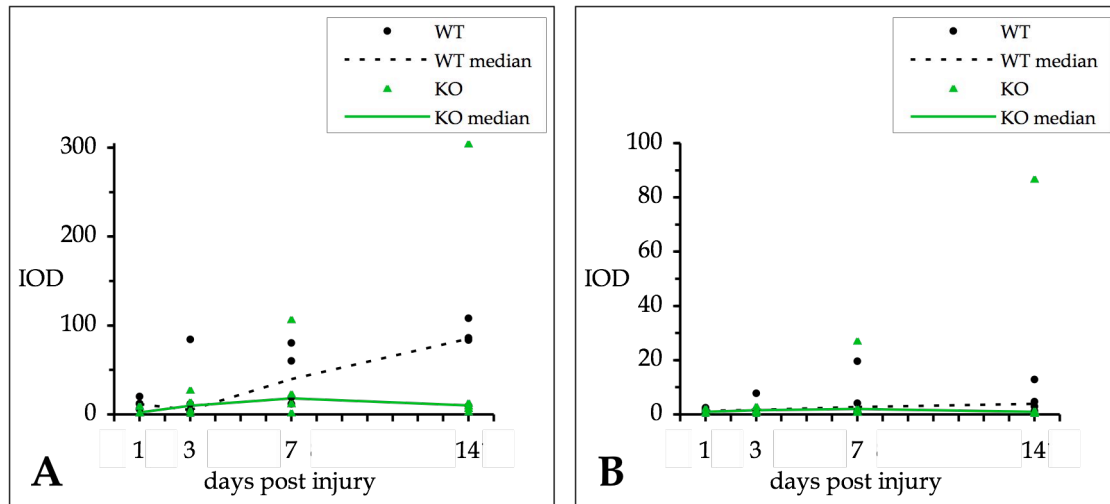


Fig. 48: Integrated optical density (IOD) for laminin immunoreactivity at the incision site (A) and in the surrounding area (B) for TNC^{+/+} wild type (WT, ●) and TNC^{-/-} knock out (KO, ▲) mice from one to fourteen days after spinal cord hemisection. Measurements are shown for three to six animals per day. For both genotypes the difference between the incision site and the surrounding area is significant ($p \leq 0.001$) over the time period tested. Although on day fourteen the incision site of TNC^{-/-} knock out mice revealed lower IOD values compared to TNC^{+/+} wild type mice, a significant difference between genotypes is not detected.

4.2.4. Fibronectin

4.2.4.1. Morphology

The normal control of TNC^{-/-} knock out animals displayed similar characteristics of fibronectin immunolabelling as observed in TNC^{+/+} wild type mice.

On the first day post injury, the incision site and the surrounding area showed markedly weaker fibronectin immunoreactivity than seen in TNC^{+/+} wild type animals (Fig. 49A₁). Near the incision site, all TNC^{-/-} knock out mice showed fewer and more weakly labelled fibronectin-positive strands (Fig. 49A₁, A₂). In the surrounding area fibronectin-positive strands were orientated perpendicular to the incision site, but seen less frequently compared to TNC^{+/+} wild type mice.

On the third and seventh day post surgery, both regions examined for fibronectin immunoreactivity showed morphological characteristics and labelling intensity indistinguishable from TNC^{+/+} wild type mice (Fig. 49B, C₁, C₂). For a detailed description of fibronectin immunoreactivity see chapter 4.1.4.1.

Fourteen days following surgery, all TNC^{-/-} knock out mice revealed considerably less immunoreactivity at the incision site compared to TNC^{+/+} wild type animals. However, fibronectin distribution pattern was very similar. The incision edges displayed moderately labelled fibronectin deposits (Fig. 49D₁, D₂).

In the surrounding area, morphological characteristics and staining intensity were identical to TNC^{+/+} wild type findings (Fig. 49D₁). For a detailed description of fibronectin immunoreactivity see chapter 4.1.4.1.

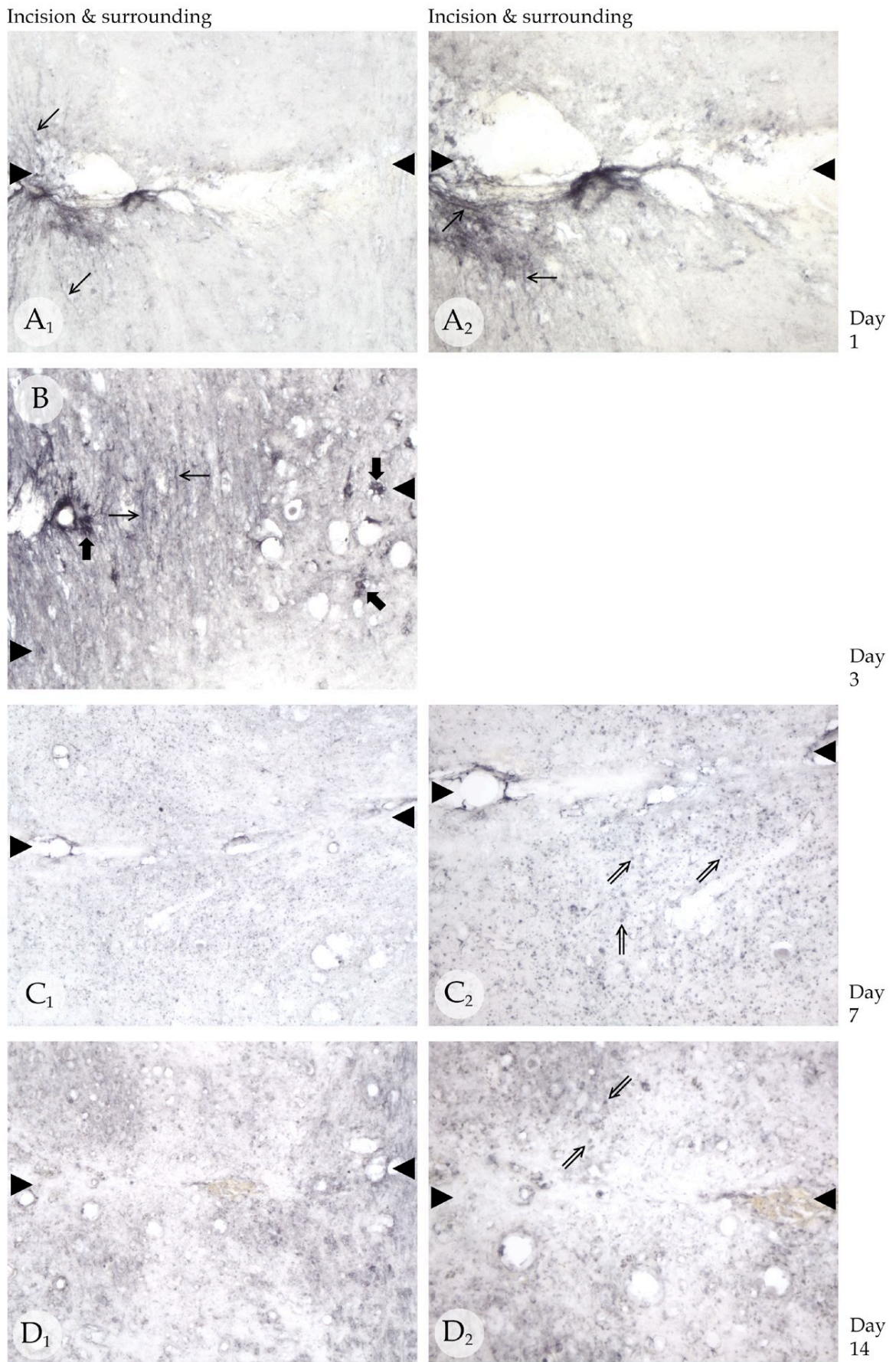


Fig. 49: Summary of fibronectin immunoreactivity at the incision site for TNC^{-/-} knock out mice (for legend see next page).

Fig. 49: Summary of fibronectin immunoreactivity at the incision site for TNC^{-/-} knock out mice after one (A₁, A₂), three (B), seven (C₁, C₂) and fourteen (D₁, D₂) days following spinal cord hemisection. Arrowheads (▶) indicate the location of incision. (A₁, A₂) One day post injury fibronectin-positive strands (→) at the incision site and in the surrounding area are seen less frequently compared to TNC^{+/+} wild type mice; (B) Three days post injury fibronectin-positive strands (→) have decreased and now intensively labelled fibronectin deposits (➡) are seen near the incision site; (C₁) Seven days post injury diffusely labelled fibronectin immunoreactivity with (C₂) lightly labelled spherical fibronectin deposits (⇒), presumably strands in a transverse cut are seen in the surrounding area; (D₁) Fourteen days post injury the overall immunoreactivity at the incision site is markedly lower than in TNC^{+/+} wild type animals. However, similar morphological features like (D₂) fibronectin round deposits (⇒) are seen at the incision site and in the surrounding area.

In summary, on day one fibronectin immunoreactivity at the incision site and in the surrounding area of TNC^{-/-} knock out mice is markedly lower compared to TNC^{+/+} wild type animals. On day three and seven no difference is observed between strains. However, on day fourteen the incision site displays a markedly lower fibronectin immunoreactivity compared to TNC^{+/+} wild type findings. A₁, B, C₁, D₁: 100x; A₂, C₂, D₂: 200x

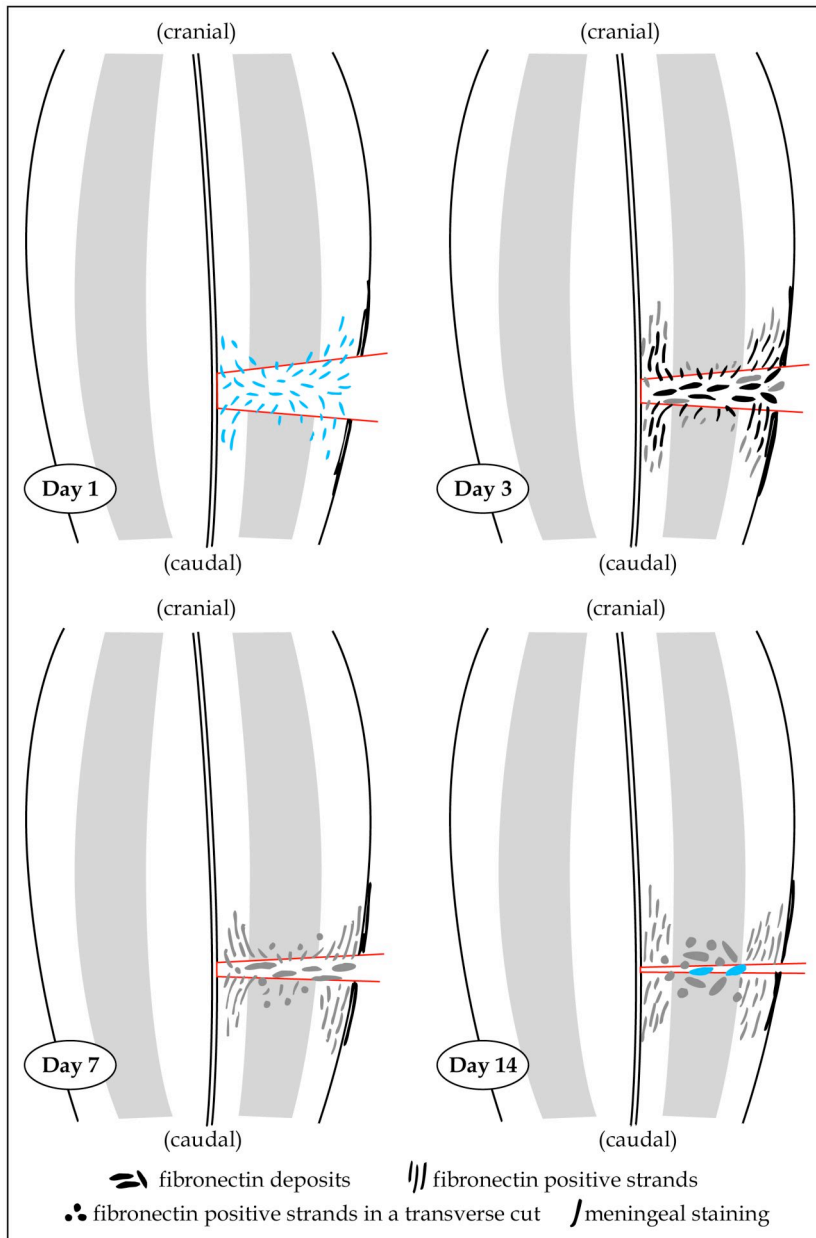


Fig. 50: Summary of changes for fibronectin for TNC^{-/-} knock out mice after one, three, seven and fourteen days following spinal cord hemisection. The intensity of the immunoreactivity is coded: black - strong; grey - weak. Objects highlighted in blue demonstrate less fibronectin immunoreactivity compared to TNC^{+/+} wild type animals. For fibronectin immunoreactivity a significant difference between genotypes is observed. On day one the incision site and the surrounding area show significantly less fibronectin-positive strands compared to TNC^{+/+} wild type mice. On day three and day seven, no difference in fibronectin immunoreactivity between genotypes is observed. On day fourteen, the incision site displays a markedly lower fibronectin immunoreactivity and fewer fibronectin deposits compared to TNC^{+/+} wild type animals, while in the surrounding area no difference between genotypes is observed.

4.2.4.2. Quantitative densitometry

On day one, the incision site showed a median IOD of 23.7, followed by a steep increase, to the maximum median IOD of 61.4 on day three. Subsequently a steady decline was seen to a median IOD of 4.0 and 1.4 on day seven and fourteen, respectively. On day one, the incision site of TNC^{-/-} knock out mice showed markedly lower IOD levels compared to TNC^{+/+} wild type findings; all IOD values of TNC^{-/-} knock out mice were lower compared to TNC^{+/+} wild type IOD values. On day three and seven IOD levels were similar between genotypes. Whereas on day fourteen, TNC^{-/-} knock out mice showed a considerably lower median IOD at the incision site than seen in TNC^{+/+} wild type animals. Again all IOD values of TNC^{-/-} knock out animals were situated below TNC^{+/+} wild type values.

On day one, the surrounding area of TNC^{-/-} knock out mice showed an extremely low median IOD of 0.1. The median IOD remained on a low level throughout the time course, being 1.6, 1.4 and 0.4 on day three, seven and fourteen, respectively. For the surrounding area, a difference between genotype was seen on day one. Whereas the median IOD in TNC^{-/-} knock out mice was as low as 0.1, TNC^{+/+} wild type animals showed a maximum level of 18.8. Between day three and day fourteen similar low IOD levels were observed for both genotypes.

The difference between the incision site and the surrounding area was significant ($p < 0.0001$) over the time period studied. Although a significant influence of the day ($p = 0.038$) was detected with ANOVA for repeated measurements, indicating a trend, post-hoc comparisons by the method of Games-Howell did not reveal any significant differences between post injury days. However, a significant influence of the genotype ($p = 0.036$) over the time period and for both regions was detected. This means that fibronectin immunoreactivity at the incision site and in the surrounding area was significantly decreased in TNC^{-/-} knock out mice compared to TNC^{+/+} wild type mice over the entire time period tested.

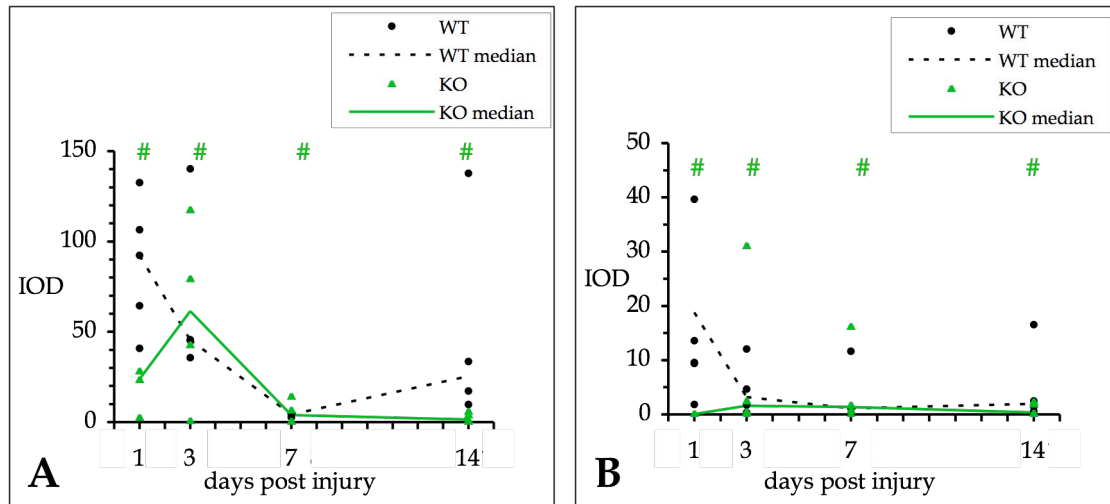


Fig. 51: Integrated optical density (IOD) for fibronectin immunoreactivity at the incision site (A) and in the surrounding area (B) for TNC^{+/+} wild type (WT, ●) and TNC^{-/-} knock out (KO, ▲) mice from one to fourteen days after spinal cord hemisection. Measurements are shown for three to six animals per day. For both genotypes the difference between the incision site and the surrounding area is significant ($p \leq 0.0001$) over the time period tested. A significant ($p = 0.036$) difference between the genotype (#) for both regions and for all post injury days is demonstrated, indicating that fibronectin immunoreactivity is significantly reduced in TNC^{-/-} knock out mice, compared to TNC^{+/+} wild type mice.

4.2.5. F4/80

4.2.5.1. Morphology

The normal control of TNC^{-/-} knock out mice revealed the same distribution of resting microglia as seen in TNC^{+/+} wild type animals.

Throughout the time course investigated, no difference in F4/80 immunoreactivity (microglia) was discovered between TNC^{-/-} knock out and TNC^{+/+} wild type mice (Fig. 52A, B₁-B₃, C₁-C₃, D₁-D₃, 53A, B₁, B₂, C₁, C₂, D, 54A, B₁, B₂, C₁, C₂, D₁, D₂). For a detailed description of F4/80 immunoreactivity see chapter 4.1.5.1.

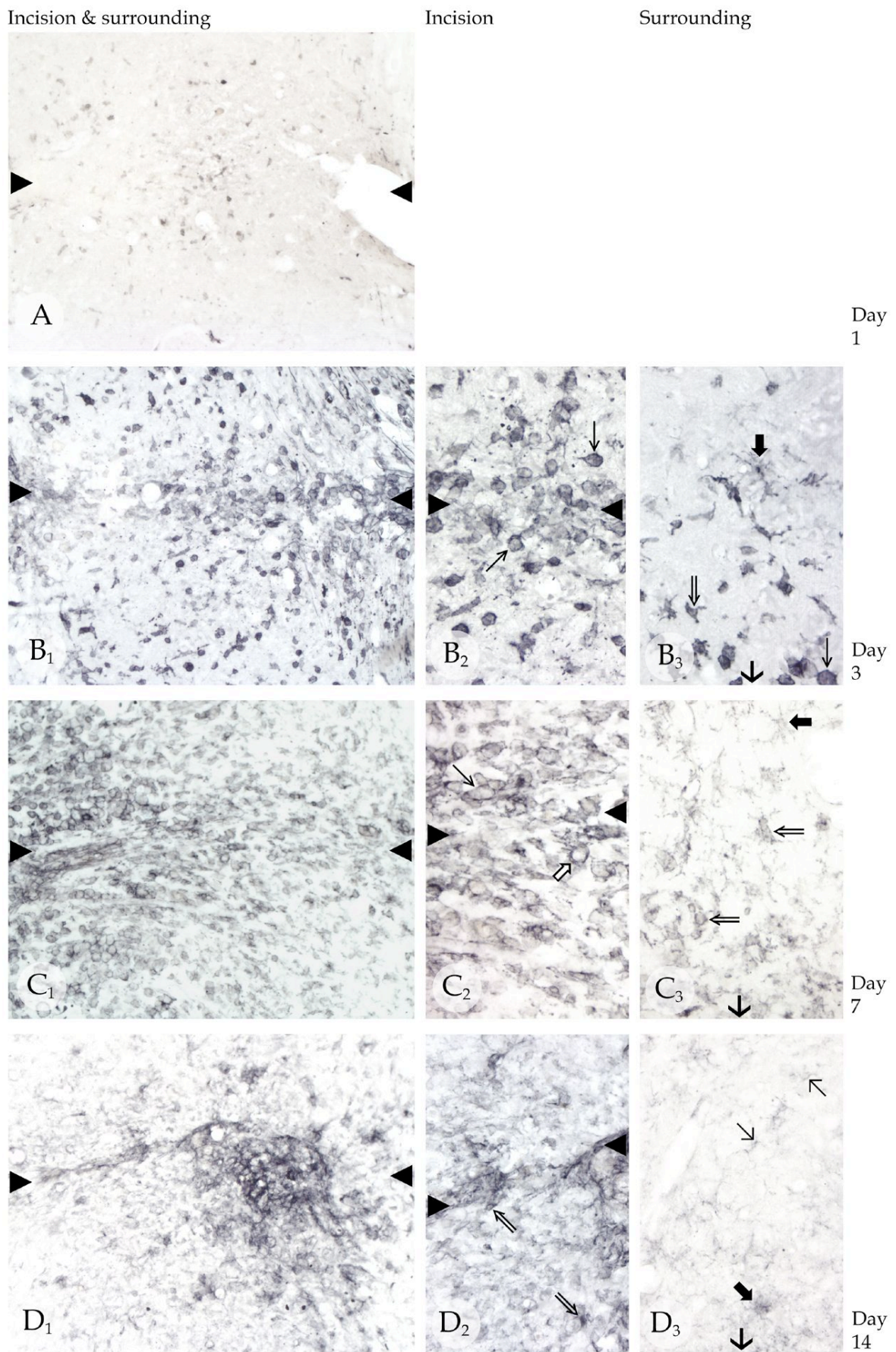


Fig. 52: Summary of F4/80 immunoreactivity at the incision site and the surrounding area for TNC^{-/-} knock out mice (for legend see next page).

Fig. 52: Summary of F4/80 immunostaining at the incision site for TNC^{-/-} knock out mice after one (A), three (B₁, B₂), seven (C₁, C₂) and fourteen (D₁, D₂) days and for the surrounding area after three (B₃), seven (C₃) and fourteen (D₃) days following spinal cord hemisection. Arrowheads (▶) indicate the location of incision. Arrows (→) indicate the direction of the incision. (A) One day post injury no F4/80-positive cells are seen at the incision site; (B₁) Three days post injury heavily labelled F4/80-positive cells, (B₂) mainly phagocytes (→) are seen at the incision site. (B₃) The surrounding area shows F4/80-positive phagocytes (→) close to the incision site, activated microglial cells (⇒) in the intermediate zone and hyper-ramified cells (➤) towards the distant spinal cord; (C₁, C₂) Seven days post injury, the density of phagocytes (→) decreased compared to day three and few F4/80-positive pericytes (⇒) are seen. (C₃) The surrounding area displays activated microglial cells (⇒) near the incision site and hyper-ramified cells (➤) towards the distant spinal cord; (D₁, D₂) Fourteen days post injury the incision site displays activated microglia (⇒). The number of phagocytes has decreased. (D₃) The surrounding area shows few hyper-ramified microglia (➤) near the incision site and resting F4/80-positive microglial cells (→) towards the distant spinal cord.

In summary, F4/80 immunoreactivity at the incision site and the surrounding area shows no difference between genotypes throughout the time course investigated. A, B₁, C₁, D₁: 100x; B₂, B₃, C₂, C₃, D₂, D₃: 200x

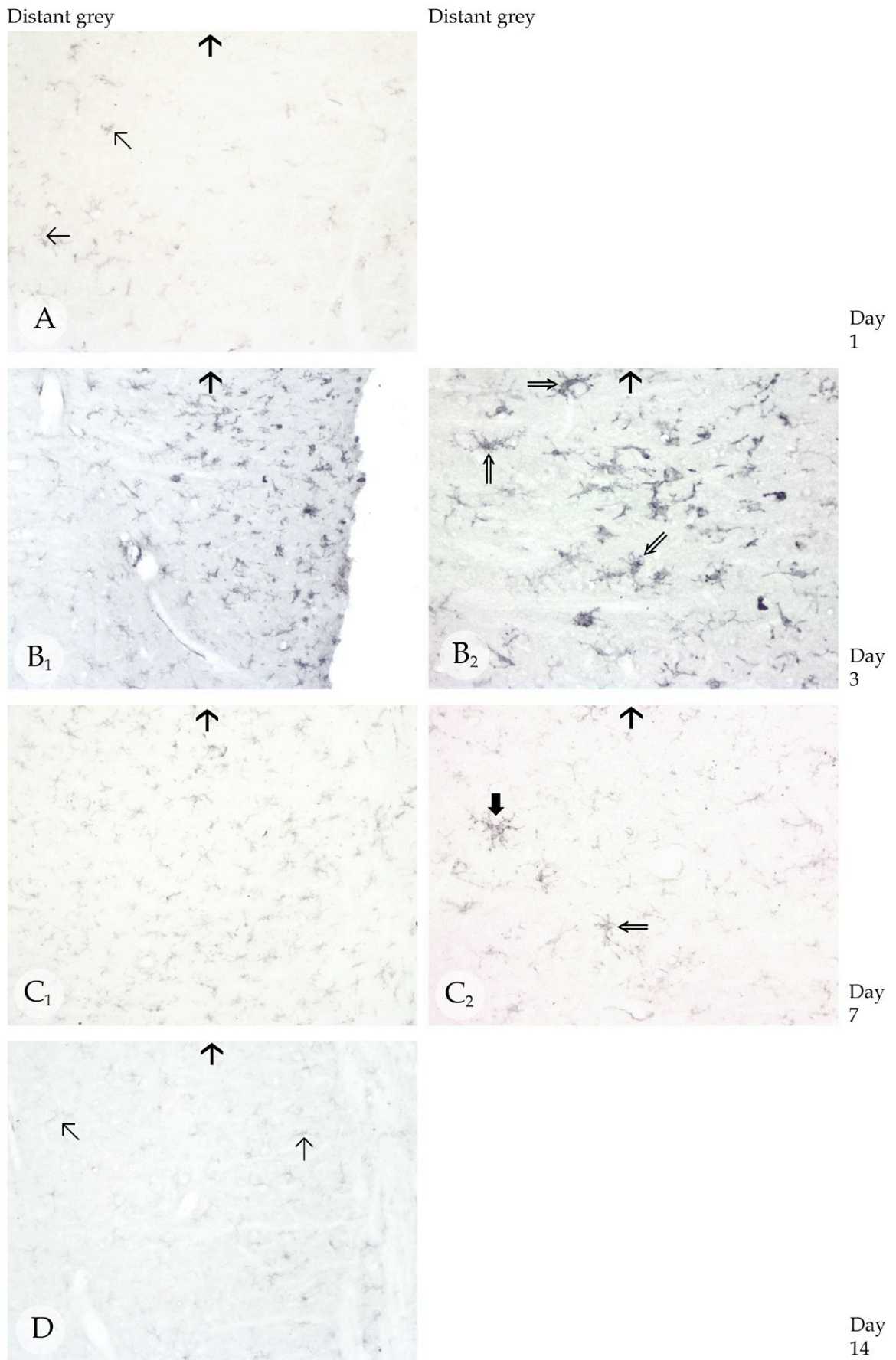


Fig. 53: Summary of F4/80 immunoreactivity at the ipsilateral grey matter distant from the incision site for TNC^{-/-} knock out mice (for legend see next page).

Fig. 53: Summary of F4/80 immunostaining at the ipsilateral grey matter distant from the incision site (distant grey) for TNC^{-/-} knock out mice after one (A), three (B₁, B₂), seven (C₁, C₂) and fourteen (D) days following spinal cord hemisection. Arrows (→) indicate the direction of the incision. (A) One day post injury the distant grey shows F4/80-positive resting microglia (→); (B₁) Three days post injury heavily labelled F4/80 positive cells are seen in the distant grey, (B₂) predominantly activated microglia (⇒); (C₁) Seven days post injury F4/80 immunoreactivity in the distant grey matter has decreased compared to day three, showing (C₂) less activated microglial cells (⇒) and some hyper-ramified microglia (➤); (D) Fourteen days post injury F4/80 immunoreactivity has decreased compared to day seven, predominantly showing resting microglia (→).

In summary, F4/80 immunoreactivity at the ipsilateral distant grey matter shows no difference between genotypes throughout the time course investigated. A, B₁, C₁, D: 100x; B₂, C₂: 200x

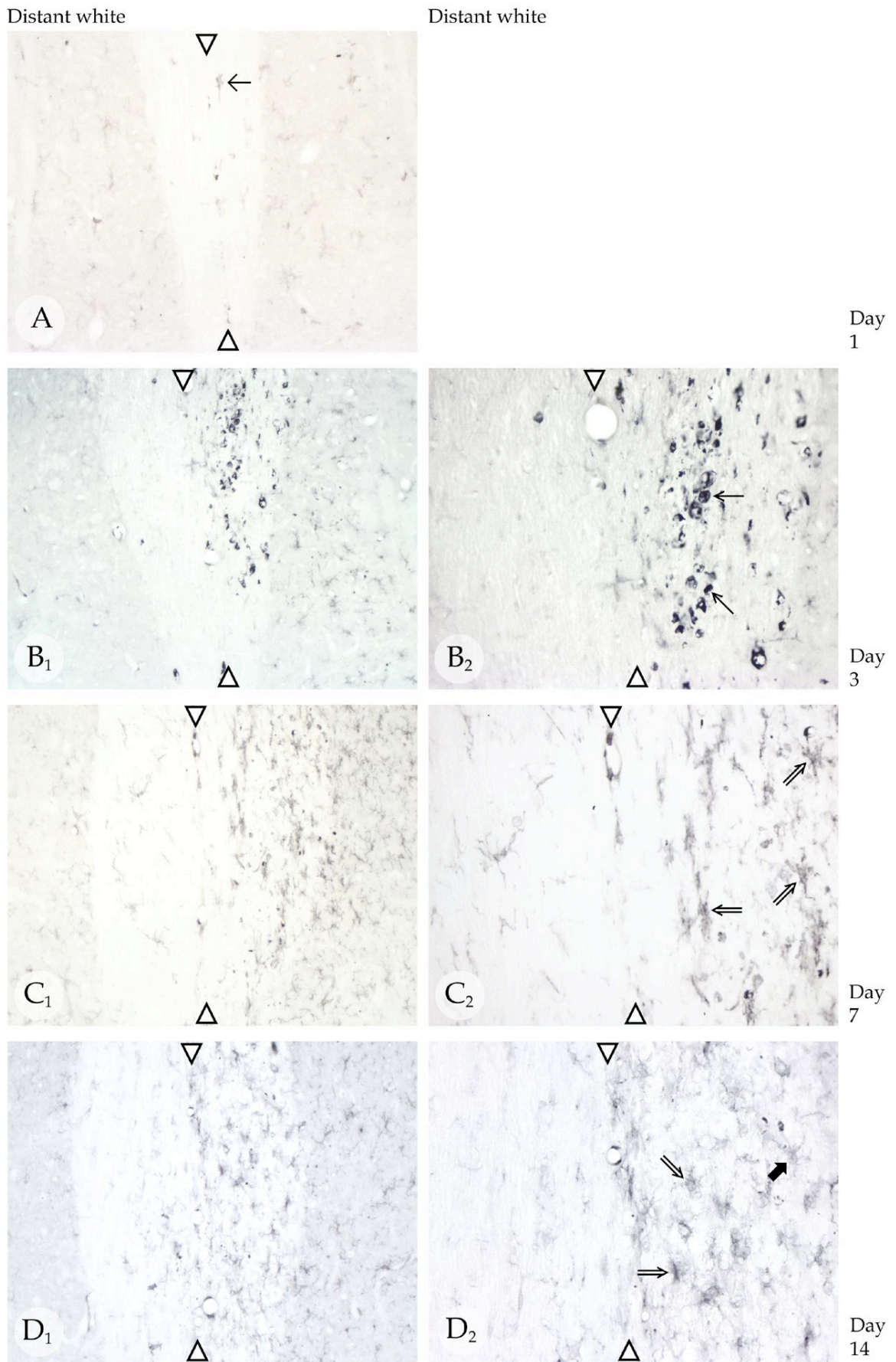


Fig. 54: Summary of F4/80 immunoreactivity at the ipsilateral white matter distant from the incision site for TNC^{-/-} knock out mice (for legend see next page).

Fig. 54: Summary of F4/80 immunoreactivity at the ipsilateral white matter distant from the incision site (distant white) for TNC^{-/-} knock out mice after one (A), three (B₁, B₂), seven (C₁, C₂) and fourteen (D₁, D₂) days following spinal cord hemisection. Arrowheads (▷) indicate the border between ipsilateral (right hand side, incision) and contralateral (left hand side) of the spinal cord. (A) One day post injury the distant white shows faintly labelled F4/80-positive resting microglia (→); (B₁) Three days post injury heavily labelled F4/80-positive cells, (B₂) mainly phagocytes (⇒) and are seen in the distant white matter; (C₁) Seven days post injury, the density of phagocytes in the distant white matter has decreased compared to day three, now (C₂) activated microglial cells (⇒) are the predominant cell type; (D₁) Fourteen days post injury F4/80-positive cells, (D₂) mainly activated microglia (⇒) and hyper-ramified cells (➤) are seen.

In summary, for F4/80 immunoreactivity at the distant white matter, no difference between genotypes is observed throughout the time course investigated. A, B₁, C₁, D₁: 100x; B₂, C₂, D₂: 200x

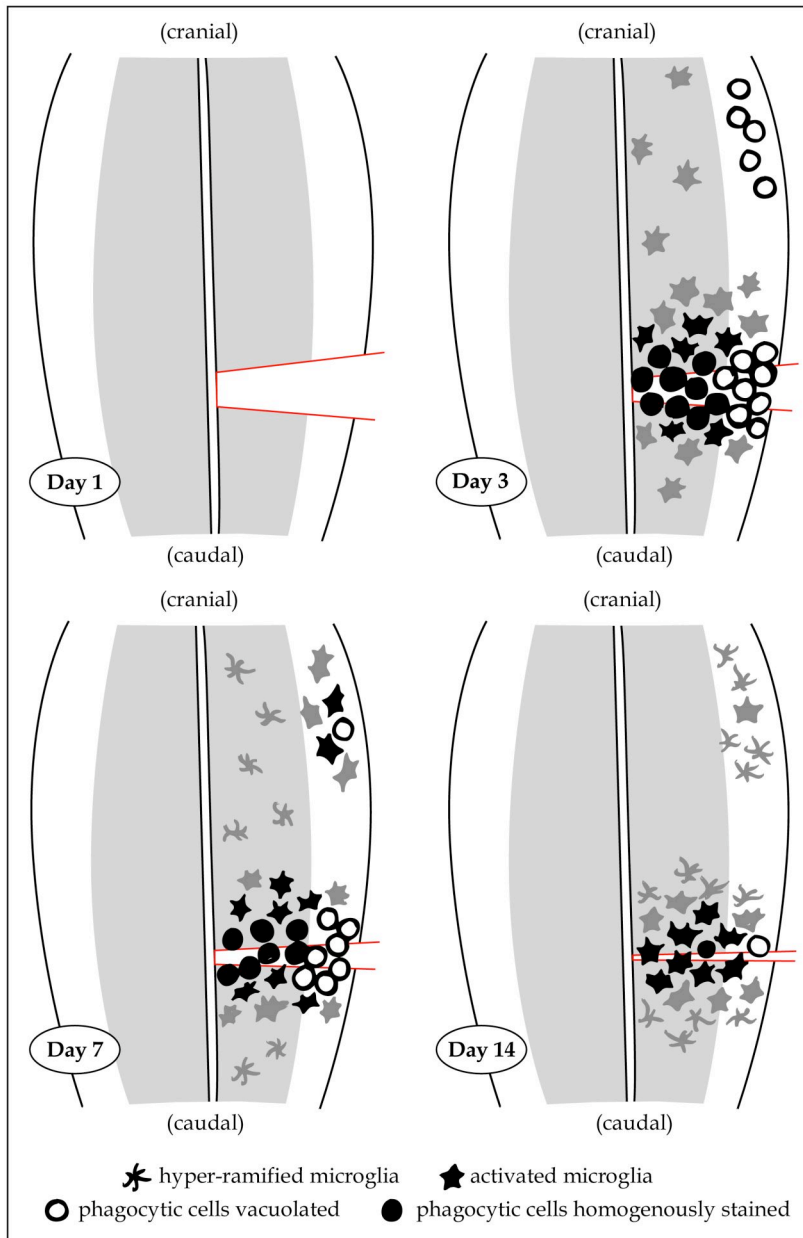


Fig. 55: Summary of changes for F4/80-positive microglia/macrophages for TNC^{-/-} knock out mice after one, three, seven and fourteen days following spinal cord hemisection. The intensity of the immunoreactivity is coded: black - strong; grey - weak. Resting microglia is not shown. Microglial/macrophage activation visualized with F4/80 immunoreactivity is undistinguishable between TNC^{+/+} wild type and TNC^{-/-} knock out mice throughout the time course investigated. For a detailed description see page 76.

4.2.5.2. Quantitative densitometry

On the first day, the median IOD at the incision site was measured as low as 0.5. A steady rise to a median IOD of 23.5 was seen on day three, followed by a steep increase to 82.3 on day seven. On day fourteen, the median IOD reached a maximum of 89.3.

In the surrounding area a median IOD of 0.2 on day one was followed by an increase to 9.0 IOD on day three. The median IOD reached it's maximum on day seven (37.1) and thereafter declined slowly to 13.5 on day fourteen. TNC-/- knock out IOD levels at the incision site and the surrounding area were comparable to TNC+/+ wild type findings.

IOD levels of F4/80 immunoreactivity in the distant grey matter cranial to the incision site showed a straight line. The median IOD on day one (0.1), three (0.6), seven (0.4) and fourteen (0.1) never exceeded levels above one.

Similar to that, the distant grey matter far caudal to the incision site displayed low IOD levels for all post surgery days investigated. Starting with a median IOD of 0.2 on day one, the highest median IOD with 1.3 was reached on day three. On day seven and fourteen the median IOD was 0.8 and 1.1, respectively. TNC-/- knock out IOD values for the distant grey matter far cranial and far caudal were similar to TNC+/+ wild type findings.

F4/80 immunoreactivity at the incision site was significantly higher compared to all other regions throughout the time course investigated. The differences between the incision site and the surrounding area ($p < 0.0001$), between the incision site and the ipsilateral distant grey matter, cranial to the incision ($p < 0.0001$), as well as between the incision site and the ipsilateral distant grey matter, caudal to the incision ($p < 0.0001$) were significant. In addition, a significant influence of the day ($p < 0.0001$) was detected for all regions investigated: The first day differed significantly from day seven ($p = 0.015$) and day fourteen ($p < 0.0001$).

Moreover, the third day differed significantly from day fourteen ($p=0.033$). Genotypes ($p=0.539$) did not differ significantly from each other.

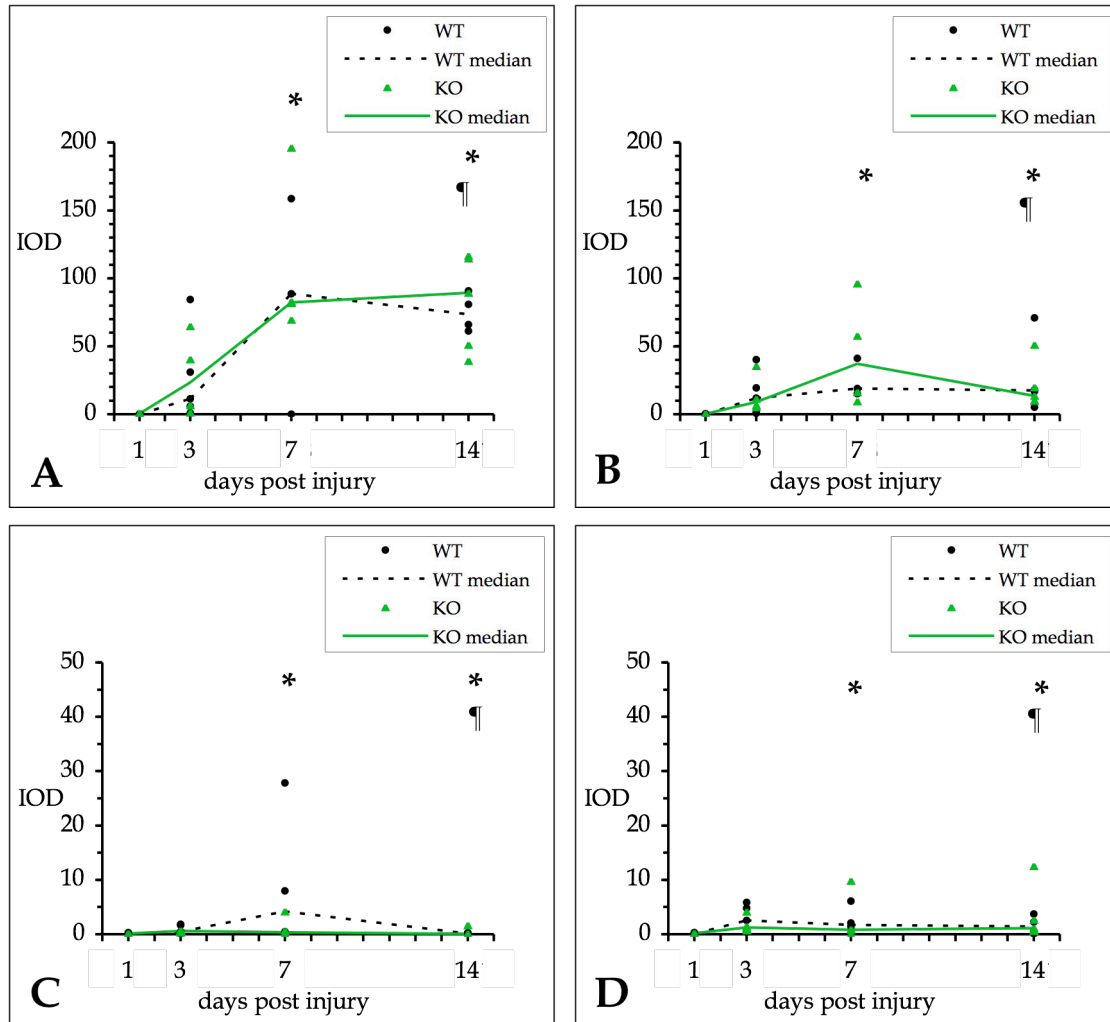


Fig. 56: Integrated optical density (IOD) for F4/80 immunoreactivity as a microglial marker is shown for TNC+/+ wild type (WT, ●) and TNC-/- knock out (KO, ▲) mice from one to fourteen days after spinal cord hemisection at the incision site (A), the surrounding area (B), the distant grey matter approximately 1.5 mm cranial (C) and 1.5 mm caudal (D) to the incision site. Measurements for three to six animals per day are shown. The surrounding area ($p \leq 0.0001$), the distant grey matter, cranial ($p \leq 0.0001$) and the distant grey matter, caudal ($p \leq 0.0001$) show a significant difference to the incision site for both genotypes over the time period investigated. In addition, in both genotypes, the first day differs significantly from day seven ($p \leq 0.05$) (*) and day fourteen ($p \leq 0.0001$) (*); and the third day differs significantly from day fourteen ($p \leq 0.05$) (¶) for all regions investigated. A significant difference between genotypes is not detected.

4.2.6. GFAP

4.2.6.1. Morphology

GFAP-positive astrocytes in the normal control of TNC^{-/-} knock out mice showed the same shape, distribution and staining intensity of astrocytes seen in the normal control of TNC^{+/+} wild type mice.

Throughout the time course investigated, no difference for GFAP immunoreactivity, i. e. astroglial reaction was observed between TNC^{-/-} knock out and TNC^{+/+} wild type mice (Fig. 57A, B₁, B₂, C₁, C₂, D₁, D₂, 58A, B₁, B₂, C₁, C₂, D, 59A, B₁, B₂, C₁, C₂, D). For a detailed description of GFAP immunoreactivity see chapter 4.1.6.1.

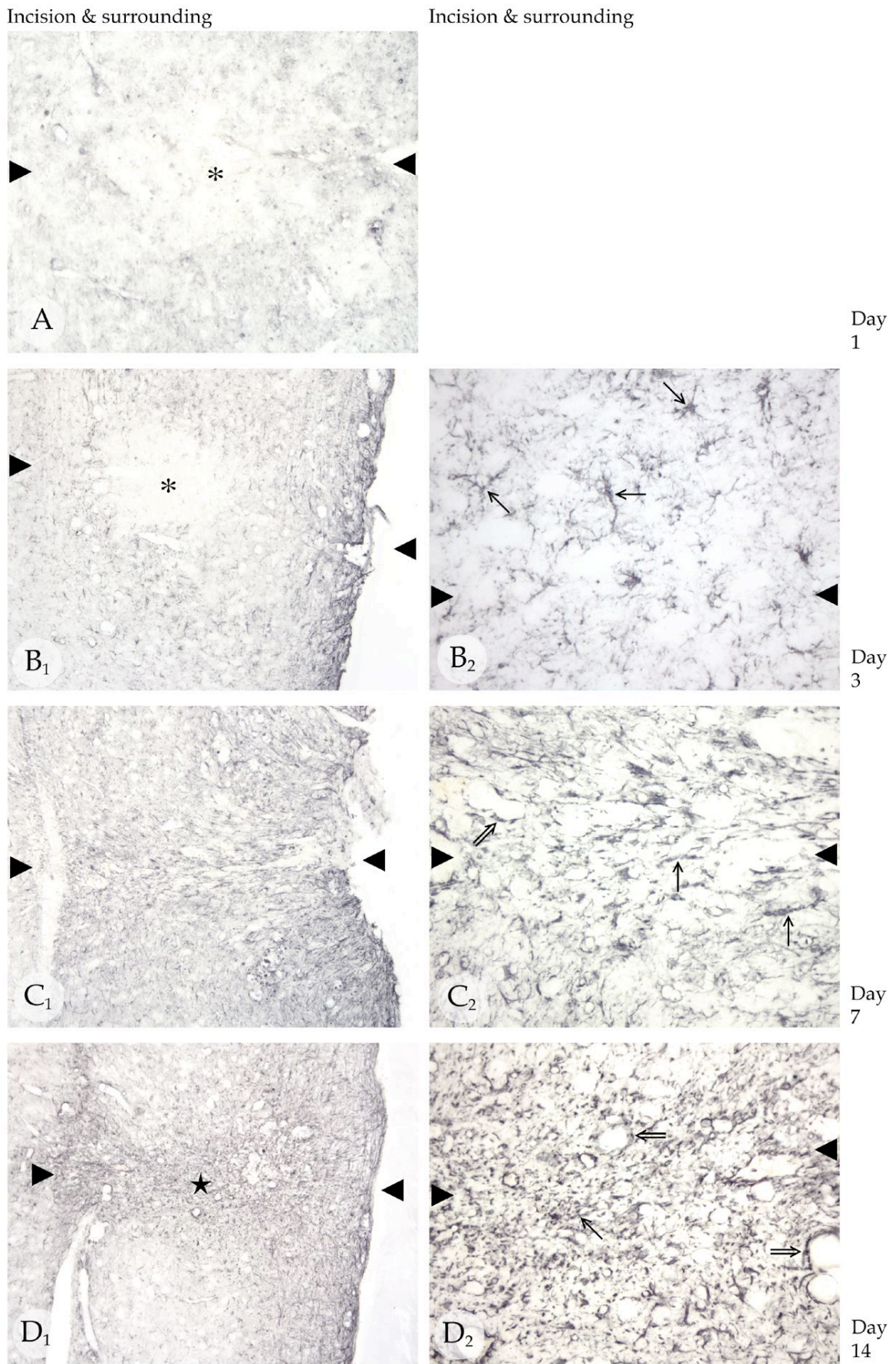


Fig. 57: Summary of GFAP immunoreactivity at the incision site for TNC^{-/-} knock out mice (for legend see next page).

Fig. 57: Summary of GFAP immunoreactivity at the incision site for TNC^{-/-} knock out mice after one (A), three (B₁, B₂), seven (C₁, C₂) and fourteen (D₁, D₂) days following spinal cord hemisection. Arrowheads (►) indicate the location of incision. (A) One day post injury the incision site is GFAP-negative (*); (B₁) Three days post injury GFAP immunoreactivity spares the incision centre (*), while (B₂) reactive astrocytes (→) form a rim around the incision site; (C₁) Seven days post injury GFAP immunoreactivity at the incision site has increased compared to day three, showing (C₂) reactive astrocytes (→) along the incision site and GFAP-positive cells (⇒) around small cavitations; (D₁) Fourteen days post injury the strongest immunoreactivity for GFAP is seen, showing a fully developed astroglial scar (★), with (D₂) tightly interwoven processes of reactive astrocytes (→) and GFAP-positive cells (⇒) lining small cavitations.

In summary, no difference in GFAP immunoreactivity, i. e. astroglial scarring is observed between genotypes throughout the time course investigated. A, B₁, C₁, D₁: 100x; B₂, C₂, D₂: 200x

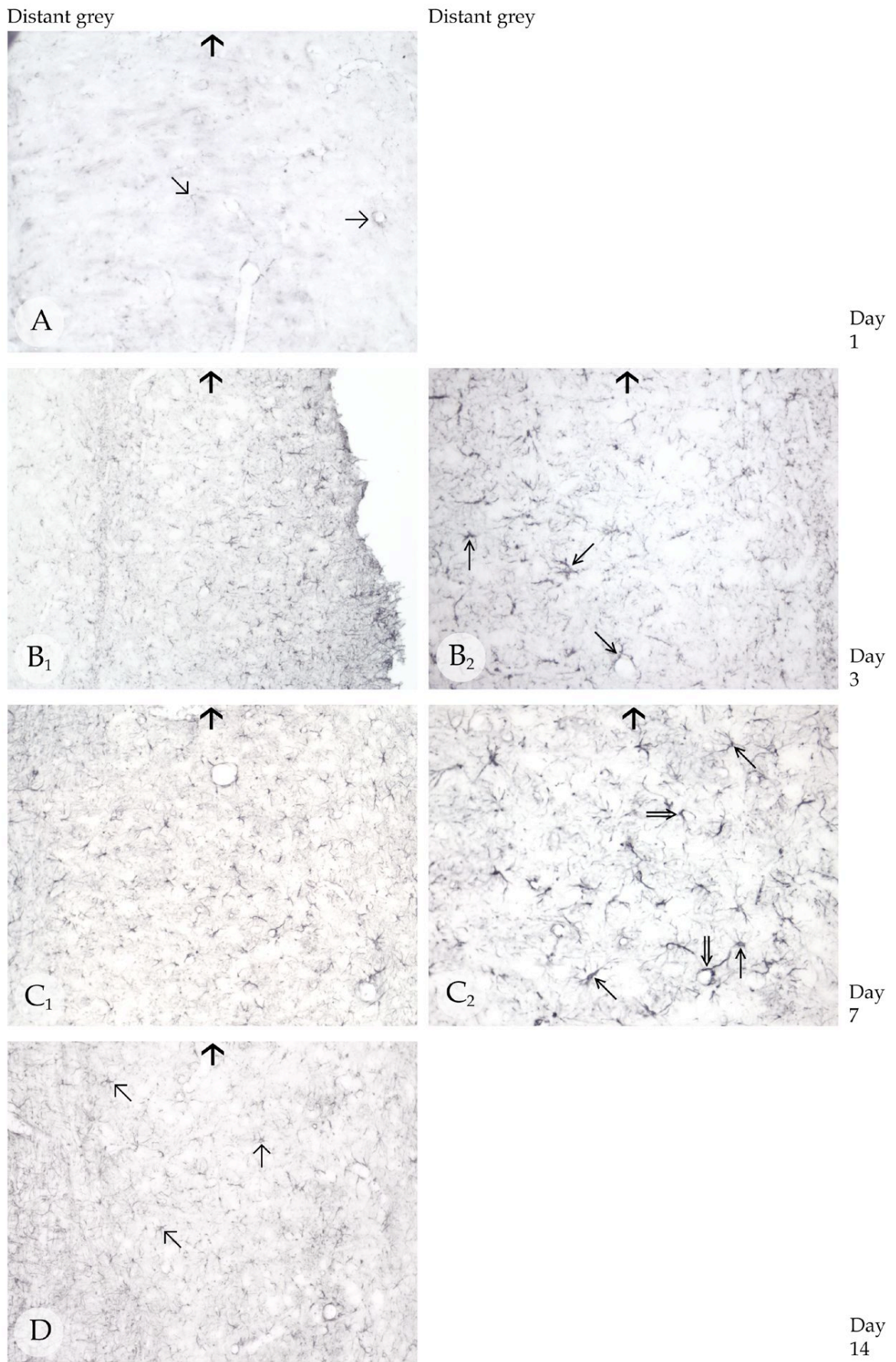


Fig. 58: Summary of GFAP immunoreactivity at the ipsilateral grey matter distant from the incision site for TNC^{-/-} knock out mice (for legend see next page).

Fig. 58: Summary of GFAP immunoreactivity at the ipsilateral grey matter distant from the incision site (distant grey) for TNC^{-/-} knock out mice after one (A), three (B₁, B₂), seven (C₁, C₂) and fourteen (D) days following spinal cord hemisection. Arrows (→) indicate the direction of the incision. (A) One day post injury the distant grey shows GFAP-positive protoplasmatic astrocytes (→); (B₁) Three days post injury GFAP immunoreactive cells in the distant grey matter, (B₂) mainly reactive astrocytes (→) are seen; (C₁) Seven days post injury GFAP immunoreactivity in the distant grey matter is similar compared to day three, (C₂) still showing reactive astrocytes (→) and some GFAP-positive cells surrounding vessels (⇒) are seen; (D) Fourteen days post injury GFAP immunoreactivity in the distant grey matter has decreased compared to day seven, now showing protoplasmatic astrocytes (→).

In summary, GFAP immunoreactivity at the ipsilateral grey matter distant from the incision site shows no difference between genotypes for the time period studied. A, B₁, C₁, D: 100x; B₂, C₂: 200x

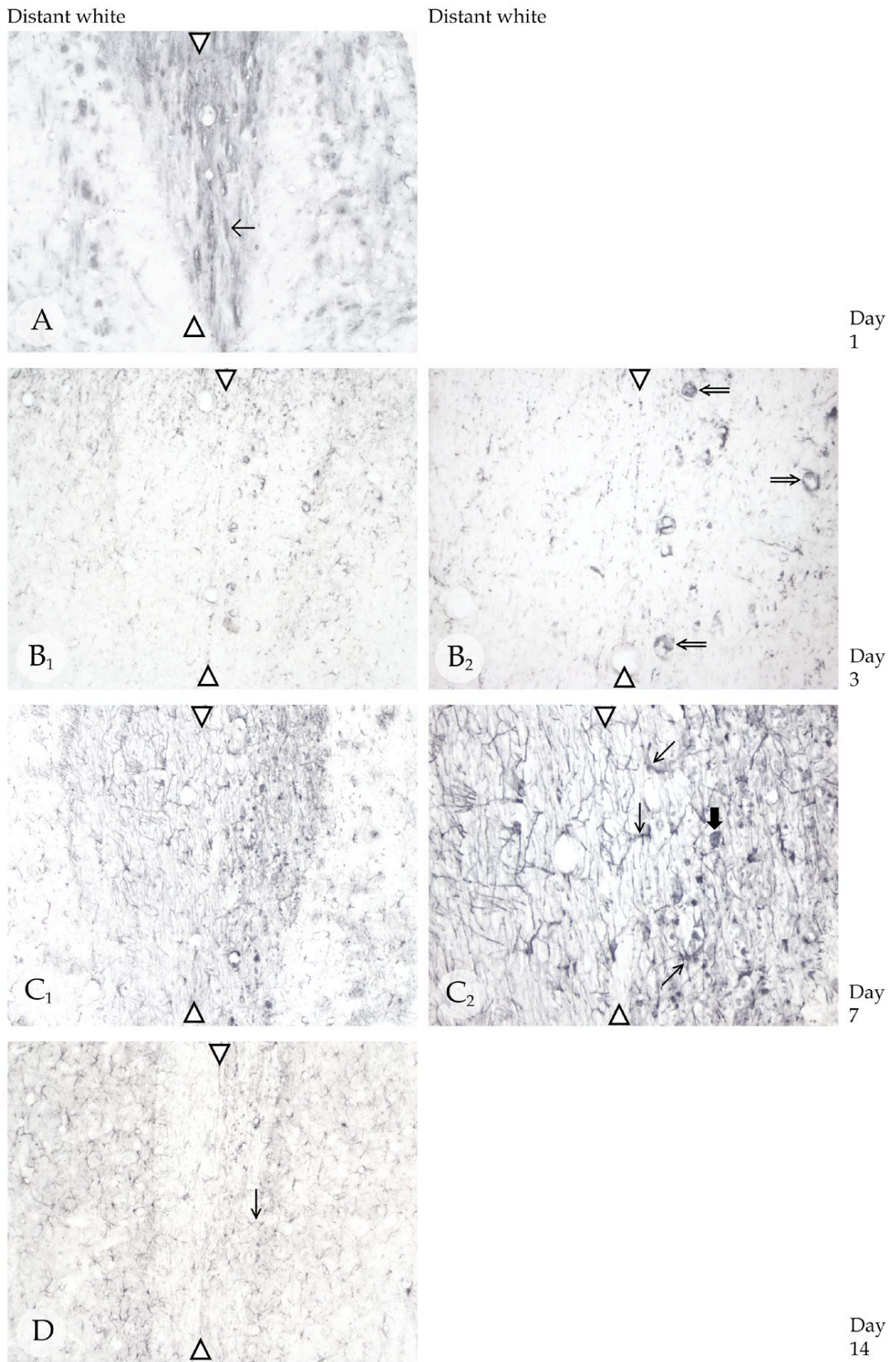


Fig. 59: Summary of GFAP immunoreactivity at the ipsilateral white matter distant from the incision site for TNC^{-/-} knock out mice (for legend see next page).

Fig. 59: Summary of GFAP immunoreactivity at the ipsilateral white matter distant from the incision site (distant white) for TNC^{-/-} knock out mice after one (A), three (B₁, B₂), seven (C₁, C₂) and fourteen (D) days following spinal cord hemisection. Arrowheads (▷) indicate the border between ipsilateral (right hand side, incision) and contralateral (left hand side) of the spinal cord. (A) One day post injury the distant white matter shows fibrous astrocytes (→); (B₁) Three days post injury GFAP-positive cells, (B₂) mainly vacuolated phagocytic-like astrocytes (⇒) are seen in the distant white matter; (C₁) Seven days post injury, phagocytic-like astrocytes have decreased, instead GFAP-positive reactive astrocytes (→) with multiple cytoplasmatic extensions are seen. In addition, non-specific labelling of cell debris (➤) is frequently seen; (D) Fourteen days post injury GFAP immunoreactivity in the distant white matter has decreased compared to day seven, now showing fewer reactive astrocytes (→).

In summary, for GFAP immunoreactivity at the ipsilateral white matter distant from the incision site, no difference between genotypes is observed for the time period tested. A, B₁, C₁, D: 100x; B₂, C₂: 200x

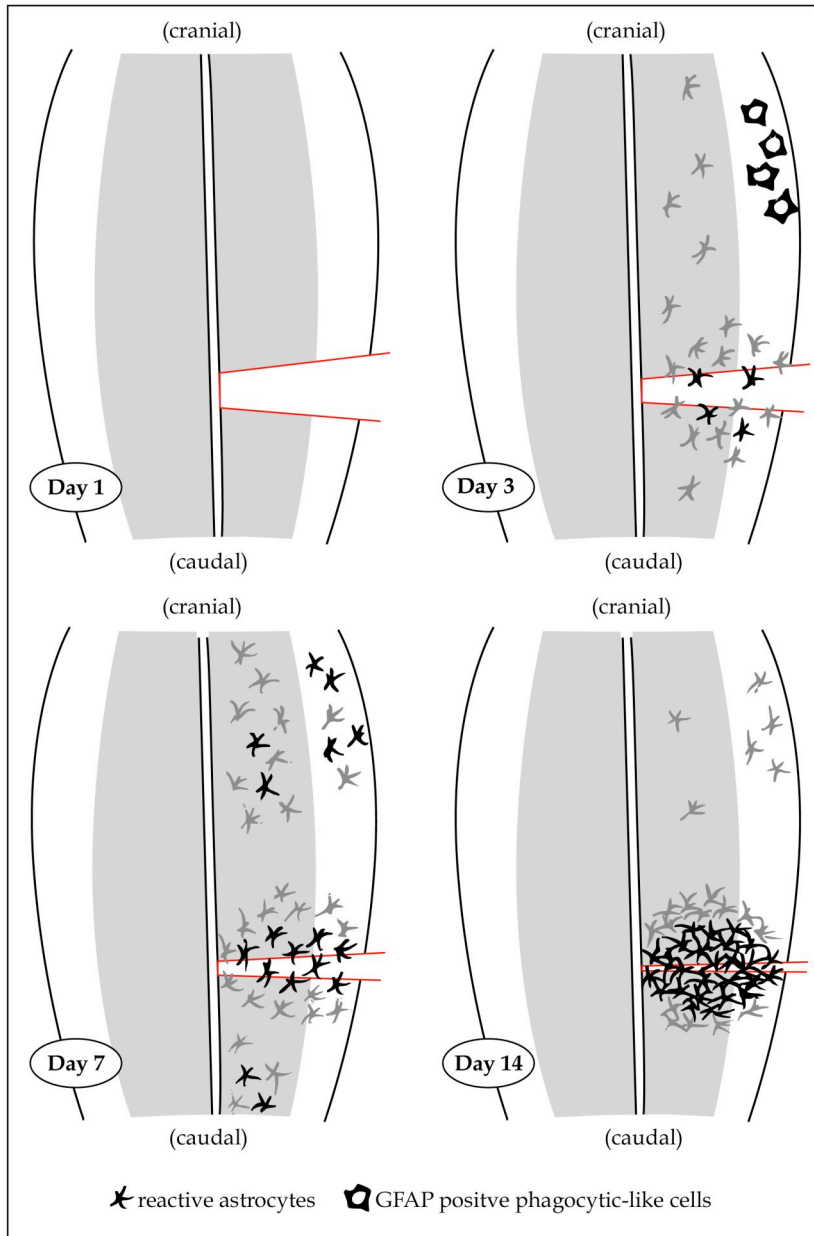


Fig. 60: Summary of changes for GFAP-positive astrocytes for TNC^{-/-} knock out mice after one, three, seven and fourteen days following spinal cord hemisection. The intensity of the immunoreactivity is coded: black - strong; grey - weak. Non-reactive protoplasmatic and fibrous astrocytes are not shown. GFAP staining; i. e. astroglial reaction is undistinguishable between TNC^{+/+} wild type and TNC^{-/-} knock out mice throughout the time course investigated. For a detailed description see page 88.

4.2.6.2. Quantitative densitometry

IOD levels of GFAP immunoreactivity (astrocytes) at the incision site showed a steady rise throughout the time course. Starting off with a median IOD of 0.0 on day one and 3.6 on day three, the level of 6.7 was reached on day seven, resulting in a maximum median IOD of 15.3 on day fourteen.

GFAP immunoreactivity in the surrounding area showed a slight curve, beginning with a median IOD of 0.7 on day one. An increase to a median IOD of 7.0 on day three was followed by a maximum median IOD of 7.4 on day seven. Subsequently a slight decline to a median IOD of 4.6 on day fourteen was observed. Median IOD levels of TNC^{-/-} knock out mice were comparable to TNC^{+/+} wild type findings at the incision site and the surrounding area.

Astrocytes in the distant grey matter far cranial to the incision site showed low median IOD levels of 0.1 and 0.4 on day one and day three, respectively. A maximum of 2.5 IOD on day seven followed a decline to a median IOD level of 0.9 on day fourteen.

Astrocytes in the distant grey matter far caudal to the incision site also showed low median IOD levels with 0.1 and 1.9 on day one and three, respectively. The maximum was reached with a median IOD of 4.8 on day seven, followed by a steady decline to a median IOD of 1.4 on day fourteen. For both regions, the distant grey matter far cranial and far caudal from the incision site, TNC^{-/-} knock out mice showed IOD values similar to TNC^{+/+} wild type findings.

GFAP distribution at the incision site was significantly higher than in the distant grey matter cranially ($p < 0.0001$) and caudally ($p = 0.001$) from the incision site throughout the time period investigated. The difference between the incision site and the surrounding area was not significant ($p = 0.391$) throughout the time course tested. A significant influence of the day ($p = 0.001$) was detected with ANOVA for repeated measurements. Post-hoc comparisons by the method of

Games-Howell revealed that the first day differed significantly from day seven ($p=0.014$) and day fourteen ($p<0.0001$) for all regions tested. No significant difference between the genotype ($p=0.875$) for all regions and for all post surgery days investigated was observed.

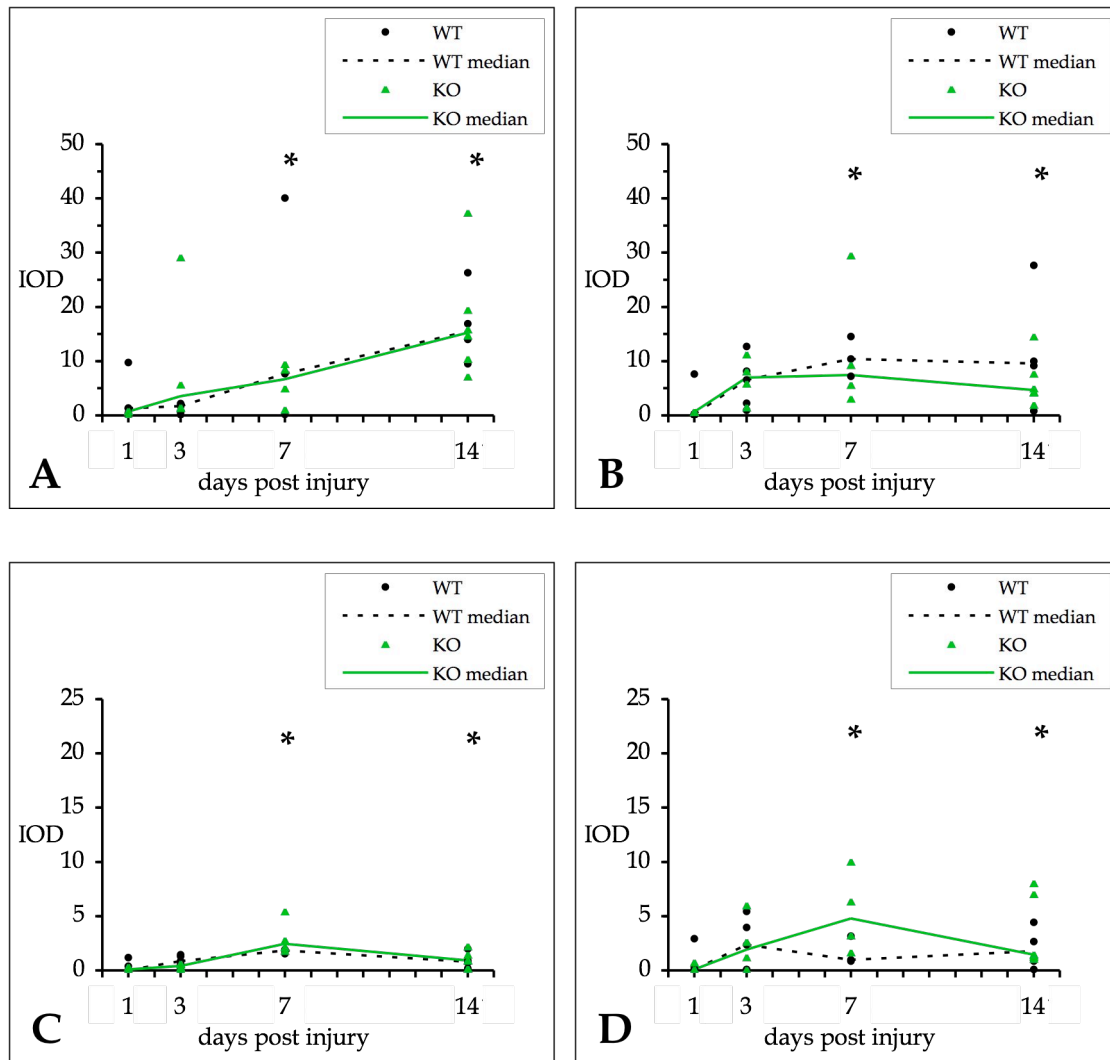


Fig. 61: Integrated optical density (IOD) for GFAP immunoreactivity as an astroglial marker is shown for TNC+/+ wild type (WT, ●) and TNC-/- knock out (KO, ▲) mice from one to fourteen days after spinal cord hemisection at the incision site (A), the surrounding area (B), the distant grey matter approximately 1.5 mm cranial (C) and 1.5 mm caudal (D) to the incision site. Measurements for three to six animals per day are shown. The distant grey matter, cranial ($p\leq 0.0001$), and the distant grey matter, caudal ($p\leq 0.001$) show a significant difference to the incision site for both genotypes throughout the time period investigated. The difference between the incision site and the surrounding area is not significant. For both genotypes the first day differs significantly from day seven ($p\leq 0.05$) (*) and day fourteen ($p\leq 0.0001$) (*) for all regions tested. The genotype has no significant influence on astrocyte distribution.

4.2.7. Neurofilament

4.2.7.1. Morphology

The normal control of TNC^{-/-} knock out mice showed the same distribution and staining intensity of NF immunoreactivity, compared to TNC^{+/+} wild type animals. No difference in the symmetry of white and grey matter or any structural abnormality was observed between genotypes.

On the first day post surgery, a difference between TNC^{-/-} knock out and TNC^{+/+} wild type mice was observed. The surrounding white matter in TNC^{-/-} knock out animals displayed a markedly lower staining intensity of thick NF-positive fibres compared to TNC^{+/+} wild type mice. However, the morphology of the surrounding white matter was similar in both genotypes, i. e. swollen and deformed thick NF-positive fibres (Fig. 62A₃).

The incision site (Fig. 62A₁), the surrounding grey matter (Fig. 62A₂) and the distant CST cranial to the incision site (Fig. 63A) were unaltered, compared to TNC^{+/+} wild type findings on the first day post surgery. For a detailed morphological description of NF immunoreactivity see chapter 4.1.7.1.

Three days post surgery, the surrounding white matter again showed a difference in NF immunoreactivity. NF immunoreactivity in the surrounding white matter was considerably lower, compared to TNC^{+/+} wild type mice. In addition, thick NF-positive fibres were seen less frequently compared to TNC^{+/+} wild type findings, demonstrating the early collapse of the formerly well-defined axons in the surrounding white matter (Fig. 62B₃). Thin NF-positive fibres, which were only seen in large quantities on days seven in TNC^{+/+} wild type mice, were already scattered throughout the surrounding white matter.

The remaining regions on day three were indistinguishable between genotypes. The incision site (Fig. 62B₁), the surrounding grey matter (Fig. 62B₂) and the distant CST (Fig. 63B₁, B₂) were unaltered, compared to TNC^{+/+} wild type findings. For a detailed morphological description see chapter 4.1.7.1.

On day seven, none of the regions studied revealed a difference in NF immunoreactivity between genotypes (Fig. 62C₁-C₃, 63C₁, C₂). For a detailed morphological description of NF immunoreactivity see chapter 4.1.7.1.

Fourteen days after injury, the incision site adjacent to the grey matter surrounding showed a marked difference between genotypes. Along the incision edges of the grey matter, a higher density of thin NF-positive fibres was observed compared to TNC^{+/+} wild type findings (Fig. 62D₂).

The surrounding grey and white matter (Fig. 62D₃), as well as the distant CST (Fig. 63D₁, D₂) showed no difference in NF immunoreactivity between TNC^{-/-} knock out and TNC^{+/+} wild type mice on day fourteen. For a detailed morphological description of NF immunoreactivity see chapter 4.1.7.1.

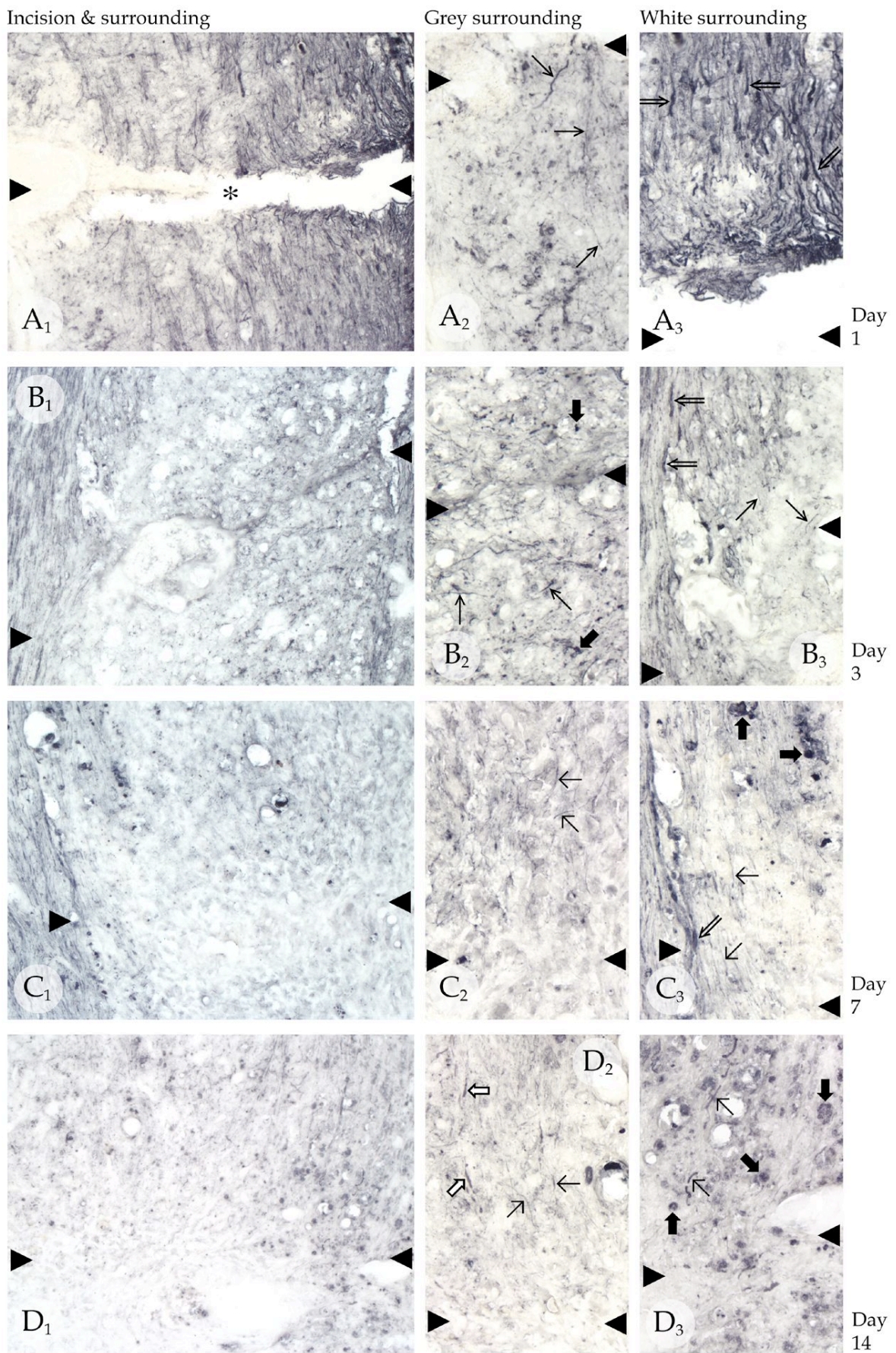


Fig. 62: Summary of neurofilament immunoreactivity at the incision site and in the immediate grey and white surrounding for TNC^{-/-} knock out mice (for legend see next page).

Fig. 62: Summary of neurofilament (NF) immunoreactivity at the incision site and in the immediate grey and white surrounding for TNC^{-/-} knock out mice after one (A₁, A₂, A₃), three (B₁, B₂, B₃), seven (C₁, C₂, C₃) and fourteen (D₁, D₂, D₃) days following spinal cord hemisection. Arrowheads (▶) indicate the location of incision. (A₁) One day post injury the incision site is NF-negative (*). (A₂) NF-positive thin fibres (→) meander through the surrounding grey matter in a disorganized way. (A₃) The surrounding white matter displays NF-positive thick fibres (⇒), with a lower staining intensity for NF immunoreactivity compared to TNC^{+/+} wild type mice; (B₁) Three days post injury the incision edges are adjacent. (B₂) The grey surrounding displays thin NF-positive fibres (→) and NF-positive necrotic material (◆). (B₃) The surrounding white matter displays less thick NF-positive fibres (⇒) compared to TNC^{+/+} wild type mice. Instead thin NF-positive fibres (→) are already seen in the surrounding white matter of TNC^{-/-} knock out mice; (C₁) Seven days post injury the incision site is pale, NF immunoreactivity being lower compared to day three. (C₂) Thin NF-positive fibres (→), with a club shaped end, representing growth cones are obvious in the surrounding grey matter. (C₃) Thick NF-positive fibres (⇒) are seen less frequently in the surrounding white matter compared to day three. Instead thin NF-positive fibres (→) are seen more often and NF-positive necrotic material (◆) is prominent in surrounding white matter; (D₁, D₂) Fourteen days post injury the incision site adjacent to the grey matter shows thin NF-positive fibres (→) more frequently compared to TNC^{+/+} wild type mice, where these fibres are only seen sporadically. These thin NF-positive fibres often show growth cones (⇨). (D₃) The usually well-defined white matter tract has completely disappeared. NF-positive necrotic material (◆) dominates the picture and some thin NF-positive fibres (→) are seen in the surrounding white matter.

In summary, on the first and third day TNC^{-/-} knock out animals show a considerably lower staining intensity for NF immunoreactivity in the surrounding white matter, indicating an earlier collapse of axons compared to TNC^{+/+} wild type mice. On day seven no difference in NF immunoreactivity is observed between genotypes. However, on day fourteen, a considerable difference between genotypes is seen at the incision site adjacent to the grey matter. TNC^{-/-} knock out animals show a markedly higher density of thin NF-positive fibres along the incision edges compared to TNC^{+/+} wild type findings. A₁, B₁, C₁, D₁: 100x; A₂, A₃, B₂, B₃, C₂, C₃, D₂, D₃: 200x

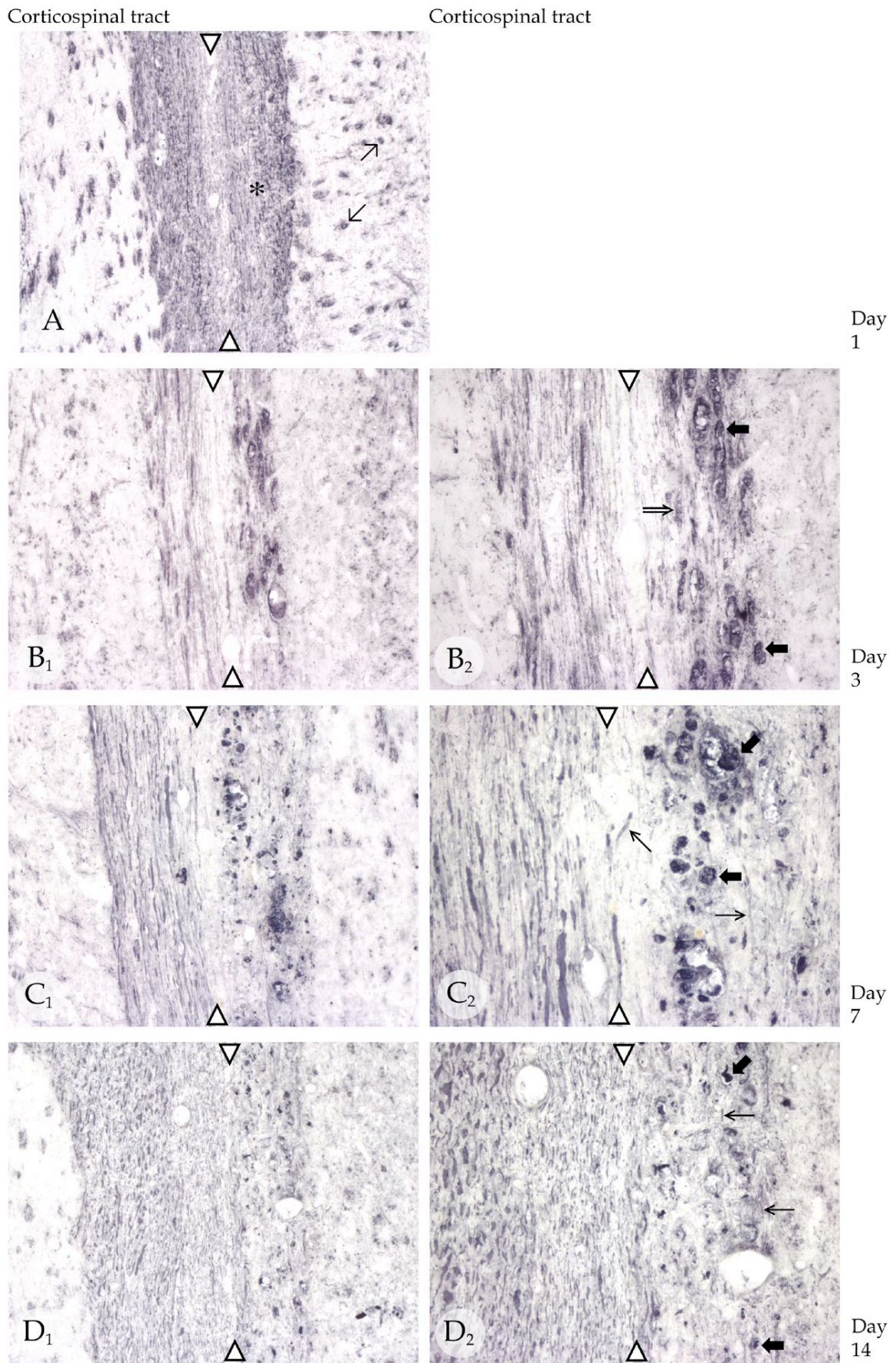


Fig. 63: Summary of neurofilament immunoreactivity at the ipsilateral corticospinal tract distant from the incision site for TNC^{-/-} knock out mice (for legend see next page).

Fig. 63: Summary of neurofilament (NF) immunoreactivity at the ipsilateral white matter distant from the incision site (distant corticospinal tract (CST)) for TNC^{-/-} knock out mice after one (A), three (B₁, B₂), seven (C₁, C₂) and fourteen (D₁, D₂) days following spinal cord hemisection. Arrowheads (\triangleright) indicate the border between ipsilateral (right hand side, incision) and contralateral (left hand side) of the spinal cord. (A) One day post injury the distant CST shows thick NF-positive fibres in a regular distribution. The ipsilateral grey matter distant from the incision site displays strongly labelled NF-positive round spots, representing axons in a transverse cut (\rightarrow); (B₁) Three days post injury the distant CST shows an irregular pattern of (B₂) oedematous NF-positive fibres (\Rightarrow) and necrotic material (\blacktriangleright); (C₁, C₂) Seven days post injury NF immunoreactivity in the distant CST displays severe axonal damage. NF-positive necrotic material (\blacktriangleright) dominates the picture. NF-positive fibres (\rightarrow), which are now lightly labelled are seen less frequently, compared to day three; (D₁) Fourteen days post injury the formerly well-defined distant CST is completely destroyed. (D₂) Necrotic material (\blacktriangleright) dominates the picture with few thin NF-positive fibres (\rightarrow).

In summary, for NF immunoreactivity at the distant CST, no difference is observed between TNC ^{+/+} wild type and TNC ^{-/-} knock out mice throughout the time course investigated. A, B₁, C₁, D₁: 100x; B₂, C₂, D₂: 200x

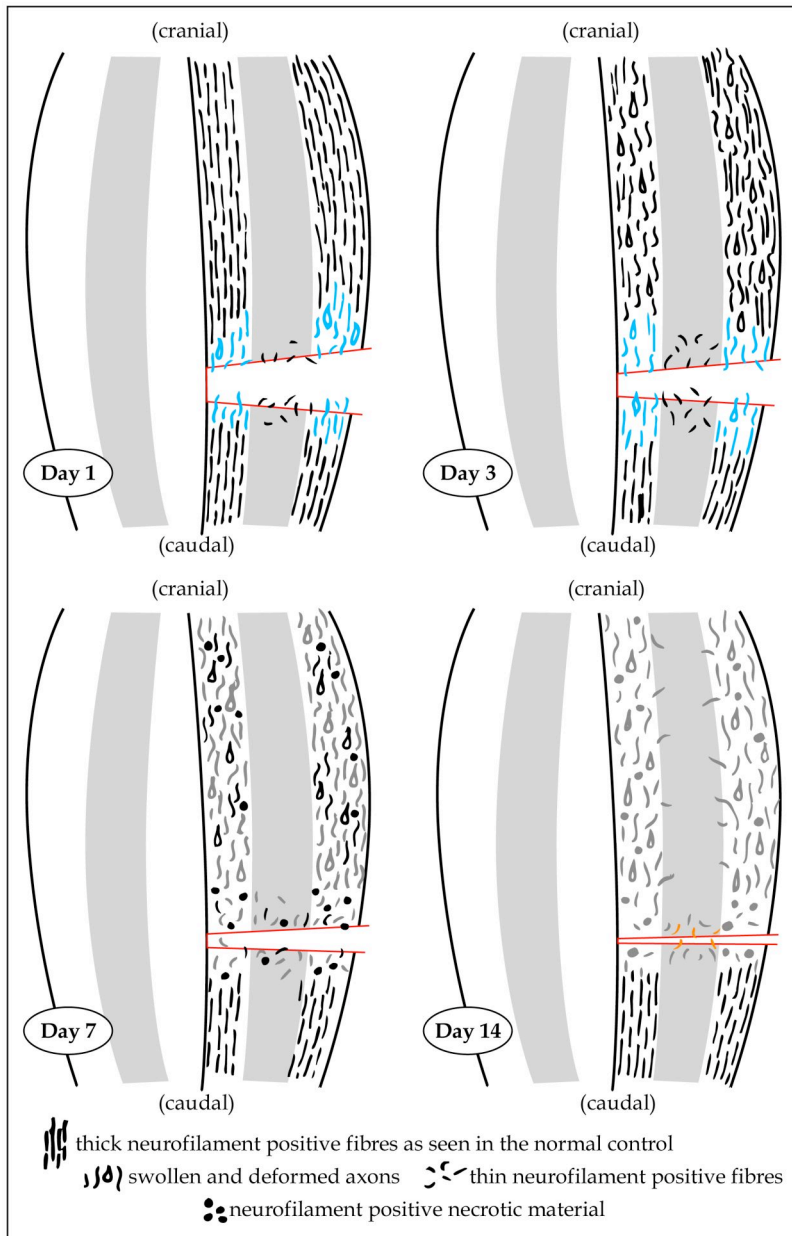


Fig. 64: Summary of changes for neurofilament (NF) for TNC^{-/-} knock out mice after one, three, seven and fourteen days following spinal cord hemisection. The intensity of the immunoreactivity is coded: black - strong; grey - weak. Normal NF staining pattern on the contralateral site of the incision is not shown. Objects highlighted in blue demonstrate less NF immunoreactivity, objects highlighted in orange demonstrate more NF immunoreactivity compared to TNC^{+/+} wild type animals. For NF immunoreactivity a considerable difference between the two genotypes is observed. On the first and third day post surgery TNC^{-/-} knock out animals show a considerably lesser staining intensity for NF immunoreactivity in the surrounding white matter. Thick NF-positive fibres on day one are less intensely labelled in TNC^{-/-} knock out mice than in TNC^{+/+} wild type mice. On day three fibres are seen less frequently in the surrounding white matter compared to TNC^{+/+} wild type mice. On day seven, no difference in NF immunoreactivity is observed between genotypes. However, on day fourteen, a considerable difference between genotypes is seen at the incision site adjacent to the grey matter. TNC^{-/-} knock out mice show a markedly higher density of thin NF fibres along the incision edges in the grey matter compared to TNC^{+/+} wild type animals.

4.2.7.2. Quantitative densitometry

As in TNC^{+/+} wild type mice, measurements in the grey matter revealed much lower IOD levels compared to measurements in the white matter.

The incision site next to the grey matter showed a median IOD of 10.6 on day one and 16.1 on day three. A slow decline to a median IOD of 2.0 was seen on day seven, followed by a considerable rise to a median IOD of 33.7 on day fourteen. All, but one TNC^{-/-} knock out animal, revealed markedly higher IOD values on day fourteen, compared to TNC^{+/+} wild type mice. The median IOD of TNC^{+/+} wild type mice on day fourteen was only 0.2, compared to 33.7 in TNC^{-/-} knock out mice. This indicated a higher NF immunoreactivity along the incision edges adjacent to the grey matter in TNC^{-/-} knock out mice, compared to TNC^{+/+} wild type animals.

The incision site next to the white matter showed a median IOD of 37.8 on day one and a maximum of 42.5 on day three. This was followed by a decline to a medium IOD of 7.1 on day seven and a considerable increase to 20.9 on day fourteen. For the incision site adjacent to the white matter, NF immunoreactivity was similar in both genotypes.

The surrounding grey matter cranial to the incision site showed its maximum on day one with a median IOD of 35.6. On day three a steep decline to the lowest point of 6.9 was observed. Subsequently, a median IOD of 13.0 and 15.0 was seen on day seven and fourteen, respectively. The surrounding grey matter, cranial to the incision site, showed IOD levels comparable to TNC^{+/+} wild type mice.

The surrounding grey matter caudal to the incision site showed the highest level on day one with a median IOD of 17.4. A decline to the lowest point with a median IOD of 10.2 was seen on day three. Subsequently, the curve stabilized on a median IOD of 16.0 and 20.5 on day seven and fourteen, respectively. In the surrounding grey matter, caudal to the incision site quantitative densitometry was comparable between genotypes.

The surrounding white matter cranial to the incision site showed a maximum median IOD of 111.3 on day one. The curve steadily declined to a median IOD of 47.7 on day three and to the lowest point of 39.4 IOD on day seven. Subsequently, a slow increase of the median IOD was seen up to 66.0 on day fourteen. For the surrounding white matter, cranial to the incision site a difference between genotypes was observed. On day one and three, the median IOD of TNC^{-/-} knock out mice was considerably lower compared to TNC^{+/+} wild type animals. For TNC^{-/-} knock out mice the median IOD of day one was 111.3 compared to 196.8 in TNC^{+/+} wild type animals. On day three, the median IOD of TNC^{-/-} knock out mice was as low as 50.4 compared to a median IOD of 128.0 of TNC^{+/+} wild type animals.

The surrounding white matter caudal to the incision site showed a peak of 171.8 on day one. This was followed by a steady fall to a median IOD of 68.2 on day three reaching the lowest median IOD (39.8) on day seven. From then on a slow rise up to 68.1 IOD on day fourteen was observed. The surrounding white matter, caudal to the incision site of TNC^{-/-} knock out mice, showed comparable IOD levels to TNC^{+/+} wild type animals.

Several differences between the regions over the time period tested were detected: The difference between the incision site next to the white matter and the surrounding white matter, cranial ($p=0.001$) and the surrounding white matter, caudal ($p<0.0001$) was statistically highly significant. In addition, the difference between the incision site next to the grey matter and the surrounding grey matter cranial ($p=0.034$) was significant. A significant difference between the incision site next to the grey matter and surrounding grey matter caudal ($p=0.098$) was not proven. Post injury days ($p=0.051$) did almost not differ significantly from each other. Morphologically less NF immunoreactivity was observed in the surrounding white matter of TNC^{-/-} knock out mice, compared to TNC^{+/+} wild type animals. In addition the incision site next to the grey matter of TNC^{-/-} knock out mice revealed more NF immunoreactivity compared to TNC^{+/+} wild type animals. However, the difference between the genotype ($p=0.061$) did barely not reach statistical significance.

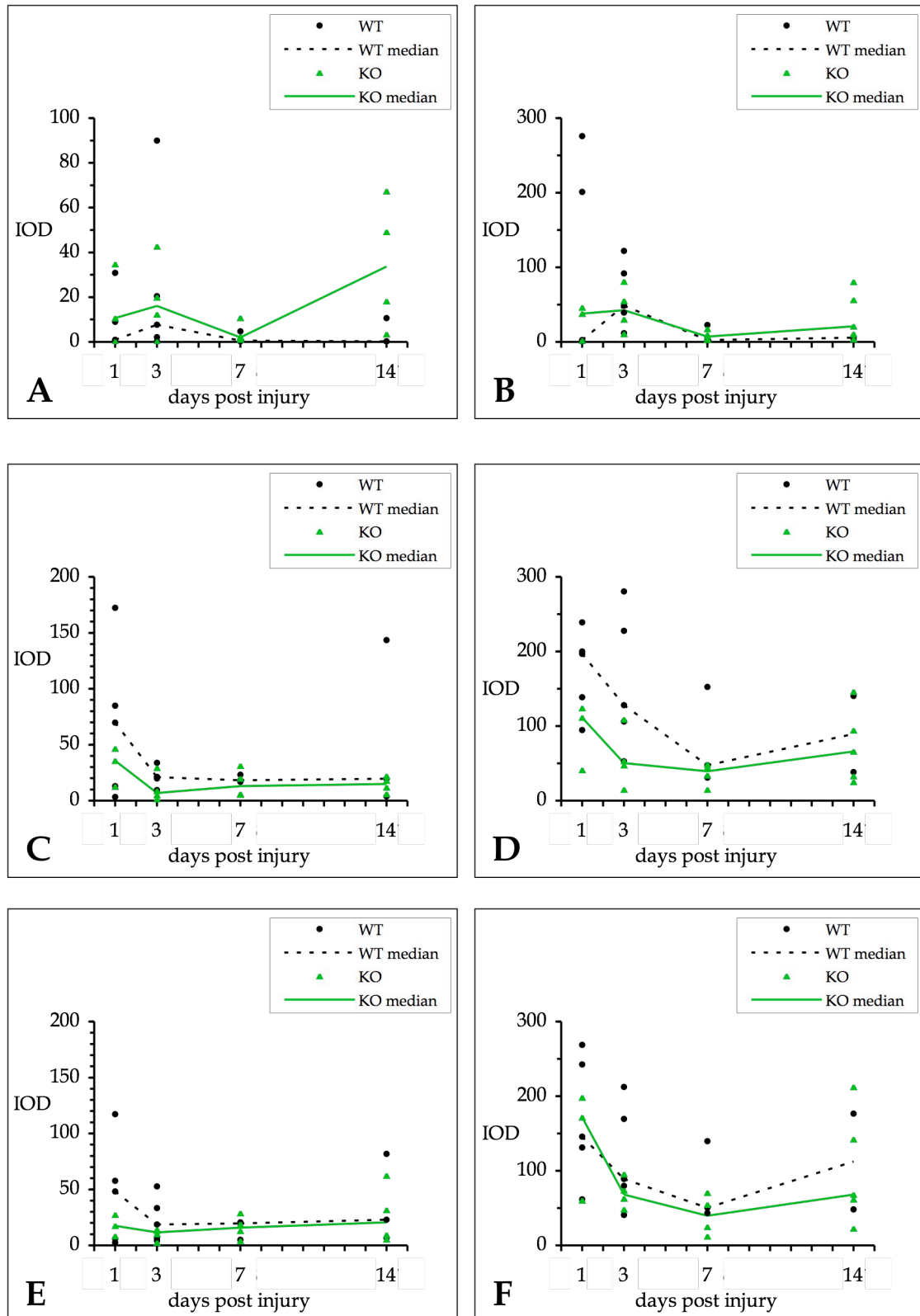


Fig. 65: Integrated optical density for neurofilament immunoreactivity as an axonal marker for TNC+/+ wild type and TNC-/- knock out mice (for legend see next page).

Fig. 65: Integrated optical density (IOD) for neurofilament (NF) immunoreactivity as an axonal marker is shown for TNC^{+/+} wild type (WT, ●) and TNC^{-/-} knock out (KO, ▲) mice from one to fourteen days after spinal cord hemisection at the incision site next to the grey matter (A), in the surrounding grey matter cranial (C) and caudal (E) to the incision site, at the incision site next to the white matter (B), and in the surrounding white matter cranial (D) and caudal (F) to the incision site. Measurements for three to six animals per day are shown. For both genotypes, the difference between the incision site next to the white matter and the surrounding white matter, cranial ($p \leq 0.001$), and the surrounding white matter, caudal ($p \leq 0.0001$) are significant for the time course investigated. In addition, for both genotypes the difference between the incision site next to the grey matter and the surrounding grey matter, cranial to the incision site ($p = 0.034$) is significant for the time period tested. For all regions, the difference between genotypes ($p = 0.061$) has barely not reached statistical significance.

5. Discussion

5.1. TNC^{+/+} wild type mice

The present study was performed to elucidate the role of TNC in wound repair after spinal cord injury. Therefore both TNC^{+/+} wild type mice and TNC^{-/-} knock out animals underwent spinal cord hemisection and the results in both strains of mice were compared. To provide basic information on the process of wound repair, a thorough examination of the temporal and spatial course of the response to injury in TNC^{+/+} wild type mice is described first. Neuronal response, inflammatory cells, microglia and astrocytes as well as the ECM molecules collagen type IV, laminin and fibronectin are discussed in detail below. Alterations found in TNC^{-/-} knock out mice are highlighted in chapter 5.2.

The process of wound healing is an integration of well-coordinated sequences of events, involving the release of various soluble mediators, cellular interactions and ECM components (Bethea 2000). In general, this process is artificially categorized into four steps, i. e. early inflammatory response (0-24 hours post injury), late inflammatory response (two to three days post injury), proliferation phase (three to seven days post injury) and maturation phase (weeks to months after injury). These phases are not independent of one another, but overlap in time and cellular makeup (Clark 1996). In line with our observation, wound repair after spinal cord injury is, unlike in other tissues, not a typical regenerative process, but a fibro-proliferative event that results in a fibrotic scar, that *patches* rather than restores the damaged tissue (Clark 1996).

During the early inflammatory response, oedema and neuronal damage have been seen in H&E stain following hemisection in TNC^{+/+} wild type mice. This has also been seen after spinal cord compression injury in rats. Oedematous tissue was seen as early as one hour post injury (Curtis et al. 1993). Neuronal damage in terms of shrunken hyperchromatic neurons with signs of chromatolysis has been

observed one day after spinal cord hemisection in TNC^{+/+} wild type mice and as early as four hours following spinal cord compression in rats (Farooque et al. 1992).

The incision site of TNC^{+/+} wild type mice has been devoid of NF-positive fibres, indicating an adequately performed hemisection. The surrounding grey matter of TNC^{+/+} wild type mice has shown randomly orientated thin NF-positive fibres, while in the surrounding white matter several swollen, darkly labelled NF-positive fibres have been seen. One hour after spinal cord compression in rats, separation of axon fascicles was seen (Curtis et al. 1993), which has also been obvious one day after injury in TNC^{+/+} wild type mice. Fifteen minutes after cortical impact injury in rats, modest changes of NF-positive fibres were described, while one day following injury a loss of normal NF morphology is seen throughout the soma and dendritic processes (Posmantur et al. 2000), which is consistent with our findings. In our series, TNC^{+/+} wild type mice have shown a down-regulation of NF immunoreactivity in axonal fibres in the white matter tract adjacent to the incision site, representing Wallerian degeneration. During Wallerian degeneration axons are swollen and staining intensity is generally down-regulated (Zenker 1994), due to a decrease in the synthesis of NF protein, which has previously been described following axotomy in motorneurons (Bisby and Tetzlaff 1992; Kreutzberg 1996).

Neurofilaments are neuron-specific intermediate filaments, predominantly found in large myelinated axons (Fuchs and Weber 1994). They are synthesized in neuronal perikarya and transported along the axon. In the uninjured CNS, NF immunoreactivity is predominantly found along axons, not in cell bodies or dendrites (Lasek 1988). Although axotomy can lead to transient detection of NF in perikarya of spinal cord neurons (Goldstein et al. 1987; Mansour et al. 1989), we have never detected NF immunoreactivity within perikarya in our series. Neurofilaments are presumed to regulate and maintain the axonal calibre to provide a cellular matrix for axonal transport and thereby ensure a normal conduction velocity (Lasek 1981; Lazarides 1982; Al-Chalabi and Miller 2003). A reduction in NF synthesis, as seen in the white matter tracts in our series, may be due to a decreased synthesis of NF protein or an increased degradation of NF

protein. This reduction of NF immunoreactivity may permit an increased transport velocity of other cytoskeletal proteins (Bisby and Tetzlaff 1992), which are needed for axonal growth after axotomy.

One day after hemisection, we have observed ruptured blood vessels in the surrounding area of TNC^{+/+} wild type mice, which resulted in minor haemorrhages. This is in agreement with previous findings. Minutes to hours following spinal cord crush injury in mice (Zhang et al. 1996) and compression injury in rats (Farooque et al. 1992; Beattie et al. 2000), swelling of tissue, petechial haemorrhage and extravasated blood with a rapid development of necrotic damage and complete cellular destruction has been observed.

Throughout the time course, small pseudocysts, devoid of endothelial lining have been obvious around the incision site of TNC^{+/+} wild type mice in our study. Pseudocysts occurring after spinal cord injury are categorized as cavitations and are thought to develop due to secondary inflammation after spinal cord injury (Zhang et al. 1996). It is well documented that cavitations after spinal cord injury in mice are less common and rather small, compared to cavitations found after spinal cord injury in rats (Kuhn and Wrathall 1998; Guth et al. 1999; Steward et al. 1999; Jakeman et al. 2000). In mice the lesion gap decreases in size and fills with cells and connective tissue (Zhang et al. 1996; Zhang and Guth 1997; Jakeman et al. 2000).

During the early inflammatory response, we have observed the presence of neutrophilic granulocytes in the surrounding area of TNC^{+/+} wild type mice. The temporal and spatial appearance of neutrophils after spinal cord hemisection in our study is in good agreement with several spinal cord injury models performed in mice and rats (Dusart and Schwab 1994; Zhang et al. 1996; Guth et al. 1999; Schnell et al. 1999; McTigue et al. 2000). Between six and 12 hours after injury, neutrophils appear in postcapillary venules near the incision site. After 24 hours, neutrophil recruitment peaks and neutrophils start to migrate into the surrounding tissue.

While neutrophils have been readily seen during the early inflammatory response, monocytes have not been observed in TNC^{+/+} wild type mice. This has been confirmed with F4/80 immunostaining. The incision site has been devoid of F4/80 immunostaining one day following spinal cord hemisection in TNC^{+/+} wild type mice. Solely, resting F4/80-positive microglia have been observed in the surrounding area and in the ipsilateral distant grey and white matter. This is in contrast to findings of other authors (see below). Microglial activation is reported as early as one day after spinal cord contusion in rats (Carlson et al. 1998; Popovich et al. 2002) and one day after brain injury in mice (Schauwecker and Steward 1997).

Using F4/80 antibody, we have observed a distinct staining pattern of resting microglia in the normal control and a massive F4/80 labelling of activated microglia and macrophages in the injured spinal cord at later time points, indicating that our immunohistochemistry was technically sound.

Differences in the visualization of microglia/macrophages by immunohistochemistry might be caused by the use of different antibodies. F4/80 antibody is specific for mice (Austyn and Gordon 1981) and labels macrophages, including microglial cells in the brain (van den Berg and Kraal 2005). Schnell et al. (1999) report a slight activation of few F4/80-positive resident microglia in the lesion vicinity one day following a bilateral spinal cord transection in mice.

A different mode of spinal cord injury is most likely responsible for the absence of F4/80 immunoreactivity in TNC^{+/+} wild type mice during the early inflammatory response. A unilateral hemisection, which has been performed in our study, may well result in minor microglial activation due to a cytokine reaction that differs somewhat from that seen in a bilateral transection performed by Schnell et al. (1999). This theory is supported by the fact, that F4/80 molecules on microglia/macrophages can be down-regulated by interferon- γ (IFN- γ) (van den Berg and Kraal 2005), which is detected following spinal cord injury in mice (Ricci-Vitiani et al. 2006). Hence, in a less invasive injury, the F4/80 antigen might not yet be expressed at the cell surface, since surface molecules on microglia/macrophages can change with the morphological change of microglial activation (Perry and Gordon 1987).

A strain difference in mice is rather not responsible for the different temporal activation of microglia, since strain differences after spinal cord contusion were detected in the *late*, and not in the *early* course of microglial activation (Ma et al. 2004).

During the early inflammatory response, we have detected immunoreactivity for ECM molecules, i. e. collagen type IV, laminin and fibronectin. Collagen type IV has been confined to vessels in the surrounding area of TNC^{+/+} wild type mice. At that time no extracellular deposits of collagen type IV has been detected.

Collagen type IV is a non-fibril forming collagen, which is restricted to the basal membrane (Hermanns et al. 2001). Collagen type IV stabilizes and enhances the elasticity of various tissues. Traditionally collagen type IV, as other ECM molecules, is thought to be produced by invading fibroblasts (Hermanns et al. 2001). However, collagen type IV has been present one day following hemisection, long before fibroblasts eventually invade the incision site. According to Bernstein et al. (1985) astrocytes in the spinal cord are capable of synthesizing all precursor proteins required for basement membrane formation at all/or some portions of their life circle. This theory is supported by Liesi and Kauppila (2002), who demonstrate that reactive astrocytes transiently express collagen type IV after spinal cord injury in rats.

However, reactive GFAP-positive astrocytes in TNC^{+/+} wild type mice have only been seen at later stages during wound repair and are therefore unlikely the producers of collagen type IV. Morphologically, visualized with GFAP immunoreactivity, astrocytes are not responding to injury one day after surgery. Indeed, the term *reactive astrocyte* is a generic one, used to demonstrate a morphological change in cell shape, which does not necessarily reflect the function of the individual cell. GFAP-positive astrocytes are classified into diverse subgroups and may well demonstrate a distinct production pattern of proteins. Therefore it may be possible that astroglial cells may well respond to spinal cord hemisection long before they turn morphologically into a reactive state.

Generally, collagens are synthesized intracellularly as longer precursor proteins called procollagens, which are secreted into the extracellular space where they become tropocollagen due to the removal of pro-domains by certain enzymes (Drenckhahn and Kugler 1994). That we have never observed collagen type IV-positive astrocytes throughout the time course investigated is most likely explained by the fact that the intracellular precursor protein procollagen is not detected with a conventional anti-collagen type IV antibody. Hence, astrocytes in TNC^{+/+} wild type mice may produce procollagen during this early stage, which we cannot prove or disprove with conventional anti-collagen type IV immunohistochemistry.

On the other hand, leptomeningeal cells, which are present throughout the time course after spinal cord injury are also known to produce ECM molecules (Sosale et al. 1988; Fawcett and Asher 1999; Hermanns et al. 2001). In our series, collagen type IV-positive vessels adjacent to the meninges have shown a stronger immunoreactivity, compared to vessels situated more medially. Hence, the most likely source of collagen type IV during the early inflammatory response after spinal cord hemisection are leptomeningeal cells, although quiescent astrocytes may play a minor role.

Parallel to collagen type IV findings, laminin immunoreactivity in TNC^{+/+} wild type mice has been confined to vessels in the surrounding area during the early inflammatory response. Laminin-positive capillaries are also seen near the injury site one day after neurotoxin injection to the rat's brain (Liesi et al. 1984).

Laminin is thought to be produced by fibroblasts (Hermanns et al. 2001), which as stated above have not invaded the incision site yet, hence may only account for a laminin production at later time points. Although we have never observed intracellular laminin, Liesi et al. (1984) noticed laminin-positive astrocytes near the lesion site, implying astrocytes as a possible source of laminin production. Liesi and Ristelli (1989) postulate, that laminin synthesized by glial cells is a variant form of laminin and might not be detected by a conventional laminin antibody. In addition, region-specific differences in the ability of

astrocytes to synthesize laminin are well known (Hatten et al 1991; Alonso and Privat 1993). Both facts explain the circumstance that we have not observed intracellular laminin deposits throughout the time course.

In our study, laminin-positive vessels found near the meninges have shown a stronger immunoreactivity, compared to laminin-positive vessels located further away from the meninges. Hence, it is most likely that large amounts of laminin are produced by leptomeningeal cells (Sosale et al. 1988; Fawcett and Asher 1999; Hermanns et al. 2001,) in the early stage of wound repair, while astrocytes might simultaneously take part in producing laminin.

In contrast to collagen type IV and laminin, fibronectin has not been associated with vessels and has been exclusively found as extracellular deposits during the early inflammatory response. Fibronectin-positive strands have been observed along the incision edges and in the surrounding area of TNC+/+ wild type mice. In accordance with our study, Farooque et al. (1992) state that 24 hours after spinal cord compression in rats, fibronectin is found in multiple regions of irregular configuration and sizes in the parenchyma.

In contrast to our observations, after rat spinal cord compression and following neurotoxin injection to the rat's brain, fibronectin is also seen in neurons, glial cells and around capillaries (Farooque et al. 1992, Liesi et al. 1984). Fibronectin in TNC+/+ wild type mice has never been seen within cells nor has it been associated with vascular structures. This difference in fibronectin immunoreactivity pattern might be due to a different location and mode of injury. In compression injury and in deep brain injury, ECM deposits are seen less frequently compared to spinal cord transection.

Depending on their location in the CNS, astrocytes have different capacities to produce fibronectin (Liesi et al. 1986). In addition, fibronectins are a heterogeneous group of molecules that differ in their splicing variants depending on their origin. For instance, cultured astrocytes synthesize a fibronectin form that differs from fibroblast-fibronectin by alternative splicing (Price and Hynes 1985; Liesi et al. 1986; Liesi 1990) and Liesi et al. (1986) failed to demonstrate significant

fibronectin immunoreactivity in the adult rat, which was synthesized by cultured astrocytes. Furthermore, glial cells *in vivo* may fail to exhibit intracellular fibronectin, because they rapidly secrete it (Liesi et al. 1986). In addition, fibroblasts (Hermanns et al. 2001) and leptomeningeal cells (Sosale et al. 1988; Fawcett and Asher 1999; Chesney and Bucala 2000; Hermanns et al. 2001) are thought to produce fibronectin.

More likely, however, seems a theory by Farooque et al. (1992). They postulate that fibronectin deposits in the wound are likely to originate from extravasated fibronectins through early haemorrhage, and are not necessarily produced by local cells (as discussed by Lorke and Möller 1985). Cellular fibronectin is structurally and antigenically similar to insoluble globulin derived from plasma. Therefore polyclonal antibodies, as ours, usually cross-react with both forms. We suggest that fibronectin in the early stage of wound repair mainly originates from extravasated blood, while local leptomeningeal may play a minor role.

Around three days following hemisection, the late inflammatory phase is ending and slowly merges into the proliferation phase. During the late inflammatory response, thin NF-positive fibres have entered, but never traversed the incision site of TNC^{+/+} wild type animals. In agreement with our observation, after a bilateral spinal cord transection in rats NF-positive fibres are seen adjacent the lesion (Joosten et al. 2000). In the surrounding grey matter of TNC^{+/+} wild type mice, we have observed thin NF-positive fibres. Similar findings of few axonal elements observed within the perilesioned grey matter are documented by Joosten et al. (2000). The surrounding white matter of TNC^{+/+} wild type mice has shown signs of axonal damage, which is in agreement with findings after spinal cord contusion injury in mice. Necrotic tissue and NF-positive fibres are seen in the surrounding white matter three days following injury (Ma et al. 2004). In addition to morphological changes at the incision site, we have observed severe axonal damage and necrotic material in the distant CST, indicating ongoing Wallerian degeneration.

During the late inflammatory response, a shift from the neutrophilic influx to a predominantly mononuclear infiltration at the incision site has been observed for TNC+/+ wild type mice. This is well documented after different spinal cord injuries in mice and rats (Zhang et al. 1996; Popovich et al. 1997; Guth et al. 1999; Schnell et al. 1999; McTigue et al. 2000).

As seen in our series, neutrophils rapidly decline about two days post injury (Bethea 2000). Three days following hemisection lymphocytes have first appeared at the incision site of TNC+/+ wild type mice. The relatively low density of lymphocytes throughout the time course is confirmed by several studies after spinal cord injury in mice (Schnell et al. 1999) and in rats (Popovich et al. 1996; Popovich et al. 2002).

During the late inflammatory response, invading monocytes have been observed in TNC+/+ wild type mice. It is known that blood-borne mononuclear cells invade the site of injury and show a peak between two and three days after spinal cord injury. Soon after that, they differentiate into macrophages and show phagocytic activity (Popovich et al. 1997). Once blood-borne monocytes have entered the incision site they remain similar in number (Norton 1999) and persist for several weeks following spinal cord injury (Popovich et al. 1997).

Our observations on blood-borne macrophages in H&E stain have been confirmed with F4/80 immunoreactivity. Three days following hemisection in TNC+/+ wild type mice, phagocytes have occurred in great number at the incision site, while activated and hyper-ramified microglia have been seen in the surrounding area. Phagocytes are characterized by a large, round cytoplasm, while activated microglial cells display frequently branching ramifications, which are short and thick (Streit et al. 1999). In contrast, hyper-ramified microglial cells show fewer ramifications with more slender processes (Streit et al. 1999).

The temporal activation of microglia has previously been described in several studies utilising spinal cord injury in mice (Fujiki et al. 1996; Zhang et al. 1996; Schauwecker and Steward 1997; Sroga et al. 2003; Ma et al. 2004) and in rats (Dusart and Schwab 1994; Popovich et al. 1997; Zhang et al. 1997a). A recent study performed a species comparison between mice and rats after spinal cord contusion

injury and consolidated similar findings of microglial/macrophage activation between the two species (Sroga et al. 2003). Subtle differences between mice and rats for microglial morphology are only observed in the *chronically* injured animal.

Besides microglial activation at the incision site, F4/80 immunoreactivity in TNC+/+ wild type mice has been observed in the ipsilateral spinal cord distant from the incision site. A concurrent activation of microglia distant from the actual lesion site is well known. After spinal cord crush injury in mice, microglial activation is observed in the dorsal column (Fujiki et al. 1996). Microglial activation distant from the lesion develops with a time course comparable to the increase in immunoreactivity at the crush site (Fujiki et al. 1996), which has also been observed in TNC+/+ wild type mice.

After CNS injury it is difficult to differentiate whether an individual phagocyte is originating from resident microglia or recruited from monocytes circulating in the blood. Microglia are found throughout the CNS, comprising between five and 15 % of the cells (Kreutzberg 1996). It is known that resident microglial cells enter the CNS during embryonic development (Jordan and Thomas 1988). Hence both resident microglia and blood-borne monocytes derive from the monocyte cell line (Chugani et al. 1991).

Carson et al. (1998) postulated to distinguish resident microglia from blood-borne monocytes by characterizing the relative expression levels of only few macrophage antigens *in vitro*. However, surface markers used to identify the different developmental derivatives of the monocytic line are themselves modulated by the processes of phagocytic activation (Perry and Gordon 1987). Using conventional F4/80 immunohistochemistry, it is not possible to determine whether an activated phagocyte derives from a blood-borne monocyte or from resident microglia, which many other authors agree on (Blight 1992; Fujiki et al. 1996; Norton 1999; Schnell et al. 1999; McTigue et al. 2000).

Previous studies have suggested that the preferential involvement of resident microglia and blood-borne monocytes depends on the nature of the injury (Streit et al. 1988). Non-invasive CNS injury involves the exclusive participation of resident microglia (Norton 1999), while a lesion involving a compromised blood-

brain barrier due to damaged vasculature also contains blood-derived monocytes (Fawcett and Asher 1999). In conclusion, spinal cord hemisection results in a mixture of invading monocytes and activated microglial cells (Stichel-Gunkel 1997; Fawcett and Asher 1999). While blood-borne monocytes are washed into the injury site with the blood stream, microglial cells rapidly divide after spinal cord injury and migrate to the injury site where they transform into an activated state (Streit and Kreutzberg 1988; Norton 1999; McTigue et al. 2000).

During the late inflammatory response, phagocytes secrete chemoattractants, which serve to promote fibroblast activation and replication (Bethea 2000). Three days following hemisection, numerous activated fibroblasts have appeared at the incision site of TNC^{+/+} wild type mice. It is known that fibroblasts rapidly invade the site of injury three to five days following spinal cord injury where they initiate wound repair (Fawcett and Asher 1999).

The precise origin of fibroblasts-like cells found within wounds has been controversially discussed (Chesney and Bucala 2000). Traditionally it has been thought that peripheral fibroblasts are recruited from a circulating precursor population in the blood (Abe et al. 2001; Quan et al. 2004). In particular, with every disruption of the continuity of the blood-brain-barrier, peripheral fibroblasts are likely to invade the incision site. However, peripheral fibroblasts and leptomeningeal cells look very much alike, so that it is difficult to distinguish them morphologically and determine their source of origin (Chesney and Bucala 2000; Grimpe and Silver 2002; Seitz et al. 2002). Fibroblasts in a spinal cord injury, which penetrate the meningeal layers, are expected to originate predominantly from the meningeal surface (Fawcett and Asher 1999). This hypothesis is supported by the fact that, in mice, following a spinal cord transection that leaves the dura intact, fibroblast infiltration is minimal (Seitz et al. 2002). After spinal cord hemisection in TNC^{+/+} wild type mice, where the dura has been cut open and the blood-brain-barrier has been impaired, the massive invasion of fibroblasts at the injury site is almost certainly a mixture of both, peripheral fibroblasts and meningeal cells.

During the end of the late inflammatory response, activated fibroblasts begin to secrete ECM proteins (Carbonell and Boya 1988). In general tumour necrosis factor- α (TNF- α) and transforming growth factor- β 1 (TGF- β 1) have been implicated in the stimulation of ECM production *in vivo* (Fawcett et al. 1992). TGF- β 1, in part derived from blood-borne macrophages, increases rapidly after a spinal cord contusion injury in rats (Semple-Rowland et al. 1995; McTigue et al. 2000). In response to TGF- β 1, cultured fibroblasts of murine origin up-regulate collagen type I in the injured tissue (Abe et al. 2001, Quan et al. 2004). Consistent with that observation, three days following hemisection in TNC+/+ wild type mice we have first observed collagen fibres in combined Masson trichrome and Verhoeff stain, demonstrating collagen type I. After spinal cord transection in rats, a similar temporal appearance of collagen type I is described (Hermanns et al. 2001).

Besides collagen type I, invading fibroblasts of either peripheral or leptomeningeal origin, begin to produce large amounts of collagen type IV and laminin during the late inflammatory response (Fawcett and Asher 1999; Hermanns et al. 2001). In particular, TGF- β 1 induces collagen type IV production in cultured fibroblasts (Abe et al. 2001; Quan et al. 2004), which is different from the early inflammatory response, where meningeal cells are seen as the major source of collagen type IV and laminin.

In TNC+/+ wild type animals, elevated collagen type IV and laminin immunoreactivity has still been seen around blood vessels three days following hemisection. This is also documented after brain injury in rats (Maxwell et al. 1984; Stichel-Gunkel 1997) and following spinal cord hemisection in cats (Risling et al. 1993). During the late inflammatory response, extracellular collagen type IV and laminin deposits, not associated with vessels have first appeared at the incision site of TNC+/+ wild type mice. Earlier work has shown a similar spatiotemporal distribution of extracellular collagen type IV and laminin. After spinal cord transection and hemisection in rats extracellular collagen type IV and laminin deposits are seen three days following injury (Sosale et al. 1988; Joosten et al. 2000; Hermanns et al. 2001). One could speculate, that the first appearance of extracellular ECM deposition is associated with the shift of ECM production from

a formerly predominant leptomeningeal source towards invading activated fibroblasts from a peripheral origin.

In contrast to our observation, three days after a contusion injury in mice, laminin is still restricted to blood vessels, and extracellular laminin is only observed later (Ma et al. 2004). This is a typical difference between transection and contusion injury models. The loss of integrity of meningeal layers results in a more pronounced ECM deposition in transection injuries. This theory is supported by the fact that three days after a deep brain injury to the rat, collagen type IV and laminin staining is less abundantly deposited (Stichel-Gunkel 1997). The characteristic difference between brain and spinal cord injuries is, that ECM deposits are detected less frequently in deep brain lesions compared to spinal cord injuries, where meningeal layers are much closer to the incision site and fibroblasts invasion is more prominent.

During the late inflammatory reaction, less fibronectin deposits have been seen in TNC+/+ wild type mice compared to the early inflammatory response. This finding is in agreement with Egan and Vijayan (1991), who observed diffuse fibronectin staining adjacent to the wound after brain injury in rats. Extravasated fibronectin, the main source of fibronectin immediately after hemisection, has gradually decreased due to restored vascular leakage during the late inflammatory response. Concurrently a temporal shift from fibronectin produced by local fibroblasts is very likely. One could speculate, that compared to extravasated fibronectin, which has been observed in large quantities, fibronectin of fibroblast origin is secreted in smaller amounts in TNC+/+ wild type mice, since local fibroblasts are also producing large quantities of other ECM molecules (Carbonell and Boya 1988) and the capacities for fibronectin production are somewhat limited.

Due to a fibronectin receptor on mature astrocytes (Pesheva et al. 1988), fibronectin facilitates proliferation and migration of astrocytes after injury (Goetschy et al. 1987). Three days following hemisection in TNC+/+ wild type

mice, we have observed GFAP-positive reactive astrocytes forming a rim in the surrounding area, leaving the incision site devoid of GFAP-positive astrocytes. This striking GFAP-negative area during the late inflammatory response is a well-described feature in the formation of astrogliosis after stab wound, contusion, crush or complete transection injury of the spinal cord in mice (Adrian and Williams 1973; Inman et al. 2002; Faulkner et al. 2004; Ma et al. 2004) and in rats (Frisén et al. 1995; Stichel-Gunkel 1997).

Besides GFAP immunoreactivity at the incision site, three days following hemisection, TNC+/+ wild type mice have first shown GFAP-positive astrocytes in the grey and white matter distant from the incision site. A widespread astroglial activation in the white and grey matter has been documented in previous studies after spinal cord hemisection in rats (Fawcett and Asher 1999; Leme and Chadi 2001). In rats this widespread astroglial reaction may extend for up to one cm from the injury (Fawcett and Asher 1999).

Reactive astrocytes in the grey and white matter are known to express different morphologies. Astrocytes reacting directly to a penetrating injury result in *anisomorphic gliosis*, while astrocytes reacting to the occurrence of Wallerian degeneration cause *isomorphic gliosis* (Mansour et al. 1990). This is in line with our observation, that during the late inflammatory response GFAP-positive cells of TNC+/+ wild type mice show a different morphology according to their location. In our study reactive astrocytes have been seen in the grey matter. In contrast, GFAP-positive astrocytes in white matter tracts distant from the incision site have shown large, round vacuolated cytoplasm with a flat nucleus, indicating phagocytosis of myelin sheath during Wallerian degeneration. Astrocytic-like phagocytic cells are previously reported in the lateral geniculate nucleus following optic enucleation (McClung 1972). GFAP-positive phagocytic-like cells, seen in TNC+/+ wild type mice, are reminiscent of gemistocytes. Gemistocytes are glial cells characterized by voluminous, eosinophilic cytoplasm and a peripherally positioned often flattened nucleus. Gemistocytes are usually present in anoxic-ischemic brains, regularly encountered in glial neoplasm (Kros et al. 2000). Although the function of these cells is far from clear, morphologically these cells

impress as GFAP-positive phagocytes that may clear debris in the white matter tracts together with phagocytes of other origin.

Seven days following injury, the proliferation phase of wound repair merges into the maturation phase. During the proliferation phase the incision site of TNC+/+ wild type mice has been devoid of NF-positive fibres. This is also seen seven days after spinal cord crush injury in mice. The lesion is devoid of intact axons and NF-positive axonal debris impress as beaded fragments (Zhang et al. 1996; Inman and Steward 2003). Similar to that, in the surrounding white matter of TNC+/+ wild type mice, we have observed gradually diminishing thick NF-positive fibres resulting in necrotic material. Degenerating remnants of axons in the surrounding white matter indicating dead or dying axons have previously been documented after spinal cord crush injury (Zhang et al. 1996; Inman and Steward 2003). In TNC+/+ wild type mice, white matter tracts near the incision site have appeared to end bluntly, demonstrating Wallerian degeneration. This has been described earlier in spinal cord crush injury (Zhang et al. 1996; Inman and Steward 2003).

In the surrounding grey matter of TNC+/+ wild type mice, fine NF-positive fibres have been seen. Likewise to our observation, thin axons of the grey matter have a fine corkscrew or varicose configuration, indicating axonal sprouting (Zhang et al. 1996). While three days after hemisection we have observed NF-positive fibres entering the incision site, during the proliferation phase the scar has become more rugged and seemed to inhibit axonal growth at the incision site. During the proliferation phase sprouting axons have only been observed in the surrounding grey matter of TNC+/+ wild type mice and no NF-positive fibre has been seen at the incision site.

The origin of NF labelled axonal sprouts in TNC+/+ wild type mice is difficult to determine using immunohistochemistry alone. Collateral axonal sprouting (Schwegler et al. 1995; Goldstein et al. 1997) and spinal cord interneurons (Nacimiento et al. 1997) are proposed to be a source of axonal sprouting. In addition, ingrowth and intraspinal sprouting of dorsal root fibres

due to PNS attachment to the cord has been described (Lampert and Cressman 1964; Nacimiento et al. 1997). Although we have observed attachments of a spinal root to the cord on the level of incision, we have observed a comparable density of axonal sprouts in TNC^{+/+} wild type animals regardless of PNS attachment. Methodically we cannot rule out that dorsal root fibres have entered the spinal cord, but PNS attachment to the cord in TNC^{+/+} wild type mice does not necessarily result in a quantitatively significantly enhanced sprouting.

The lasting proliferation phase is characterized by a high density of activated fibroblasts and reactive astrocytes, indicating the ongoing scar formation. The preceding GFAP-negative area at the incision site of TNC^{+/+} wild type mice has been replaced by heavily labelled GFAP-positive astrocytes. Processes of reactive astrocytes have been tightly interwoven with each other and penetrated the incision site and the surrounding area. This is in line with previous reports of spinal cord stab wound, bilateral transection and contusion injury in mice (Adrian and Williams 1973; Ma et al. 2001; Faulkner et al. 2004). During the process of astrogliosis, astrocytes proliferate and are strongly positive for GFAP immunoreactivity (Tacconi 1998). Furthermore, they show cytoplasmic processes, which are apposed to one another and bound together by tight or gap junctions (Fawcett and Asher 1999, Tacconi 1998). This dense astroglial scar fills the space vacated by dead neurons and glial cells (Stichel and Müller 1998).

As already mentioned, GFAP-positive astrocytes are a heterogeneous class of cells with different properties in different parts of the CNS (Stichel-Gunkel 1997, Tacconi 1998). The astrocytic response varies with the proximity to the site of injury. During the proliferation phase, reactive astrocytes at the incision site of TNC^{+/+} wild type mice have shown an extensive response compared to astrocytes distant from the incision site, which has previously been reported after spinal cord hemisection in rats (Leme and Chadi 2001). GFAP immunoreactivity in the distant grey and white matter of TNC^{+/+} wild type mice has decreased during the proliferation phase. Furthermore, astrocytic-like phagocytes in the distant white matter have now been replaced by reactive astrocytes. This indicates

that myelin sheaths, which accumulated due to Wallerian degeneration, have been almost cleared in TNC^{+/+} wild type mice.

During the proliferation phase, activated fibroblasts and reactive astrocytes continue to produce large amounts of various ECM proteins in high quantities, i. e. collagen type IV, laminin and fibronectin, which are deposited in a rather disorderly way (Bernstein et al. 1985, Chesney and Bucala 2000, Hermanns et al. 2001). The ECM is a dynamic structure that changes in composition, density and architecture at different time points following injury. ECM molecules bind by homophilic and heterophilic interactions to one another (Yamagata et al. 1986). Their deposition is mainly regulated by transforming growth factor- α (TGF- α) and transforming growth factor- β (TGF- β) (Sandvig et al. 2004). TGF- β reaches its maximum seven days post injury (Semple-Rowland et al. 1995), which is in line with the finding that ECM deposition in TNC^{+/+} wild type mice is very prominent during the proliferation phase.

Seven days following hemisection in TNC^{+/+} wild type mice, extracellular collagen type IV deposits have fully extended the incision site, which has been previously seen seven days after bilateral spinal cord transection of the rat (Weidner et al. 1999; Joosten et al. 2000; Hermanns et al. 2001). Collagen type I deposits have also widely extended the incision site and the surrounding area of TNC^{+/+} wild type mice, which is confirmed after previous spinal cord injury models in rats (Guth et al. 1999; Hermanns et al. 2001). Collagen type IV spontaneously forms a sheet-like network (Hermanns et al. 2001), where other ECM molecules anchor on (Liesi 1985; Stichel et al. 1999c).

Moderately labelled extracellular laminin deposits have been observed at the incision site of TNC^{+/+} wild type animals during the proliferation phase. Similar findings are observed six days following spinal cord hemisection in rats (Bernstein et al. 1985). Laminin forms an independent network after spinal cord injury (Stichel and Müller 1998), which is then seen to intermingle with the existing collagen type IV network at around seven days after brain injury in rats (Stichel et al. 1999c).

Fibronectin, which makes up a large amount of the ECM formation (Sandvig et al. 2004), is also present in TNC^{+/+} wild type mice during the proliferative phase.

The up-regulation of TGF- β on day seven suppresses the activation of microglia and blocks microglial proliferation (Böttner et al. 2000), which is in line with our observation in TNC^{+/+} wild type mice. F4/80-positive phagocytes have been widely replaced by activated microglia at the incision site and in the surrounding area of TNC^{+/+} wild type mice. Simultaneously, F4/80 immunoreactivity in the distant grey and white matter of TNC^{+/+} wild type mice has abated. An analogous course of microglial/macrophage activation has previously been reported in spinal cord contusion and crush injury as well as in a brain injury in mice (Zhang et al. 1996; Schauwecker and Steward 1997; Ma et al. 2001; Sroga et al. 2003) and in rats (Popovich et al. 1997; Zhang et al. 1997b; Leme and Chadi 2001). In all studies, including the current study, immunohistochemical evidence of microglial/macrophage activation is maximal at the incision site between three and seven days post injury.

F4/80-positive cells located around small cavitations have been observed in TNC^{+/+} wild type mice. Small cavities, which are typically lined with macrophages, are also reported after a spinal cord contusion injury in mice (Ma et al. 2001).

Fourteen days following hemisection, the maturation phase is in progress. The incision site of TNC^{+/+} wild type mice has remained free of NF-positive fibres, which has recently been documented fourteen days after spinal cord crush injury in mice (Faulkner et al. 2004). No axonal sprouts were found within the incision site and one is again tempted to point out the spatiotemporal coincidence of the ongoing fibroglial scar formation. The imminent stop of axonal fibres at the wound border has previously been described fourteen days after brain injury in rats (Stichel et al. 1999a). Of note, six days after a brain injury with experimentally

reduced ECM deposits, axons either extended into or even traversed the lesion centre (Stichel et al. 1999a; Stichel et al. 1999b).

Throughout the surrounding grey matter of TNC^{+/+} wild type mice, we have observed NF-positive sprouting fibres without apparent orientation. This distribution of sprouts is also observed three weeks following spinal cord transection (Seitz et al. 2002) and eight weeks after spinal cord crush injury in mice (Zhang et al. 1996).

Due to Wallerian degeneration in the surrounding white matter of TNC^{+/+} wild type mice, thick NF-positive fibres have been replaced by necrotic material and for the first time thin NF-positive fibres, indicating axonal sprouting have been observed during the maturation phase. An increase of NF-positive axons in the immediate surrounding of the lesion is reported with increased post-injury survival times following spinal cord crush injury in mice (Zhang et al. 1996; Inman and Steward 2003).

The distant CST in TNC^{+/+} wild type mice has shown intense Wallerian degeneration. In contrast to the white matter tract adjacent to the incision site, only few NF-positive thin fibres have been observed in the distant CST, indicating that growth-promoting factors are rather found in the proximity of the lesion site. The strong mononuclear infiltration, which has been seen in the distant CST, may be an additional cause for the limited number of axonal sprouts. In contrast, leucocytes and monocytes around the incision site of TNC^{+/+} wild type mice have greatly decreased during the maturation phase and axonal sprouts in the surrounding grey and white matter have been readily seen.

During the maturation phase, the scar in TNC^{+/+} wild type mice has contracted and diminished in size. The tendency for lesions to decrease in size is well known (Zhang et al. 1996; Inman et al. 2002) and commonly takes place between five and 15 days after injury (Romo 2008). The expression of α -smooth muscle actin by fibroblasts may be responsible for wound contraction (Abe et al. 2001; Sroga et al. 2003). Due to the breakdown of provisional ECM molecules, activated fibroblasts are gradually triggered to stop migrating and proliferating

(Scholar and Stadelmann 2006). Indeed, quiescent fibroblasts are the predominant cell type in TNC^{+/+} wild type mice during the maturation phase, indicating that activated fibroblasts have returned to their resting state.

Whether fibroblasts are beneficial or harmful to axonal growth is still unclear. Fibroblasts are probably not in themselves a mechanical barrier to axonal growth, since NF-positive axons grow along meningeal interfaces (Hermanns et al. 2001). It is more likely that fibroblasts are the major source of inhibitory molecules, especially during the proliferation and maturation phase and therefore indirectly prevent axonal growth (Grimpe and Silver 2002). Fibroblasts, for instance, produce chondroitin sulphate proteoglycan (CS-PG) (Culav et al. 1999), which is the most inhibitory molecule to axonal growth observed so far (Schwab et al. 1993; Fawcett and Asher 1999).

During the maturation phase, a vast amount of strongly GFAP-positive astrocytes has been found at the incision site of TNC^{+/+} wild type mice. Tightly interwoven astroglial processes throughout the incision site and the surrounding area present a distinct astroglial scar. This spatiotemporal distribution of astroglial activation and the subsequent formation of the astroglial scar have been described earlier after spinal cord injury in mice and rats (Fawcett and Asher 1999; Ma et al. 2001; Faulkner et al 2004). The astroglial scar reaches its maximum within weeks, thereafter, astrocytes slowly return to their resting state (Norenberg 1994, Tacconi 1998). Reactive astrocytes in the distant grey and white matter of TNC^{+/+} wild type mice have returned to their protoplasmic or fibrous state fourteen days following hemisection.

Whether reactive astrocytes are valuable or detrimental to axonal growth is still controversial. First of all, it is unknown whether astroglial scarring occurs as a result of axonal elongation not having proceeded, or whether the scar prevents long distance elongation of axons in the first place (Nicholls et al. 1999). Numerous studies revealed that astroglial scarring is one of the major impediments to axonal growth and therefore reactive astrocytes are widely regarded as detrimental to overall outcome after spinal cord injury (Ramon y Cajal 1928; Reier and Houle

1988; Fawcett and Asher 1999; Giménez y Ribotta et al. 2001; Giménez y Ribotta et al. 2002; Faulkner et al. 2004). On the other hand, many studies demonstrate that astrocytes may support axonal growth during development and under certain other conditions in adults (Gage et al. 1988; Smith et al. 1990; Kawaja and Gage 1991; Stichel and Müller 1994; Li and Raisman 1995). Moreover, axons are reported to readily penetrate fibrous scars formed after spinal cord injury (Matthews et al. 1979a; Frisé et al. 1993). This is confirmed in monolayer cultures of astrocytes, where axons tend to regrow well (Noble et al. 1984). However, monolayer cultures tend to be less permissive with time *in vitro* (Smith et al. 1990) and in three-dimensional tissue cultures, neurones almost completely fail to regrow their axons, resembling their behaviour *in vivo* (Fawcett and Asher 1999).

For a long time the astroglial scar has been thought to act as a mechanical barrier to growing axons (Reier and Houle 1988; Jakeman and Reier 1991; Stichel et al. 1999b). However, fenestrations within the fibrous scar, which have a diameter of 0.5-5 μm , are sufficient to allow a penetration of regrowing *thin* axons (Stichel et al. 1999b). In a further elaboration of the barrier theory, the hypothesis of a biochemical barrier emerged, which postulated the fact that either down-regulation of growth-promoting or up-regulation of growth-inhibiting molecules are responsible for the barrier function (Fawcett and Asher 1999; Fitch and Silver 1999). Reactive astrocytes are known to produce ECM molecules that may have positive or negative influence on axonal growth (Bush et al. 1999). A particular subgroup of astrocytes, for instance produces a variety of CS-PGs (Fitch and Silver 1997; Fawcett and Asher 1999) and CS-PGs incorporated within the ECM are inhibitory to axonal growth. Other molecules produced by astrocytes that may interfere with axonal growth are certain tenascins (Grierson et al. 1990; Ajemian et al. 1994; Qiu et al. 2000). While tenascin-R impedes recovery after a nerve lesion, TNC is more likely to promote axonal growth (Guntinas-Lichius et al. 2005).

During the maturation phase, also named remodelling phase ECM molecules, which were previously laid down in a disorganized manner, are now rearranged and cross-linked (Lorenz and Longaker, 2003), resulting in a scar that patches the tissue disruption.

Fourteen days after hemisection, fibronectin immunoreactivity in TNC+/+ wild type mice has nearly ceased, which is also seen fifteen days after penetrating brain lesion in the rat (Egan and Vijayan 1991). In contrast, collagen type I has been most prominent at the incision site and in the surrounding area of TNC+/+ wild type mice during the maturation phase, which is described in previous studies (Matthews et al. 1979b; Stichel et al. 1999c). During the maturation phase, the incision site of TNC+/+ wild type mice has been filled with extracellular collagen type IV and laminin deposits. This is in agreement with previous studies fourteen days after spinal cord injury in mice and rats (Frisén et al. 1995; Weidner et al. 1999; Joosten et al. 2000; Hermanns et al. 2001).

Besides extracellular deposits, both collagen type IV and laminin immunoreactivity in TNC+/+ wild type mice have been detected in blood vessels throughout the time points investigated. The appearance of collagen type IV and laminin-positive blood vessel at the lesion site is a well-known phenomenon of postlesional changes and often related to lesion-induced angiogenesis (Maxwell et al. 1984; Sosale 1988; Risling et al. 1993; Stichel-Gunkel 1997). Vasodilation has been a prominent feature in TNC+/+ wild type mice until the proliferation phase. In our series, an increase in capillaries adjacent to the incision site, indicated by enhanced collagen type IV and laminin immunoreactivity has been first seen during the proliferation phase and has been most striking fourteen days following hemisection. It is known that after CNS injury the mean number of capillaries in the lesion is twice that of uninjured regions and that newly formed blood vessels often exhibit an increased luminal diameter (Blight 1991; Jaeger and Blight 1997), which is in accordance with the present study.

ECM-mediated sprouting of vessels is important for wound healing in restoring blood supply and providing nutrition for the formation of granulation tissue (Hermanns et al. 2001). Microglia/macrophages and fibroblasts contribute to new blood vessel formation, in that they produce angiogenetic factors, like TNF- α (Blight 1992; Chesney and Bucala 1997; Chesney and Bucala 2000; Hartlapp et al. 2001).

During the maturation phase, the incision site of TNC^{+/+} wild type mice has still shown activated microglia, while in the surrounding area microglial cells have already returned to a hyper-ramified or resting state. The decrease in microglia/macrophage activation fourteen days after spinal cord lesion has been described earlier in mice (Zhang et al. 1996; Schauwecker and Steward 1997; Ma et al. 2001; Sroga et al. 2003). Although a consistent decrease in immunoreactivity for microglia/macrophage is seen over the time (Popovich et al. 2002), cells persist in various stages of activation at the injury site for many weeks (Fawcett and Asher 1999). In concordance with the decreased activation of microglia/macrophage at the incision site, cells in the distant grey and white matter of TNC^{+/+} wild type mice have also predominantly returned to a resting state.

The role of activated microglia and blood-borne macrophages with regard to their influence upon axonal growth is also controversial. Traditionally microglial/macrophage response to injury is thought to be detrimental to the wound healing process (Leskovar et al. 2000). A better anatomical and functional outcome in animals after CNS injuries is for instance observed when invading monocyte numbers are reduced experimentally (Blight 1994; Popovich et al. 1999).

Interestingly, in certain fish and amphibians, where axonal regeneration takes place a massive microglia/macrophage activation occurs in the early response to CNS injury (McGlade-McCulloh et al. 1989; Dowding et al. 1991; Wilson et al. 1992). In addition, an increase in macrophages/microglia following CNS injury due to macrophages/microglia transplantation or administering macrophage-attracting agents is associated with an improvement of axonal regeneration (Stichel-Gunkel 1997; Leskovar et al. 2000). This suggests that the presence of activated microglia or blood-borne macrophages *per se* is probably neither harmful nor helpful to axonal growth (Rabchevsky and Streit 1997; Fawcett and Asher 1999). Most probably the profile of cytokines, chemokines and other growth factors, which are produced by activated microglia/macrophages determine the beneficial or detrimental effect to axonal growth.

In conclusion, this is the most comprehensively performed immunohistochemical study after spinal cord hemisection in mice. TNC+/+ wild type mice following spinal cord hemisection over a period of fourteen days generally resemble previous findings of diverse spinal cord injuries in rodents.

5.2. TNC^{-/-} knock out mice

This is the first survey to characterize the inflammatory response, scar formation and axonal growth following spinal cord hemisection in TNC^{-/-} knock out mice over a time period of fourteen days. In this study a detailed morphological description of the lesion is provided, including NF, F4/80 (microglia), GFAP (astrocytes), collagen type IV, laminin and fibronectin immunohistochemical analysis of the lesion. Besides morphological analysis, quantitative densitometric measurements have been performed for all six immunohistochemical reactions.

As expected, TNC^{-/-} knock out mice show abnormalities in the spatiotemporal course of the formation of ECM, the inflammatory response and subtle alterations in axonal growth. Alterations in TNC^{-/-} knock out mice are discussed in detail below.

During the early inflammatory response, alterations in fibronectin immunoreactivity and in lymphocytic influx have been observed in TNC^{-/-} knock out mice.

Quantitative densitometry for fibronectin immunoreactivity revealed a significant difference between genotypes ($p=0.036$) over the time period and for both regions (i. e. incision site, surrounding area) investigated. As this is the first study to evaluate scar formation in TNC^{-/-} knock out mice following spinal cord hemisection, animal numbers on each evaluation day had to be kept small due to restrictions of animal welfare reasons. Therefore statistical analysis has focused on the overall chronological sequence of fourteen days. During the early inflammatory response and during the maturation phase, IOD values for fibronectin immunoreactivity have been significantly lower in TNC^{-/-} knock out mice than in TNC^{+/+} wild type mice. In particular, one day following hemisection, the median IOD at the incision site for fibronectin immunoreactivity has been 23.7 in TNC^{-/-} knock out mice, compared to 92.3 in TNC^{+/+} wild type

mice. In addition, the median IOD at the surrounding area of TNC^{-/-} knock out mice has been as low as 0.1, compared to 18.8 in TNC^{+/+} wild type animals.

A marked down-regulation of fibronectin has also previously been reported in skin and cornea wounds of mice lacking TNC (for review see Mackie and Tucker 1999). This down-regulation of fibronectin observed in skin and cornea can now be extended to the spinal cord, indicating that this down-regulation of fibronectin is a general feature of TNC deficient mice.

The reduced fibronectin level may be a direct influence of absent TNC deposition in the ECM. Fibronectin has several binding sites to other ECM molecules and binding between TNC and fibronectin is possible with homologous FNIII repeats (Hauzenberger et al. 1999). Absent TNC might be the cause for a reduced capacity of binding sites for fibronectin, so that less fibronectin anchors at previously laid down TNC molecules. Additionally, TNC may have a direct influence on the expression of fibronectin. An intriguing reason for low fibronectin levels one day after hemisection in TNC^{-/-} knock out mice is an early onset of lymphocytic infiltration.

During the early inflammatory response, lymphocytic infiltration has already been seen in the surrounding area of the incision site in TNC^{-/-} knock out mice. In contrast, lymphocytic infiltration in TNC^{+/+} wild type animals has only been seen three days after injury, which is known to be the normal temporal course for lymphocytes in wound healing. Lymphocytes generally penetrate skin wounds when wound closure has been completed and then accumulate with an approximate delay of four days after injury (Eming et al. 2007).

TNC appears to regulate several aspects of lymphocyte behaviour. In particular, it is suggested to alter the adhesion properties of B- and T-lymphocytes (Rüegg et al. 1989). TNC acts as an anti-adhesive substrate for T-lymphocytes (Rüegg et al. 1989; Gundersen et al. 1997). Moreover, the TNC subunit FN1-5 and the alternatively spliced FNIII-A1A2 domain both suppress T-lymphocyte proliferation (Hibino et al. 1998; Hauzenberger et al. 1999; Puente Navazo et al. 2001). In lung cancer, TNC is known to inhibit lymphocytes that infiltrate the tumour (Parekh et al. 2005). This generally immunosuppressive function of TNC

strongly suggests an increase and/or early onset of lymphocytic infiltration in wounds of TNC deficient mice. Our study highly corroborates this theory, since one day after spinal cord hemisection, TNC^{-/-} knock out mice show an early onset lymphocytic infiltration. During the late inflammatory phase, the proliferation and the maturation phase of wound repair, numbers of lymphocytes in TNC^{-/-} knock out mice have been indistinguishable from TNC^{+/+} wild type animals. This indicates that during later stages of wound repair other aspects contribute to regulate lymphocytic maintenance in both TNC^{-/-} knock out and TNC^{+/+} wild type mice. At the same time, TNC seems to be responsible for a suppression of lymphocytic influx during the early inflammatory response.

The interaction of ECM molecules with T-lymphocytes is of vital importance for several lymphocytic functions, such as adhesion, migration, activation and proliferation (Shimizu and Shaw 1991; Hauzenberger et al. 1995). A direct interaction between fibronectin and lymphocytes has been described. T-lymphocytes are known to express fibronectin receptors and adhere to fibronectin (Lazarovits and Karsh 1993; Sundqvist et al. 1994). In addition, fibronectin is used by T-lymphocytes for local positioning (Lazarovits and Karsh 1993; Sundqvist et al. 1994).

In TNC^{-/-} knock out mice, where fibronectin levels are reduced, local positioning of lymphocytes is expected to be abnormal. However, we have observed the same spatial distribution of invading lymphocytes in TNC^{-/-} knock out mice during the early inflammatory response as we have seen in TNC^{+/+} wild type mice three days following hemisection. This finding indicates that the early onset of lymphocytic influx, due to the lack of immunosuppressive TNC, is not altered with regard to its arrangement. One could speculate, that due to low fibronectin levels fibronectin receptors on lymphocytes are compensatory up-regulated resulting in a premature, but widely normal local positioning of lymphocytes in TNC^{-/-} knock out mice. It is highly likely that other factors, especially later during the course of inflammation, contribute to lymphocytic maintenance and local positioning (for review see Ley et al. 2007). However, the

contradiction that an early onset, but normal distribution of lymphocytes in TNC deficient mice occurs remains to be clarified.

During the late inflammatory response, no difference between genotypes has been detected. In particular, fibroblast invasion, microglia/macrophage activation and astroglial scarring has been observed in a comparable spatiotemporal course in TNC^{+/+} wild type and TNC^{-/-} knock out mice.

Fibroblasts, evaluated by semi-quantitative analysis have shown a similar spatial distribution and temporal course in both genotypes throughout the time course investigated. This is in accordance with findings in skin wounds of TNC deficient mice. Proliferation and apoptosis of fibroblasts in the granulation tissue of TNC deficient mice was not changed (Forsberg et al. 1996).

In our series, collagen type I has been normally deposited in TNC^{-/-} knock out mice over a time period of fourteen days. Again, this is in agreement with findings by Forsberg et al. (1996), who found that collagen type I in skin wounds is expressed equally in TNC deficient and wild type mice. In addition, healing rate and wound contraction has been indistinguishable between TNC^{-/-} knock out and TNC^{+/+} wild type mice in our series and after skin wounds in TNC deficient mice (Forsberg et al. 1996).

Our semi-quantitative analysis in H&E stain has shown a similar density and distribution of macrophages in both genotypes. This finding corroborates earlier findings in skin wounds of TNC deficient mice, showing that macrophage numbers were not altered in comparison to wild type mice (Forsberg et al. 1996). In our study, this has been confirmed with quantitative densitometry. For F4/80 immunoreactivity (microglia/macrophage) no significant difference between the genotype ($p=0.539$) for any region (i. e. incision site, surrounding area, distant grey matter) throughout the time course investigated has been detected. Our observation is in line with a recent study, which revealed no significant alteration in the density of microglial cells in the somatosensory and motor cortex of TNC deficient mice (Irintchev et al. 2005).

Although *in vitro* studies suggest a role for TNC in regulating chemotaxis and adhesion properties of monocytes (Rüegg et al. 1989; Loike et al. 2001), this *in vivo* study indicates that TNC only plays a minor role, if any in regulating microglia/macrophage response after spinal cord hemisection.

The spatiotemporal distribution of GFAP-positive astrocytes and the subsequent scar formation has been indistinguishable between TNC^{+/+} wild type and TNC^{-/-} knock out mice throughout the time course investigated. In accordance with this finding, the glial scar after a cortical stab wound in TNC deficient mice followed the same time course and spatial distribution as the one seen in wild type mice (Steindler et al. 1995). However, that study indicated that there might be a higher number of astrocytes in TNC deficient mice, but failed to present quantitative data (Steindler et al. 1995). The present study performed a quantitative analysis for GFAP immunoreactivity, which has revealed no significant difference between genotypes ($p=0.875$) for all regions (i. e. incision site, surrounding area, distant grey matter) throughout the time course tested.

An abnormal high number of astrocytes in astroglial scarring as described by Steindler et al. (1995) may be due to a different location of injury in the CNS, i. e. brain vs. spinal cord injury. More likely, however, seems that in TNC deficient mice an abnormal high number of astrocytes already occurs during development, since astrocytes cultured on TNC revert to a quiescent, non-activated state and TNC significantly reduces the proliferation rate of astrocytes (Holley et al. 2005). This hypothesis is corroborated by Irintchev et al. (2005), who found abnormally high astrogliosis in the somatosensory and motor cortices of TNC deficient mice. This indicates that in TNC deficient mice abnormal high astrogliosis in the cortex may already occur during development and is not necessarily associated with the presence of a cortical stab wound.

Whether abnormal high numbers of astrocytes are also present in the uninjured spinal cord of TNC deficient mice remains to be clarified. However, the present study suggests, that after spinal cord hemisection TNC has no influence on the number of astrocytes and the formation of astroglial scarring.

During the proliferation phase of wound repair leucocytic infiltration generally diminishes. In contrast to TNC^{+/+} wild type animals, TNC^{-/-} knock out mice have shown a much stronger neutrophilic infiltration seven days after spinal cord hemisection. In our series, semi-quantitative analysis has only revealed abnormally high numbers of neutrophils during the proliferation phase. During the maturation phase neutrophils have equally receded in both genotypes.

In experimentally induced nephritis and dermatitis inflammation is more severe in TNC deficient mice, compared to wild type animals (Koyama et al. 1998; Nakao et al. 1998). Moreover, in chemically induced dermatitis granulocytes persist for a longer time in TNC deficient mice, compared to wild type animals. After five days granulocytes are still abundant in TNC deficient mice (Koyama et al. 1998). The findings by Koyama et al. (1998) and Nakao et al. (1998) are corroborated by our series, where an abnormal strong infiltration of neutrophilic granulocytes in TNC^{-/-} knock out mice has been observed seven days after spinal cord hemisection.

The abundance of granulocytes during the proliferation phase in TNC deficient mice may be due to the fact that TNC is known to block chemotaxis of polymorphonuclear cells (Loike et al. 2001). Hence, in TNC deficient mice polymorphonuclear cells are probably increased and their temporal course of migration may be altered. Generally TNC immunoreactivity peaks at about six days following penetrating cortical injury (Steindler 1993; Tang et al. 2003). During that time the repellent capacity of TNC provides that neutrophilic infiltration diminishes in TNC^{+/+} wild type mice. During the maturation phase, where neutrophils have been equally reduced in both genotypes other factors, such as altered cytokine levels may be responsible for the decline of neutrophils.

This study suggests, that TNC blocks neutrophilic influx in TNC^{+/+} wild type mice after spinal cord hemisection. Furthermore, absent TNC seems to be responsible for a prolonged neutrophilic infiltration after spinal cord hemisection in TNC^{-/-} knock out mice.

During the maturation phase, a decreased staining intensity for fibronectin immunoreactivity and subtle alterations in NF immunoreactivity have been observed in TNC^{-/-} knock out mice.

Compared to TNC^{+/+} wild type mice, significantly fewer fibronectin deposits have been observed in TNC^{-/-} knock out mice during the maturation phase. Quantitative densitometry for fibronectin immunoreactivity has revealed a significant difference between genotypes ($p=0.036$) for both regions throughout the time course investigated. The median IOD at the incision site of TNC^{-/-} knock out mice has been as low as 1.4 compared to a median IOD of 25.4 fourteen days following hemisection. This demonstrates a distinct down-regulation of fibronectin immunoreactivity at the incision site during the maturation phase.

As stated above, a marked down-regulation of fibronectin in TNC deficient mice is also reported in skin and cornea wounds (Forsberg et al. 1996; Matsuda et al. 1999). In particular, thirteen days following skin wound, Forsberg et al. (1996) observed a decrease in fibronectin immunoreactivity within the wound bed in TNC deficient mice. In addition, fibronectin deposition in TNC deficient mice has been reduced up to fourteen days after artificially induced glomerulonephritis (Nakao et al. 1998), which corroborates our finding of reduced fibronectin deposition fourteen days after spinal cord hemisection. The present study and previous observations indicate that fibronectin deposition is decreased during the first fourteen days of wound healing in TNC deficient mice. Whether fibronectin deposition continues to be down-regulated at later time points remains to be clarified in a further study.

It is an intriguing possibility, that in TNC deficient mice fibroblasts down-regulate fibronectin expression to compensate for the absence of TNC protein within wounds (Iglesia et al. 2000). Fibronectin is largely produced by fibroblasts (Reier and Houle 1988; Hermanns et al. 2001) and fibronectin in our series has been significantly reduced in TNC^{-/-} knock out mice. Since fibroblast density has not been altered in TNC^{-/-} knock out mice after spinal cord hemisection or after skin wounds (Forsberg et al. 1996), one could speculate that fibroblasts have an altered expression pattern of fibronectin. Altered cytokine levels in TNC deficient mice may be responsible for a low fibronectin release by fibroblasts. TNC is

required for a normal TGF- β 1 response and TGF- β 1 levels are reduced in TNC deficient mice (Nakao et al. 1998). In TNC $^{-/-}$ knock out mice reduced TGF- β 1 levels are likely to be associated with a reduced deposition of fibronectin after spinal cord injury. However, whether the expression pattern of fibroblasts in TNC $^{-/-}$ knock out mice with regard to fibronectin production is truly altered remains to be clarified in a further study.

As a multifunctional protein, fibronectin has an increasing number of interactive sites to other ECM molecules. In particular, fibronectin can bind collagen type IV (Leblond and Inoue 1989), which in turn possess binding sites to laminin (Drenckhahn and Kugler 1994). Due to reduced fibronectin deposition a subsequent down-regulation of collagen type IV in TNC $^{-/-}$ knock out mice may be feasible.

However, quantitative densitometry for collagen type IV ($p=0.651$) and laminin ($p=0.895$) has revealed no significant difference between genotypes for both regions (i. e. incision site and surrounding area) over the time period tested. This finding indicates, that deposition of collagen type IV and laminin occurs independently from TNC deposition. Indeed after CNS injury, laminin forms an independent network (Stichel and Müller 1998), which is then seen to intermingle with a preexisting collagen type IV network (Stichel et al. 1999c).

The coincidence of the imminent stop of axonal fibres is thought to be associated with the formation of ECM after wounding. Degradation of ECM molecules in CNS lesions has been shown to promote fibre growth across the incision site (Stichel et al. 1999a; Stichel et al. 1999c). Hence, an altered ECM composition as seen in TNC $^{-/-}$ knock out mice demonstrated by reduced fibronectin levels may be associated with enhanced axonal sprouting. In addition, *in vitro*, TNC selectively inhibits fibronectin-dependent neurite outgrowth (Pesheva et al. 1994), which strongly suggests enhanced axonal sprouting in TNC deficient mice.

This hypothesis is corroborated by a higher density of NF-positive axonal sprouts in TNC^{-/-} knock out mice, as compared to TNC^{+/+} wild type mice, fourteen days following hemisection. Quantitative densitometry for NF immunoreactivity has just not reached significance between genotypes ($p=0.061$) for all regions throughout the time course tested. This finding indicates a trend that NF-positive fibres are seen more frequently in TNC^{-/-} knock out mice, compared to TNC^{+/+} wild type animals. In particular, during the maturation phase a higher density of axonal sprouts has been morphologically apparent at the incision site next to the grey matter. Quantitative analysis between post injury days has also just not reached significance ($p=0.051$). However, fourteen days after spinal cord hemisection a marked difference in median IOD levels between genotypes at the incision site adjacent to the grey matter has been obvious. In that region, the median IOD for NF immunoreactivity has been 33.7 in TNC^{-/-} knock out mice, compared to a median IOD of 0.2 for TNC^{+/+} wild type mice. This is more than a 150-fold increase for NF immunoreactivity in TNC^{-/-} knock out mice. All other regions tested (i.e. incision site next to the white matter, surrounding white matter cranial, surrounding white matter caudal, surrounding grey matter cranial, surrounding grey matter caudal), have mostly shown a two-fold increase, but never exceeded an 18-fold increase of median IOD values between genotypes.

Many abnormalities found in TNC deficient mice are subtle and not discovered at first sight (Forsberg et al. 1996). In fact, the closer one looks, the more evident it becomes that TNC deficient mice are far from normal (Jones and Jones 2000). Hence, the trend of enhanced axonal sprouting in TNC^{-/-} knock out mice during the maturation phase is not surprising and should be confirmed in a further study with a larger cohort of animals fourteen after spinal cord hemisection. In addition, later time points may clarify the beneficial effect of TNC depletion for axonal growth.

Traditionally TNC is thought to be growth-promoting (Wehrle and Chiquet 1990; Lochter and Schachner 1993; Taylor et al. 1993; Götz et al. 1996; Cybulska-Klosowicz et al. 2004; Guntinas-Lichius et al. 2005), hence poor axonal growth in TNC deficient mice would be anticipated. However, reduced axonal sprouting has never been observed in TNC^{-/-} knock out mice.

In recent years it became apparent, that *in vitro* TNC can be both neurite-outgrowth promoting and repellent (Bartsch 1996). For example, soluble TNC in culture inhibits outgrowth of axons and dendrites (Lochter et al. 1991). Similarly, certain neurons in the brain avoid to grow neurites on to TNC containing areas, when plated on patterned TNC substrates (Faissner and Kruse 1990). Moreover, in choice situations neurites are deflected from TNC containing areas and purified TNC constitutes an inhospitable substrate for neural cell cultures (Cybulska-Klosowicz et al. 2004).

The effects of TNC on neurite elongation are strongly dependent on how the molecule is offered to the nerve cell (Bartsch 1996). For example, the action of TNC may differ depending upon whether it is part of the ECM or an isolated soluble molecule (Meiners et al. 2000). In addition, neurite growth promoting and neurite inhibitory effects can be associated with different domains of the molecule (Bartsch 1996), hence alternative splice variants of TNC may well lead to different functions.

A recent *in vivo* study has shown that an abnormally high neuronal density is found in the somatosensory and motor cortices of adult TNC deficient mice (Irintchev et al. 2005), demonstrating that enhanced neuronal density in the CNS occurs in the absence of TNC. In addition, in neuron-glia co-cultures a subclass of astrocytes produces a TNC-rich ECM that deflects neurite outgrowth (Grierson et al. 1990; Meiners et al. 1995). Both studies indicate that enhanced NF immunoreactivity in TNC deficient mice is highly likely and most probable associated with an altered ECM composition due to the lack of TNC.

It is still unclear whether the ECM produced in TNC deficient mice is truly normal (Jones and Jones 2000) and a change in the quality of ECM may be a benefit for axonal growth. In the ECM, down-regulation of growth-promoting or up-regulation of growth-inhibiting molecules are thought to be responsible for the biochemical barrier that impedes axonal growth (Fawcett and Asher 1999; Fitch and Silver 1999). CS-PG for instance, is one the most inhibitory molecules to axonal growth (Schwab et al. 1993; Fawcett and Asher 1999). One could assume, that due to the lack of TNC CS-PGs may be more accessible to degradation,

leading to an enhanced axonal sprouting in TNC deficient mice. It is also possible, that less binding sites for CS-PGs are present in an ECM that lacks TNC.

On the other hand, one could speculate, that growth-promoting molecules incorporated into an ECM that lacks TNC are more exposed and able to express their capacity to promote axonal growth more effectively. *In vitro* laminin has been shown to be one of the most potent supporters of neurite outgrowth and predominantly promotes neurite outgrowth of long neurites (Liesi 1990; Costa et al. 2002). Moreover, in a lesioned co-culture model high levels of laminin and its bioavailability in the ECM were associated with axonal growth (Costa et al. 2002). In an ECM that lacks TNC, laminin may not be augmented as the present study has shown, but may now have the potential to express its growth-promoting role more effectively.

The molecular mechanism of the altered ECM in TNC^{-/-} knock out mice is not yet known, but this *in vivo* study points to an important role of TNC in the composition of ECM after wounding. In summary, TNC seems to have no direct influence on axonal growth after spinal cord hemisection. This survey rather suggests that the lack of TNC fundamentally alters ECM composition in a way that axonal sprouting is more likely to penetrate spinal cord scar tissue.

To elucidate the spatiotemporal course of wound repair mechanisms with regard to the role of TNC, we have examined the inflammatory response, microglia, astrocytes, ECM components and axonal growth in TNC^{-/-} knock out mice following spinal cord hemisection.

In summary, the most marked alterations in TNC^{-/-} knock out mice have been observed in ECM composition and NF-positive fibres. The present study has chosen the time duration of fourteen days, resembling the inflammatory reaction and scar formation during wound healing. In our study the most marked alterations in TNC^{-/-} knock out mice have been observed fourteen days after injury. Hence a further study should be carried out at later time points to clarify the beneficial effect of TNC depletion with regard to axonal growth.

The evaluation of other ECM molecules in TNC deficient mice after spinal cord hemisection could yield important insights into the altered ECM composition. The generation of double or multiple knock out models for TNC and other ECM molecules (i. e. fibronectin) might identify further components that play a role in the success of axonal growth after spinal cord injury.

Developing a more thorough understanding of those different processes during wound repair will be essential for developing effective therapeutic and reparative strategies for treating spinal cord injuries.

6. Summary

Patients suffering from spinal cord (SC) injury are challenged to maintain an acceptable quality of life and complete functional recovery after SC injury has not been described to date. Tenascin C (TNC), an extracellular matrix (ECM) glycoprotein is involved in wound healing and its role is somewhat paradoxical, because *in vitro* it can be both neurite-outgrowth promoting and repellent.

To assess its effects *in vivo*, 20 TNC^{-/-} knock out (TNC^{-/-}) and 20 TNC^{+/+} wild type (TNC^{+/+}) mice underwent lumbar SC hemisection. According to the sequence of the inflammatory response, systemic perfusion was performed at 1, 3, 7 and 14 days post surgery. Cryostat sections were examined in H&E and combined Masson trichrome and Verhoeff stain as well as by immunohistochemistry using antibodies against neurofilament (NF), GFAP (astrocytes), F4/80 (microglia) and the ECM molecules collagen type IV, laminin and fibronectin. Staining intensity was quantified by measuring Integrated Optical Density at the incision site, the surrounding area and distant from the lesion site.

TNC^{+/+} mice resembled the findings of previous studies in normal mice. However, distinct alterations after SC hemisection were seen in TNC^{-/-} mice. After one day, an early onset lymphocytic infiltration was seen in TNC^{-/-} mice. Seven days after injury neutrophil influx was more prominent in TNC^{-/-} mice compared to TNC^{+/+} mice. Quantitative densitometry demonstrated that microglial and astrocytic responses to injury were identical in TNC^{-/-} and TNC^{+/+} mice. However, after fourteen days, fibronectin was significantly ($p=0.036$) decreased in TNC^{-/-} mice. At the same time, NF-positive axonal sprouts were markedly increased along the incision edges of TNC^{-/-} mice.

The increase in NF-positive sprouts in TNC^{-/-} mice indicates that lack of TNC fundamentally alters ECM composition in a way that axonal fibres are more likely to penetrate SC scar tissue. These differences between TNC^{+/+} and TNC^{-/-} mice were detected fourteen days after injury. Hence further *in vivo* studies should be carried out at later time points in order to assess the beneficial effect of TNC depletion in axonal regeneration further.

7. References

Abe R, Donnelly SC, Peng T, Bucala R, Metz CN (2001) Peripheral blood fibrocytes: Differentiation pathway and migration to wound sites. *J Immunol.* 166: 7556-62

Adrian EK, Williams MG (1973) Cell proliferation in injured spinal cord. An electron microscopic study. *J Comp Neurol.* 151: 1-24

Ajemian A, Ness R, David S (1994) Tenascin in the injured rat optic nerve and in non-neuronal cells in vitro: potential role in neural repair. *J Comp Neurol.* 340: 233-42

Al-Chalabi A, Miller CC (2003) Neurofilaments and neurological disease. *Bioessays.* 25: 346-55

Alonso G, Privat A (1993) Reactive astrocytes involved in the formation of lesional scars differ in the mediobasal hypothalamus and in other forebrain regions. *J Neurosci Res.* 34: 523-38

Austyn JM, Gordon S (1981) F4/80, a monoclonal antibody directed specifically against the mouse macrophage. *Eur J Immunol.* 11: 805-15

Aziz SM, Toborek M, Hennig B, Mattson MP, Guo H, Lipke DW (1997) Oxidative stress mediates monocrotaline-induced alterations in tenascin expression in pulmonary artery endothelial cells. *Int J Biochem Cell Biol.* 29: 75-87

Bähr M, Bonhoeffer F (1994) Perspectives on axonal regeneration in the mammalian CNS. *Trends Neurosci.* 17: 473-9

Bannister LH (1995) Cells and Tissues. In: Williams PL (ed) *Gray's Anatomy, The anatomical basis of medicine and surgery*, Churchill Livingstone, New York Edinburgh London Tokyo Madrid and Melbourne, p 76

Bartsch U (1996) The extracellular matrix molecule tenascin-C: expression in vivo and functional characterization in vitro. *Prog Neurobiol.* 49: 145-68

Beattie MS, Li Q, Bresnahan JC (2000) Cell death and plasticity after spinal cord injury. *Prog Brain Res.* 128: 9-21

Bernstein JJ, Getz R, Jefferson M, Kelemen M (1985) Astrocytes secrete basal lamina after hemisection of rat spinal cord. *Brain Res.* 327: 135-41

Bethea JR (2000) Spinal cord injury-induced inflammation: a dual-edged sword. *Prog Brain Res.* 128: 33-42

Bisby MA, Tetzlaff W (1992) Changes in cytoskeletal protein synthesis following axon injury and during axon regeneration. *Mol Neurobiol.* 6: 107-23

Blight AR (1991) Morphometric analysis of blood vessels in chronic experimental spinal cord injury: hypervascularity and recovery of function. *J Neurol Sci.* 106: 158-74

Blight AR (1992) Macrophages and inflammatory damage in spinal cord injury. *J Neurotrauma.* 9 Suppl 1: S83-91

Blight AR (1994) Effects of silica on the outcome from experimental spinal cord injury: implication of macrophages in secondary tissue damage. *Neuroscience*. 60: 263-73

Böttner M, Kriegelstein K, Unsicker K (2000) The transforming growth factor-betas: structure, signaling, and roles in nervous system development and functions. *J Neurochem*. 75: 2227-40

Bregman BS, Coumans JV, Dai HN, Kuhn PL, Lynskey J, McAtee M, Sandhu F (2002) Transplants and neurotrophic factors increase regeneration and recovery of function after spinal cord injury. *Prog Brain Res*. 137: 257-73

Bush TG, Puvanachandra N, Horner CH, Polito A, Ostenfeld T, Svendsen CN, Mucke L, Johnson MH, Sofroniew MV (1999) Leukocyte infiltration, neuronal degeneration, and neurite outgrowth after ablation of scar-forming, reactive astrocytes in adult transgenic mice. *Neuron*. 23: 297-308

Carbonell AL, Boya J (1988) Ultrastructural study on meningeal regeneration and meningo-glial relationships after cerebral stab wound in the adult rat. *Brain Res*. 439: 337-44

Carlson SL, Parrish ME, Springer JE, Doty K, Dossett L (1998) Acute inflammatory response in spinal cord following impact injury. *Exp Neurol*. 151: 77-88

Carson MJ, Reilly CR, Sutcliffe JG, Lo D (1998) Mature microglia resemble immature antigen-presenting cells. *Glia*. 22: 72-85

Chesney J, Bucala R (1997) Peripheral blood fibrocytes: novel fibroblast-like cells that present antigen and mediate tissue repair. *Biochem Soc Trans*. 25: 520-4

Chesney J, Bucala R (2000) Peripheral blood fibrocytes: mesenchymal precursor cells and the pathogenesis of fibrosis. *Curr Rheumatol Rep*. 2: 501-5

Chilosi M, Lestani M, Benedetti A, Montagna L, Pedron S, Scarpa A, Menestrina F, Hirohashi S, Pizzolo G, Semenzato G (1993) Constitutive expression of tenascin in T-dependent zones of human lymphoid tissues. *Am J Pathol*. 143: 1348-55

Chiquet-Ehrismann R (1995) Tenascins, a growing family of extracellular matrix proteins. *Experientia*. 51(9-10): 853-62

Chugani DC, Kedersha NL, Rome LH (1991) Vault immunofluorescence in the brain: new insights regarding the origin of microglia. *J Neurosci*. 11: 256-68

Cifuentes-Diaz C, Velasco E, Meunier FA, Goudou D, Belkadi, Faille L, Murawsky M, Angaut-Petit D, Molgo J, Schachner M, Saga Y, Aizawa S, Rieger F (1998) The peripheral nerve and the neuromuscular junction are affected in the tenascin-C deficient mouse. *Cell Mol Biol (Noisy-le-grand)*. 44: 357-79

Cifuentes-Diaz C, Faille L, Goudou D, Schachner M, Rieger F, Angaut-Petit D (2002) Abnormal reinnervation of skeletal muscle in a tenascin-C deficient mouse. *J Neurosci Res*. 67: 93-9

Clark, RAF (Ed) (1996) *The Molecular and Cellular Biology of Wound Repair*, 2nd ed. Plenum Press, New York

Costa S, Planchenault T, Charriere-Bertrand C, Mouchel Y, Fages C, Juliano S, Lefrançois T, Barlovatz-Meimon G, Tardy M (2002) Astroglial permissivity for neurite outgrowth in neuron-astrocyte cocultures depends on regulation of laminin bioavailability. *Glia*. 37: 105-13

- Culav EM, Clark CH, Merrilees MJ (1999) Connective tissues: matrix composition and its relevance to physical therapy. *Phys Ther.* 79: 308-19
- Curtis R, Green D, Lindsay RM, Wilkin GP (1993) Up-regulation of GAP-43 and growth of axons in rat spinal cord after compression injury. *J Neurocytol.* 22: 51-64
- Cybulska-Klosowicz A, Zakrzewska R, Pyza E, Kossut M, Schachner M (2004) Reduced plasticity of cortical whisker representation in adult tenascin-C-deficient mice after vibrissotomy. *Eur J Neurosci.* 20: 1538-44
- Dowding AJ, Maggs A, Scholes J (1991) Diversity amongst the microglia in growing and regenerating fish CNS: immunohistochemical characterization using FL1, an anti-macrophage monoclonal antibody. *Glia.* 4: 345-64
- Drenckhahn D, Kugler P (1994) Systematik der Gewebe: Bindegewebe. In: Drenckhahn D, Zenker W (eds) *Benninghoff Anatomie, Makroskopische Anatomie, Embryologie und Histologie des Menschen*, Urban and Schwarzenberg. München, Wien, Baltimore, 15th edition, Volume 1, p 140
- Dusart I, Schwab ME (1994) Secondary cell death and the inflammatory reaction after dorsal hemisection of the rat spinal cord. *Eur J Neurosci.* 6: 712-24
- Egan RA, Vijayan VK (1991) Fibronectin immunoreactivity in neural trauma. *Brain Res.* 568: 330-4
- Eming SA, Krieg T, Davidson JM (2007) Inflammation in wound repair: molecular and cellular mechanisms. *J Invest Dermatol.* 127: 514-25
- Erickson HP (1993) Tenascin-C, tenascin-R and tenascin-X: a family of talented proteins in search of functions. *Curr Opin Cell Biol.* 5: 869-76
- Erickson HP, Bourdon MA (1989) Tenascin: an extracellular matrix protein prominent in specialized embryonic tissues and tumors. *Annu Rev Cell Biol.* 5: 71-92
- Evers MR, Salmen B, Bukalo O, Rollenhagen A, Bosl MR, Morellini F, Bartsch U, Dityatev A, Schachner M (2002) Impairment of L-type Ca²⁺ channel-dependent forms of hippocampal synaptic plasticity in mice deficient in the extracellular matrix glycoprotein tenascin-C. *J Neurosci.* 22: 7177-94
- Faissner A (1997) The tenascin gene family in axon growth and guidance. *Cell Tissue Res.* 290: 331-41
- Faissner A, Kruse J (1990) J1/tenascin is a repulsive substrate for central nervous system neurons. *Neuron.* 5: 627-37
- Farooque M, Zhang Y, Holtz A, Olsson Y (1992) Exudation of fibronectin and albumin after spinal cord injury in rats. *Acta Neuropathol (Berl).* 84: 613-20
- Faulkner JR, Herrmann JE, Woo MJ, Tansey KE, Doan NB, Sofroniew MV (2004) Reactive astrocytes protect tissue and preserve function after spinal cord injury. *J Neurosci.* 24: 2143-55
- Fawcett JW, Geller HM (1998) Regeneration in the CNS: optimism mounts. *Trends Neurosci.* 21: 179-80

Fawcett JW, Asher RA (1999) The glial scar and central nervous system repair. *Brain Res Bull.* 49: 377-91

Fawcett JW, Fersht N, Housden L, Schachner M, Pesheva P (1992) Axonal growth on astrocytes is not inhibited by oligodendrocytes. *J Cell Sci.* 103: 571-9

Fitch MT, Silver J (1997) Activated macrophages and the blood-brain barrier: inflammation after CNS injury leads to increases in putative inhibitory molecules. *Exp Neurol.* 148: 587-603

Forsberg E, Hirsch E, Frohlich L, Meyer M, Ekblom P, Aszodi A, Werner S, Fassler R (1996) Skin wounds and severed nerves heal normally in mice lacking tenascin-C. *Proc Natl Acad Sci U S A.* 93: 6594-9

Frisén J, Fried K, Sjögren AM, Risling M (1993) Growth of ascending spinal axons in CNS scar tissue. *Int J Dev Neurosci.* 11: 461-75

Frisén J, Haegerstrand A, Risling M, Fried K, Johansson CB, Hammarberg H, Elde R, Hokfelt T, Cullheim S (1995) Spinal axons in central nervous system scar tissue are closely related to laminin-immunoreactive astrocytes. *Neuroscience.* 65: 293-304

Fuchs E, Weber K (1994) Intermediate filaments: structure, dynamics, function, and disease. *Annu Rev Biochem.* 63: 345-82

Fujiki M, Zhang Z, Guth L, Steward O (1996) Genetic influences on cellular reactions to spinal cord injury: activation of macrophages/microglia and astrocytes is delayed in mice carrying a mutation (WldS) that causes delayed Wallerian degeneration. *J Comp Neurol.* 371: 469-84

Gage FH, Olejniczak P, Armstrong DM (1988) Astrocytes are important for sprouting in the septohippocampal circuit. *Exp Neurol.* 102: 2-13

Giménez y Ribotta M, Menet V, Privat A (2001) The role of astrocytes in axonal regeneration in the mammalian CNS. *Prog Brain Res.* 132: 587-610

Giménez y Ribotta M, Gaviria M, Menet V, Privat A (2002) Strategies for regeneration and repair in spinal cord traumatic injury. *Prog Brain Res.* 137: 191-212

Goetschy JF, Ulrich G, Aunis D, Ciesielski-Treska J (1987) Fibronectin and collagens modulate the proliferation and morphology of astroglial cells in culture. *Int J Dev Neurosci.* 5: 63-70

Götz B, Scholze A, Clement A, Joester A, Schütte K, Wigger F, Frank R, Spiess E, Ekblom P, Faissner A (1996) Tenascin-C contains distinct adhesive, anti-adhesive, and neurite outgrowth promoting sites for neurons. *J Cell Biol.* 132: 681-99

Goldstein B, Little JW, Harris RM (1997) Axonal sprouting following incomplete spinal cord injury: an experimental model. *J Spinal Cord Med.* 20: 200-6

Goldstein ME, Cooper HS, Bruce J, Carden MJ, Lee VM, Schlaepfer WW (1987) Phosphorylation of neurofilament proteins and chromatolysis following transection of rat sciatic nerve. *J Neurosci.* 7: 1586-94

Grierson JP, Petroski RE, Ling DS, Geller HM (1990) Astrocyte topography and tenascin cytotactin expression: correlation with the ability to support neuritic outgrowth. *Brain Res Dev Brain Res.* 55: 11-9

- Grimpe B, Silver J (2002) The extracellular matrix in axon regeneration. *Prog Brain Res.* 137: 333-49
- Gundersen D, Trân-Thang C, Sordat B, Mourali F, Rüegg C (1997) Plasmin-induced proteolysis of tenascin-C: modulation by T lymphocyte-derived urokinase-type plasminogen activator and effect on T lymphocyte adhesion, activation, and cell clustering. *J Immunol.* 158: 1051-60
- Guntinas-Lichius O, Angelov DN, Morellini F, Lenzen M, Skouras E, Schachner M, Irintchev A (2005) Opposite impacts of tenascin-C and tenascin-R deficiency in mice on the functional outcome of facial nerve repair. *Eur J Neurosci.* 22: 2171-9
- Guth L, Zhang Z, Steward O (1999) The unique histopathological responses of the injured spinal cord. Implications for neuroprotective therapy. *Ann N Y Acad Sci.* 890: 366-84
- Hagios C, Koch M, Spring J, Chiquet M, Chiquet-Ehrismann R (1996) Tenascin-Y: a protein of novel domain structure is secreted by differentiated fibroblasts of muscle connective tissue. *J Cell Biol.* 134: 1499-512
- Hartlapp I, Abe R, Saeed RW, Peng T, Voelter W, Bucala R, Metz CN (2001) Fibrocytes induce an angiogenic phenotype in cultured endothelial cells and promote angiogenesis in vivo. *FASEB J.* 15: 2215-24
- Hatten ME, Liem RK, Shelanski ML, Mason CA (1991) Astroglia in CNS injury. *Glia.* 4: 233-43
- Hauzenberger D, Klominek J, Bergström SE, Sundqvist KG (1995) T lymphocyte migration: the influence of interactions via adhesion molecules, the T cell receptor, and cytokines. *Crit Rev Immunol.* 15: 285-316
- Hauzenberger D, Olivier P, Gundersen D, Rüegg C (1999) Tenascin-C inhibits beta1 integrin-dependent T lymphocyte adhesion to fibronectin through the binding of its fnIII 1-5 repeats to fibronectin. *Eur J Immunol.* 29: 1435-47
- Hermanns S, Klapka N, Müller HW (2001) The collagenous lesion scar - an obstacle for axonal regeneration in brain and spinal cord injury. *Restor Neurol Neurosci.* 19: 139-48
- Hibino S, Kato K, Kudoh S, Yagita H, Okumura K (1998) Tenascin suppresses CD3-mediated T cell activation. *Biochem Biophys Res Commun.* 250(1): 119-24
- Holley JE, Gveric D, Whatmore JL, Gutowski NJ (2005) Tenascin C induces a quiescent phenotype in cultured adult human astrocytes. *Glia.* 52(1): 53-8
- Iglesia DD, Gala PH, Qiu T, Stepp MA (2000) Integrin expression during epithelial migration and re-stratification in the tenascin-C-deficient mouse cornea. *J Histochem Cytochem.* 48: 363-76
- Inman D, Guth L, Steward O (2002) Genetic influences on secondary degeneration and wound healing following spinal cord injury in various strains of mice. *J Comp Neurol.* 451: 225-35
- Inman DM, Steward O (2003) Ascending sensory, but not other long-tract axons, regenerate into connective tissue matrix that forms at the site of a spinal cord injury in mice. *J Comp Neurol.* 462: 431-49
- Irintchev A, Rollenhagen A, Troncoso E, Kiss JZ, Schachner M (2005) Structural and functional aberrations in the cerebral cortex of tenascin-C deficient mice. *Cereb Cortex.* 15: 950-62

Jaeger CB, Blight AR (1997) Spinal cord compression injury in guinea pigs: structural changes of endothelium and its perivascular cell associations after blood-brain barrier breakdown and repair. *Exp Neurol.* 144: 381-99

Jakeman LB, Reier PJ (1991) Axonal projections between fetal spinal cord transplants and the adult rat spinal cord: a neuroanatomical tracing study of local interactions. *J Comp Neurol.* 307: 311-34

Jakeman LB, Guan Z, Wei P, Ponnappan R, Dzwonczyk R, Popovich PG, Stokes BT (2000) Traumatic spinal cord injury produced by controlled contusion in mouse. *J Neurotrauma.* 17: 299-319

Jones FS, Jones PL (2000) The tenascin family of ECM glycoproteins: structure, function, and regulation during embryonic development and tissue remodeling. *Dev Dyn.* 218: 235-59

Joosten EA (1997) Corticospinal tract regrowth. *Prog Neurobiol.* 53: 1-25

Joosten EA, Dijkstra S, Brook GA, Veldman H, Bar PR (2000) Collagen IV deposits do not prevent regrowing axons from penetrating the lesion site in spinal cord injury. *J Neurosci Res.* 62: 686-91

Jordan FL, Thomas WE (1988) Brain macrophages: Questions of origin and interrelationship. *Brain Res. Rev.* 13: 165-178

Kawaja MD, Gage FH (1991) Reactive astrocytes are substrates for the growth of adult CNS axons in the presence of elevated levels of nerve growth factor. *Neuron.* 7: 1019-30

Kiernan BW, Garcion E, Ferguson J, Frost EE, Torres EM, Dunnett SB, Saga Y, Aizawa S, Faissner A, Kaur R, Franklin RJ, ffrench-Constant C (1999) Myelination and behaviour of tenascin-C null transgenic mice. *Eur J Neurosci.* 11: 3082-92

Kliesch WF, Cruse JM, Lewis RE, Bishop GR, Brackin B, Lampton JA (1996) Restoration of depressed immune function in spinal cord injury patients receiving rehabilitation therapy. *Paraplegia.* 34: 82-90

Koyama Y, Kusubata M, Yoshiki A, Hiraiwa N, Ohashi T, Irie S, Kusakabe M (1998) Effect of tenascin-C deficiency on chemically induced dermatitis in the mouse. *J Invest Dermatol.* 111: 930-5

Kreutzberg GW (1996) Principles of neuronal regeneration. *Acta Neurochir Suppl.* 66: 103-6

Kros JM, Waarsenburg N, Hayes DP, Hop WC, van Dekken H (2000) Cytogenetic analysis of gemistocytic cells in gliomas. *J Neuropathol Exp Neurol.* 59: 679-86

Kuhn PL, Wrathall JR (1998) A mouse model of graded contusive spinal cord injury. *J Neurotrauma.* 15: 125-40

Lampert P, Cressman M (1964) Axonal regeneration in the dorsal columns of the spinal cord of adult rats. An electron microscopic study. *Lab Invest.* 13: 825-39

Lasek RJ (1981) The dynamic ordering of neuronal cytoskeletons. *Neurosci Res Program Bull.* 19: 7-32

Lasek RJ (1988) Studying the intrinsic determinants of neuronal form and function. In: Lasek RJ, Black MM (eds) *Intrinsic Determinations of Neuronal Form and Function*. New York: Alan R. Liss pp: 1-60

Lazarides E (1982) Intermediate filaments: a chemically heterogeneous, developmentally regulated class of proteins. *Annu Rev Biochem.* 51: 219-50

Lazarovits AI, Karsh J (1993) Differential expression in rheumatoid synovium and synovial fluid of alpha 4 beta 7 integrin. A novel receptor for fibronectin and vascular cell adhesion molecule-1. *J Immunol.* 151: 6482-9

Leblond CP, Inoue S (1989) Structure, composition, and assembly of basement membrane. *Am J Anat.* 185: 367-90

Leme RJ, Chadi G (2001) Distant microglial and astroglial activation secondary to experimental spinal cord lesion. *Arq Neuropsiquiatr.* 59(3-A): 483-92

Leskovar A, Moriarty LJ, Turek JJ, Schoenlein IA, Borgens RB (2000) The macrophage in acute neural injury: changes in cell numbers over time and levels of cytokine production in mammalian central and peripheral nervous systems. *J Exp Biol.* 203: 1783-95

Ley K, Laudanna C, Cybulsky MI, Nourshargh S (2007) Getting to the site of inflammation: the leukocyte adhesion cascade updated. *Nat Rev Immunol.* 7: 678-89

Li Y, Raisman G (1995) Sprouts from cut corticospinal axons persist in the presence of astrocytic scarring in long-term lesions of the adult rat spinal cord. *Exp Neurol.* 134: 102-11

Liesi P (1985) Laminin-immunoreactive glia distinguish regenerative adult CNS systems from non-regenerative ones. *EMBO J.* 4: 2505-11

Liesi P (1990) Extracellular matrix and neuronal movement. *Experientia.* 46: 900-7

Liesi P, Kaakkola S, Dahl D, Vaheri A (1984) Laminin is induced in astrocytes of adult brain by injury. *EMBO J.* 3: 683-6

Liesi P, Kauppila T (2002) Induction of type IV collagen and other basement-membrane-associated proteins after spinal cord injury of the adult rat may participate in formation of the glial scar. *Exp Neurol.* 173: 31-45

Liesi P, Kirkwood T, Vaheri A (1986) Fibronectin is expressed by astrocytes cultured from embryonic and early postnatal rat brain. *Exp Cell Res.* 163: 175-85

Liesi P, Risteli L (1989) Glial cells of mammalian brain produce a variant form of laminin. *Exp Neurol.* 105: 86-92

Lochter A, Schachner M (1993) Tenascin and extracellular matrix glycoproteins: from promotion to polarization of neurite growth in vitro. *J Neurosci.* 13: 3986-4000

Lochter A, Vaughan L, Kaplony A, Prochiantz A, Schachner M, Faissner A (1991) J1/tenascin in substrate-bound and soluble form displays contrary effects on neurite outgrowth. *J Cell Biol.* 113: 1159-71

- Loike JD, Cao L, Budhu S, Hoffman S, Silverstein SC (2001) Blockade of alpha 5 beta 1 integrins reverses the inhibitory effect of tenascin on chemotaxis of human monocytes and polymorphonuclear leukocytes through three-dimensional gels of extracellular matrix proteins. *J Immunol.* 166: 7534-42
- Lorenz HP, Longaker MT (2003) Wounds: Biology, Pathology, and Management. In: Norton JA, Bollinger RR, Chang AE, Lowry SF, Mulvihill SJ, Pass HI, Thompson RW (eds) *Essential Practice of Surgery*, Springer New York, p 77-88
- Lorke D, Möller P (1985) The early appearance of fibronectin in the course of metastatic tumor growth in lymph nodes. *J Cancer Res Clin Oncol* 109: 65-71
- Ma M, Basso DM, Walters P, Stokes BT, Jakeman LB (2001) Behavioral and histological outcomes following graded spinal cord contusion injury in the C57Bl/6 mouse. *Exp Neurol.* 169: 239-54
- Ma M, Wei P, Wei T, Ransohoff RM, Jakeman LB (2004) Enhanced axonal growth into a spinal cord contusion injury site in a strain of mouse (129X1/SvJ) with a diminished inflammatory response. *J Comp Neurol.* 474: 469-86
- Mackie EJ (1997) Molecules in focus: tenascin-C. *Int J Biochem Cell Biol.* 29: 1133-7
- Mackie EJ, Tucker RP (1999) The tenascin-C knockout revisited. *J Cell Sci.* 112: 3847-53
- Mackie EJ, Halfter W, Liverani D (1988) Induction of tenascin in healing wounds. *J Cell Biol.* 107: 2757-67
- Mackie EJ, Thesleff I, Chiquet-Ehrismann R (1987) Tenascin is associated with chondrogenic and osteogenic differentiation in vivo and promotes chondrogenesis in vitro. *J Cell Biol.* 105: 2569-79
- Mansour H, Asher R, Dahl D, Labkovsky B, Perides G, Bignami A (1990) Permissive and non-permissive reactive astrocytes: immunofluorescence study with antibodies to the glial hyaluronate-binding protein. *J Neurosci Res.* 25: 300-11
- Mansour H, Bignami A, Labkovsky B, Dahl D (1989) Neurofilament phosphorylation in neuronal perikarya following axotomy: a study of rat spinal cord with ventral and dorsal root transection. *J Comp Neurol.* 283: 481-5
- Maseruka H, Bonshek RE, Tullo AB (1997) Tenascin-C expression in normal, inflamed, and scarred human corneas. *Br J Ophthalmol.* 81: 677-82
- Matsuda A, Yoshiki A, Tagawa Y, Matsuda H, Kusakabe M (1999) Corneal wound healing in tenascin knockout mouse. *Invest Ophthalmol Vis Sci.* 40: 1071-80
- Matthews MA, St Onge MF, Faciane CL, Gelderd JB (1979a) Axon sprouting into segments of rat spinal cord adjacent to the site of a previous transection. *Neuropathol Appl Neurobiol.* 5: 181-96
- Matthews MA, St Onge MF, Faciane CL, Gelderd JB (1979b) Spinal cord transection: a quantitative analysis of elements of the connective tissue matrix formed within the site of lesion following administration of piromen, cytoxan or trypsin. *Neuropathol Appl Neurobiol.* 5: 161-80
- Maxwell WL, Duance VC, Lehto M, Ashurst DE, Berry M (1984) The distribution of types I, III, IV and V collagens in penetrant lesions of the central nervous system of the rat. *Histochem J.* 16: 1215-29

- McClung JR (1972) Phagocytosis of degenerating retinogeniculate terminals in the squirrel monkey, *Saimiri sciureus*. *Brain Res.* 44: 656-60
- McGlade-McCulloh E, Morrissey AM, Norona F, Muller KJ (1989) Individual microglia move rapidly and directly to nerve lesions in the leech central nervous system. *Proc Natl Acad Sci U S A.* 86: 1093-7
- McTigue DM, Popovich PG, Jakeman LB, Stokes BT (2000) Strategies for spinal cord injury repair. *Prog Brain Res.* 128: 3-8
- Meiners S, Powell EM, Geller HM (1995) A distinct subset of tenascin/CS-6-PG-rich astrocytes restricts neuronal growth in vitro. *J Neurosci.* 15(12): 8096-108
- Meiners S, Mercado ML, Geller HM (2000) The multi-domain structure of extracellular matrix molecules: implications for nervous system regeneration. *Prog Brain Res.* 128: 23-31
- Morellini F, Schachner M (2006) Enhanced novelty-induced activity, reduced anxiety, delayed resynchronization to daylight reversal and weaker muscle strength in tenascin-C-deficient mice. *Eur J Neurosci.* 23: 1255-68
- Nacimiento W (1999) Nervenregeneration nach Rückenmarkstrauma: Fortschritte in der Neurobiologie, Perspektiven für die Klinik. *Dtsch Arztebl* 96(19): A-1279 / B-1091 / C-1019
- Nacimiento W, Brook GA, Noth J (1997) Lesion-induced neuronal reorganization in the spinal cord: morphological aspects. *Adv Neurol.* 73: 37-59
- Nacimiento W, Schmitt AB, Brook GA (1999) Nerve regeneration after spinal cord trauma. Neurobiological progress and clinical expectations. *Nervenarzt.* 70: 702-13
- Nakao N, Hiraiwa N, Yoshiki A, Ike F, Kusakabe M (1998) Tenascin-C promotes healing of Habu-snake venom-induced glomerulonephritis: studies in knockout congenic mice and in culture. *Am J Pathol.* 152: 1237-45
- Nicholls JG, Adams WB, Eugenin J, Geiser R, Lepre M, Luque JM, Wintzer M (1999) Why does the central nervous system not regenerate after injury? *Surv Ophthalmol.* 43 Suppl 1: S136-41
- Noble M, Fok-Seang J, Cohen J (1984) Glia are a unique substrate for the in vitro growth of central nervous system neurons. *J Neurosci.* 4: 1892-903
- Norenberg MD (1994) Astrocyte responses to CNS injury. *J Neuropathol Exp Neurol.* 53: 213-20
- Norton WT (1999) Cell reactions following acute brain injury: a review. *Neurochem Res.* 24(2): 213-8
- Parekh K, Ramachandran S, Cooper J, Bigner D, Patterson A, Mohanakumar T (2005) Tenascin-C, over expressed in lung cancer down regulates effector functions of tumor infiltrating lymphocytes. *Lung Cancer.* 47: 17-29
- Perry VH, Gordon S (1987) Modulation of CD4 antigen on macrophages and microglia in rat brain. *J Exp Med.* 166: 1138-43
- Pesheva P, Juliano RL, Schachner M (1988) Expression and localization of the fibronectin receptor in the mouse nervous system. *J Neurosci Res.* 20: 420-30

- Pesheva P, Probstmeier R, Skubitz AP, McCarthy JB, Furcht LT, Schachner M (1994) Tenascin-R (J1 160/180) inhibits fibronectin-mediated cell adhesion-functional relatedness to tenascin-C. *J Cell Sci.* 107: 2323-33
- Popovich PG, Guan Z, McGaughy V, Fisher L, Hickey WF, Basso DM (2002) The neuropathological and behavioral consequences of intraspinal microglial/macrophage activation. *J Neuropathol Exp Neurol.* 61: 623-33
- Popovich PG, Guan Z, Wei P, Huitinga I, van Rooijen N, Stokes BT (1999) Depletion of hematogenous macrophages promotes partial hindlimb recovery and neuroanatomical repair after experimental spinal cord injury. *Exp Neurol.* 158: 351-65
- Popovich PG, Stokes BT, Whitacre CC (1996) Concept of autoimmunity following spinal cord injury: possible roles for T lymphocytes in the traumatized central nervous system. *J Neurosci Res.* 45: 349-63
- Popovich PG, Wei P, Stokes BT (1997) Cellular inflammatory response after spinal cord injury in Sprague-Dawley and Lewis rats. *J Comp Neurol.* 377: 443-64
- Posmantur RM, Newcomb JK, Kampf A, Hayes RL (2000) Light and confocal microscopic studies of evolutionary changes in neurofilament proteins following cortical impact injury in the rat. *Exp Neurol.* 161: 15-26
- Price J, Hynes RO (1985) Astrocytes in culture synthesize and secrete a variant form of fibronectin. *J Neurosci.* 5: 2205-2211
- Puente Navazo MD, Valmori D, Rüegg C (2001) The alternatively spliced domain TnFnIII A1A2 of the extracellular matrix protein tenascin-C suppresses activation-induced T lymphocyte proliferation and cytokine production. *J Immunol.* 167: 6431-40
- Qiu J, Cai D, Filbin MT (2000) Glial inhibition of nerve regeneration in the mature mammalian CNS. *Glia.* 29: 166-74
- Quan TE, Cowper S, Wu SP, Bockenstedt LK, Bucala R (2004) Circulating fibrocytes: collagen-secreting cells of the peripheral blood. *Int J Biochem Cell Biol.* 36: 598-606
- Rabchevsky AG, Streit WJ (1997) Grafting of cultured microglial cells into the lesioned spinal cord of adult rats enhances neurite outgrowth. *J Neurosci Res.* 47: 34-48
- Ramon y Cajal S (1928) *Degeneration and Regeneration of the Nervous System.* New York, Hafner
- Reier PJ, Houle JD (1988) The glial scar: its bearing on axonal elongation and transplantation approaches to CNS repair. *Adv Neurol.* 47: 87-138
- Ricci-Vitiani L, Casalbore P, Petrucci G, Lauretti L, Montano N, Larocca LM, Falchetti ML, Lombardi DG, Gerevini VD, Cenciarelli C, D'Alessandris QG, Fernandez E, De Maria R, Maira G, Peschle C, Parati E, Pallini R (2006) Influence of local environment on the differentiation of neural stem cells engrafted onto the injured spinal cord. *Neurol Res.* 28: 488-92
- Risling M, Fried K, Linda H, Carlstedt T, Cullheim S (1993) Regrowth of motor axons following spinal cord lesions: distribution of laminin and collagen in the CNS scar tissue. *Brain Res Bull.* 30: 405-14

- Romo T (2008) Wound Healing, Skin. In: eMedicine, accessed March 2008
- Rossignol S, Schwab M, Schwartz M, Fehlings MG (2007) Spinal cord injury: time to move? *J Neurosci.* 31; 27: 11782-92
- Roth-Kleiner M, Hirsch E, Schittny JC (2004) Fetal lungs of tenascin-C-deficient mice grow well, but branch poorly in organ culture. *Am J Respir Cell Mol Biol.* 30(3): 360-6
- Rüegg CR, Chiquet-Ehrismann R, Alkan SS (1989) Tenascin, an extracellular matrix protein, exerts immunomodulatory activities. *Proc Natl Acad Sci U S A.* 86: 7437-41
- Saga Y, Yagi T, Ikawa Y, Sakakura T, Aizawa S (1992) Mice develop normally without tenascin. *Genes Dev.* 6: 1821-31
- Sandvig A, Berry M, Barrett LB, Butt A, Logan A (2004) Myelin-, reactive glia-, and scar-derived CNS axon growth inhibitors: expression, receptor signaling, and correlation with axon regeneration. *Glia.* 46: 225-51
- Schachner M (1994) Lessons from genetic knockout mice deficient in neural recognition molecules. *Prog Brain Res.* 100: 25-30
- Schauwecker PE, Steward O (1997) Genetic influences on cellular reactions to brain injury: activation of microglia in denervated neuropil in mice carrying a mutation (Wld(S)) that causes delayed Wallerian degeneration. *J Comp Neurol.* 380: 82-94
- Schenk S, Chiquet-Ehrismann R, Battegay EJ (1999) The fibrinogen globe of tenascin-C promotes basic fibroblast growth factor-induced endothelial cell elongation. *Mol Biol Cell.* 10: 2933-43
- Schnell L, Fearn S, Klassen H, Schwab ME, Perry VH (1999) Acute inflammatory responses to mechanical lesions in the CNS: differences between brain and spinal cord. *Eur J Neurosci.* 11: 3648-58
- Scholar A, Stadelmann W (2006) Wound healing: Chronic wounds. In: eMedicine accessed December 2006
- Schwab ME, Bartholdi D (1996) Degeneration and regeneration of axons in the lesioned spinal cord. *Physiol Rev.* 76: 319-70
- Schwab JM, Brechtel K, Mueller CA, Kaps HP, Meyerman R, Schluesener HJ (2004) Akute Rückenmarkverletzung: Experimentelle Strategien als Basis zukünftiger Behandlungen. In: *Dtsch Arztebl;* 101: A-1422 / B-1183 / C-1137
- Schwab ME, Kapfhammer JP, Bandtlow CE (1993) Inhibitors of neurite growth. *Annu Rev Neurosci.* 16: 565-95
- Schwegler G, Schwab ME, Kapfhammer JP (1995) Increased collateral sprouting of primary afferents in the myelin-free spinal cord. *J Neurosci.* 15: 2756-67
- Schwerdtfeger K, Steudel WI, Pitzen T, Mautes AEM (2004) Spinales Trauma: Spinal injury epidemiology, management, therapy and prognosis. *Intensivmedizin und Notfallmedizin* 41: 71-131
- Seitz A, Aglow E, Heber-Katz E (2002) Recovery from spinal cord injury: a new transection model in the C57Bl/6 mouse. *J Neurosci Res.* 67: 337-45

- Semple-Rowland SL, Mahatme A, Popovich PG, Green DA, Hassler G Jr, Stokes BT, Streit WJ (1995) Analysis of TGF-beta 1 gene expression in contused rat spinal cord using quantitative RT-PCR. *J Neurotrauma*. 12: 1003-14
- Shimizu Y, Shaw S (1991) Lymphocyte interactions with extracellular matrix. *FASEB J*. 5: 2292-9
- Smith GM, Rutishauser U, Silver J, Miller RH (1990) Maturation of astrocytes in vitro alters the extent and molecular basis of neurite outgrowth. *Dev Biol*. 138: 377-90
- Sofroniew MV (2005) Reactive astrocytes in neural repair and protection. *Neuroscientist*. 11: 400-7
- Sosale A, Robson JA, Stelzner DJ (1988) Laminin distribution during corticospinal tract development and after spinal cord injury. *Exp Neurol*. 102: 14-22
- Sroga JM, Jones TB, Kigerl KA, McGaughy VM, Popovich PG (2003) Rats and mice exhibit distinct inflammatory reactions after spinal cord injury. *J Comp Neurol*. 462: 223-40
- Steindler DA (1993) Glial boundaries in the developing nervous system. *Annu Rev Neurosci*. 16: 445-70
- Steindler DA, Settles D, Erickson HP, Laywell ED, Yoshiki A, Faissner A, Kusakabe M (1995) Tenascin knockout mice: barrels, boundary molecules, and glial scars. *J Neurosci*. 15: 1971-83
- Steward O, Schauwecker PE, Guth L, Zhang Z, Fujiki M, Inman D, Wrathall J, Kempermann G, Gage FH, Saatman KE, Raghupathi R, McIntosh T (1999) Genetic approaches to neurotrauma research: opportunities and potential pitfalls of murine models. *Exp Neurol*. 157: 19-42
- Stichel-Gunkel CC (1997) The role of microenvironment in axonal regeneration. Influences of lesion-induced changes and glial implants on the regeneration of the postcommissural fornix. *Adv Anat Embryol Cell Biol*. 137: I-VII, 1-81
- Stichel CC, Müller HW (1994) Relationship between injury-induced astrogliosis, laminin expression and axonal sprouting in the adult rat brain. *J Neurocytol*. 23: 615-30
- Stichel CC, Müller HW (1998) The CNS lesion scar: new vistas on an old regeneration barrier. *Cell Tissue Res*. 294: 1-9
- Stichel CC, Hermanns S, Luhmann HJ, Lausberg F, Niermann H, D'Urso D, Servos G, Hartwig HG, Müller HW (1999a) Inhibition of collagen IV deposition promotes regeneration of injured CNS axons. *Eur J Neurosci*. 11: 632-46
- Stichel CC, Lausberg F, Hermanns S, Müller HW (1999b) Scar modulation in subacute and chronic CNS lesions: Effects on axonal regeneration. *Restor Neurol Neurosci*. 15: 1-15
- Stichel CC, Niermann H, D'Urso D, Lausberg F, Hermanns S, Müller HW (1999c) Basal membrane-depleted scar in lesioned CNS: characteristics and relationships with regenerating axons. *Neuroscience*. 93: 321-33
- Streit WJ, Graeber MB, Kreutzberg GW (1988) Functional plasticity of microglia: a review. *Glia*. 1: 301-7
- Streit WJ, Kreutzberg GW (1988) Response of endogenous glial cells to motor neuron degeneration induced by toxic ricin. *J Comp Neurol*. 268: 248-63

- Streit WJ, Walter SA, Pennell NA (1999) Reactive microgliosis. *Prog Neurobiol.* 57: 563-81
- Strekalova T, Sun M, Sibbe M, Evers M, Dityatev A, Gass P, Schachner M (2002) Fibronectin domains of extracellular matrix molecule tenascin-C modulate hippocampal learning and synaptic plasticity. *Mol Cell Neurosci.* 21: 173-87
- Sundqvist KG, Ström H, Arencibia I, Hauzenberger D (1994) Fibronectin and lymphocytes in inflammatory tissue. Studies of blood and synovial fluid lymphocytes from patients with rheumatoid arthritis and other inflammatory arthritides. *Cell Adhes Commun.* 2: 239-47
- Tacconi MT (1998) Neuronal death: is there a role for astrocytes? *Neurochem Res.* 23: 759-65
- Talts JF, Wirl G, Dictor M, Muller WJ, Fässler R (1999) Tenascin-C modulates tumor stroma and monocyte/macrophage recruitment but not tumor growth or metastasis in a mouse strain with spontaneous mammary cancer. *J Cell Sci.* 112: 1855-64
- Tang X, Davies JE, Davies SJ (2003) Changes in distribution, cell associations, and protein expression levels of NG2, neurocan, phosphacan, brevican, versican V2, and tenascin-C during acute to chronic maturation of spinal cord scar tissue. *J Neurosci Res.* 71: 427-44
- Tate MC, Shear DA, Hoffman SW, Stein DG, Archer DR, LaPlaca MC (2002) Fibronectin promotes survival and migration of primary neural stem cells transplanted into the traumatically injured mouse brain. *Cell Transplant.* 11: 283-95
- Taylor J, Pesheva P, Schachner M (1993) Influence of janusin and tenascin on growth cone behavior in vitro. *J Neurosci Res.* 35: 347-62
- Thesleff I, Mackie E, Vainio S, Chiquet-Ehrismann R (1987) Changes in the distribution of tenascin during tooth development. *Development.* 101: 289-96
- Thomas WE (1999) Brain macrophages: on the role of pericytes and perivascular cells. *Brain Res Brain Res Rev.* 31: 42-57
- Uematsu J, Ono K, Yamano T, Shimada M (1996) Development of corticospinal tract fibers and their plasticity I: quantitative analysis of the developing corticospinal tract in mice. *Brain Dev.* 18: 29-34
- van den Berg TK, Kraal G (2005) A function for the macrophage F4/80 molecule in tolerance induction. *Trends Immunol.* 26: 506-9
- Wallner K, Li C, Shah PK, Fishbein MC, Forrester JS, Kaul S, Sharifi BG (1999) Tenascin-C is expressed in macrophage-rich human coronary atherosclerotic plaque. *Circulation.* 99: 1284-9
- Webb CM, Zaman G, Mosley JR, Tucker RP, Lanyon LE, Mackie EJ (1997) Expression of tenascin-C in bones responding to mechanical load. *J Bone Miner Res.* 12: 52-8
- Wehrle B, Chiquet M (1990) Tenascin is accumulated along developing peripheral nerves and allows neurite outgrowth in vitro. *Development.* 110: 401-15
- Weidner N, Grill RJ, Tuszynski MH (1999) Elimination of basal lamina and the collagen "scar" after spinal cord injury fails to augment corticospinal tract regeneration. *Exp Neurol.* 160: 40-50

Wilson MA, Gaze RM, Goodbrand IA, Taylor JS (1992) Regeneration in the *Xenopus* tadpole optic nerve is preceded by a massive macrophage/microglial response. *Anat Embryol (Berl)*. 186: 75-89

Yamagata M, Yamada KM, Yoneda M, Suzuki S, Kimata K (1986) Chondroitin sulfate proteoglycan (PG-M-like proteoglycan) is involved in the binding of hyaluronic acid to cellular fibronectin. *J Biol Chem*. 261: 13526-35

Zenker W (1994) Feinstruktur des Nervengewebes. In: Drenckhahn D, Zenker W (eds) *Benninghoff Anatomie, Makroskopische Anatomie, Embryologie und Histologie des Menschen*, Urban and Schwarzenberg. München, Wien, Baltimore, 15th edition, Volume 2, p 262

Zhang Y, Winterbottom JK, Schachner M, Lieberman AR, Anderson PN (1997a) Tenascin-C expression and axonal sprouting following injury to the spinal dorsal columns in the adult rat. *J Neurosci Res*. 49: 433-50

Zhang Z, Guth L (1997) Experimental spinal cord injury: Wallerian degeneration in the dorsal column is followed by revascularization, glial proliferation, and nerve regeneration. *Exp Neurol*. 147: 159-71

Zhang Z, Fujiki M, Guth L, Steward O (1996) Genetic influences on cellular reactions to spinal cord injury: a wound-healing response present in normal mice is impaired in mice carrying a mutation (WldS) that causes delayed Wallerian degeneration. *J Comp Neurol*. 371: 485-95

Zhang Z, Krebs CJ, Guth L (1997b) Experimental analysis of progressive necrosis after spinal cord trauma in the rat: etiological role of the inflammatory response. *Exp Neurol*. 143: 141-52

Zhao Y, Young SL, McIntosh JC (1998) Induction of tenascin in rat lungs undergoing bleomycin-induced pulmonary fibrosis. *Am J Physiol*. 274: L1049-57

8. Appendix

8.1. Acknowledgement

The experimental part of this work was produced in the Institute of Anatomy II, Experimental Morphology at the University Medical Centre Hamburg-Eppendorf between 2001 and 2003. Quantitative evaluation of this study was performed during 2003 at the Institute of Anatomy at the Chinese University of Hong Kong, with the support of the German Academic Exchange Service (DAAD, PKZ D/03/36817).

First of all, I would like to express my special thanks to Prof. Dr. D. Lorke for the opportunity to work on this subject. I enjoyed the professional supervision and am grateful for his exchange of ideas about research. In particular I liked the extensive and deep discussions about the scientific work. I would also like to thank him deeply for his advices in life and the talks while having lunch in either Hamburg or Hong Kong – they were always fun.

I would like to thank Prof. Dr. U. Schumacher, Head of Department of the Institute of Anatomy II for his ongoing encouragement and for being part of the laboratory team. I appreciate his support throughout the project and his hanseatic sense of humour.

I thank Prof. Dr. M. Schachner, Head of Centre of Molecular Neurobiology Hamburg (ZMNH) for her cooperation and providing animals.

I am grateful to Prof. Dr. M. Davidoff, Institute of Anatomy I of the Cellular Neurobiology at the University Medical Centre Hamburg-Eppendorf who always managed to fit me into his tight schedule for suddenly upcoming problems and questions. I enjoyed our fruitful talks and life saving advices with regard to cryo tissue conservation and immunohistochemistry.

I would like to express my thanks to Prof. D. Yew, Head of Department of Anatomy at the Chinese University of Hong Kong for his cheerful reception and

the highly productive time in his department. I very much enjoyed our talks over Yum Cha lunches and I am still looking forward to travel along the Silk Road.

I am grateful to Cornelia Babista, who spent hours with me operating in the laboratories. I appreciate her help, and advice. I thank Christine Knies for her advices and support on immunohistochemistry. To the laboratory team in Hamburg, namely Susanne Feldhaus, Renate Gehrke, Maike Märker and Klaus Siebert, I am grateful for their excellent assistance and technical help.

At the laboratory in Hong Kong I would like to thank Corinna Au for her skilful technical assistance in preparing photographs and for introducing me to the Metamorph software.

I would like to thank Ulrike Schulz, who performed statistical analysis of this work in an excellent way.

I am grateful to Michael Schreiber, who helped me creating schematic diagrams and editing photographs. In spite of spending hours with Photoshop, we had an excellent familial collaboration. Without his assistance I would have been lost in the desert of computer layout techniques. I am deeply grateful to Michael and Renate Schreiber, who have both encouraged me throughout my life and supported me financially.

Finally I am thankful to Lars, for his everlasting support, which helped me to overcome every possible crisis related to this dissertation.

Last, but not least, I thank Emma who motivated me to eventually bring this thesis to an end.

For revision of this work I thank Michael Schreiber, Prof. Dr. Lorke and Prof. Dr. Schumacher.

8.2. Curriculum Vitae

Jenny Schreiber, 31st December 1977

Academic Studies

1999-2008	Asian-Africa Institute, University of Hamburg Languages and Cultures of Austronesia
1999-2007	Faculty of Medicine, University of Hamburg Medicine
2007	Third State Exam (3. Staatsexamen)
2005	Second State Exam (2. Staatsexamen)
2004	Faculty of Medicine, University of Sydney, Australia Medicine
2002	First State Exam (1. Staatsexamen)
2001	Preclinical Exam (Physikum)

Clinical Elective (Praktisches Jahr)

2007	Neurosurgery (4 months) Asklepios Klinik Altona, Hamburg
2007	Neurosurgery (1 month) Yale New Haven Hospital, University of Yale, Connecticut, USA
2006	Trauma and Reconstructive Surgery (4 months) Asklepios Klinik Barmbek, Hamburg
2006	Internal Medicine, Infectious Diseases (2 months) Singapore General Hospital, National University of Singapore
2005	Internal Medicine (2 months) Israelitisches Krankenhaus, Hamburg

Clinical Placements (Famulaturen)

2004	Neurosurgery (4 weeks) Westmead Hospital, University of Sydney, Australia
2004	Accident and Emergency Medicine (4 weeks) Dubbo Base Hospital, University of Sydney, Australia
2003	Neurology (4 weeks) Cipto Mangunkusumo Hospital, University of Indonesia, Jakarta
2003	Neurosurgery (4 weeks) University Medical Centre Hamburg-Eppendorf

8.3. Statistical tables

1 Deskriptive Statistiken

1.1 Bindegewebige Antikörper

Deskriptive Statistiken								
	N	Mittelwert	Standardab- weichung	Minimum	Maximum	Perzentile		
						25.	50. (Median)	75.
Collagen IV - surrounding area	35	2,21853	4,017966	,000	17,844	,06017	,59825	2,49392
Collagen IV - Incision	35	14,51852	19,284482	,103	72,756	,88566	5,48216	23,25273
Laminin - surrounding area	34	5,83552	15,422756	,063	86,887	,88000	1,55212	3,01409
Laminin - Incision	34	34,34242	58,074434	,650	304,758	5,07563	11,96727	35,90940
Fibronektin - surrounding area	32	5,79284	9,360940	,011	39,660	,28111	1,77273	9,51144
Fibronektin - Incision	32	38,94097	45,509561	,413	140,264	3,17738	20,47350	59,75267

Kolmogorov-Smirnov-Anpassungstest								
		Collagen IV - surrounding area	Collagen IV - Incision	Laminin - surrounding area	Laminin - Incision	Fibronektin - surrounding area	Fibronektin - Incision	
N		35	35	34	34	32	32	
Parameter der Normalverteilung ^{a,b}	Mittelwert	2,21853	14,51852	5,83552	34,34242	5,79284	38,94097	
	Standardabweichung	4,017966	19,284483	15,422756	58,074432	9,360940	45,509560	
Extremste Differenzen	Absolut	,290	,263	,381	,309	,321	,109	
	Positiv	,284	,263	,381	,309	,321	,101	
	Negativ	-,290	-,227	-,354	-,281	-,268	-,109	
Kolmogorov-Smirnov-Z		1,718	1,494	2,223	1,804	1,817	1,124	
Asymptotische Signifikanz (2-seitig)		,006	,023	,000	,003	,003	,160	

a. Die zu testende Verteilung ist eine Normalverteilung.

b. Aus den Daten berechnet.

1.2 Gliale Marker

Deskriptive Statistiken								
	N	Mittelwert	Standardab- weichung	Minimum	Maximum	Perzentile		
						25.	50. (Median)	75.
F4-B0 - surrounding area	32	18,84800	23,080510	,051	98,293	,92469	11,63500	19,70388
F4-B0 - Incision	32	51,09106	51,498096	,000	198,104	1,03649	45,76241	83,94910
F4-B0 - ipsilateral remaining spinal cord, cranial	33	1,54727	4,969381	,010	27,956	,04542	,17895	,66089
F4-B0 - ipsilateral remaining spinal cord, caudal	33	2,06024	2,918044	,024	12,545	,23092	,81175	2,60264
GFAP - surrounding area	34	6,83843	7,022358	,024	29,484	,91929	5,73429	9,45785
GFAP - Incision	34	8,88243	10,771258	,000	40,049	1,01210	5,32515	14,19788
GFAP - ipsilateral remaining spinal cord, cranial	34	1,02514	1,100332	,008	5,427	,15335	,78953	1,60660
GFAP - ipsilateral remaining spinal cord, caudal	34	2,36943	2,625181	,025	10,009	,09613	1,31714	3,40192

Kolmogorov-Smirnov-Anpassungstest

N	Parameter der Normalverteilung	F4-B3 - surrounding area	F4-B3 - Incision	F4-B3 - ipsilateral remaining spinal cord, cranial	F4-B3 - ipsilateral remaining spinal cord, caudal	GFAP - surrounding area	GFAP - Incision	GFAP - ipsilateral remaining spinal cord, cranial	GFAP - ipsilateral remaining spinal cord, caudal
		32	32	32	32	32	34	34	34
Mittelwert	18,04830	51,03105	1,54727	2,00324	8,02940	8,98242	1,02514	2,26943	
Standardabweichung	22,060535	51,488355	4,582261	2,516045	7,022258	10,771258	1,103322	2,525181	
Extremste Differenzen	Absolut	,294	,125	,285	,245	,195	,205	,179	,195
	Positiv	,294	,125	,285	,245	,195	,205	,152	,195
	Negativ	-,230	-,151	-,279	-,243	-,195	-,205	-,179	-,195
Kolmogorov-Smirnov-Z	1,425	1,053	2,215	1,435	,957	1,194	1,025	1,125	
Asymptotische Signifikanz (2-seitig)	,029	,217	,000	,032	,207	,115	,234	,152	

a. Die zu testende Verteilung ist eine Normalverteilung.

b. Aus den Daten berechnet.

1.3 Neuronale Marker

Deskriptive Statistiken

	N	Mittelwert	Standardabweichung	Minimum	Maximum	Perzentile		
						25.	50. (Median)	75.
Neurofilament-white matter, centre	31	41,03831	61,860344	,200	275,865	3,55212	17,21879	54,86107
Neurofilament-white matter, cranial	31	99,37972	71,855827	14,859	280,489	41,27000	94,38816	140,45425
Neurofilament-white matter, caudal	31	105,79594	70,703586	12,095	258,660	50,29097	73,61576	169,45752
Neurofilament-grey matter, centre	31	14,60150	21,779185	,079	89,903	,27459	4,70610	19,86951
Neurofilament-grey matter, cranial	31	30,11069	38,951476	1,517	172,389	8,77688	19,58593	31,22304
Neurofilament-grey matter, caudal	31	24,85791	26,268545	2,364	117,298	6,56079	17,41000	31,58633

Kolmogorov-Smirnov-Anpassungstest

N	Parameter der Normalverteilung	Neurofilament -white matter, centre	Neurofilament -white matter, cranial	Neurofilament -white matter, caudal	Neurofilament -grey matter, centre	Neurofilament -grey matter, cranial	Neurofilament -grey matter, caudal
		31	31	31	31	31	31
Mittelwert	41,03831	99,37972	105,79594	14,60150	30,11069	24,85792	
Standardabweichung	61,860344	71,855827	70,703583	21,779186	38,951477	26,268545	
Extremste Differenzen	Absolut	,250	,191	,192	,250	,253	,211
	Positiv	,215	,191	,192	,251	,253	,211
	Negativ	-,250	-,120	-,093	-,252	-,231	-,126
Kolmogorov-Smirnov-Z	1,392	1,066	1,067	1,408	1,573	1,175	
Asymptotische Signifikanz (2-seitig)	,042	,208	,205	,038	,014	,126	

a. Die zu testende Verteilung ist eine Normalverteilung.

b. Aus den Daten berechnet.

2 Collagen IV

Tests der Innersubjekteffekte

Maß: MASS_1

Quelle		Quadratsumme vom Typ III	df	Mittel der Quadrate	F	Signifikanz
COLL	Sphärizität angenommen	2765,696	1	2765,696	23,898	,000
	Greenhouse-Geisser	2765,696	1,000	2765,696	23,898	,000
	Huynh-Feldt	2765,696	1,000	2765,696	23,898	,000
	Untergrenze	2765,696	1,000	2765,696	23,898	,000
COLL * GENOTYP	Sphärizität angenommen	23,085	1	23,085	,199	,659
	Greenhouse-Geisser	23,085	1,000	23,085	,199	,659
	Huynh-Feldt	23,085	1,000	23,085	,199	,659
	Untergrenze	23,085	1,000	23,085	,199	,659
COLL * TAG	Sphärizität angenommen	1086,312	3	362,104	3,129	,042
	Greenhouse-Geisser	1086,312	3,000	362,104	3,129	,042
	Huynh-Feldt	1086,312	3,000	362,104	3,129	,042
	Untergrenze	1086,312	3,000	362,104	3,129	,042
COLL * GENOTYP * TAG	Sphärizität angenommen	617,935	3	205,978	1,780	,175
	Greenhouse-Geisser	617,935	3,000	205,978	1,780	,175
	Huynh-Feldt	617,935	3,000	205,978	1,780	,175
	Untergrenze	617,935	3,000	205,978	1,780	,175
Fehler(COLL)	Sphärizität angenommen	3124,633	27	115,727		
	Greenhouse-Geisser	3124,633	27,000	115,727		
	Huynh-Feldt	3124,633	27,000	115,727		
	Untergrenze	3124,633	27,000	115,727		

Tests der Innersubjektcontrast

Maß: MASS_1

Quelle	COLL	Quadratsumme vom Typ II	df	Mittel der Quadrate	F	Signifikanz
COLL	Stufe 1 gegen Stufe 2	5531,373	1	5531,373	23,898	,000
COLL * GENOTYP	Stufe 1 gegen Stufe 2	46,169	1	46,169	,199	,659
COLL * TAG	Stufe 1 gegen Stufe 2	2172,625	3	724,208	3,129	,042
COLL * GENOTYP * TAG	Stufe 1 gegen Stufe 2	1235,869	3	411,956	1,780	,175
Fehler(COLL)	Stufe 1 gegen Stufe 2	6249,266	27	231,454		

Tests der Zwischensubjekteffekte

Maß: MASS_1
Transformierte Variable: Mittel

Quelle	Quadratsumme vom Typ III	df	Mittel der Quadrate	F	Signifikanz
Intercept	2552,124	1	2552,124	24,144	,000
GENOTYP	22,185	1	22,185	,210	,651
TAG	890,225	3	296,742	2,807	,059
GENOTYP * TAG	419,225	3	139,408	1,319	,289
Fehler	2854,028	27	105,705		

Mehrfachvergleiche

Maß: MASS_1
Games-Howell

(I) post OP day	(J) post OP day	Mittlere Differenz (I-J)	Standardfehler	Signifikanz	95% Konfidenzintervall	
					Untergrenze	Obergrenze
1	1					
	3	-3,81300	4,995804	,273	-9,74491	2,11890
	7	-14,22931	5,140640	,193	-34,80747	6,34884
	14	-6,24959	4,876840	,272	-16,05289	3,55371
3	1	3,81300	4,995804	,273	-2,11890	9,74491
	3					
	7	-10,41631	4,995804	,424	-31,04507	10,21245
	14	-2,43659	4,723922	,903	-12,82246	7,94929
7	1	14,22931	5,140640	,193	-6,34884	34,80747
	3	10,41631	4,995804	,424	-10,21245	31,04507
	7					
	14	7,97972	4,876840	,670	-13,12982	29,08927
14	1	6,24959	4,876840	,272	-3,55371	16,05289
	3	2,43659	4,723922	,903	-7,94929	12,82246
	7	-7,97972	4,876840	,670	-29,08927	13,12982
	14					

Basiert auf beobachteten Mittelwerten.

3 Laminin

Tests der Innersubjekteffekte

Maß: MASS_1

Quelle		Quadratsumme vom Typ III	df	Mittel der Quadrate	F	Signifikanz
LAM	Sphäricität angenommen	12924,793	1	12924,793	13,024	,001
	Greenhouse-Geisser	12924,793	1,000	12924,793	13,024	,001
	Huynh-Feldt	12924,793	1,000	12924,793	13,024	,001
	Untergrenze	12924,793	1,000	12924,793	13,024	,001
LAM * GENOTYP	Sphäricität angenommen	409,166	1	409,166	,412	,526
	Greenhouse-Geisser	409,166	1,000	409,166	,412	,526
	Huynh-Feldt	409,166	1,000	409,166	,412	,526
	Untergrenze	409,166	1,000	409,166	,412	,526
LAM * TAG	Sphäricität angenommen	6555,777	3	2185,259	2,202	,112
	Greenhouse-Geisser	6555,777	3,000	2185,259	2,202	,112
	Huynh-Feldt	6555,777	3,000	2185,259	2,202	,112
	Untergrenze	6555,777	3,000	2185,259	2,202	,112
LAM * GENOTYP * TAG	Sphäricität angenommen	68,452	3	22,817	,023	,995
	Greenhouse-Geisser	68,452	3,000	22,817	,023	,995
	Huynh-Feldt	68,452	3,000	22,817	,023	,995
	Untergrenze	68,452	3,000	22,817	,023	,995
Fehler(LAM)	Sphäricität angenommen	25802,243	26	992,384		
	Greenhouse-Geisser	25802,243	26,000	992,384		
	Huynh-Feldt	25802,243	26,000	992,384		
	Untergrenze	25802,243	26,000	992,384		

Tests der Innersubjektkontraste

Maß: MASS_1

Quelle	LAM	Quadratsumme vom Typ III	df	Mittel der Quadrate	F	Signifikanz
LAM	Stufe 1 gegen Stufe 2	25849,585	1	25849,585	13,024	,001
LAM * GENOTYP	Stufe 1 gegen Stufe 2	818,333	1	818,333	,412	,526
LAM * TAG	Stufe 1 gegen Stufe 2	13111,555	3	4370,518	2,202	,112
LAM * GENOTYP * TAG	Stufe 1 gegen Stufe 2	136,905	3	45,635	,023	,995
Fehler(LAM)	Stufe 1 gegen Stufe 2	51604,485	26	1984,788		

Tests der Zwischensubjekteffekte

Maß: MASS_1

Transformierte Variable: Mittel

Quelle	Quadratsumme vom Typ III	df	Mittel der Quadrate	F	Signifikanz
Intercept	12624,374	1	12624,374	9,036	,006
GENOTYP	24,652	1	24,652	,018	,895
TAG	6716,008	3	2238,669	1,602	,213
GENOTYP * TAG	108,034	3	36,011	,026	,994
Fehler	36324,372	26	1397,091		

4 Fibronectin

Tests der Innersubjekteffekte

Maß: MASS_1

Quelle		Quadratsumme vom Typ III	df	Mittel der Quadrate	F	Signifikanz
FIBRO	Sphäricität angenommen	15254,717	1	15254,717	31,317	,000
	Greenhouse-Geisser	15254,717	1,000	15254,717	31,317	,000
	Huynh-Feldt	15254,717	1,000	15254,717	31,317	,000
	Untergrenze	15254,717	1,000	15254,717	31,317	,000
FIBRO * GENOTYP	Sphäricität angenommen	2707,483	1	2707,483	5,558	,027
	Greenhouse-Geisser	2707,483	1,000	2707,483	5,558	,027
	Huynh-Feldt	2707,483	1,000	2707,483	5,558	,027
	Untergrenze	2707,483	1,000	2707,483	5,558	,027
FIBRO * TAG	Sphäricität angenommen	6978,674	3	2326,225	4,776	,010
	Greenhouse-Geisser	6978,674	3,000	2326,225	4,776	,010
	Huynh-Feldt	6978,674	3,000	2326,225	4,776	,010
	Untergrenze	6978,674	3,000	2326,225	4,776	,010
FIBRO * GENOTYP * TAG	Sphäricität angenommen	1945,750	3	648,583	1,331	,287
	Greenhouse-Geisser	1945,750	3,000	648,583	1,331	,287
	Huynh-Feldt	1945,750	3,000	648,583	1,331	,287
	Untergrenze	1945,750	3,000	648,583	1,331	,287
Fehler(FIBRO)	Sphäricität angenommen	11690,586	24	487,108		
	Greenhouse-Geisser	11690,586	24,000	487,108		
	Huynh-Feldt	11690,586	24,000	487,108		
	Untergrenze	11690,586	24,000	487,108		

Tests der Innersubjektkontraste

Maß: MASS_1

Quelle	FIBRO	Quadratsumme vom Typ II	df	Mittel der Quadrate	F	Signifikanz
FIBRO	Stufe 1 gegen Stufe 2	30509,434	1	30509,434	31,317	,000
FIBRO * GENOTYP	Stufe 1 gegen Stufe 2	5414,966	1	5414,966	5,558	,027
FIBRO * TAG	Stufe 1 gegen Stufe 2	13957,349	3	4652,450	4,778	,010
FIBRO * GENOTYP * TAG	Stufe 1 gegen Stufe 2	3891,501	3	1297,167	1,331	,287
Fehler(FIBRO)	Stufe 1 gegen Stufe 2	23381,172	24	974,216		

Tests der Zwischensubjekteffekte

Maß: MASS_1

Transformierte Variable: Mittel

Quelle	Quadratsumme vom Typ III	df	Mittel der Quadrate	F	Signifikanz
Intercept	13826,729	1	13826,729	30,916	,000
GENOTYP	2199,979	1	2199,979	4,919	,036
TAG	4415,101	3	1471,700	3,291	,038
GENOTYP * TAG	2391,605	3	797,202	1,783	,177
Fehler	10733,490	24	447,229		

Mehrfachvergleiche

Maß: MASS_1

Games-Howell

(I) post OP day	(J) post OP day	Mittlere		Signifikanz	95% Konfidenzintervall	
		Differenz (I-J)	Standardfehler		Untergrenze	Obergrenze
1	1					
	3	,28009	10,573892	1,000	-39,43248	39,99267
	7	30,65922	10,945018	,061	-1,49491	62,81334
	14	22,20943	10,275976	,337	-14,57726	59,09613
3	1	-,28009	10,573892	1,000	-39,99267	39,43248
	3					
	7	30,37913	10,945018	,061	-1,43947	62,19772
	14	21,92934	10,275976	,343	-14,71216	58,57084
7	1	-30,65922	10,945018	,061	-62,81334	1,49491
	3	-30,37913	10,945018	,061	-62,19772	1,43947
	7					
	14	-8,44978	10,657481	,754	-34,87251	17,97294
14	1	-22,20943	10,275976	,337	-59,09613	14,67726
	3	-21,92934	10,275976	,343	-58,57084	14,71216
	7	8,44978	10,657481	,754	-17,97294	34,87251
	14					

Basiert auf beobachteten Mittelwerten.

5 F4-80

Tests der Innersubjekteffekte

Maß: MASS_1

Quelle		Quadratsumme vom Typ III	df	Mittel der Quadrate	F	Signifikanz
F4_80	Sphärizität angenommen	46835,836	3	15611,945	35,662	,000
	Greenhouse-Geisser	46835,836	1,466	31956,325	35,662	,000
	Huynh-Feldt	46835,836	1,993	23506,016	35,662	,000
	Untergrenze	46835,836	1,000	46835,836	35,662	,000
F4_80 * GENOTYP	Sphärizität angenommen	372,211	3	124,070	,283	,837
	Greenhouse-Geisser	372,211	1,466	253,961	,283	,686
	Huynh-Feldt	372,211	1,993	186,805	,283	,754
	Untergrenze	372,211	1,000	372,211	,283	,599
F4_80 * TAG	Sphärizität angenommen	25708,369	9	2856,485	6,525	,000
	Greenhouse-Geisser	25708,369	4,397	5846,983	6,525	,000
	Huynh-Feldt	25708,369	5,978	4300,847	6,525	,000
	Untergrenze	25708,369	3,000	8569,456	6,525	,002
F4_80 * GENOTYP * TAG	Sphärizität angenommen	826,841	9	91,871	,210	,992
	Greenhouse-Geisser	826,841	4,397	188,053	,210	,943
	Huynh-Feldt	826,841	5,978	138,325	,210	,972
	Untergrenze	826,841	3,000	275,614	,210	,889
Fehler(F4_80)	Sphärizität angenommen	31519,938	72	437,777		
	Greenhouse-Geisser	31519,938	35,175	896,092		
	Huynh-Feldt	31519,938	47,820	659,136		
	Untergrenze	31519,938	24,000	1313,331		

Tests der Innersubjekt kontraste

Maß: MASS_1

Quelle	F4_80	Quadratsumme vom Typ II	df	Mittel der Quadrate	F	Signifikanz
F4_80	Stufe 1 gegen Stufe 4	29586,847	1	29586,847	23,858	,000
	Stufe 2 gegen Stufe 4	71884,144	1	71884,144	45,568	,000
	Stufe 3 gegen Stufe 4	68535,261	1	68535,261	44,058	,000
F4_80 * GENOTYP	Stufe 1 gegen Stufe 4	211,067	1	211,067	,171	,683
	Stufe 2 gegen Stufe 4	601,505	1	601,505	,381	,543
	Stufe 3 gegen Stufe 4	508,166	1	508,166	,327	,573
F4_80 * TAG	Stufe 1 gegen Stufe 4	18791,350	3	6263,783	5,072	,007
	Stufe 2 gegen Stufe 4	39626,894	3	12875,631	8,162	,001
	Stufe 3 gegen Stufe 4	37920,336	3	12640,112	8,126	,001
F4_80 * GENOTYP * TAG	Stufe 1 gegen Stufe 4	244,041	3	81,347	,066	,977
	Stufe 2 gegen Stufe 4	759,474	3	253,158	,160	,922
	Stufe 3 gegen Stufe 4	640,217	3	213,406	,137	,937
Fehler(F4_80)	Stufe 1 gegen Stufe 4	29638,825	24	1234,951		
	Stufe 2 gegen Stufe 4	37860,046	24	1577,502		
	Stufe 3 gegen Stufe 4	37333,834	24	1555,576		

Tests der Zwischensubjekteffekte

Maß: MASS_1

Transformierte Variable: Mittel

Quelle	Quadratsumme vom Typ II	df	Mittel der Quadrate	F	Signifikanz
Intercept	9379,174	1	9379,174	57,317	,000
GENOTYP	63,709	1	63,709	,389	,539
TAG	4517,491	3	1505,830	9,202	,000
GENOTYP * TAG	150,710	3	50,237	,307	,820
Fehler	3927,308	24	163,638		

Mehrfachvergleiche

Maß: MASS_1
Games-Howell

(I) post OP day	(J) post OP day	Mittlere Differenz (I-J)	Standardfehler	Signifikanz	95% Konfidenzintervall	
					Untergrenze	Obergrenze
1	1					
	3	-11,15461	6,446611	,063	-22,92270	,61348
	7	-34,33457*	6,837664	,015	-60,45704	-8,21210
	14	-26,29981*	6,446611	,000	-36,76908	-15,83054
3	1	11,15461	6,446611	,063	-,61348	22,92270
	3					
	7	-23,17996	6,446611	,087	-49,49636	3,13643
	14	-15,14520*	6,030253	,033	-29,23828	-1,05212
7	1	34,33457*	6,837664	,015	8,21210	60,45704
	3	23,17996	6,446611	,087	-3,13643	49,49636
	7					
	14	8,03476	6,446611	,766	-18,12099	34,19051
14	1	26,29981*	6,446611	,000	15,83054	36,76908
	3	15,14520*	6,030253	,033	1,05212	29,23828
	7	-8,03476	6,446611	,766	-34,19051	18,12099
	14					

Basiert auf beobachteten Mittelwerten.

*. Die mittlere Differenz ist auf der Stufe ,05 signifikant.

6 GFAP

Tests der Innersubjekteffekte

Maß: MASS_1

Quelle		Quadratsumme vom Typ III	df	Mittel der Quadrate	F	Signifikanz
GFAP	Sphäritizität angenommen	1314,548	3	438,183	13,325	,000
	Greenhouse-Geisser	1314,548	1,669	787,519	13,325	,000
	Huynh-Feldt	1314,548	2,250	584,143	13,325	,000
	Untergrenze	1314,548	1,000	1314,548	13,325	,001
GFAP * GENOTYP	Sphäritizität angenommen	27,803	3	9,268	,282	,838
	Greenhouse-Geisser	27,803	1,669	16,656	,282	,716
	Huynh-Feldt	27,803	2,250	12,355	,282	,781
	Untergrenze	27,803	1,000	27,803	,282	,600
GFAP * TAG	Sphäritizität angenommen	753,019	9	83,669	2,544	,013
	Greenhouse-Geisser	753,019	5,008	150,373	2,544	,042
	Huynh-Feldt	753,019	6,751	111,539	2,544	,025
	Untergrenze	753,019	3,000	251,006	2,544	,078
GFAP * GENOTYP * TAG	Sphäritizität angenommen	352,133	9	39,126	1,190	,313
	Greenhouse-Geisser	352,133	5,008	70,319	1,190	,330
	Huynh-Feldt	352,133	6,751	52,159	1,190	,323
	Untergrenze	352,133	3,000	117,378	1,190	,333
Fehler(GFAP)	Sphäritizität angenommen	2564,975	78	32,884		
	Greenhouse-Geisser	2564,975	43,400	59,101		
	Huynh-Feldt	2564,975	58,510	43,838		
	Untergrenze	2564,975	26,000	98,653		

Tests der Innersubjektkontraste

Maß: MASS_1

Quelle	GFAP	Quadratsumme vom Typ III	df	Mittel der Quadrate	F	Signifikanz
GFAP	Stufe 1 gegen Stufe 4	99,312	1	99,312	,760	,391
	Stufe 2 gegen Stufe 4	1907,615	1	1907,615	21,981	,000
	Stufe 3 gegen Stufe 4	1349,854	1	1349,854	14,746	,001
GFAP * GENOTYP	Stufe 1 gegen Stufe 4	1,675	1	1,675	,013	,911
	Stufe 2 gegen Stufe 4	7,226	1	7,226	,083	,775
	Stufe 3 gegen Stufe 4	31,026	1	31,026	,339	,565
GFAP * TAG	Stufe 1 gegen Stufe 4	484,074	3	161,358	1,235	,317
	Stufe 2 gegen Stufe 4	1066,233	3	355,411	4,095	,017
	Stufe 3 gegen Stufe 4	936,053	3	312,018	3,409	,032
GFAP * GENOTYP * TAG	Stufe 1 gegen Stufe 4	424,668	3	141,555	1,083	,373
	Stufe 2 gegen Stufe 4	388,331	3	129,444	1,492	,240
	Stufe 3 gegen Stufe 4	455,205	3	151,735	1,658	,201
Fehler(GFAP)	Stufe 1 gegen Stufe 4	3396,964	26	130,652		
	Stufe 2 gegen Stufe 4	2256,406	26	86,785		
	Stufe 3 gegen Stufe 4	2379,976	26	91,536		

Tests der Zwischensubjekteffekte

Maß: MASS_1

Transformierte Variable: Mittel

Quelle	Quadratsumme vom Typ III	df	Mittel der Quadrate	F	Signifikanz
Intercept	731,961	1	731,961	76,594	,000
GENOTYP	,241	1	,241	,025	,875
TAG	229,375	3	76,458	8,001	,001
GENOTYP * TAG	14,443	3	4,814	,504	,683
Fehler	249,466	26	9,556		

Mehrfachvergleiche

Maß: MASS_1
Games-Howell

(I) post OP day	(J) post OP day	Mittlere			95% Konfidenzintervall	
		Differenz (I-J)	Standardfehler	Signifikanz	Untergrenze	Obergrenze
1	1					
	3	-2,61504	1,502121	,179	-6,15412	,92403
	7	-6,00090*	1,599920	,014	-10,65505	-1,34674
	14	-6,39724*	1,466351	,000	-9,71198	-3,08261
3	1	2,61504	1,502121	,179	-,92403	6,15412
	3					
	7	-3,38585	1,557888	,248	-8,45653	1,68482
	14	-3,78220	1,420372	,081	-7,92848	,36409
7	1	6,00090*	1,599920	,014	1,34674	10,65505
	3	3,38585	1,557888	,248	-1,68482	8,45653
	7					
	14	-,39634	1,523428	,995	-5,37173	4,57904
14	1	6,39724*	1,466351	,000	3,08261	9,71198
	3	3,78220	1,420372	,081	-,36409	7,92848
	7	,39634	1,523428	,995	-4,57904	5,37173
	14					

Basiert auf beobachteten Mittelwerten.

*. Die mittlere Differenz ist auf der Stufe ,05 signifikant.

7 Neurofilament

Tests der Innersubjekteffekte

Maß: MASS_1

Quelle		Quadratsumme vom Typ III	df	Mittel der Quadrate	F	Signifikanz
NF	Sphärizität angenommen	207838,070	5	41567,614	22,481	,000
	Greenhouse-Geisser	207838,070	2,715	76540,898	22,481	,000
	Huynh-Feldt	207838,070	4,120	50440,442	22,481	,000
	Untergrenze	207838,070	1,000	207838,07	22,481	,000
NF * GENOTYP	Sphärizität angenommen	18287,760	5	3657,552	1,978	,087
	Greenhouse-Geisser	18287,760	2,715	6734,866	1,978	,132
	Huynh-Feldt	18287,760	4,120	4438,276	1,978	,103
	Untergrenze	18287,760	1,000	18287,760	1,978	,174
NF * TAG	Sphärizität angenommen	34562,669	15	2304,178	1,246	,240
	Greenhouse-Geisser	34562,669	8,146	4242,819	1,246	,288
	Huynh-Feldt	34562,669	12,361	2796,017	1,246	,263
	Untergrenze	34562,669	3,000	11520,890	1,246	,317
NF * GENOTYP * TAG	Sphärizität angenommen	15761,896	15	1050,793	,568	,893
	Greenhouse-Geisser	15761,896	8,146	1934,887	,568	,802
	Huynh-Feldt	15761,896	12,361	1275,090	,568	,866
	Untergrenze	15761,896	3,000	5253,965	,568	,642
Fehler(NF)	Sphärizität angenommen	203391,502	110	1849,014		
	Greenhouse-Geisser	203391,502	59,738	3404,698		
	Huynh-Feldt	203391,502	90,650	2243,695		
	Untergrenze	203391,502	22,000	9245,068		

Tests der Innersubjektkontraste

Maß: MASS_1

Quelle	NF	Quadratsumme vom Typ III	df	Mittel der Quadrate	F	Signifikanz
NF	Stufe 2 gegen Stufe 1	93421,280	1	93421,280	15,437	,001
	Stufe 3 gegen Stufe 1	130644,138	1	130644,14	35,280	,000
	Stufe 4 gegen Stufe 1	580,733	1	580,733	,069	,763
	Stufe 5 gegen Stufe 1	3685,350	1	3685,350	,738	,390
	Stufe 6 gegen Stufe 1	14843,390	1	14843,390	3,707	,067
NF * GENOTYP	Stufe 2 gegen Stufe 1	14963,450	1	14963,450	2,473	,130
	Stufe 3 gegen Stufe 1	1586,593	1	1586,593	,428	,520
	Stufe 4 gegen Stufe 1	1337,320	1	1337,320	,215	,648
	Stufe 5 gegen Stufe 1	4,945	1	4,945	,001	,975
	Stufe 6 gegen Stufe 1	3676,784	1	3676,784	,918	,348
NF * TAG	Stufe 2 gegen Stufe 1	2122,210	3	707,403	,117	,949
	Stufe 3 gegen Stufe 1	16353,448	3	5451,149	1,472	,250
	Stufe 4 gegen Stufe 1	14625,975	3	4875,325	,783	,516
	Stufe 5 gegen Stufe 1	13791,597	3	4597,199	,921	,447
	Stufe 6 gegen Stufe 1	10171,476	3	3390,492	,847	,483
NF * GENOTYP * TAG	Stufe 2 gegen Stufe 1	5164,349	3	1721,450	,284	,836
	Stufe 3 gegen Stufe 1	7647,148	3	2549,049	,688	,569
	Stufe 4 gegen Stufe 1	12674,050	3	4224,683	,678	,575
	Stufe 5 gegen Stufe 1	6053,849	3	2017,950	,404	,751
	Stufe 6 gegen Stufe 1	6450,565	3	2150,188	,537	,662
Fehler(NF)	Stufe 2 gegen Stufe 1	133136,595	22	6051,663		
	Stufe 3 gegen Stufe 1	81467,589	22	3703,072		
	Stufe 4 gegen Stufe 1	137032,358	22	6228,744		
	Stufe 5 gegen Stufe 1	109823,251	22	4991,966		
	Stufe 6 gegen Stufe 1	88080,895	22	4003,677		

Tests der Innersubjektkontraste

Maß: MASS_1

Quelle	NF	Quadratsumme vom Typ II	df	Mittel der Quadrate	F	Signifikanz
NF	Stufe 1 gegen Stufe 6	14843,390	1	14843,390	3,707	,067
	Stufe 2 gegen Stufe 6	182741,203	1	182741,20	42,047	,000
	Stufe 3 gegen Stufe 6	233560,268	1	233560,27	50,732	,000
	Stufe 4 gegen Stufe 6	9552,142	1	9552,142	5,111	,034
	Stufe 5 gegen Stufe 6	3736,433	1	3736,433	2,979	,098
NF * GENOTYP	Stufe 1 gegen Stufe 6	3676,784	1	3676,784	,918	,348
	Stufe 2 gegen Stufe 6	33474,975	1	33474,975	7,702	,011
	Stufe 3 gegen Stufe 6	10093,929	1	10093,929	2,193	,153
	Stufe 4 gegen Stufe 6	9448,983	1	9448,983	5,056	,035
	Stufe 5 gegen Stufe 6	3951,415	1	3951,415	3,150	,090
NF * TAG	Stufe 1 gegen Stufe 6	10171,476	3	3390,492	,847	,483
	Stufe 2 gegen Stufe 6	18916,569	3	6305,523	1,451	,255
	Stufe 3 gegen Stufe 6	33139,472	3	11046,491	2,399	,095
	Stufe 4 gegen Stufe 6	8395,701	3	2798,567	1,497	,243
	Stufe 5 gegen Stufe 6	3172,712	3	1057,571	,843	,485
NF * GENOTYP * TAG	Stufe 1 gegen Stufe 6	6450,565	3	2150,188	,537	,662
	Stufe 2 gegen Stufe 6	4054,267	3	1351,422	,311	,817
	Stufe 3 gegen Stufe 6	92,282	3	30,761	,007	,999
	Stufe 4 gegen Stufe 6	8160,803	3	2720,268	1,455	,254
	Stufe 5 gegen Stufe 6	2709,566	3	901,189	,718	,552
Fehler(NF)	Stufe 1 gegen Stufe 6	88080,895	22	4003,677		
	Stufe 2 gegen Stufe 6	95614,331	22	4346,106		
	Stufe 3 gegen Stufe 6	101283,139	22	4603,779		
	Stufe 4 gegen Stufe 6	41117,286	22	1868,968		
	Stufe 5 gegen Stufe 6	27594,334	22	1254,288		

Tests der Zwischensubjekteffekte

Maß: MASS_1

Transformierte Variable: Mittel

Quelle	Quadratsumme vom Typ III	df	Mittel der Quadrate	F	Signifikanz
Intercept	72217,562	1	72217,562	80,582	,000
GENOTYP	3486,745	1	3486,745	3,891	,061
TAG	8126,229	3	2708,743	3,022	,051
GENOTYP * TAG	1313,541	3	437,847	,489	,694
Fehler	19716,308	22	896,196		

9. Statement of Originality

The work described in this thesis was carried out on a part-time basis by the candidate under the supervision of Prof. Dr. Lorke at the University Medical Centre Hamburg-Eppendorf.

I herewith declare that I have performed the work for this thesis independently and without improper help. This work does not contain any material written or published by another person except where acknowledged. References in word or content are stated with edition, year, volume and page. I have listed all persons who directly participated in the process of this thesis. This body of work has not previously been submitted for a degree at this or any other university.

25. August 2008

Jenny Schreiber